

# **DNA as Supramolecular Scaffold for Porphyrin Arrays**

**Inauguraldissertation**

Zur

Erlangung der Würde eines  
Doktors der Philosophie

vorgelegt der  
Philosophisch-Naturwissenschaftlichen Fakultät  
Der University of Basel

von

**Imenne Bouamaied**  
Aus Mulhouse (Frankreich)

Basel, 2007

Genehmigt von der Philosophisch-Naturwissenschaftlichen Fakultät der Universität Basel auf  
Antrag der Professoren:

Dr. Eugen Stulz  
Prof. Dr. Bernd Giese  
Prof. Dr. Edwin Constable

Basel, den 26. Juni 2007

Prof. Dr. Hans-Peter Hauri (Dekan)

The work presented herein was initiated and guided by Dr. Eugen Stulz at the Institute of Organic Chemistry of the Philosophic-Scientific Faculty of the University of Basel (Switzerland) and at the School of Chemistry at the University of Southampton (UK), during the time period from September 2003 to June 2007.

Excerpts from this work have been published in the following journals:

- “E. Porphyrin substituted DNA with an unusually stable secondary structure”, *submitted*.
- “Porphyrin-DNA: a supramolecular scaffold for functional molecules on the nanometre scale”, *NN&NA*, in press.
- “Tetranucleotides as scaffold for diporphyrin arrays, **2006**”, *Pure Appl. Chem.*, **78**, 2003–2014.
- “Porphyrin-substituted dinucleotides: Synthesis and spectroscopie”, *Chimia*, **2005**, 59 (3), 1001-104.
- “Synthesis and spectroscopic properties of porphyrin-substituted uridine and deoxyuridine”, *Synlett*, **2004**, (9), 1579-1583.

Excerpts from this work have been presented at the following Conferences:

- Presentation: “Porphyrin substituted DNA: synthesis and spectroscopy”
  - Fall Meeting, Zürich, 2006.
  - 4<sup>th</sup> French-Tunisian Symposium on Organic Chemistry , Tunisia, 2006.
- Poster: “Tetra Nucleotides as Scaffold for Diphenylporphyrin Arrays”
  - PILS, Murten, 2006.
- Poster: “Porphyrin substituted Nucleotides”
  - 14<sup>th</sup> European Symposium on Organic Chemistry (ESOC), Helsinki, 2005.

- Poster: “Tetra Nucleotides as Scaffold for Diphenylporphyrin Arrays”
  - Fall Meeting, Lausanne, 2005.
  
- Poster: “Porphyrin substituted dinucleotides”
  - NRP47 Spring School on “Supramolecular Chemistry”, Murten, 2005.
  - Fall Meeting, Zürich, 2004. *Poster presentation awarded by the Swiss Chemical Society.*

«Rien ne se perd, rien ne se crée, tout se transforme»

Lavoisier



**“A mes parents”**





## Acknowledgements

I would like to thank the following people for their help and support during the years devoted to this work.

First, I would like to thank my supervisor, Dr. Eugen Stulz for the challenging problems, numerous inspiring discussions, and for his continuous interest and support during my work.

Prof. Dr. Bernd Giese for his help, support and to give me the opportunity to stay in Basel in his group.

I am grateful to Prof. Dr. Edwin Constable for accepting to co-referee this thesis.

I thank Dr. Nicolas Amiot for the helpful discussions.

I would like to thank the entire Giese group, past and present, especially Eng. Karine Heintz, for the nice and familiar atmosphere, and for their help.

Special thanks to Dr. Jessica Grun for her advices and help through the last four years.  
(Thank you also to care about my fish when I was away.)

Many thanks to Dr. Deepali Gupta and Thao Nguyen for their help and pleasant time spend together in Southampton.

I gratefully acknowledge the Swiss National Science Foundation and the University of Basel for their financial support.

And my family for giving me the opportunity to come so far in my studies, and for their support and love in everything I decided.

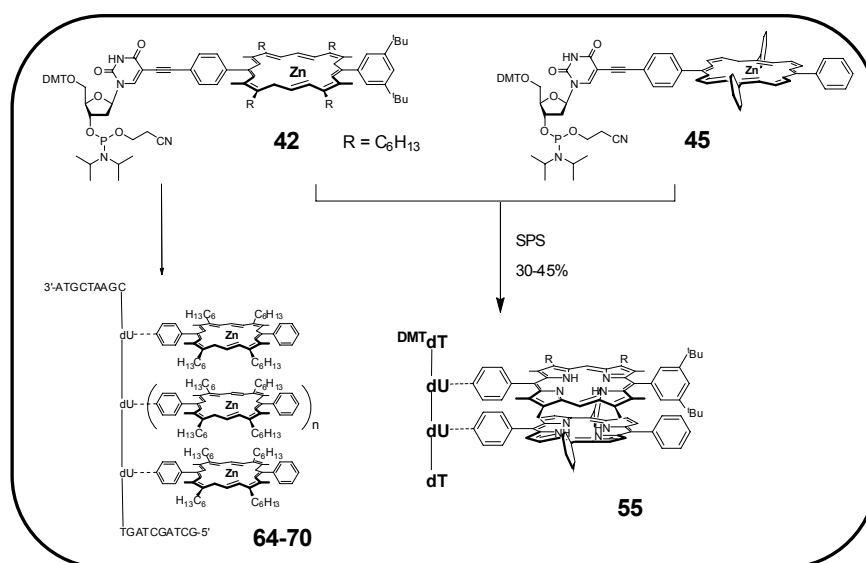


## Abstract

Modified nucleotides are becoming increasingly attractive, e.g. to create supramolecular assemblies by using the Watson-Crick base pairing motif, or to incorporate various functionalities such as fluorophores or amino acid side chain mimics into the DNA itself. Here, we present a general synthetic route to porphyrinyl-nucleosides **31-38**, where the substitution pattern and the metallation state of the porphyrin residue can be varied to introduce diversity. Based on the synthetic route, the corresponding phosphoramidites **39-42** were synthesized.

First, diphenylporphyrin dimers were synthesised both in solution (**46a**, **46b**) and on solid support **47**. The building block was then successfully incorporated into trimer **57**, tetranucleotides **54-56** and 21-mer oligo-deoxynucleotides **64-70** on solid support via an automated DNA synthesiser. The 21-mer DNA contains one central modification, two porphyrins separated by one thymidine, three consecutive and five consecutive porphyrins. These strands were purified by hybridisation of the complementary strand on support solid or by fluoruous affinity chromatography.

First results on the interaction of the dimer, the tetramer, and the 21-mer with the complementary strands are discussed. The UV-Visible and fluorescence spectroscopy show an electronic interaction between the different porphyrins in the hetero-tetranucleotide **55**. Similarly, in the 21-mer porphyrin DNA strands, an electronic coupling between the chromophore is evident from the broadened UV-Vis absorbances (porphyrin B-band).



**Scheme 1:** Solid phase synthesis of oligonucleotides.



## Table of contents

<b>1</b>	<b>INTRODUCTION</b>	<b>21</b>
<b>1.1</b>	<b>Porphyryns</b>	<b>21</b>
1.1.1	Structure	21
1.1.2	Supramolecular multiporphyrin arrays	25
1.1.2.1	Mode of connectivity : Coordination	25
1.1.2.2	Mode of connectivity : Covalent	27
1.1.2.3	Mode of connectivity : combined Covalent-Coordination	28
1.1.3	Templated porphyrin assemblies	29
1.1.4	Photoinduced electron transfer	32
1.1.5	Electron transfer: electronic wires	34
1.1.6	Antenna complex of the natural photosynthetic system	36
1.1.7	Optoelectronic devices	39
<b>1.2</b>	<b>DNA</b>	<b>42</b>
1.2.1	The molecular structure of DNA	42
1.2.2	DNA in nanotechnology and supramolecular chemistry	45
1.2.3	Porphyryns-DNA interactions	49
1.2.3.1	Non-covalent interaction	49
1.2.3.2	Covalent DNA-porphyrin conjugates	51
<b>1.3</b>	<b>Project</b>	<b>55</b>
1.3.1	Research	55
1.3.2	Plan of the synthetic route	57
<b>2</b>	<b>SYNTHESES</b>	<b>59</b>
<b>2.1</b>	<b>Porphyrin synthesis</b>	<b>59</b>
2.1.1	Methodology	59
2.1.2	Synthetic route	61
2.1.2.1	Porphyrin components	62
2.1.2.2	Porphyrin synthesis	66
<b>2.2</b>	<b>Nucleotide Synthesis</b>	<b>69</b>
<b>2.3</b>	<b>Synthesis of the Porphyrin Building Blocks</b>	<b>71</b>
2.3.1	Methodology	71
2.3.2	Results	71
<b>2.4</b>	<b>Synthesis of the Phosphoramidite Building Blocks</b>	<b>73</b>
2.4.1	Methodology	73
2.4.2	Results	74
<b>3</b>	<b>PORPHYRIN-SUBSTITUTED DINUCLEOTIDES</b>	<b>75</b>
<b>3.1</b>	<b>Modified Dinucleotides Synthesis</b>	<b>75</b>
3.1.1	Dimerisation in solution	75
3.1.2	Dimerisation on solid phase	78
<b>3.2</b>	<b>Syntheses of the Adenosine dimer</b>	<b>79</b>
<b>3.3</b>	<b>Duplex Formation (or spectroscopy analysis)</b>	<b>81</b>
<b>4</b>	<b>TRI- AND TETRANUCLEOTIDE PORPHYRIN ARRAYS</b>	<b>85</b>

---

<b>4.1</b>	<b>Methodology</b> .....	<b>85</b>
<b>4.2</b>	<b>Synthesis of the tri- and tetranucleotide</b> .....	<b>87</b>
<b>4.3</b>	<b>Complementary DNA strand synthesis</b> .....	<b>89</b>
<b>4.4</b>	<b>UV-Visible Spectroscopy</b> .....	<b>90</b>
<b>4.5</b>	<b>Steady state emission spectroscopy</b> .....	<b>92</b>
<b>4.6</b>	<b>Circular dichroism spectroscopy</b> .....	<b>94</b>
<b>4.7</b>	<b><sup>1</sup>H NMR Spectroscopy</b> .....	<b>96</b>
<b>4.8</b>	<b>Peptide Nucleic Acid</b> .....	<b>98</b>
4.8.1	Solid-Phase PNA Synthesis.....	99
4.8.2	Spectroscopy studies with tetra-nucleotides.....	102
4.8.2.1	UV-Visible Spectroscopy.....	102
4.8.2.2	Circular Dichroism Spectroscopy.....	106
<b>5</b>	<b>21-MER OLIGONUCLEOTIDES</b> .....	<b>109</b>
<b>5.1</b>	<b>Synthesis</b> .....	<b>109</b>
<b>5.2</b>	<b>DNA Strands Purifications</b> .....	<b>111</b>
5.2.1	Purification <i>via</i> Solid Support.....	111
5.2.2	Purification <i>via</i> Fluorous Purification System.....	112
<b>5.3</b>	<b>UV-Visible Spectroscopy</b> .....	<b>113</b>
<b>5.4</b>	<b>Circular Dichroism Spectroscopy</b> .....	<b>115</b>
<b>5.5</b>	<b>Melting temperature</b> .....	<b>118</b>
<b>5.6</b>	<b>On-bead hybridisation</b> .....	<b>119</b>
<b>6</b>	<b>SUMMARY AND OUTLOOK</b> .....	<b>121</b>
<b>6.1</b>	<b>Summary</b> .....	<b>121</b>
<b>6.2</b>	<b>Outlook</b> .....	<b>122</b>
6.2.1	Synthesis of DNA porphyrin arrays for structural studies.....	122
6.2.2	Synthesis of Donor-Acceptor systems.....	124
6.2.3	Synthesis of electronic wires for charge separation through artificial membranes.....	125
6.2.4	Synthesis of electronic wires for electron transport in break junctions or nano-gaps.....	127
<b>7</b>	<b>GENERAL EXPERIMENTAL CONDITIONS</b> .....	<b>131</b>
<b>7.1</b>	<b>Reaction instruments and physical data</b> .....	<b>131</b>
<b>7.2</b>	<b>Assignment of protons in the <sup>1</sup>H NMR spectra</b> .....	<b>134</b>
<b>7.3</b>	<b>Separation and purification methods</b> .....	<b>135</b>
<b>7.4</b>	<b>Further Instruments</b> .....	<b>137</b>
<b>7.5</b>	<b>Solvents and chemicals</b> .....	<b>138</b>

---

7.6	Buffer and solution .....	138
<b>8</b>	<b>GENERAL SYNTHETIC PROCEDURE.....</b>	<b>141</b>
8.1	Syntheses.....	141
8.2	Reversed-Phase HPLC .....	141
8.3	Formation of the double-stranded DNA .....	141
8.4	Quantification of oligonucleotides via UV absorption.....	142
8.5	Mass determination .....	142
<b>9</b>	<b>PREPARATION OF COMPONENTS FOR THE PORPHYRIN SYNTHESIS..</b>	<b>143</b>
9.1	Synthesis of the dipyrromethane with ester chain .....	143
9.2	Synthesis of the dipyrromethane with hexyl chain .....	147
9.3	Synthesis of the derivate benzaldehyde.....	151
9.4	Synthesis of the protected oligonucleotides .....	156
<b>10</b>	<b>PORPHYRIN SYNTHESIS .....</b>	<b>161</b>
10.1	Zn Diphenylporphyrin with ester chain .....	161
10.2	Zinc diphenylporphyrin with hexyl chain .....	164
10.3	Zinc diphenylporphyrin bearing hexyl chain and di-tertbutylbenzaldehyde.....	167
10.4	Zinc diphenylporphyrin bearing hexyl chain and phosphonate group.....	170
<b>11</b>	<b>SYNTHESIS OF THE BUILDING BLOCKS .....</b>	<b>173</b>
11.1	5'-O-TBDMS-dU <sup>ZnDPP</sup> 33 .....	173
11.2	3'-O-TBDMS-dU <sup>ZnDPP</sup> 34 .....	174
11.3	3',5'-Bis-O-TBDMS-dU <sup>ZnDPP</sup> 32 .....	175
11.4	5'-O-DMT-dU <sup>ZnDPP</sup> 36 .....	177
11.5	5'-O-DMT-dU <sup>ZnDPP</sup> 35 .....	178
11.6	5'-O-DMT-dU <sup>ZnDPP</sup> 37 .....	179
11.7	dU <sup>ZnDPP</sup> 83 .....	180
<b>12</b>	<b>SYNTHESIS OF THE PHOSPHORAMIDITE BUILDING BLOCK .....</b>	<b>183</b>
12.1	5'-O-TBDMS-dU <sup>ZnDPP</sup> phosphoramidite 39.....	183
12.2	5'-O-DMT-dU <sup>ZnDPP</sup> phosphoramidite .....	185

<b>12.3</b>	<b>5'-O-DMT-dU<sup>ZnDPP</sup> phosphoramidite 42</b> .....	<b>186</b>
<b>12.4</b>	<b>Synthesis of the homo- and heterophorphyrinic dimers in solution</b> .....	<b>187</b>
12.4.1	Synthesis of the 1-phenyl-1H-imidazol-3-ium saltz.....	187
12.4.2	Synthesis of the (dU <sup>ZnDPP</sup> ) <sub>2</sub> dimer 44.....	188
12.4.3	Synthesis of the (dU <sup>ZnDPP</sup> -dU <sup>ZnTPP</sup> ) dimer.....	189
<b>13</b>	<b>SYNTHESIS OF DIADENOSINE DIMER</b> .....	<b>191</b>
<b>13.1</b>	<b>6-N-Benzoyl-2'-deoxyadenosine 50</b> .....	<b>191</b>
<b>13.2</b>	<b>5'-O-DMT-6-N-Benzoyl-2'-deoxyadenosine 51</b> .....	<b>192</b>
<b>13.3</b>	<b>5'-O-DMT-6-N-Benzoyl-2'-deoxyadenosine dimer 52</b> .....	<b>193</b>
<b>13.4</b>	<b>2'-deoxyadenosine dimer 53</b> .....	<b>195</b>
<b>14</b>	<b>MANUAL PNA FMOC-SYNTHESIS</b> .....	<b>197</b>
<b>14.1</b>	<b>Solutions for PNA synthesis:</b> .....	<b>197</b>
<b>14.2</b>	<b>Manual synthesis</b> .....	<b>198</b>
14.2.1	Swelling the resin .....	198
14.2.2	Fmoc-deprotection .....	198
14.2.3	Coupling reaction .....	199
14.2.4	Free amine acetylation .....	199
14.2.5	Cleavage of the side chain protecting groups and from MBHA Resin .....	199
14.2.6	Purification and characterisation of PNA.....	200
14.2.6.1	Purification.....	200
14.2.6.2	Characterisation.....	201
<b>15</b>	<b>SYNTHESIS OF OLIGONUCLEOTIDES</b> .....	<b>203</b>
<b>15.1</b>	<b>Principle of the Automated DNA Solid-Phase Synthesis</b> .....	<b>203</b>
<b>15.2</b>	<b>Incorporation of the Building Block</b> .....	<b>205</b>
<b>15.3</b>	<b>DNA Melting Temperatures</b> .....	<b>205</b>
<b>15.4</b>	<b>Data for the synthesized Oligonucleotides</b> .....	<b>206</b>
<b>15.5</b>	<b>Synthesis</b> .....	<b>206</b>
15.5.1	Dimer 47 .....	206
15.5.2	Trimer 57.....	207
15.5.3	Tetramers .....	208
15.5.4	21mer oligonucleotides .....	209
15.5.4.1	Modified oligonucleotides (ODN).....	209
15.5.4.2	Oligonucleotide synthesis (ON) .....	210
15.5.4.3	Purification.....	210



**Abbreviations**

A	adenine within structural formulas, adenosine within text
Å	angstrom ( $1 \text{ Å} = 10^{-10} \text{ m}$ )
aro.	aromatic
Ac	acetyl
AcOH	acetic acid
Anh.	Anhydrous
Aq.	aqueous
B	any base (adenine, cytosine, guanine or thymine)
Bhoc	benzhydryloxycarbonyl group
Boc	tert-butoxycarbonyl
B <sup>P</sup>	any protected base (adenine, cytosine or guanine)
Bz	benzoyl
C	cytosine within structural formulas, adenosine within text
°C	degree centigrade
Calcd.	calculated
CD	circular dichroism
COSY	correlated Spectroscopy
CPG	controlled pore glass
d	deoxy
DCM/CH <sub>2</sub> Cl <sub>2</sub>	dichloroethane
DMAP	N,N-dimethylamino pyridine
DMF	N,N-dimethylformamide
DMSO	dimethylsulfoxide
DMT	4,4'-dimethoxytrityl
DNA	deoxyribonucleic acid
DPP	diphenylporphyrin
eq	equivalent
ET	electron transfert
EtOAc/EA	ethyl acetate
Fmoc	9-fluorenylmethoxycarbonyl
g	guanine within structural formulas, adenosine within text
h	(s)

---

HATU	O-(7-azabenzotriazol-1-yl)N,N,N',N'-tetramethyluronium hexafluorophosphate
HPLC	high performance liquid chromatography
Hz	hertz
J	coupling constant
MALDI-TOF	matrix-assisted laser desorption ionization time-of-flight
MeOH	methanol
min	minute (s)
m.p	melting point
NMP	N-methyl-2-pyrrolidone
NMR	nuclear magnetic resonance
org.	organic
PE	petrol ether
ppm	parts per million
quant.	quantitative
R <sub>f</sub>	retention factor (TLC)
RP	reverse phase
RT.	room temperature
sat.	saturated
T	thymine structural formulas, adenosine within text
TBAF	Bu <sub>4</sub> NF
TBDMS	t-BuMe <sub>2</sub> Si
TEAA	tetraethylammonium acetate
TEA	triethylamine
TFA	trifluoroacetic acid
TIS	triisopropylsilane
THF	tetrahydrofuran
TLC	thin layer chromatography
T <sub>m</sub>	DNA melting point
TPP	tetraphenylporphyrin
Tris	tris(hydroxymethyl)aminomethane
<sup>t</sup> Bu	tert-butyl
UV	ultra violet
UV/Vis	ultra violet/ visible spectroscopy

## **Theoretical Part**



# 1 Introduction

## 1.1 Porphyrins

### 1.1.1 Structure

The porphyrins are a group of naturally occurring pigments and a typical example of zinc octaethylporphyrin<sup>[1]</sup> is shown in figure 1:

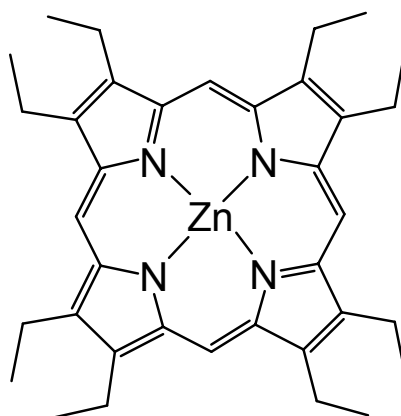


**Figure 1:** Zinc octaethylporphyrin ZnOEP.

A porphyrin is a heterocyclic macrocycle made from four pyrrole subunits linked on opposite sides ( $\alpha$  position) through four methine bridges ( $=\text{CH}-$ ). The macrocycle is fully oxidized and therefore more aromatic than the related chlorines (2,3-dihydroporphyrin) and bacteriochlorophylls (2,3,12,13-tetrahydroporphyrin). The extensive conjugated system makes the compound chromatic, hence the name porphyrin, from a Greek word for *purple*. The first porphyrin was synthesised by Fisher, more than one century ago. The porphyrin structure, with the different possible substitution position, is given in Figure 2.

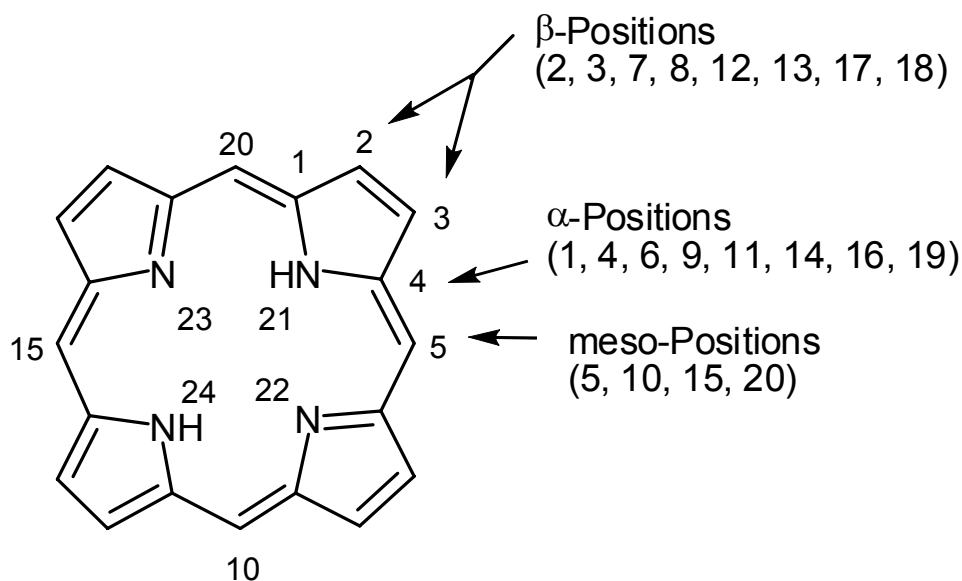


**Figure 2:** Porphyrin structure.

Porphyrins have already been complexed with nearly all metals in the central cavity. Best known are Iron-, magnesium-, zinc-, copper-, nickel-, and cobalt-containing porphyrins. A porphyrin, in which no metal is inserted in its cavity, is called a *free base*. Some iron-containing porphyrins, hemes, and *hemoproteins*, are found extensively in biochemistry, e.g. haemoglobin, where iron is the actual transfer site for oxygen and can be preferentially bound with carbon monoxide, thus poisoning by asphyxiation can occur. Some shellfish, with green-colored blood, have a copper-centered porphyrin. Porphyrin derivatives can also be found in nature, as in chlorophyll (Mg chlorine) and photosynthetic bacteria (bacteriochlorin).

The porphyrin consists of a planar system with 22  $\pi$ -electrons, 18 of which are in the conjugated system. As they follow Hückel's rule, porphyrins have aromatic properties. The delocalisation degrees through the  $\pi$ -system depend on the porphyrin being: (i) a free base, (ii) a di-anion, or (iii) a metallocomplex (Figure 3).<sup>[2]</sup> The porphyrin is an amphoteric molecule. The  $pK_a$  can vary from  $\sim 5.5$  ( $H_2P + H^+ \leftrightarrow H_3P^+$ ) to  $\sim 2$  ( $H^+ + H_3P^+ \leftrightarrow H_4P^{2+}$ ) for the protonated form and from 10-15 for the pyrrol-proton ( $H_2P \leftrightarrow HP^- + H^+$ ;  $HP^- \leftrightarrow P^{2-} + H^+$ ).

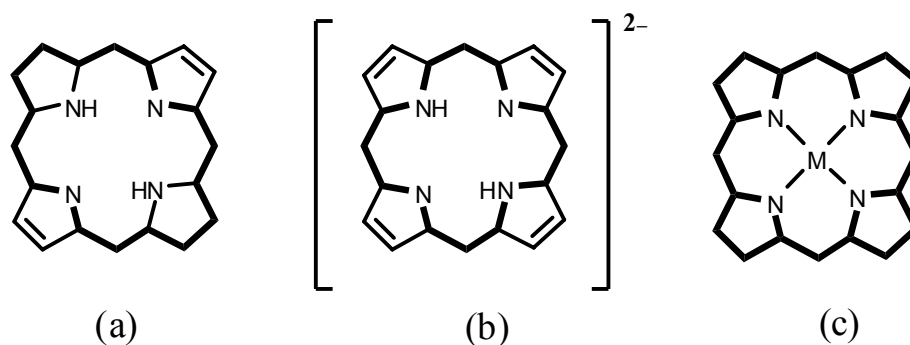


**Figure 3:** Delocalisation of the porphyrin  $\pi$ -system: in (a) free base, (b) di-anion and (c) metallocomplex.

The di-anion structure can form a metallocomplex with four equivalent coordinative donor-acceptor bonds, through labile electrostatic interaction (e.g.:  $\text{Na}^+$ ,  $\text{K}^+$ ,  $\text{Rb}^+$ ,  $\text{Cs}^+$ ,  $\text{Be}^{2+}$ ,  $\text{Sr}^{2+}$ ,  $\text{Mg}^{2+}$ ,  $\text{Ba}^{2+}$ ,  $\text{Ca}^{2+}$ ) or through covalent bonds with cations whose vacant orbital is occupied or semi-occupied (e.g.:  $\text{Fe}^{2+}$ ,  $\text{Fe}^{3+}$ ,  $\text{Co}^{2+}$ ,  $\text{Ni}^{2+}$ ,  $\text{Zn}^{2+}$ ,  $\text{Mn}^{3+}$ ,  $\text{Cr}^{3+}$ ). The porphyrin central cavity is  $\sim 1.4 \text{ \AA}$ , which is an appropriate size for a 3d metal-ion. The spectroscopic characteristic of a porphyrin is due to the  $\pi$ -delocalisation. The UV-visible spectrum shows an intensive absorption at  $\sim 400\text{-}450 \text{ nm}$  which is named “Soret-Band” or “B-Band”. Four other, smaller peaks, at  $500\text{-}700 \text{ nm}$  with  $\lg(\epsilon) \sim 4.5\text{-}5.5$ , are named “Q-Bands”, and vary with the solution, the pH, and the porphyrin structure. Figure 4 shows the UV-visible spectra of a typical porphyrin:  $\text{H}_2\text{DPP}$  and  $\text{ZnDPP}(\text{OAc})_2$ .

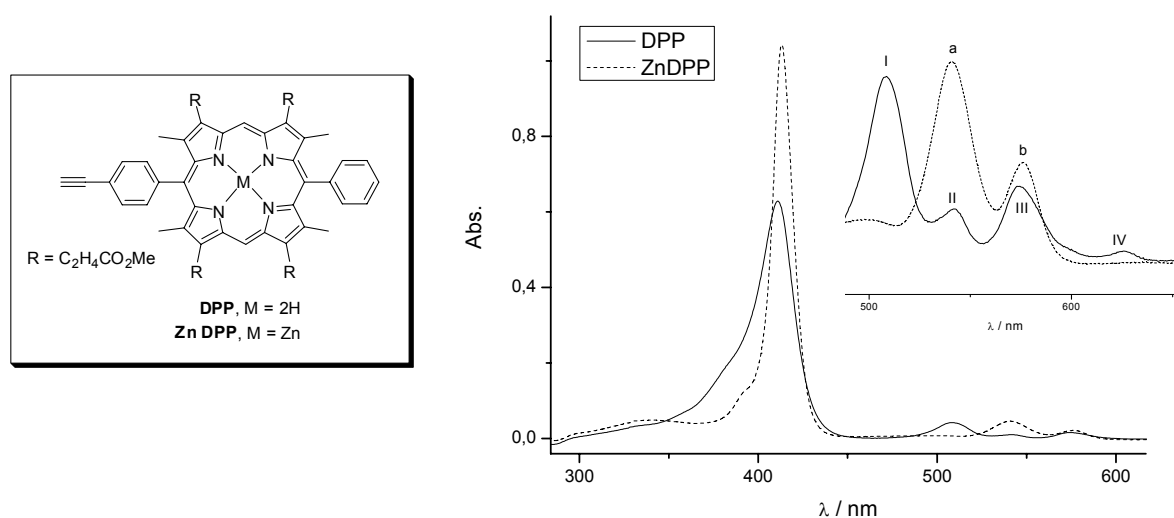


**Figure 4:** UV-Vis. spectra of  $\text{H}_2\text{DPP}$  and  $\text{ZnDPP}(\text{OAc})_2$ .

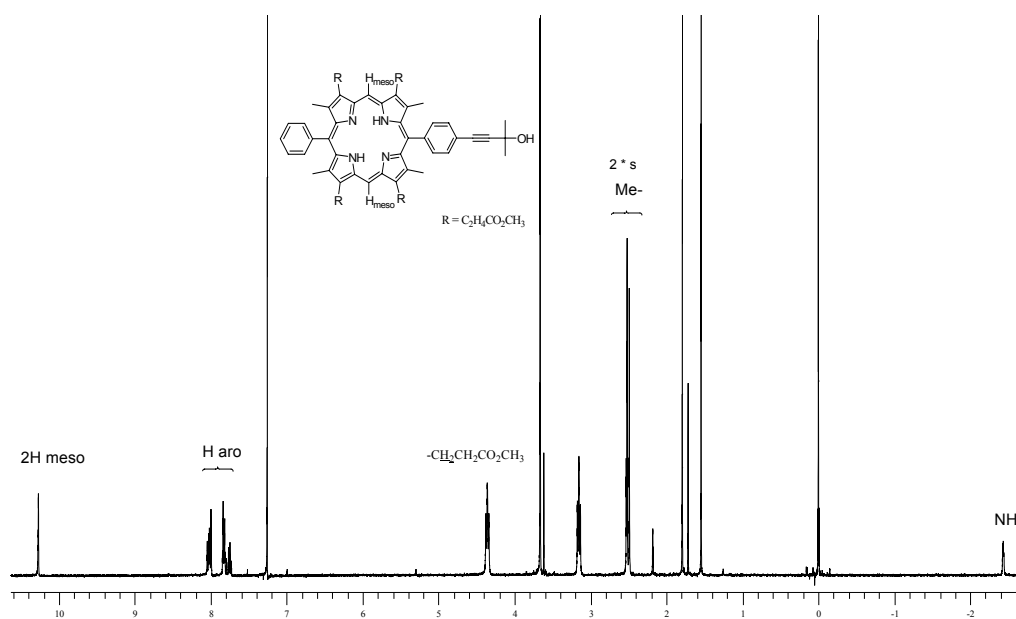


**Figure 5:**  $^1\text{H}$  NMR spectrum of the protected diphenylporphyrin **77**.

The NMR spectra of the protected diphenyl porphyrin (figure 5) show the pyrrol-NH signal at  $\delta = -2$  to  $-3$  ppm, which disappears in the Zn-DPP. Generally, the signal of the two meso-H of the porphyrin is at 10 ppm, and the aromatic protons generate a multiplet from 7.5 to 9 ppm. Due to the asymmetry of the porphyrin, the four methyl groups on the  $\beta$ -position give two singlets at 2.5 ppm. For a symmetrical porphyrin, these two singlets will be turned in one singlet. The signal of the first  $-\text{CH}_2-$  on the alkyl chain appears at 4.5 ppm.

Porphyrins are well-known pigments: they have been widely studied because of their electrochemical and photophysical properties, which can be tuned upon insertion of different metal ions and by changing the substituents on the porphyrin core. Metalloporphyrins undergo reversible redox processes at low potential values, to yield stable and nonfluorescent radical cations. Therefore, Porphyrins have been used extensively to investigate electron and energy-transfer processes. Nowadays, they are not only used in optical and electrochemical properties, but they cover a great variety of fields from photonic devices to light-harvesting antennae and molecular electronics. They offer new way to design molecular devices in the field of material chemistry.



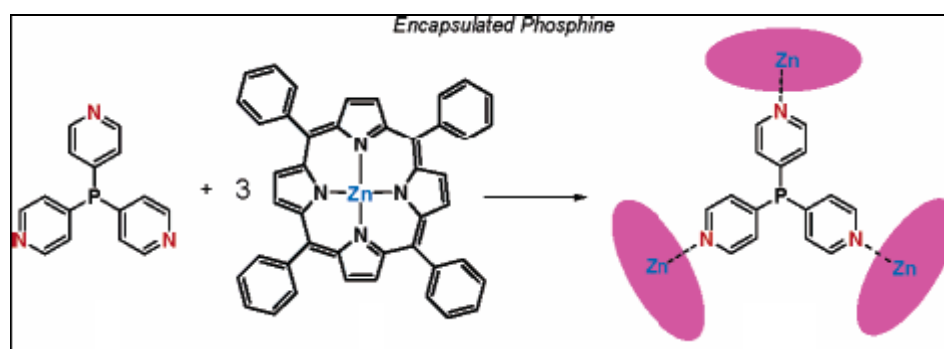
Porphyrins can form conjugated oligomers, in which they possess some extraordinary electrical properties, due to their extended  $\pi$ -systems. They can also form giant supramolecular chromophores where the metal chelation of porphyrins allows considerable control of the redox properties of such systems. The relatively large size of the monomer unit, which is about 16 Å, offers another key advantage to use porphyrins as a molecular wire. For example, a linear tetramer has a length of ca. 56 Å, which is large enough to span a gap in an electrical circuit.

### 1.1.2 Supramolecular multiporphyrin arrays

In order to construct a supramolecular assembly, the mode of connectivity between the porphyrins and the ligand should be appropriate, otherwise the systems will not be stable in solution, and dissociation to yield the individual building block will be observed.

#### 1.1.2.1 Mode of connectivity : Coordination

Porphyrins are widely used and highly versatile building blocks in supramolecular chemistry, especially the metalloporphyrins. Nearly every metal of the periodic table has been inserted into porphyrins. One application of metalloporphyrins is in catalysis, in which case the metal center is used as an active site<sup>[3]</sup>. The most common application of the metalloporphyrin is in the construction of various supramolecular assemblies via coordinative patterns. Generally, the supramolecular binding motif is represented by the axial coordination of the donor ligand to the metal center. Various Zn(II)- and Ru(II)- porphyrins complexes were used, as supramolecular building blocks that selectively associate with the nitrogen donor atoms, to form a supramolecular assembly via Zn-N<sub>pyr</sub> interaction. An example of a tris(meta-pyridyl)phosphine template used with a meso-substituted Zn- tetraphenylporphyrin to create a supramolecular encapsulated ligand assembly<sup>[4]</sup>, is given in Scheme 2.



**Scheme 2:** Formation of supramolecular Phosphine Ligand via Zn(II)- N<sub>pyr</sub> interactions using Zn(II) porphyrin building blocks.

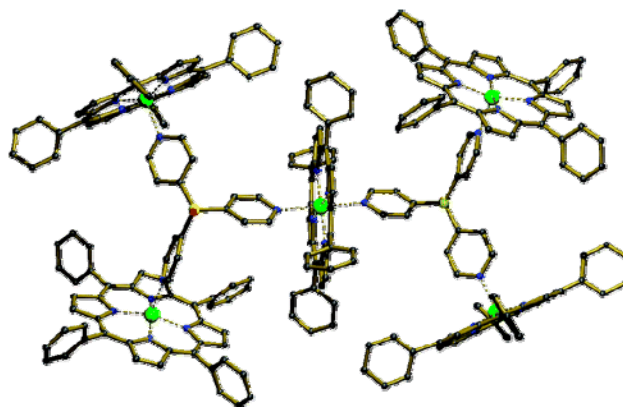


**Figure 6:** X-ray crystallography of the supramolecular ligand. (Zn = green colour).

In the solid state, the template-encapsulated structure formed do not have the expected 1:3 ratio of building blocks, but instead a 2:5 stoichiometry was observed. One of the Zn(II)porphyrin units is part of two adjacent capsule assemblies as a result of a rather unusual hexacoordinated zinc metal. The structure can therefore be described as a fusion of two '1:3' assemblies through the central Zn(II)porphyrin unit. The unique hexacoordinated Zn center bridges the two parts of the 2:5 assemblies via a double axial ligation of two pyridyl phosphines as shown in figure 6.

### 1.1.2.2 Mode of connectivity : Covalent

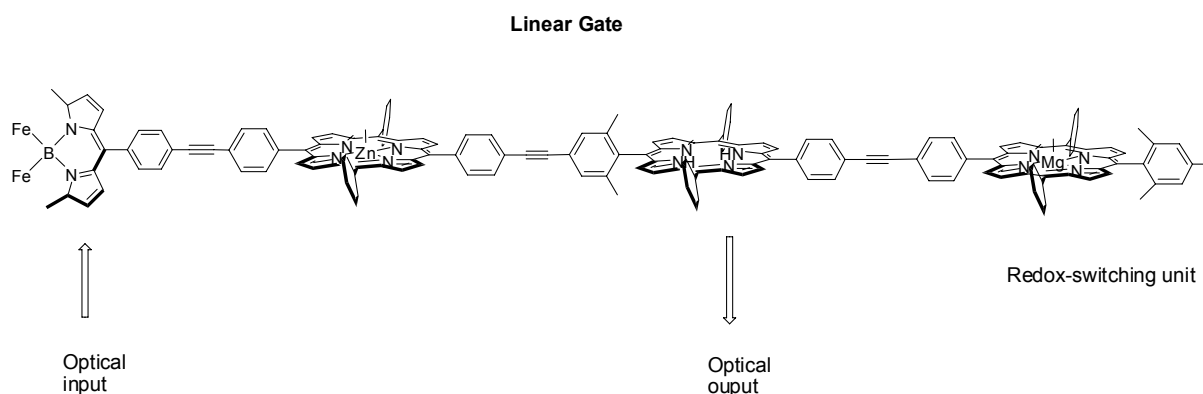


**Figure 7:** Linear gate.<sup>[5]</sup>

The construction of supramolecular assemblies using covalent linkage was used in the design and the synthesis of optoelectronic gates.<sup>[6]</sup> The porphyrins connected *via* a diphenylethyne covalent linker were used in the construction of molecular wires, where their oxidation/reduction properties were used to control the excited-state energy-migration process. An example of a linear gate and a T gate is shown in figure 7. In the linear gate a BDPY-Zn porphyrin dyad was coupled with Fb porphyrin-Mg porphyrin dimer. The synthesis of the T gate used a Zn porphyrin bearing four different meso substituents. Attachment of the three different groups to the Zn porphyrin was accomplished using successive Pd-mediated coupling reactions in the following sequence: Fb porphyrin (output unit), BDPY dye (input unit), and Mg porphyrin (redox switching unit). Both the linear gate and T gate syntheses introduce the Mg porphyrin at the final step to minimize demetalation of the Mg porphyrin. Lindsey and co-workers have studied the dynamics of the energy transfer processes in the linear- and T-shaped optoelectronic gates and their component parts. They have elucidated the dynamics and mechanism of energy flow in the gates. They showed that the energy transfer occurs very rapidly ( $k_{\text{trans}} = (9 \text{ ps})^{-1}$ ) from a Zn porphyrin to a Mg porphyrin joined via a diphenylethyne linker and the majority of the energy in the T gate initially flows to the site of switching rather than to the output unit. The electronic communication in diphenylethyne-linked multiporphyrin arrays can proceed via superexchange among distant sites, such as from a Mg porphyrin to a Fb porphyrin in an array of Mg, Zn, and Fb porphyrins (i.e., like the T gate). Thus, in the T gate, the excited-state energy that initially reaches the Mg porphyrin then proceeds to the Fb porphyrin via superexchange.

### 1.1.2.3 Mode of connectivity : combined Covalent-Coordination

A combined covalent-coordination approach was used to realise multiporphyrin arrays by Sanders *et al.* A large heterometallic porphyrin array, assembled using a combination of Sn(IV) and Rh(III) porphyrin coordination chemistry <sup>[7]</sup>, is shown in figure 8.

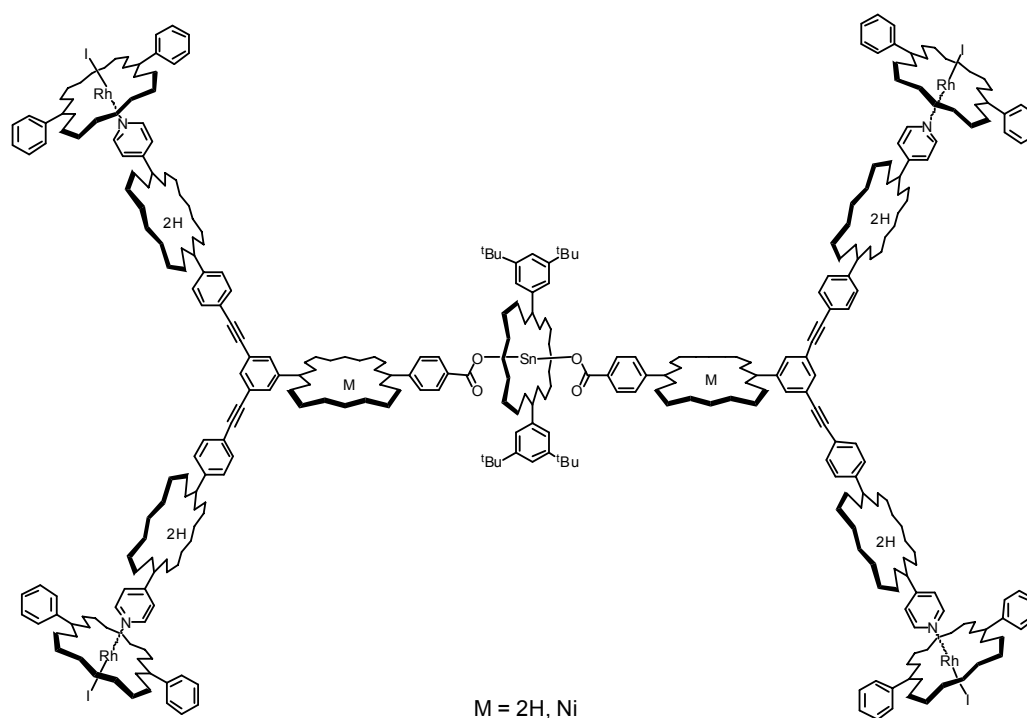


**Figure 8:** Heterometallic undecamer by Sanders using orthogonal binding mode.

A Sn(IV) porphyrin acted as a core around which were coordinated two carboxylic acid functionalized porphyrins. Rh(III) porphyrins were coordinated to pyridyl groups at the periphery of these entities. In this way an eleven porphyrin array, with four different porphyrin metallation states, was assembled. The two-dimensional <sup>1</sup>H NMR analysis proved the integrity of the eleven-porphyrin assembly. This example demonstrates that the composition of such multi-porphyrin arrays can be tuned by choosing the appropriate combination of substituted porphyrins-as-ligand together with the metalloporphyrins that act as ligand acceptor porphyrins.

### 1.1.3 Templated porphyrin assemblies

In section 1.1.7, reasons will be given for constructing supramolecular assemblies with porphyrins and fullerenes. The construction of supramolecular porphyrin-fullerene complexes is achieved through the  $\pi$ - $\pi$  stacking formed between porphyrins and fullerenes. Multiporphyrin arrays, which are based on an oligopeptide scaffold, can form clusters with  $C_{60}$ <sup>[8]</sup>, which show enhanced activity in photoelectronic devices (figure 9).

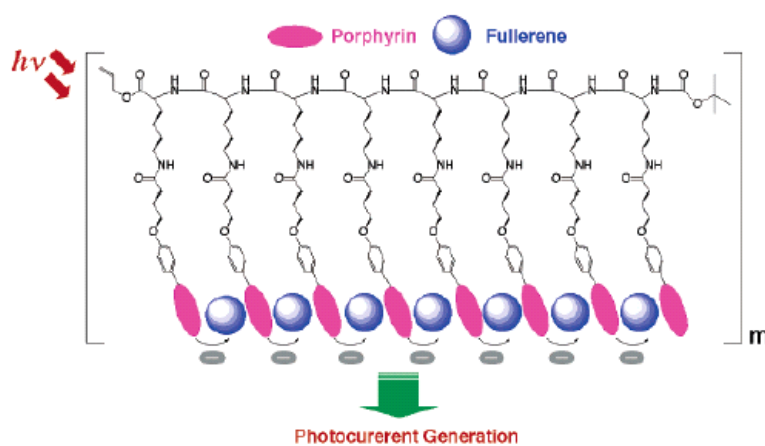


**Figure 9:** Illustration of a Supramolecular Assembly between Porphyrin-Peptide Oligomers and Fullerenes.

The porphyrin- $C_{60}$  complex forms linear arrays with an alternating porphyrin and fullerene composition. These arrays are preformed in solution (toluene-acetonitrile) and subsequently deposited on  $SnO_2$  electrodes. Such porphyrin oligomers are flexible enough to accommodate  $C_{60}$  between the porphyrin units. Compared to the monomer porphyrin, no quenching of the excited state of porphyrins occurs. The systems showed efficient photoresponse from the UV to the near-IR region. A high power conversion efficiency ( $\eta$ ) of 1.3% and a maximum incident photon-to-photocurrent efficiency (IPCE) of 42% show that the formation of a molecular assembly between fullerene and multi-porphyrin arrays with a polypeptide backbone controls the electron transfer efficiency in the supramolecular complex, which is essential for the light-to-energy conversion (chapter 1.1.6). A recently emerging trend concerned with the association of porphyrins and fullerenes could lead to new materials in the future.

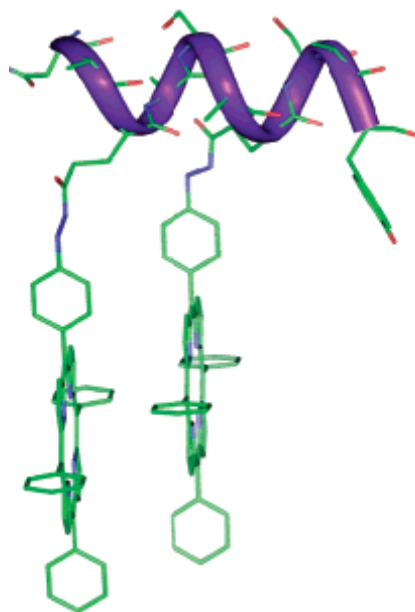


**Figure 10:** Porphyrin-Modified Peptides.

Another example of a supramolecular assembly,<sup>[9]</sup> that features long-range electronic coupling between porphyrins covalently attached to a designed peptide scaffold, is shown in figure 10. The resulting construct self-assembles to form extended organized aggregates in which porphyrins engage in exciton coupling. By this approach, Akerfeldt *et al.* aim to control the structure and the electronic properties of the assembly by manipulation of the spacing between the porphyrins along the peptide chain. They report an example where a short diporphyrinlinked peptide sequence that self-assembles in a “Lego-like” fashion to yield extended porphyrin arrays. The properties can be controlled by concentration, temperature, and pH. By adjusting the temperature, the growth of the aggregate can be monitored over time. This system could be used in the construction of photonic nanodevices that mimic the photosynthetic light-harvesting complexes.

A “classical” covalent synthesis is mostly used to obtain this multi-porphyrin supramolecular species<sup>[10-12]</sup> as seen above. The main reason for the predominance of the covalent synthesis over the noncovalent method is that the former allows finer control over the structure of the final species, intrinsic to the strength of the covalent bond. Noncovalent interactions are weaker and less addressable. Purrello *et al.*<sup>[10]</sup> give one possible way to partly overcome this limitation inherent in the noncovalent route by using a combined approach. They begin the synthesis with covalently synthesized multipart components (as porphyrin

conjugates) and then self-assemble these with the other components (or multiparts) to obtain the final species as shown in figure 11. This assembly formed by the interaction between multi-anionic and multicationic components take advantage in terms of thermodynamic stability and/or kinetic inertness. Some of these "purely" noncovalent species have good control in aqueous solution. This self-assembly is driven by the templating action of an octa-anionic calixarene on a tetracationic porphyrin and/or its metal derivatives. They started from a central 1:4 porphyrin/calixarene species; they show the possibility to pile, in a stepwise fashion, up to six porphyrins above and below the central porphyrin to form a final 7:4 array. Interestingly, the stoichiometric ratio of the complex corresponds to the ratio of the components in solution.

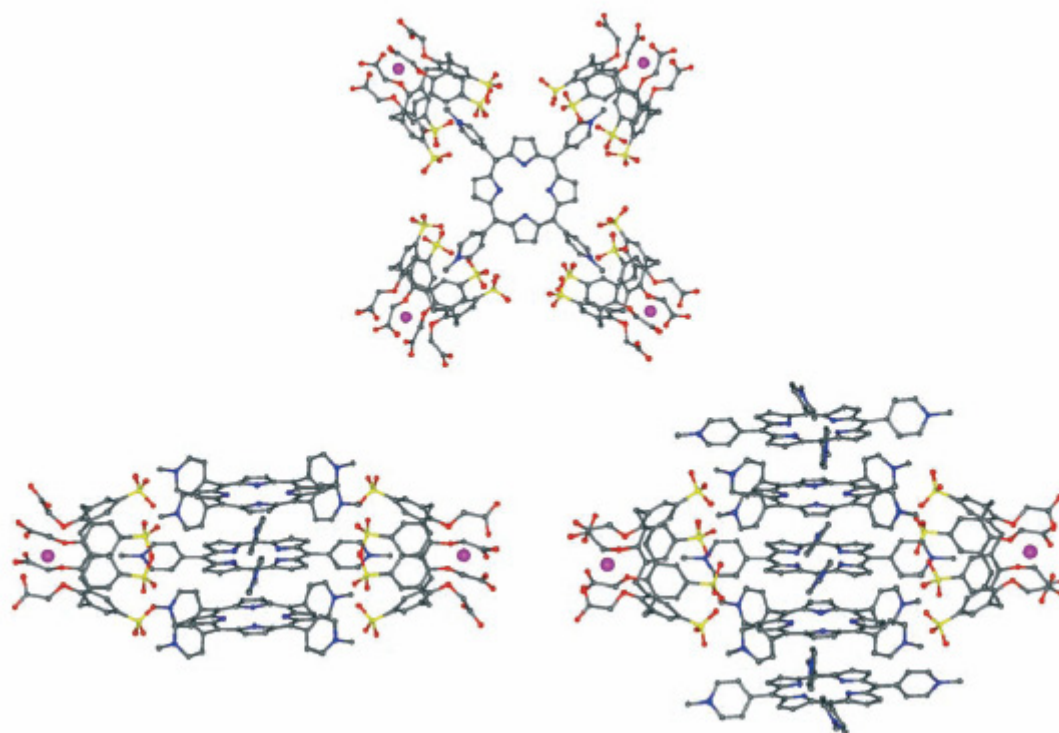


**Figure 11:** Porphyrins and Calixarenes complexes.

The top of the figure shows a host–guest interactions in the unit, formed by the central tetracationic porphyrin and four calixarenes as extracted from the structure of the complexes indicated in the lower part of this figure. Each calixarene hosts a sodium ion (violet circles) in the lower rim. On the side view, they are tri- (left) and penta-porphyrin (right) supramolecular complexes where the two calixarenes interacting with the central porphyrin above and below the figure plane have been omitted for clarity.

### 1.1.4 Photoinduced electron transfer

The design of “smart” molecular arrays, able to perform useful acts upon external stimuli, are used for the construction of nanostructures in a “bottom up” approach. The present example addresses the effect of using excitation with UV light in a series of dyads and triads (figure 12) based on porphyrins and bis-terpyridine complexes. In the models elaborated by Sauvage and co-workers, a free-base or zinc(II) porphyrin is used as chromophore and primary electron donor, while a Au(III)-metalated porphyrin serves as electron acceptor. These electro-active components are assembled around an octahedral transition metal complex of the Ir(III) terpyridine type, which can act as electron relay between two porphyrins. The construction of linear dyads and triads are fixed by intercomponent distances. The Iridium-(III) polyimine complexes was selected for its photophysical and electrochemical properties, its high energetic excited states which avoid the risk of energy transfer from a porphyrinic component, and its good ability to accept electrons.



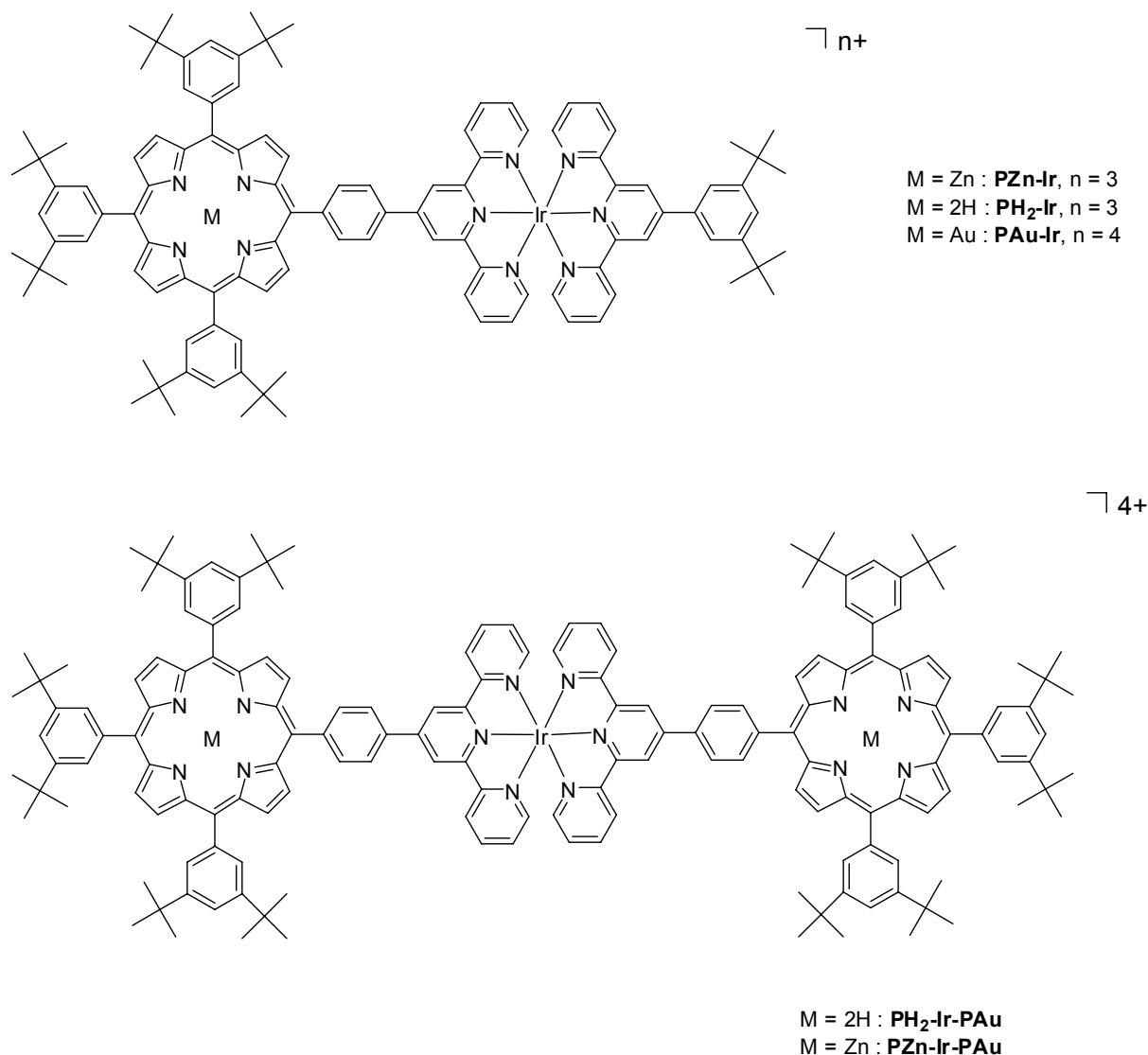


**Figure 12:** Arrays and related models.<sup>[13]</sup>

Excitation of these arrays by light in the visible range excites only the porphyrins. A selective excitation of the free base porphyrin in acetonitrile solutions of the arrays **PH<sub>2</sub>-Ir** and **PH<sub>2</sub>-Ir-PAu** dyads results in an electron-transfer process from the excited state of the free base porphyrin to the metal complex, leading to a charge separated (CS) state characterized by a reduced metal complex and an oxidized free-base porphyrin. In the triad a further electrontransfer step to the gold porphyrin moiety can compete with the back electron transfer and gives **PH<sub>2</sub><sup>+</sup>-Ir-PAu<sup>-</sup>**. Compared to the zinc metalated homologues, the excitation of the zinc porphyrin unit in the triad **PZn-Ir-PAu** in toluene produced two consecutive electron-transfer steps leading to the CS state **PZn<sup>+</sup>-Ir-PAu<sup>-</sup>**. (The corresponding **PZn-Ir** and **PAu-Ir** dyads could not be studied in the same solvent.) Excitation at 350-355 nm, of the

dyads **PAu-Ir**, **PH<sub>2</sub>-Ir** and of the triads **PH<sub>2</sub>-Ir-PAu** and **PZn-Ir-PAu**, produces to a predominant extent the excited state of the metal complex identified as a ligand centered state. The excitation of this unit leads to an energy transfer process, in contrast with the electron-transfer process observed for excitation of the porphyrin free-base photosensitizer. Switching of the type of process from electron-to energy-transfer by changing the excitation wavelength, does not occur in **PZn-Ir-PAu**, which exhibits electron-transfer irrespective of the unit which is excited.

These results reveal that in **PH<sub>2</sub>-Ir** dyads and **PH<sub>2</sub>-Ir-PAu** triads arrays, it is possible to switch the nature of the photoinduced process between energy and electron transfer by selective excitation of the different component units. The excitation of the Ir complex unit in the ultraviolet leads to energy transfer and sensitization of the triplets of the porphyrins whereas excitation of the free-base porphyrin in the visible wavelength range leads to electron transfer which yields a charge separated state.

### 1.1.5 Electron transfer: electronic wires

The field of single-molecule electronics has become a promising design concept for miniaturisation in electronics. Molecular wires are the crucial components of such electronic devices, and several types of molecules have been suggested that have the potential for charge transfer, including conjugated hydrocarbon, carbon nanotubes, porphyrins oligomers and DNA strands. All have the same key requirements, namely they have to be electron or hole conducting in order to carry a current through the circuit. Rate measurements of the electron transfer along the wires are studied by spectroscopic techniques and STM in order to obtain current-voltage characterisation. Porphyrins are one of the most attractive building blocks due to their desirable characteristics such as rigid planar geometry, high electronic stability, and a small HOMO-LUMO energy gap. The porphyrins can conduct electrons through their  $\pi$ -system which is the basis of many wires.

A non natural molecular design of directly meso-meso-linked porphyrins arrays,<sup>[14]</sup> as a model of light-harvesting antenna as well as a molecular photonic wire is shown in figure 13. The preparation of meso-meso directly linked zinc(II) porphyrins arrays up to 128-mer (Z128) is achieved by repetitive Ag(I)-salt-promoted dimerisation reaction.

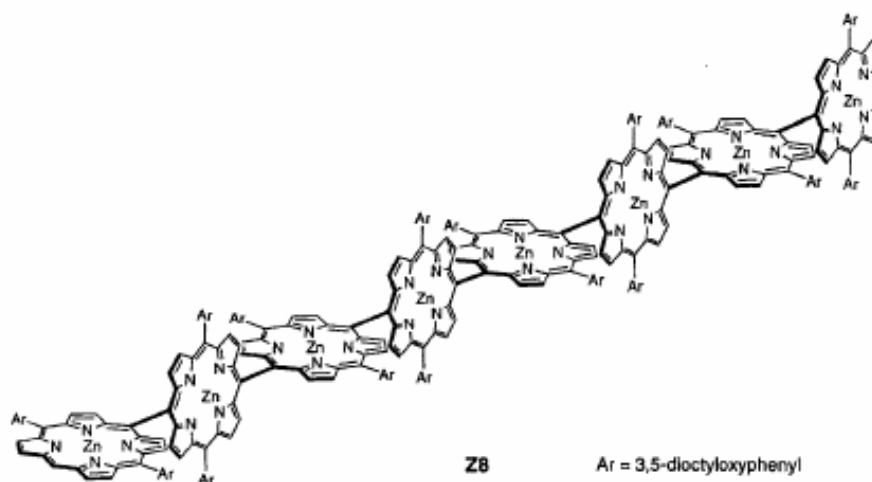


**Figure 13:** 8-mer of meso-meso directly linked zinc(II) porphyrins arrays.

Here, the porphyrin units are close enough to each other to allow for a rapid energy transfer. The properties of these giant arrays are favourable for the use as photonic molecular wires, and the linear shape allows a prediction of the entire molecular length by the number of porphyrins ( $8.35 \text{ \AA}$  per one porphyrin unit). The large electronic interactions between the neighbouring porphyrins are favourable for rapid excitation-energy hopping, and each porphyrin unit retains its individual character due to the orthogonal geometry, thus minimizing the formation of any energy sink, which will disrupt the energy flow along the arrays.

In another example,<sup>[15]</sup> linear porphyrin arrays are self-assembled by hydrogen bonding or metal ion coordination, and self-organize in lipid bilayer membranes. This illustrates the use of porphyrins as photo-switch conductors (figure 14). The incorporation of porphyrins into lipid bilayer membranes to study electron transfer reactions to quinines led to the formation of a molecular electronic device that functioned as a photogated transistor. An aqueous electron acceptor is placed on one side of the membrane and an electron donor is placed on the opposite side. When illuminated with white light, substantial photocurrents are observed. Only the assembled structures give rise to the photocurrent, as no current is observed from any of the component molecules alone.

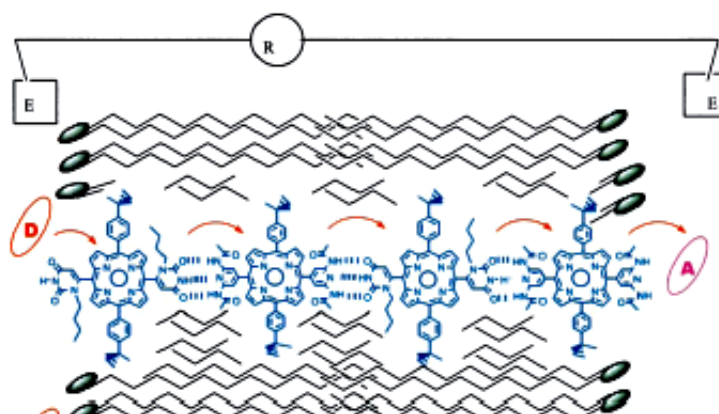


**Figure 14:** Schematic of one of four self-assembling porphyrin systems self-organized into bilayers to form a functional device.

The orientation of the porphyrins tape (top and bottom arrays) can be in any direction such that the porphyrin planes are perpendicular to the bilayer-water interface. It is difficult to quantify the yield of membrane-spanning porphyrin arrays, so it is reasonable to expect some monomers-to-trimers to be present in the system. The electron donor, D, is  $K_4Fe(CN)_6$  and the acceptor, A, is anthraquinonesulfate (AQS).

### 1.1.6 Antenna complex of the natural photosynthetic system

Multiporphyrins are not only used to study electron transfer from the photoexcited state, but they are also suitable for mimicking the antenna effect of the natural photosynthetic system. In the natural photosynthetic systems, light energy absorbed by one of the chromophores in the antenna complexes is transferred through intra- and interantenna complexes until it attained the reaction center. Porphyrin arrays, in which fast photoinduced energy transfer occurs, are useful models to mimic natural photosynthesis. Various designs of porphyrins-based artificial antennae,<sup>[16]</sup> such as stars,<sup>[17]</sup> windmill,<sup>[18]</sup> macroring,<sup>[19-21]</sup> dendrimer,<sup>[22-24]</sup> and linear arrays,<sup>[25, 26]</sup> have been studied. A linear antenna with terminal acceptors as an example is shown in figure 15, where the formation of the light-harvesting antenna-acceptor composite is achieved by heterocomplementary coordination.<sup>[6]</sup>

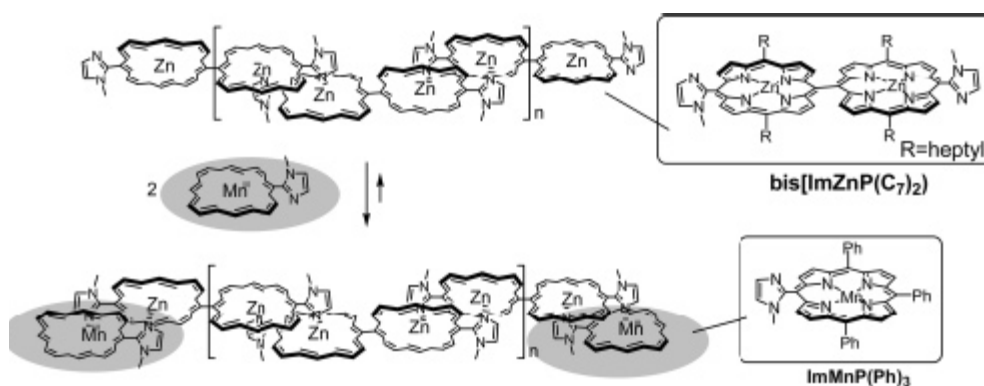


**Figure 15:** light-harvesting antenna-acceptor composite.

The linear antenna which has two free zinc imidazolyl porphyrin terminals is mixed with manganese porphyrins, an acceptor porphyrin, to obtain the large antenna acceptor composite.

In another design, complexes of porphyrins with fullerenes to form light-harvesting antenna ensembles have been studied. Photoinduced electron transfer occurs in a molecular dyad consisting of a fullerene covalently linked to synthetic porphyrin,<sup>[27]</sup> as shown in figure 16. Fullerenes, which are available since 1990, have been found to be an excellent electron acceptor moieties for incorporation into multicomponent “supermolecules” which act as artificial reaction center.

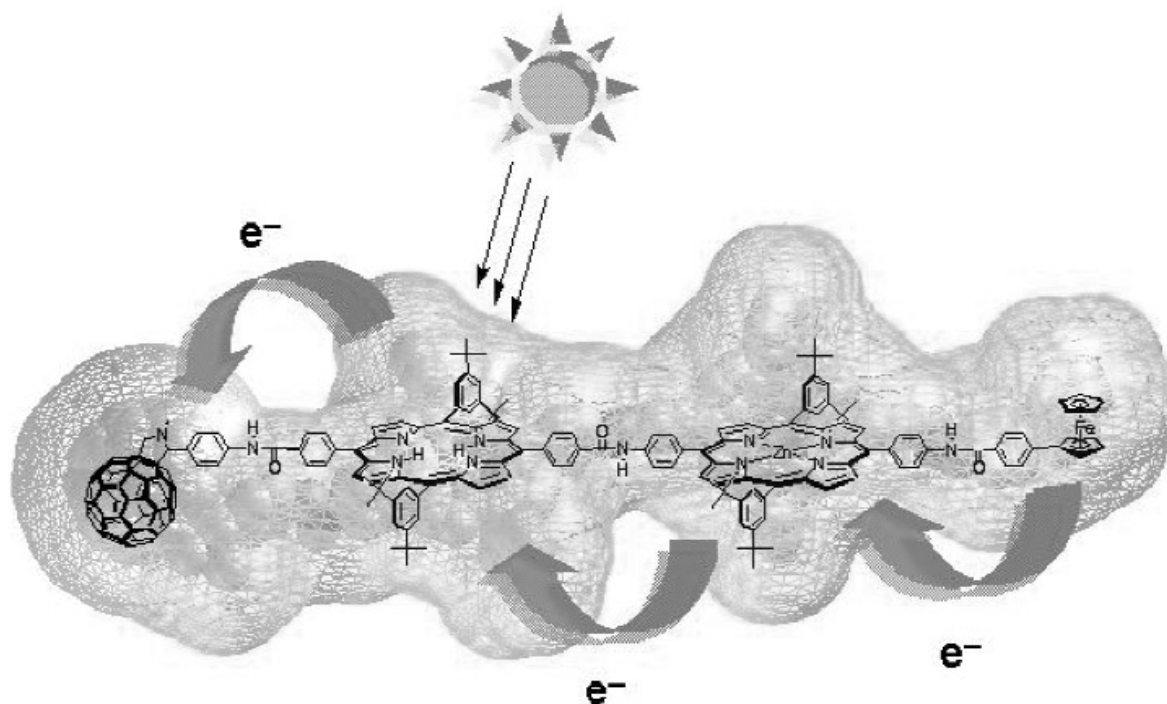


**Figure 16:** Sequence of electron-transfer reaction in photoexcited Fc-ZnP-H<sub>2</sub>P-C<sub>60</sub>.

A fullerene moiety is linked to an array of two porphyrins (i.e., ZnP and H<sub>2</sub>P). In ZnP–H<sub>2</sub>P–C<sub>60</sub>, the ZnP moiety acts as an antenna molecule, transferring its singlet excited-state energy to the lower-lying H<sub>2</sub>P. In polar benzonitrile, this energy transfer is followed by a sequential electron transfer yielding Fc–ZnP–H<sub>2</sub>P<sup>•+</sup>–C<sub>60</sub><sup>•-</sup>, then Fc–ZnP<sup>•+</sup>–H<sub>2</sub>P–C<sub>60</sub><sup>•-</sup> and Fc<sup>•+</sup>–ZnP–H<sub>2</sub>P–C<sub>60</sub><sup>•-</sup>. Considering the overall efficiency of 40 % for (i) funneling light from the antenna chromophore (i.e., ZnP) to the H<sub>2</sub>P chromophore, (ii) charge-injection into the fullerene core and (iii) charge-shift, this artificial reaction center reproduces the natural system very well.

Recent advances in understanding the photosynthetic antenna system and improvements in synthetic and spectroscopic methods allowed the development of artificial light-harvesting antennae which absorb light and then transfer this excitation energy among various chromophores.

### 1.1.7 Optoelectronic devices

The development of new photoactive molecular devices could lead to significant improvement in energy conversion and transport. The combination of both chromophores (porphyrins and fullerenes) seems ideal for fulfilling an enhanced light-harvesting efficiency of chromophores throughout the solar spectrum and a highly efficient conversion of the harvested light into the high energy state of the charge separation by photoinduced electron transfer. Self-assembled monolayers (SAMs) of fullerenes and porphyrins have been used as artificial photosynthetic materials and photonic molecular devices. In particular, the construction of photoactive ITO electrodes based on a *layer-by-layer* approach<sup>[28-30]</sup> such as the example shown in figure 17, is a promising approach. Porphyrin-linked fullerenes bearing positively charged functionalities are synthesised, which allow the control of the thickness and the control of the assembled films. The specific alignment and the orientation of the system are guaranteed by the free-base tetraphenylporphyrin-fullerene donor-acceptor ensemble which facilitate the electron transfer among adjacent layers and the repulsion of equally charged substrates restricts each assembly restructuring to single-layers.

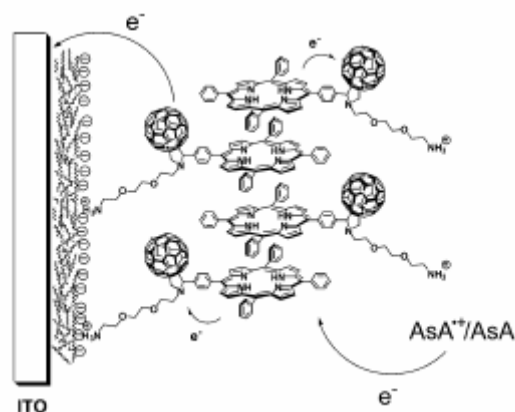


**Figure 17:** Schematic illustration of photocurrent generation in ITO electrodes covered with a single-layer film of H<sub>2</sub>P-C<sub>60</sub>.

Electrostatic and van der Waals interactions have been used for the step-by-step deposition of layers containing the fullerene-porphyrin dyad as the active layer. This photoactive ITO/H<sub>2</sub>P-C<sub>60</sub> electrode gives rise to largely improved light harvesting features in the visible light. In response to visible light irradiation, injection of electrons into the ITO conduction band occurs directly from the photochemically generated H<sub>2</sub>P<sup>+</sup>-C<sub>60</sub><sup>•-</sup> radical pair

and indirectly via electron transport mediated through suitable electron carriers. Considering the simplicity of this approach, combined with the useful efficiency found for monolayer coverage, porphyrins could be a potent alternative in fabrication of photoactive molecular devices.

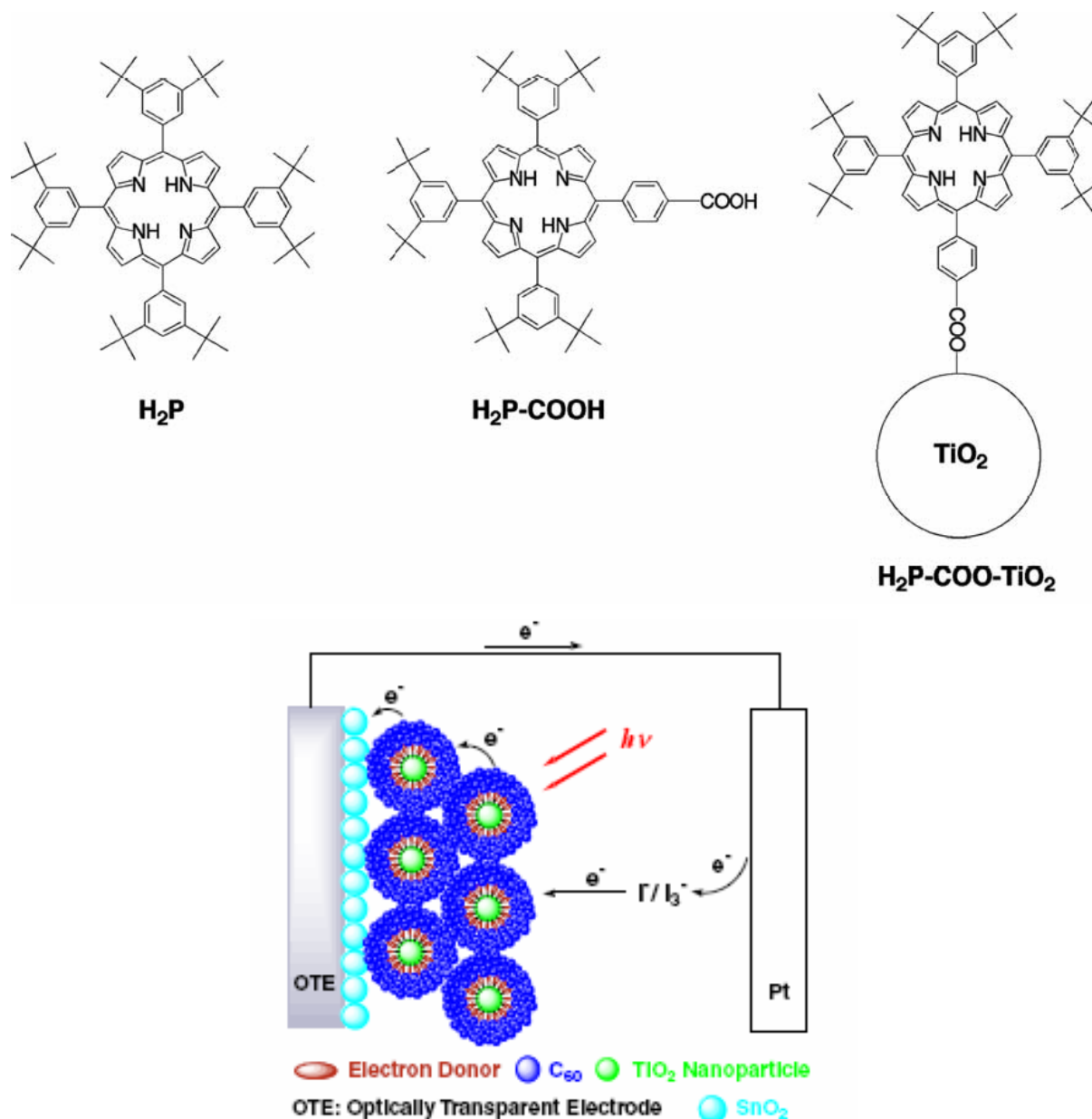


**Figure 18:** TiO<sub>2</sub> nanoparticles modified with dyes with some reference compounds employed and supramolecular assemblies of fullerene, porphyrin and fluorescein dye derivatives on TiO<sub>2</sub> nanoparticles.



Another example of organization of supramolecular assemblies of fullerene, porphyrin and fluorescein on TiO<sub>2</sub> nanoparticles developed by Fukuzumi et al.<sup>[31]</sup> is shown in figure 18. TiO<sub>2</sub> nanoparticles were modified with a porphyrin derivative and fluorescein derivatives. The dye-modified TiO<sub>2</sub> nanoparticles were deposited on nanostructured OTE/SnO<sub>2</sub> (OTE: optically transparent electrodes) together with nanoclusters of fullerene (C<sub>60</sub>) from acetonitrile/toluene (3:1, v/v) using an electrophoretic deposition technique. The dye-modified TiO<sub>2</sub> composite electrodes [OTE/SnO<sub>2</sub>/(dye + C<sub>60</sub>)<sub>n</sub>] have broad as well as high absorbance properties in the visible region, exhibiting the photo response under visible light excitation using an I<sub>3</sub>/I<sup>-</sup> redox couple. The incident photon to photocurrent efficiency (IPCE) for these electrodes increases in order: OTE/SnO<sub>2</sub>/(H<sub>2</sub>P)<sub>n</sub> < OTE/SnO<sub>2</sub>/(H<sub>2</sub>P-COO-TiO<sub>2</sub>)<sub>n</sub> < OTE/SnO<sub>2</sub>/(H<sub>2</sub>P-COO-TiO<sub>2</sub> + C<sub>60</sub>). The IPCE value can be further improved by replacing H<sub>2</sub>P-COOH with a fluorescein derivative containing an electron donor moiety.

## 1.2 DNA

### 1.2.1 The molecular structure of DNA

Carrying the hereditary information in all living cell, DNA came into the researcher's focus in the early 1950s, when its molecular structure was elucidated. In 1953, Watson and Crick proposed its structure to be a double-stranded helix.<sup>[32]</sup> DNA is built from monomeric units called nucleotides which are composed of three fragments: a sugar, a heterocycle and phosphate. The sugar deoxyribose is in the furanose form, which is connected by a  $\beta$ -glycosyl linkage with one of the four heterocyclic bases to produce the different nucleosides: adenosine, cytidine, guanosine and thymidine. In DNA, the nucleosides are linked by 3',5'-phosphodiester bonds to form a linear polymer. In the DNA duplex, hydrogen-bonded base-pairs of adenine with thymine (A-T) and guanine with cytosine (G-C) (figure 19) are stacked at 3.4 Å distance by van der Waals contact.

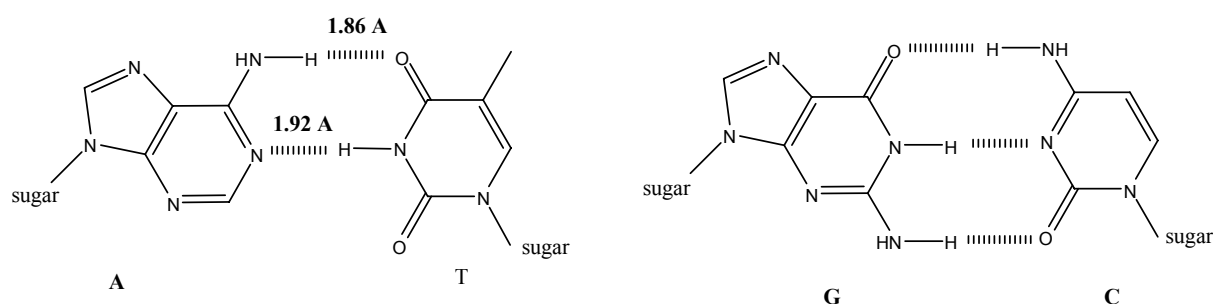


**Figure 19:** Hydrogen-bonded base-pairs.

A right-handed rotation of  $36^\circ$  between adjacent base-pairs produces a double helix of two antiparallel strands with 10.5 base-pairs per turn and 20 Å diameter. The arrangement of two strands generates two grooves with similar depth but different width along the double helix which are the major and the minor grooves (figure 20).

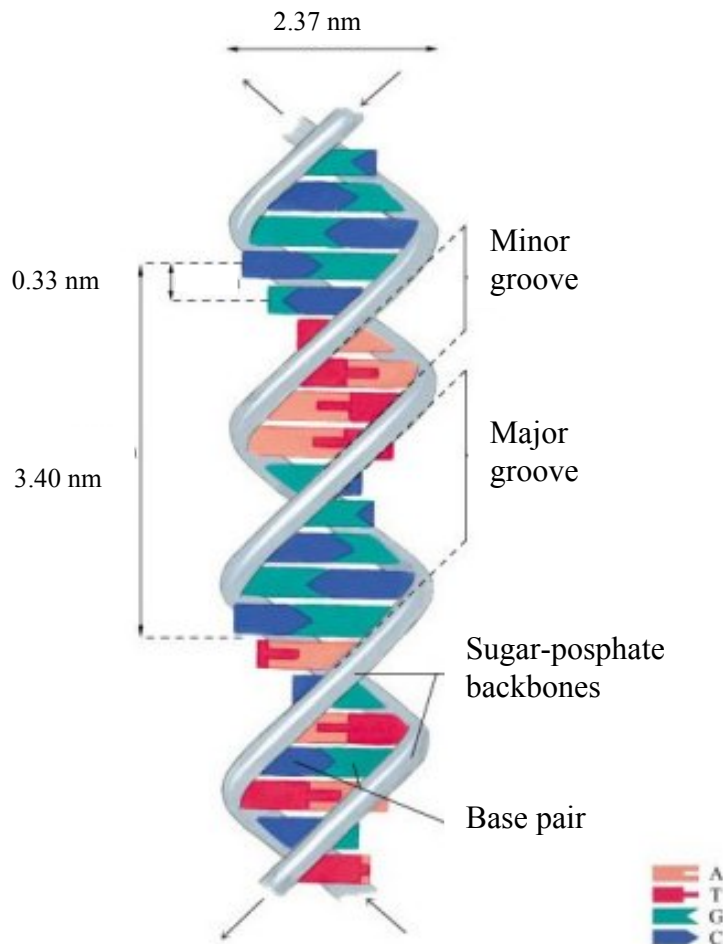


**Figure 20:** Three-dimensional structure of B-DNA.

Three DNA conformations are believed to be found in nature, A-DNA, B-DNA and Z-DNA (figure 21). The B-type described by Watson and Crick is the most commonly found in living cells. All conformations differ by their density, diameter and helical structure. An A-type helix is usually formed in RNA-RNA duplexes and RNA-DNA duplexes, whereas DNA-DNA duplexes adopt the B-type form. Depending on the sequence of the DNA and on the environmental conditions, a left-handed Z-type is formed, e.g. in GC-rich sequences under high salt concentration conditions.

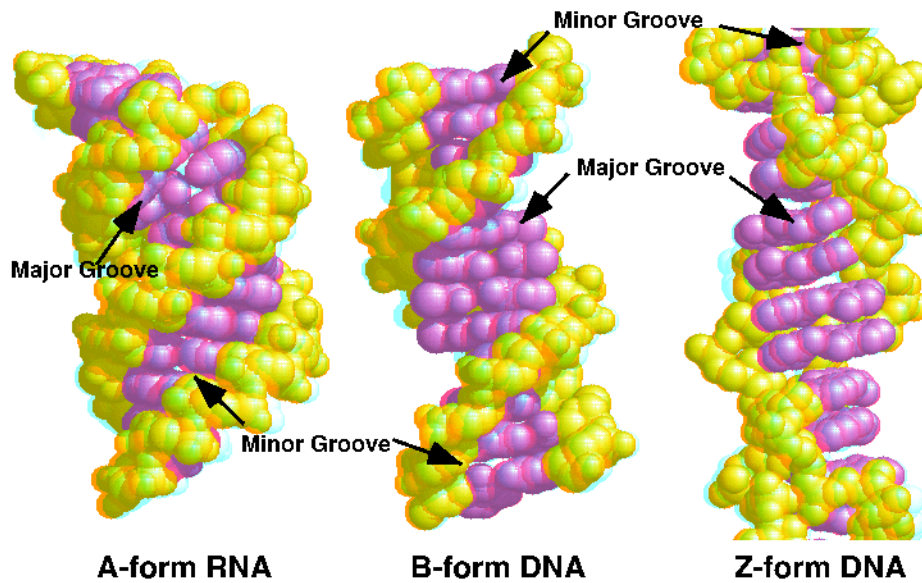


**Figure 21:** Space filling structures of A-, B-, and Z-DNA.

There are different and independent effects which may stabilize the DNA strand, depending on the environment and the sequences. The stability of the DNA double helix is due to:

- the hydrogen bonds which contribute  $15\text{-}25 \text{ kJ mol}^{-1}$  and  $25\text{-}40 \text{ kJ mol}^{-1}$  per base pair for A-T and G-C, respectively.
- the stacking of the aromatic by the partial overlap of the  $\pi$ -systems of the two neighbouring bases.
- permanent electrostatic effects, induced dipole attractions and solvophobic effects.

## 1.2.2 DNA in nanotechnology and supramolecular chemistry

DNA has recently become one of the most attractive supramolecular scaffolds to produce nanoscaled entities and shows increasing importance in nanobiotechnology,<sup>[33, 34]</sup> e.g. to specifically connect nanoparticles, to create nanomechanical devices, and to construct protein arrays and nanowires.<sup>[32, 35-37]</sup> The specific bonding of DNA base pairs can be used to direct the assembly of structured materials which leads to a new field of DNA exploitation in nanotechnology. “The nucleic-acid ‘system’ that operates in terrestrial life is optimized (through evolution) chemistry incarnate. Why not use it to allow human being to sculpt something new, perhaps beautiful, perhaps useful, certainly unnatural,” Roald Hoffmann, in *American Scientist*, 1994. Two different types of nanotechnological constructions can be used: the ‘top-down’ system, where devices are made smaller (e.g. by using lithography), and the ‘bottom-up’ construction, where atoms or molecules are used to create the desired devices (e.g. by self-assembly). Single-stranded overhangs (termed “sticky ends”) can be used to direct the intermolecular associations of different DNA molecules. Figure 22 illustrates two double-helical strands with complementary overhangs which under appropriate conditions could cohere in a sequence-specific fashion and can be ligated.

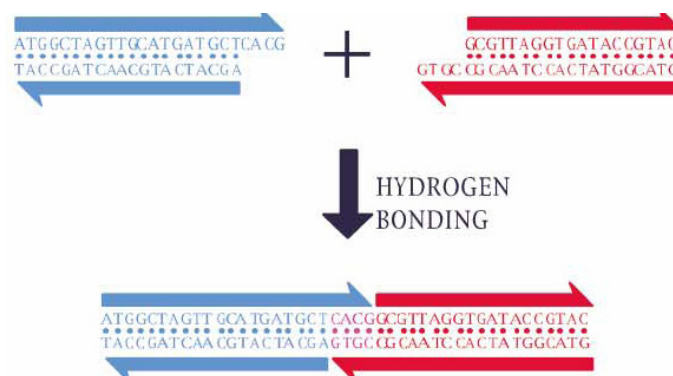


**Figure 22:** Sticky-ended cohesion.<sup>[38]</sup>

The double helix is just a line, but a ‘line’ may be curved. In biological systems, DNA branched at the level of secondary structure is found. It displays symmetry that allows its branch point to migrate. That represents a simple way to design and to assemble synthetic DNA sequences that are stable as they lack the above mentioned symmetry. The structural DNA nanotechnology combines the two concepts of stable branched DNA molecules with

sticky-ended cohesion. An example of branched sticky-ended junction assembled as a group of four units to produce a quadrilateral is shown in figure 23. The sticky ends on the outside can be extended to form a lattice in two or three dimensions by addition of further components.

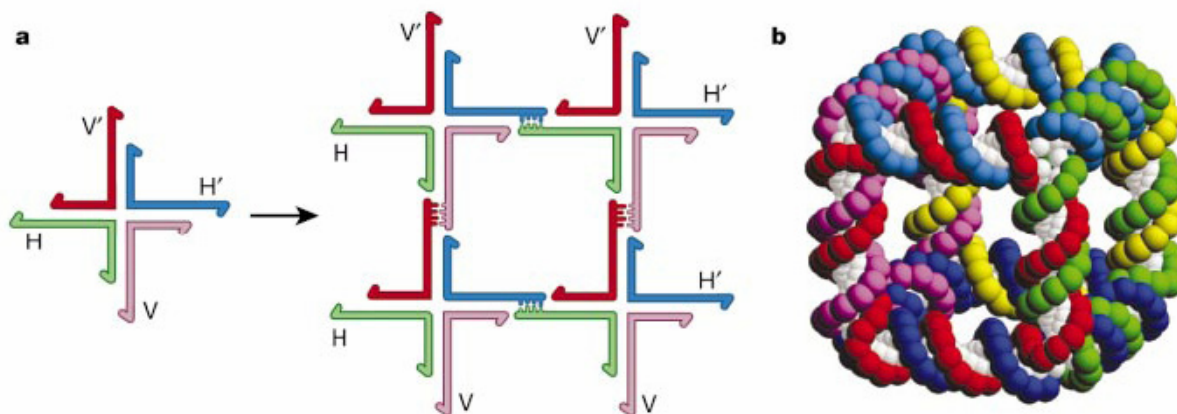


**Figure 23:** (a) Sticky-ended assembly of branched molecule, (b) A stick cube.<sup>[39]</sup>

Synthetic branched DNA molecules with programmed sticky ends self assemble into desired structures. The construction of the first artificial DNA structure was a stick-cube (Figure 23) whose edges contained two turns of the DNA double helices. The structure consists of six cyclic interlocked single strands, each linked twice to its four neighbours. Since this famous example of Seeman, more complex polyhedra and constructions have been done like Knots and Borromean rings constructed with three intricately interlinked rings.

Structurally controlled crossover DNA motifs, called “DNA tiles” have been used as building blocks for the creation of one- and multi-dimensional nanostructures. For example, a DNA nanostructure<sup>[32]</sup> self-assembles into two distinct lattice forms: nanoribbons or two-dimensional nanogrids. The 4 x 4 tile (figure 24) contains four four-arm junctions oriented with a square cavity and pointing in four directions (N, S, E, W). It is composed of nine strands where one of them is participated in all four junctions.

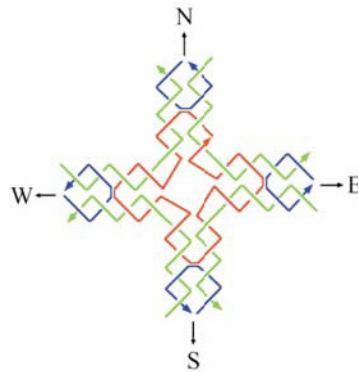


**Figure 24:** The 4 x 4 tile strand structure.

Based on this structure, other versions of the 4 x 4 tile are prepared<sup>[33]</sup>, assembled and visualised with AFM; e. g. a self-assembly of nanoribbons (figure 25). The 4 x 4 nanoribbons act, after metallization, as a scaffold for the production of highly conductive silver nanowires.

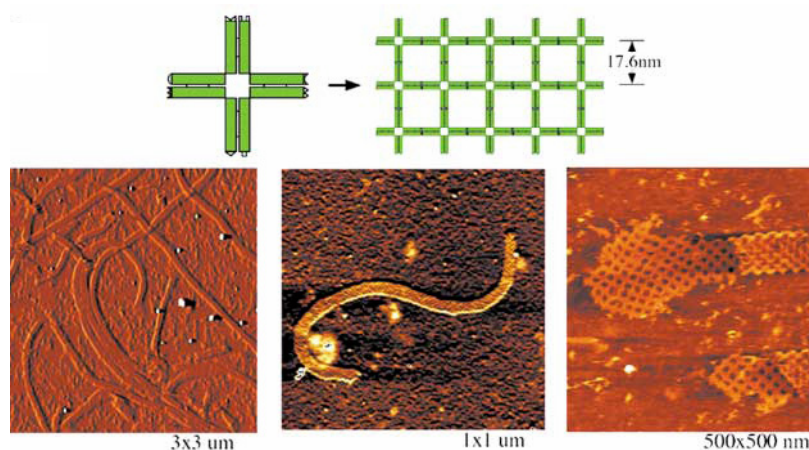


**Figure 25:** Self-assembly of nanoribbons.

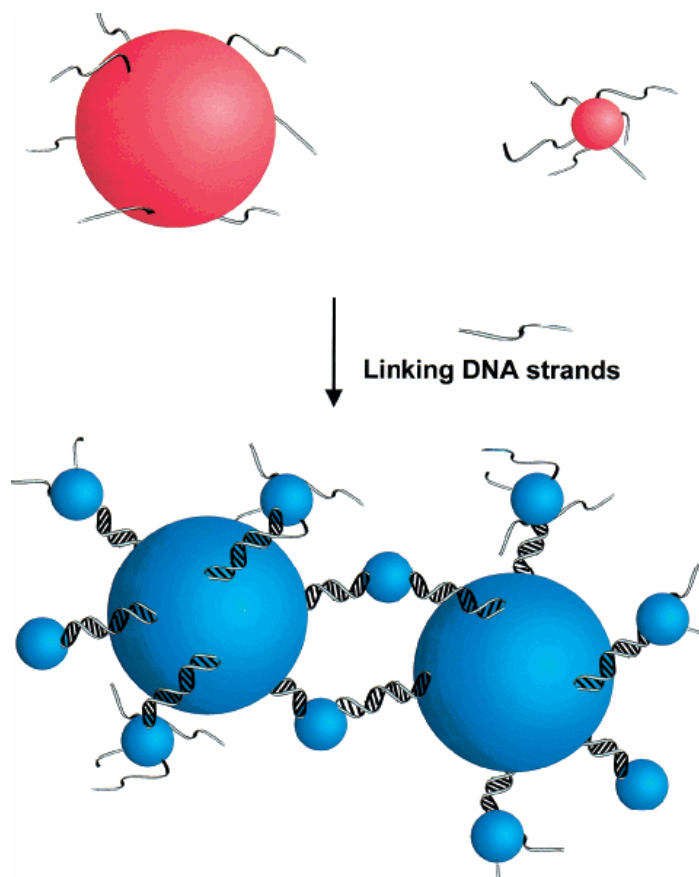


**Figure 26:** Oligonucleotides and 13-nm Au particles: DNA-induced assembly.

Recently, by utilising these crossover DNA molecules, extended structures such as DNA-nanoparticles conjugates have been created to build a variety of two and three-dimensional materials. DNA is used as a synthetically programmable assembler for nanoscale inorganic building blocks into functional materials. Both Au nanoparticles and DNA strands are mixed together, <sup>[33]</sup> and then using the molecular recognition properties associated with DNA to guide the assembly of those particles into extended structures (figure 26).



### 1.2.3 Porphyrins-DNA interactions

#### 1.2.3.1 Non-covalent interaction

The DNA-binding interactions of 5,10,15,20-tetra(*N*-methylpyridinium-4-yl) porphyrin, denoted  $H_2T_4$ , and related cationic porphyrins with DNA have long been of interest due to the potential for therapeutic applications and the novel binding interactions. The exploration of porphyrins in intracellular media is in photodynamic therapy, for targeting diseased cells or viruses. Porphyrins act as sensitizers, they absorb into the red end of the visible spectrum, at wavelengths that penetrate tissue efficiently. Cationic porphyrins, an amphiphilic molecule with good water soluble system, have a natural affinity for DNA. Fiel et al. initiated the studies and showed that cationic porphyrins like  $H_2T_4$  can bind to DNA (figure 27). In vivo, cationic porphyrins enter cells via pinocytosis and accumulate in mitochondria. Because these same cations bind to telomeric DNA, they also act as inhibitors of telomerase, an enzyme which have an important influence on tumor longevity.

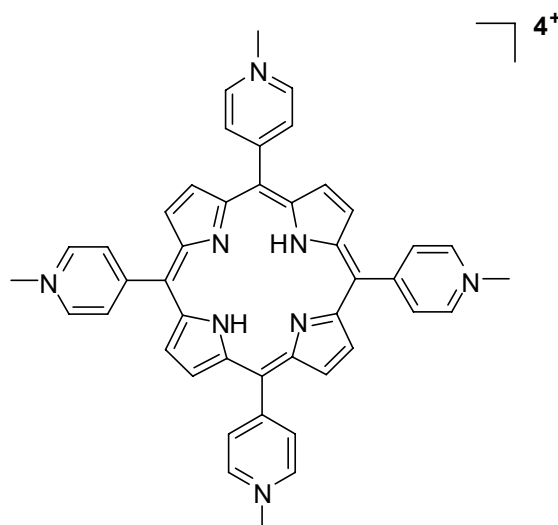


**Figure 27:**  $H_2T_4$ .<sup>[40, 41]</sup>

Depending on the nature of the DNA and the porphyrin substrate, monomeric porphyrins can bind to DNA in multiple ways. Three major binding modes have been proposed for cationic porphyrin binding to DNA: intercalation and two types of outside binding. The first type is the outside binding involving both placement of porphyrin in the minor or major groove and electronic interaction with the phosphate backbone, and the second type is the stacking of the porphyrin along the DNA helix. The binding of porphyrins

to DNA is presumably stabilized by electronic interactions between the positively charged substituents on the porphyrin periphery and the negatively charged phosphate oxygen atom of the DNA backbone. In the case of intercalation, favorable aromatic  $\pi$ - $\pi$  stacking interactions between the porphyrin macrocycle and nucleic acid bases are also involved. Coulombic interactions, van der Waals' forces, and hydrophobic effects provide for stability of the assemblies, while the pyridiniumyl substituents and axial ligands on metalated forms pose important steric constraints. Competitive binding studies involving DNA hairpin substrates reveal that the base composition, not the sequence, dictates the mode of binding. DNA sequences which are rich in guanine-cytosine (G=C) base pairs support intercalative binding. Spectroscopic consequences in the Soret region include a strong bathochromic shift ( $\Delta\lambda \geq 15$  nm), marked hypochromism ( $H \geq 35\%$ ), and an induced circular dichroic (CD) signal with a negative amplitude due to the transferred chirality of the DNA onto the porphyrin. In contrast, DNA sequences that are rich in adenine-thymine (A=T) base pairs support external binding, in which case the Soret band undergoes a smaller bathochromic shift ( $\Delta\lambda \leq 8$  nm), shows weaker hypochromism ( $H \leq 10\%$ ), and gives an induced CD signal with the opposite sign.

### 1.2.3.2 Covalent DNA-porphyrin conjugates

To study the structure and the dynamics of nucleic acids, the use of molecular probes has attracted widespread attention. There are four known ways in which small molecules can bind DNA: intercalation, groove binding, electrostatic binding and capping. Unlike the first three non-covalent binding modes, the latter mode not only specifies the binding mode and the position of the molecule, but can stabilize the oligonucleotide through the  $\pi$ - $\pi$  stacking interactions of the adjacent terminal base pairs. Capping is carried out by covalently linking a small molecule to the end of the DNA strand and is base pair specific. Berova *et al.*<sup>[42-45]</sup> worked on porphyrin-based molecular caps and explored the effect of capping on DNA structures.

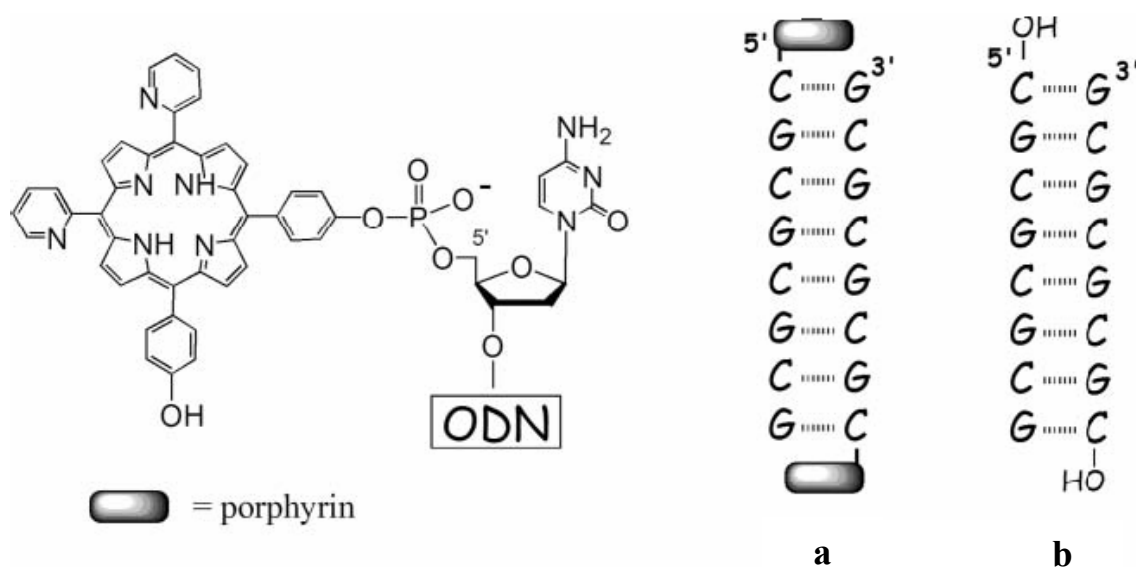


**Figure 28:** Tetraarylporphyrin attached to the cytosine *via* phosphate linker.<sup>[45]</sup>

A non-charged hydrophilic tetraarylporphyrin is attached to the 5' end of the self complementary oligonucleotide (ODN) where the porphyrin is coupled to the cytosine *via* phosphate linker (figure 28). By using CG sequences which are known to form stable Z-form structure at high salt concentration, they explored the possibility of following the B- to Z-DNA transition and to study the effect of a bulky porphyrin on the salt-induced B- to Z-DNA transition. The porphyrin chromophore allows the simultaneous detection of the B- to Z-DNA transition *via* the porphyrin Soret band circular dichroism exciton couplet signal around 420 nm and the oligonucleotide CD region below 300 nm (figure 29), at micromolar concentrations.

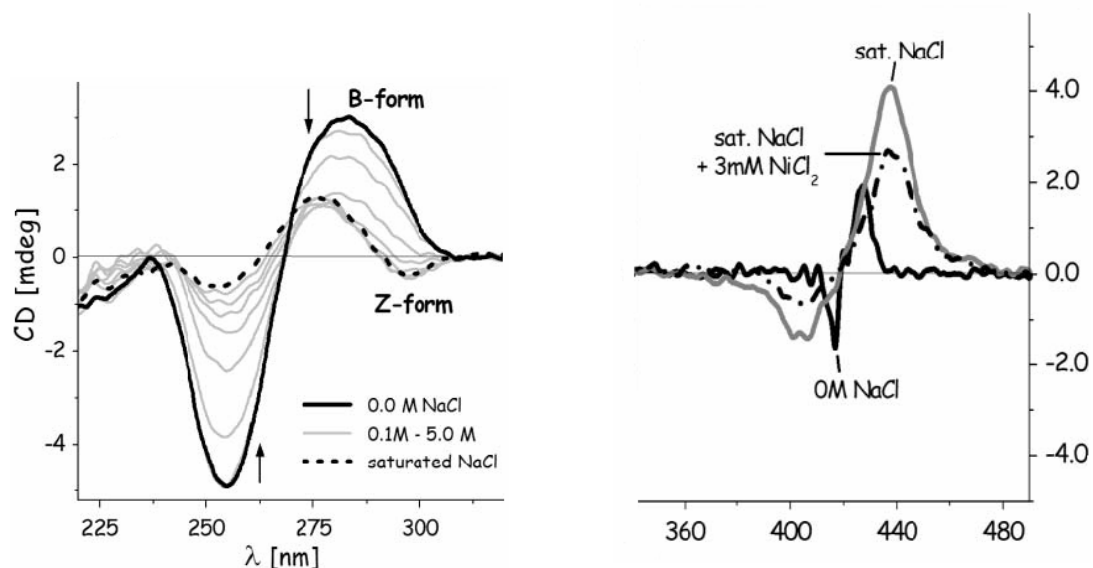


**Figure 29:** CD spectra of  $\sim 10 \mu\text{M}$  porphyrin-ODN **a** in 50 mM potassium phosphate buffer, (pH = 7.0 at different NaCl concentrations). On the left, the arrows show increasing amount of sodium chloride. On the right black line, with 0.0 M NaCl; grey line, with saturated NaCl; black dash-dotted line, with saturated NaCl and 3 mM nickel(II) chloride .

Below 300 nm increasing amounts of salt induced a dramatic change in the CD spectrum which is a consequence of the conformational change from right-handed B-DNA to left-handed Z-DNA. Without NaCl, the duplex **a** exists in the B-DNA conformation, while in saturated NaCl solution it exists predominantly, but not completely, in the Z-DNA form. In addition, an exciton coupled CD can be observed in the porphyrin Soret band absorption region (around 420 nm) in **a**. Figure 30 shows how the Soret region of the CD spectrum of 8-mer **a** sensitively reflects the change from B-DNA to Z-DNA.

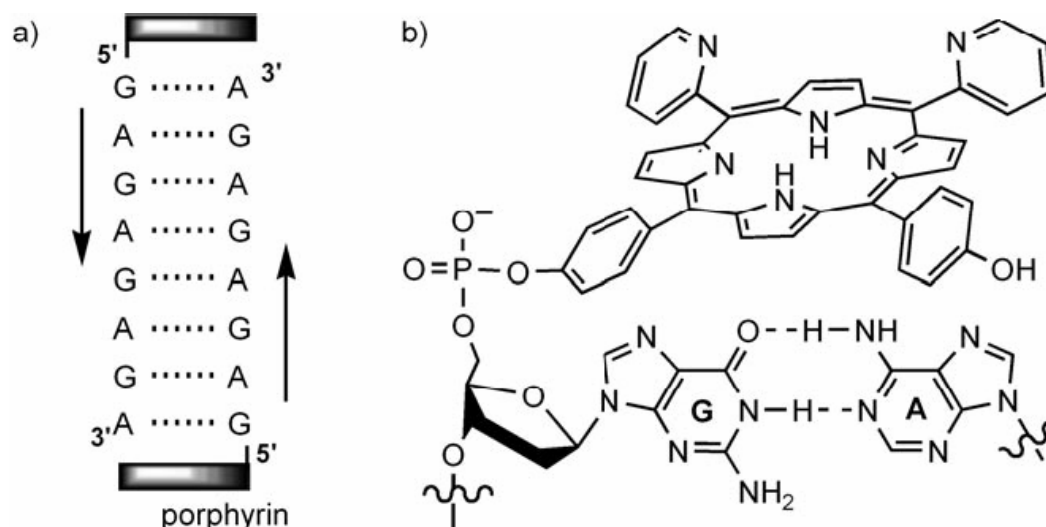


**Figure 30:** a) Schematic representation of the antiparallel duplex 1P with porphyrins serving as molecular caps. b) Diagram demonstrating the overlap of the porphyrin with a guanine–adenine base pair.<sup>[42]</sup>

Another example of an oligonucleotide duplex with noncanonical Watson-Crick guanine-adenine (G-A) base pairs by covalently linked terminal porphyrins, is shown in figure 30. Berova and coworkers attached the same neutral hydrophilic tetraarylporphyrin to the 5' position of the 5'-GAGAGAGA-3' strand through a short and flexible phosphate linker. The CD of the porphyrin-d(GA)<sub>4</sub> **a** shows a spectrum which is characteristic of a highly ordered structure with A-like features. Such characteristic CD spectrum is directly associated with an organized secondary structure in which the bases are close enough to interact with each other. Spectroscopic studies show the porphyrin-induced stabilization of the non-self-complementary DNA sequence. Depending on environmental factors, Guanine–adenine repeat strands (d(GA)<sub>n</sub>) self-associate into parallel- and antiparallel stranded homoduplexes, but the porphyrin end-capping induces a highly ordered antiparallel duplex structure which is in contrast with the uncapping ODN.

DNA provides an ideal supramolecular scaffold for assembling porphyrins in defined structures<sup>[46, 47]</sup> which are capable of self-assembly given an appropriate connectivity to a specific nucleobase. Thus Endo and Majima have synthesized a tetraphenylporphyrin-based DNA-porphyrin conjugate with linkages between each *meso*-phenyl porphyrin group and the central phosphorus atom of a 10-mer strand of DNA. The spacing of the 10 bases in a 10-mer corresponds to one helical turn. They used a thiolate tether through a phosphoramidite linkage which reacted with a maleimide-substituted porphyrin to give two synthetic oligonucleotides: CGGCT $p$ ACTCC and GTGCT $p$ AGCGG, where  $p$  denotes the position of the tetraphenylporphyrin linked to the phosphoramidite. Those DNA-porphyrin strands were then mixed with four equivalents of complementary 20-mer non-porphyrinic strands. They obtained a double-helical complex with two DNA-porphyrin strands linked to four complementary strands (figure 31).

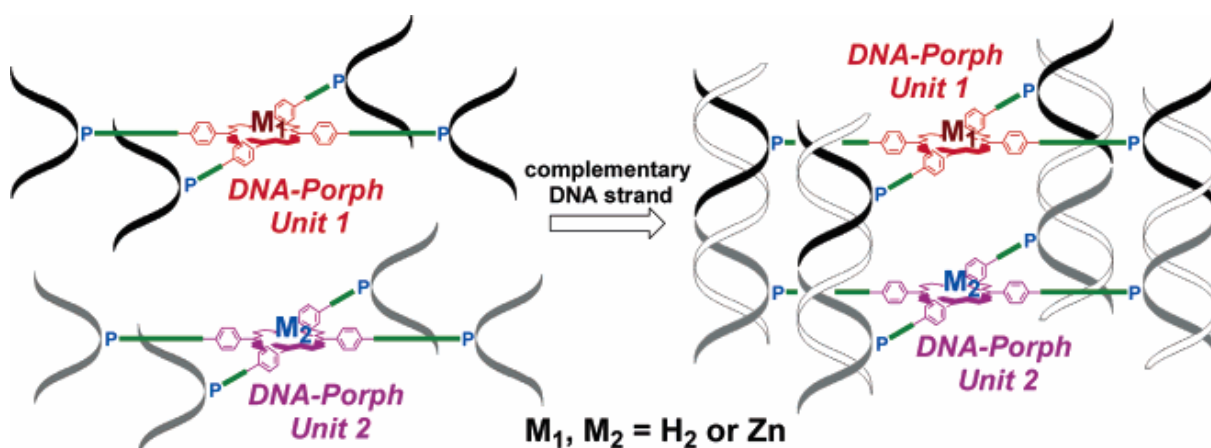


**Figure 31:** Four-DNA double-helix assembled structure containing two porphyrin derivatives.

Two different porphyrins such as a free base (H<sub>2</sub>-Porph) and a Zn-porphyrin (Zn-Porph) that show different photochemical properties were incorporated into the DNA structure. The four double-helix assembled DNA structures containing the heterogeneous porphyrin dimer were constructed, and the arrangements of these porphyrins were programmed by the sequence of the complementary strand. Fluorescent lifetimes of the systems indicated a singlet transfer between the freebase and the zinc porphyrins within the one complex, which proves the possible incorporation of multiple and different porphyrin chromophores into DNA structures by using the appropriate sequence programming of the DNA strands.

## 1.3 Project

### 1.3.1 Research

The aims of this project is to explore the use of DNA as a supramolecular template to connect specific electrochemically and photophysically active molecules, namely porphyrins, and place the units in a predetermined orientation *via* formation of the double stranded helix of DNA. This new arrangement, which can be termed DNA Architectonics, is designed to function as a scaffold to create a multifunctional molecule on the nanometre scale. Nucleotides will be substituted with different porphyrins, which are promising candidates for a variety of different applications due to their central metal binding site, their relative ease of functionalisation, and their physicochemical properties. The porphyrin units will be connected through the backbone of the DNA (Scheme 3), which is independent of the porphyrin structure. The changes in the porphyrin structure should not alter the base pairing abilities of the DNA and the capacity to form helical superstructures to provide the spatial arrangement. The reason is that the modification at the 5-position of thymine will point outwards of the DNA, and the porphyrin will be located in the major groove.

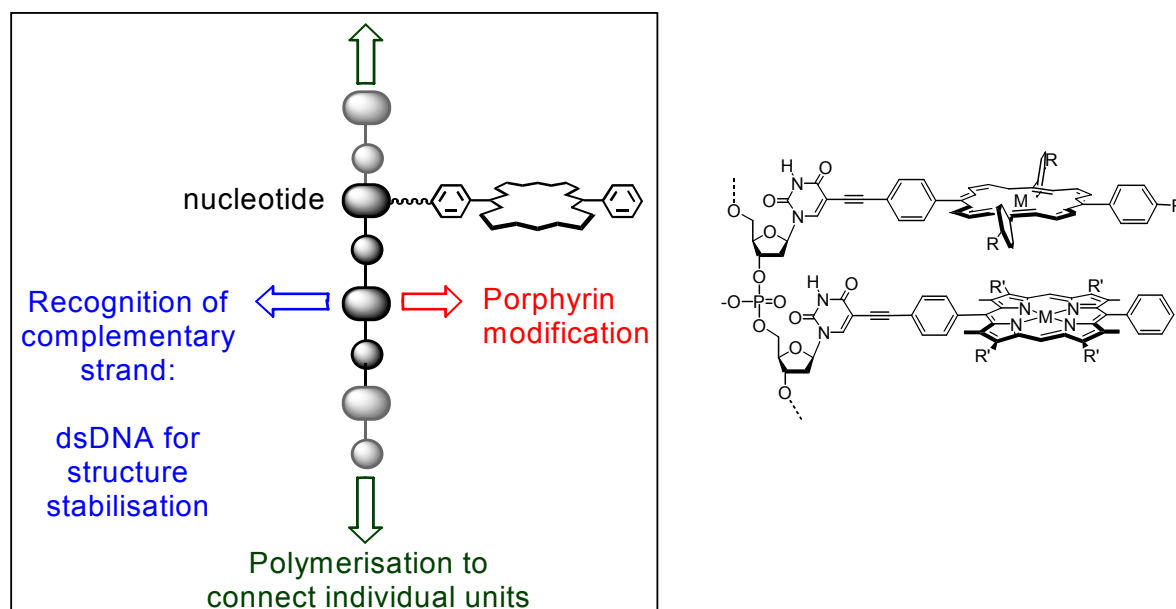


**Figure 32:** Schematic representation of the DNA-as-scaffold concept.

The order of the individual units is programmable *via* the DNA sequence; changing the sequence allows shuffling of the units without the need to redesign the building blocks. There seems to be virtually no limitation in the diversity of incorporated porphyrins, because one specific nucleobase can be substituted with variable porphyrins. The relative distance of the porphyrins can be varied easily by introducing natural nucleotides without porphyrin substituents between the modified nucleobases which is a good compromise to prevent porphyrins stacking, and allows alteration of the electronic interactions between the porphyrins. The tertiary structure of dsDNA (e.g. A, B, Z helix, see chapter 1) is highly dependent on the experimental conditions (pH, ionic strength, solvent, base sequence) allowing changes in the spatial arrangement to be made while maintaining the porphyrin structure and sequence.

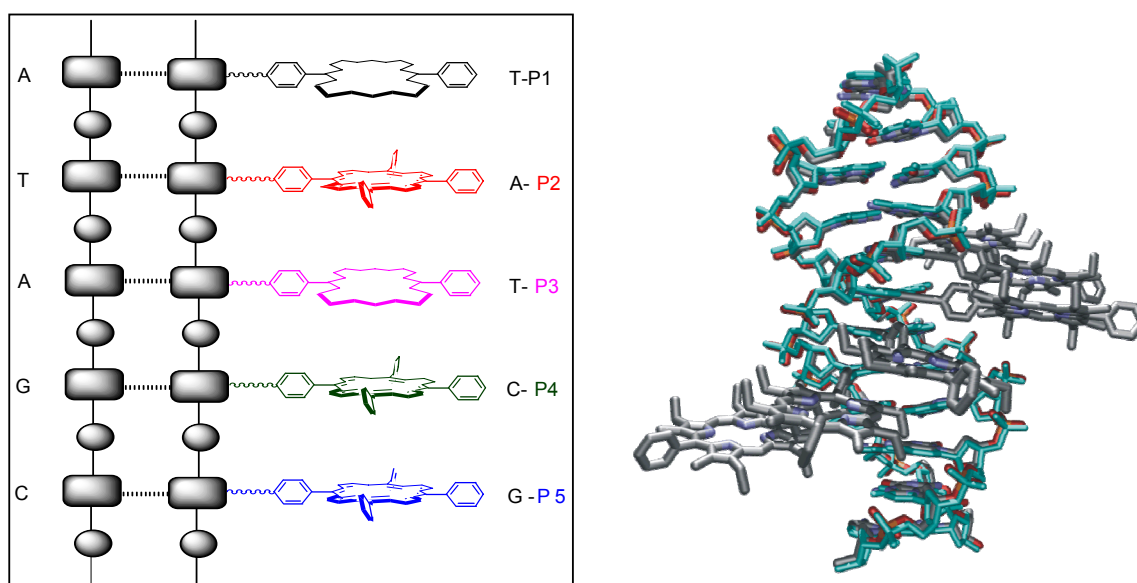


**Figure 33:** Schematic representation of the modified duplexes and superposition of the calculated structures of DNA and porphyrin-DNA.

To date, procedures where porphyrins have been coupled to the nucleobase and successfully been incorporated into DNA according to our proposed route, have not been reported; meaning that this project is unique in its design.

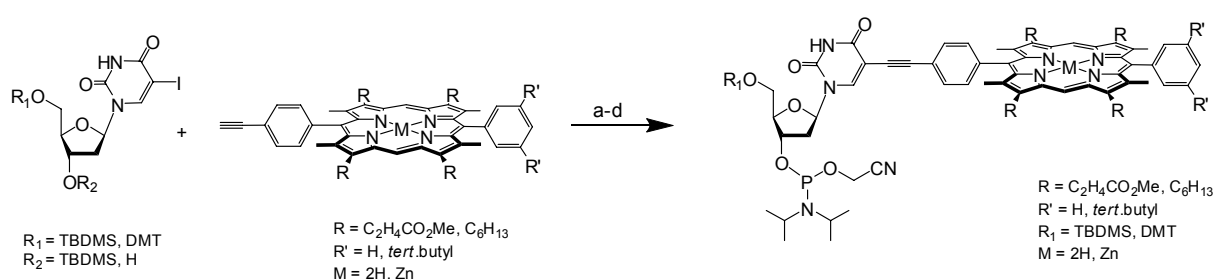
Pyrimidine-5-substituents and 7-deazapurine-7-substituents are known to be located in the major groove of dsDNA and do not destabilise the double helical structure. Chromophores for FRET analysis,<sup>[48, 49]</sup> functional groups derived from amino acid sidechains<sup>[50-53]</sup> and



4d-transition metal complexes<sup>[54-56]</sup> were successfully incorporated into DNA, using solid phase synthesis or enzymatic synthesis (PCR).<sup>[57, 58]</sup> These studies indicate that the proposed project is feasible, provided that the following requirements, which are crucial for success, are fulfilled.<sup>[54]</sup> Several aspects of the obtained porphyrinyl-DNA will be studied: electrochemical and photophysical properties, energy and/or electron transfer within the individual porphyrin units, mass spectrometry, solubility and structure of the porphyrinyl-DNA in organic solvents, and possibly other DNA-ligand interactions in the presence of the porphyrins.

### 1.3.2 Plan of the synthetic route

In order to demonstrate the concepts feasibility, several steps (Scheme 3) of the project have to be established: (i) the synthesis of the porphyrin with the appropriate substituents, (ii) protection the nucleoside, which is here the 5-iodouracile, with the right protecting group, (iii) synthesis of the porphyrin substituted nucleotides *via* Sonogashira coupling, and conversion to the phosphoramidite building blocks, (iv) and finally incorporation of the building blocks into DNA starting from small oligomers to longer oligomers with different structures and number of porphyrins.



a) Pd(OAc)<sub>2</sub>, PPh<sub>3</sub>, NEt<sub>3</sub>, CuI; b) NaOH, py; c) DMTr-Cl; py; d) CEP-Cl, iPr<sub>2</sub>NEt

**Scheme 3:** Synthesis of the building blocks.

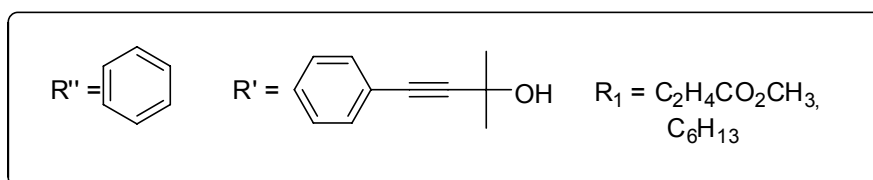


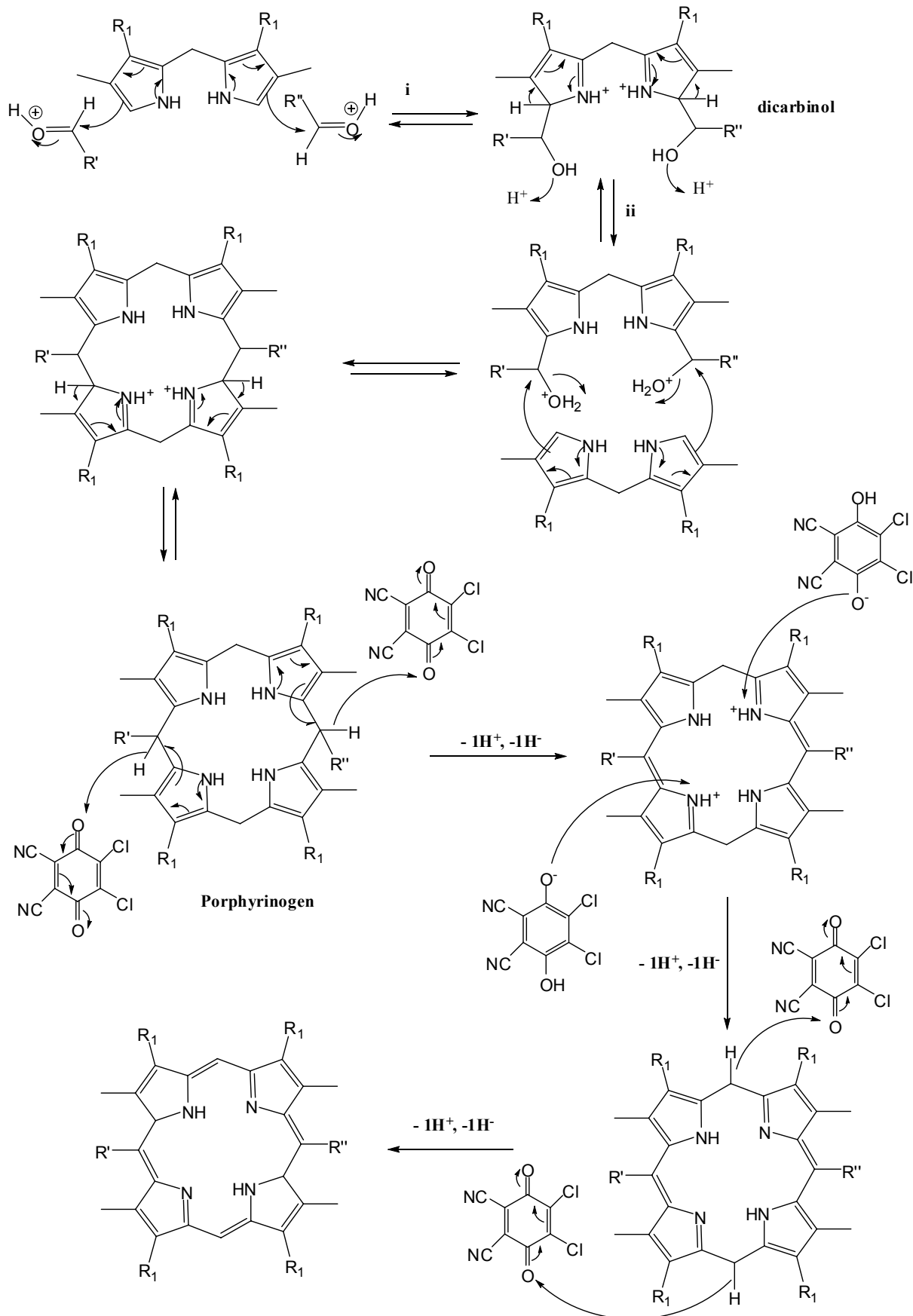
## 2 Syntheses

### 2.1 Porphyrin synthesis

#### 2.1.1 Methodology

The method used in this work allows the synthesis of porphyrins bearing different meso substituents. The dipyrromethane provides the starting point for each porphyrin. The desired porphyrin has been prepared by statistical reaction of a dipyrromethane and two different aldehydes. In each case, the resulting three porphyrins are then separated chromatographically. The synthesis starts with the deprotection of the carboxylic acid by hydrogenolysis followed by decarboxylation in acidic condition (scheme 4). The individual steps i and ii were not concerted. The dipyrromethane was first condensed with two different aldehydes to give the dicarbinol which condensed with a second dipyrromethane to give the porphyrinogen. Finally, a quinone (DDQ) is added to oxidize the porphyrinogen to the porphyrin in yield of ~10%. The low yield can be explained by the polymerisation of the tetrapyrrole intermediate formed during the reaction, which results in black polymeric side products.





**Scheme 4:** Mechanism of the porphyrin synthesis.

### 2.1.2 Synthetic route

Four structurally different diphenyl porphyrins as target compounds were chosen, which have one alkynyl phenyl substituent for the attachment to the uracil base.<sup>[59, 60]</sup> One porphyrin, the diphenyl porphyrin **22**, is bearing ester side chains, which can be hydrolysed to render the porphyrins soluble in water. The two other porphyrins **24** and **25** have alkyl chains, thus ensuring good solubility in organic solvents. The porphyrin **23** has a phosphonate group on the phenyl substituent. The phosphonic acid, obtained after deprotection, could be attached to oxide surfaces such as  $\text{TiO}_2$ .<sup>[61]</sup>

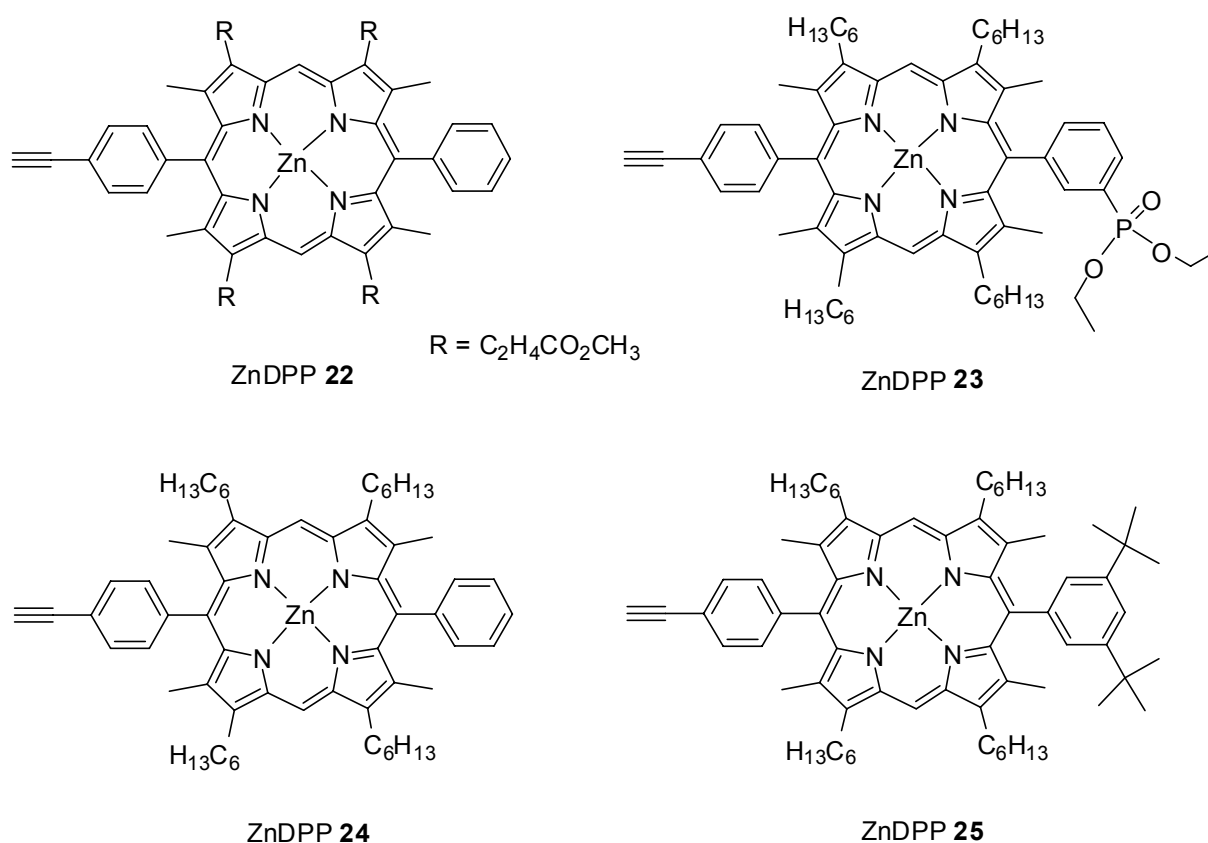
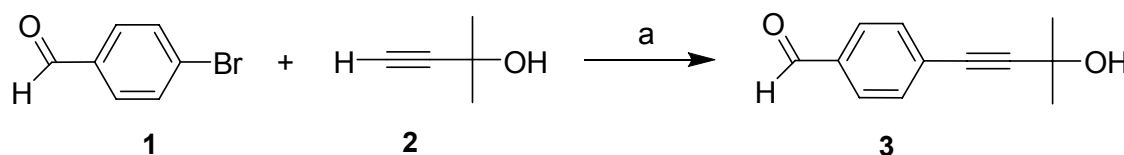


**Figure 34:** The four structurally different diphenyl porphyrins **22-25**.

### 2.1.2.1 Porphyrin components

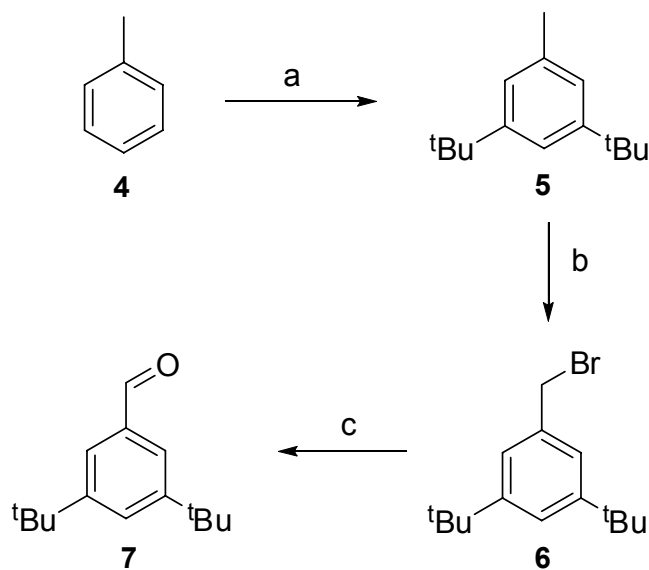
For the different porphyrins syntheses, several compounds as starting material were required. To introduce an alkynyl phenyl substituent on the porphyrin, we synthesised the 4-(3-hydroxy-3-methylbut-1-ynyl)benzaldehyde **3**.<sup>[62]</sup> The ethynyl moiety is protected with propan-2-ol for the porphyrin synthesis; this protecting group introduces a polarity in the porphyrin structure which leads to a better purification. Then, it will be removed after the porphyrin synthesis under basic conditions. Normally the most common protecting group, used for the porphyrin synthesis, is the TMS group. But in our case, the TMS group will have the same *r<sub>f</sub>*-value on the TLC plate as the tert-butyl group, and the unsymmetrical porphyrin won't be isolated from the two other symmetric ones.



(a)  $\text{K}_2\text{CO}_3$ , CuI,  $\text{PPh}_3$ , Pd/C 10%, DME/ $\text{H}_2\text{O}$ , 87%.

**Scheme 5:** The synthesis of 4-(3-hydroxy-3-methylbut-1-ynyl)benzaldehyde **3**.

The cross-coupling of *p*-bromobenzaldehyde to 2-methyl-3-butyn-2-ol was achieved in the presence of a catalytic amount of palladium on activated charcoal, copper(I) iodide, triphenylphosphine and potassium carbonate. The reaction mixture was refluxed at 80°C for 16h and the coupled product was obtained as yellow oil with good yield 87% after column chromatography.

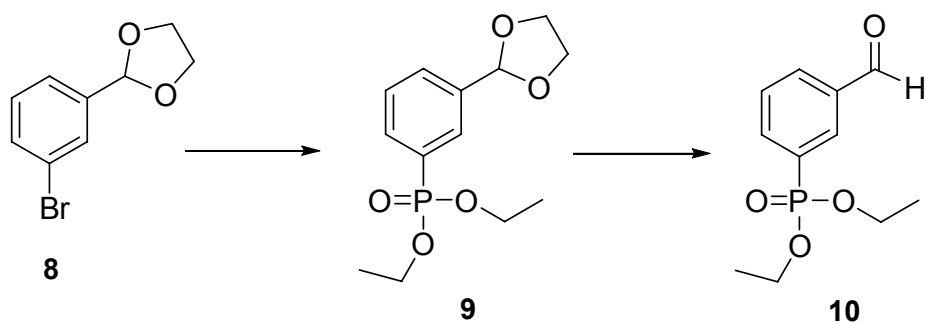


(a)  $\text{ClC}(\text{CH}_3)_3$ ,  $\text{AlCl}_3$ , toluene; (b) NBS,  $(\text{PhCO})_2\text{O}_2$ ,  $\text{CCl}_4$ ; (c)  $(\text{CH}_2)_6\text{N}_4$ , c.HCl 37%, MeOH/ $\text{H}_2\text{O}$ .

**Scheme 6:** Synthesis of 3',5'-di-tert-butylbenzaldehyde 7.

The 3,5-di-*tert*-butyltoluene was prepared by Friedel–Crafts *tert*-butylation reaction of toluene using *tert*-butyl chloride in the presence of aluminium chloride as catalyst.<sup>[63-65]</sup> Aluminium trichloride (4%) was added in portions over a period of 8h, to a rapidly stirred solution of toluene and 3',5'-di-*tert*-butyl chloride. This is an interesting reaction since the methyl group activates the *ortho* and *para* sites of toluene. The isolation of the *meta* functionalised product indicates the reversibility of the reaction and that the di-*tert*-butylation of the *meta* isomer is presumably slower than that of the first formed *ortho* or *para* isomers. After distillation, the obtained 3,5-di-*tert*-butyltoluene was brominated using N-bromosuccinimide and AIBN, to afford the bromomethyl derivative. 3,5-Di-*tert*-butylbenzaldehyde was prepared from 3,5-di-*tert*-butyl(bromomethyl)benzene by oxidation with hexamethylenetetramine.

The synthesis of the phosphonate derivate **10** is shown in scheme 7.<sup>[66]</sup>



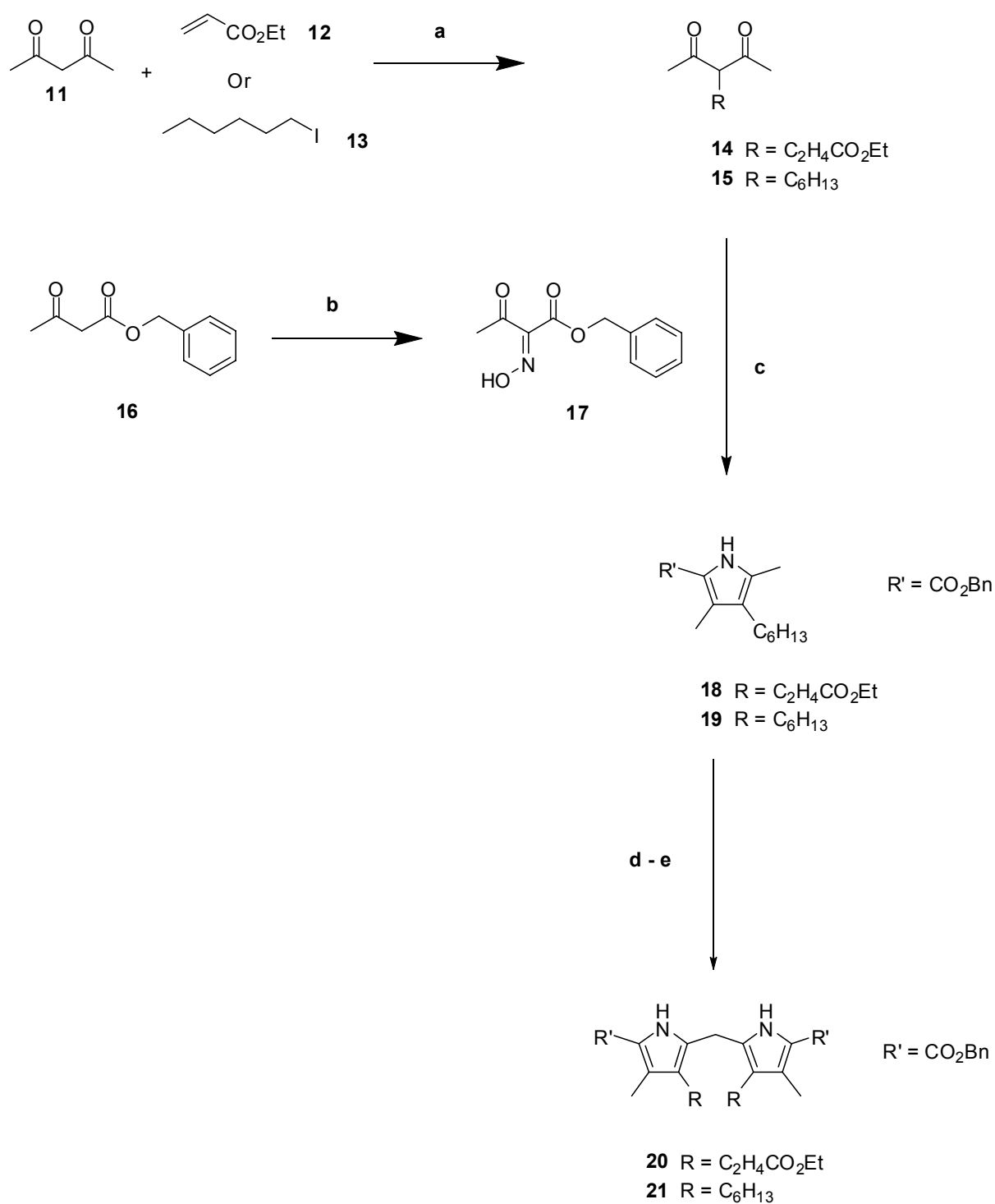
(a)  $(\text{EtO})_2\text{PHO}$ ,  $\text{Net}_3$ ,  $\text{Pd}(\text{PPh}_3)_4$ ,  $95^\circ\text{C}$ , 36h, 10%; (b) 15%  $\text{H}_2\text{SO}_4$  on silica, 24h, RT., 54%.

**Scheme 7:** diethyl (3-carbonylphenyl)phosphonate synthesis **10**.

The commercially available 2-(3-bromophenyl)-1,3-dioxolane, which provided an ideal starting material, was reacted with diethylphosphonate using palladium as catalyst in a standard Arbusov reaction. Then the aldehyde was unmasked under acidic conditions to give the phosphonate derivate **10**.



Two different dipyrromethane were synthesised<sup>[64, 67, 68]</sup> as it is shown in scheme 8.



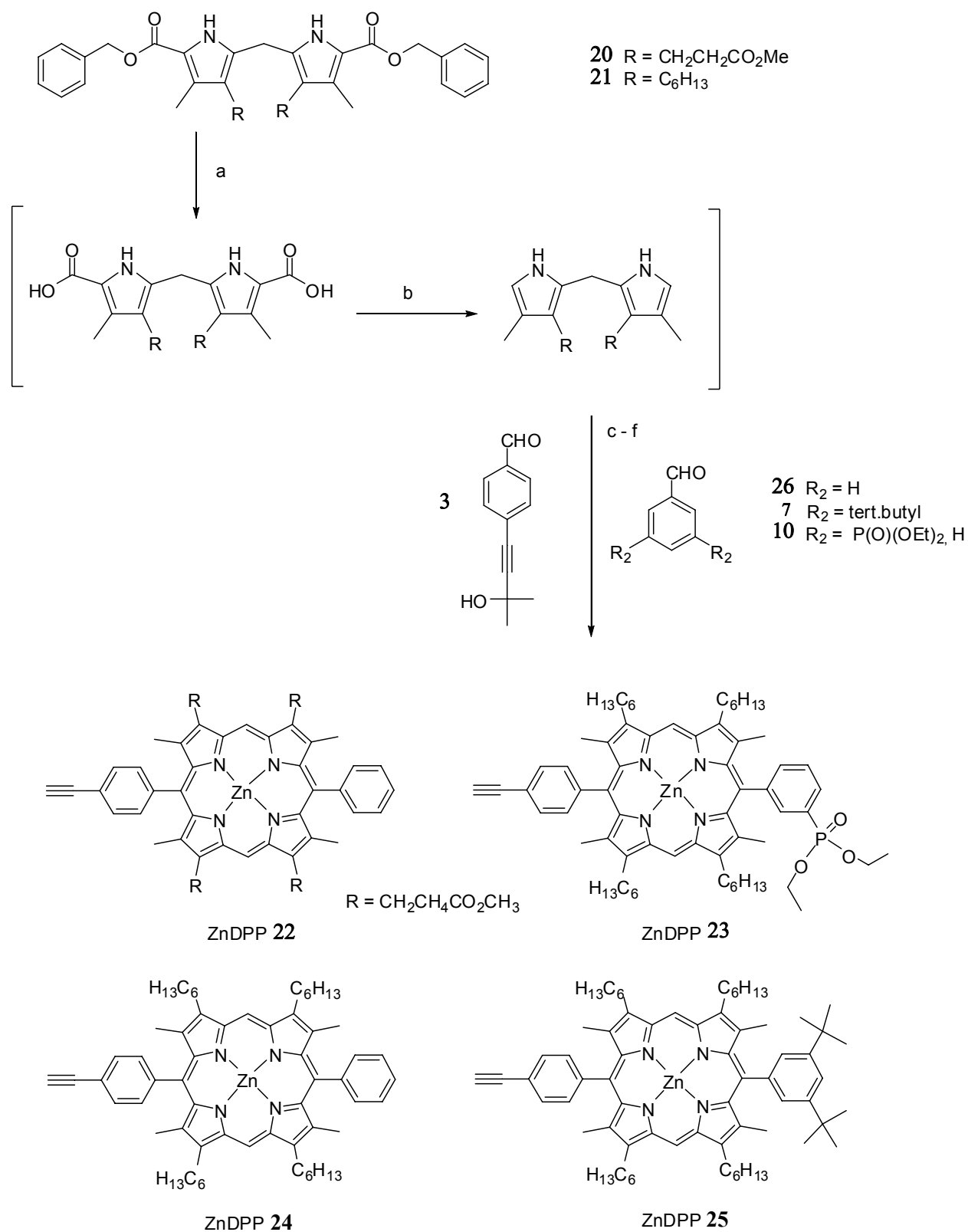
(a) Na, EtOH; (b) NaNO<sub>2</sub>, H<sub>2</sub>O/HOAc; (c) Zn, HOAc; (d) PbOAc<sub>4</sub>, HOAc; (e) HCl, MeOH.

**Scheme 8:** The synthesis of two different Dipyrromethane **20** and **21**.

1-iodohexane and 2, 4-pentadione were treated with potassium carbonate in acetone, to give the 3-hexyl-2,4-diketone **15** which could be isolated by distillation. This 3-hexyl-2,4-diketone **15** was then reacted with the oxime **17** and Zinc in acetic acid to give the hexyl substituted pyrrol **19**. The oxime **17** was readily synthesised from benzoyl acetoacetate by treatment with sodium nitrite in water.  $\alpha$ -Acetylation of the hexyl-derived pyrrole was achieved by treatment with Lead acetate in acetic acid. Dimerisation of this acetylated pyrrole was done by refluxing the compound in hydrochloric acid and methanol to obtain dipyrromethane **21**. According to the same procedure, we obtained the dipyrromethane **20** <sup>[69, 70]</sup> by using the acryl acid ester **12** instead of 1-iodohexane **13**.

### 2.1.2.2 Porphyrin synthesis

The Zinc metallated porphyrins ZnDPP (**22-25**) <sup>[67, 71]</sup> were obtained from the two different dipyrromethane (**20, 21**), the benzaldehyde derivate (**26, 7, 10**) and the alkynyl benzaldehyde **3**. Generally, 2 equivalents of the appropriate dipyrromethane (**20** or **21**), 1 equivalent of alkynyl benzaldehyde **3**, and 1 equivalent of the appropriate benzaldehyde derivate (**26** or **7** or **10**) were used. But the use of 1.5 equivalents of the protected alkynyl benzaldehyde<sup>[62]</sup> **3** increased the yield of the desired porphyrin. The yield of the porphyrin synthesis is increased by using a 3',5'-di-tert-butyl-phenyl side group instead of the benzaldehyde.



(a) H<sub>2</sub>, Pd-C, 2h; (b) TFA, 1.5h; (c) MeOH, 2h; (d) DDQ, overnight; (e) NaOMe, toluene, 125°C, 5h; (f) Zn (OAc)<sub>2</sub>·2H<sub>2</sub>O, CHCl<sub>3</sub>/MeOH.

**Scheme 9:** Synthesis of the different diphenyl porphyrins **22-25**.

The ZnDPP **22** was synthesised from the corresponding hexyl-derivatised substituted pyrrole **20**, the synthesis is shown in Scheme 9. Removal of the benzoyl protecting group from dipyrromethane **20** by hydrogenolysis gave the bis  $\alpha$ -acid. The decarboxylation of the dipyrromethane was carried out by treatment with concentrated TFA, giving the  $\alpha$ -deprotected but unstable dipyrromethane, which was used immediately without further purification.

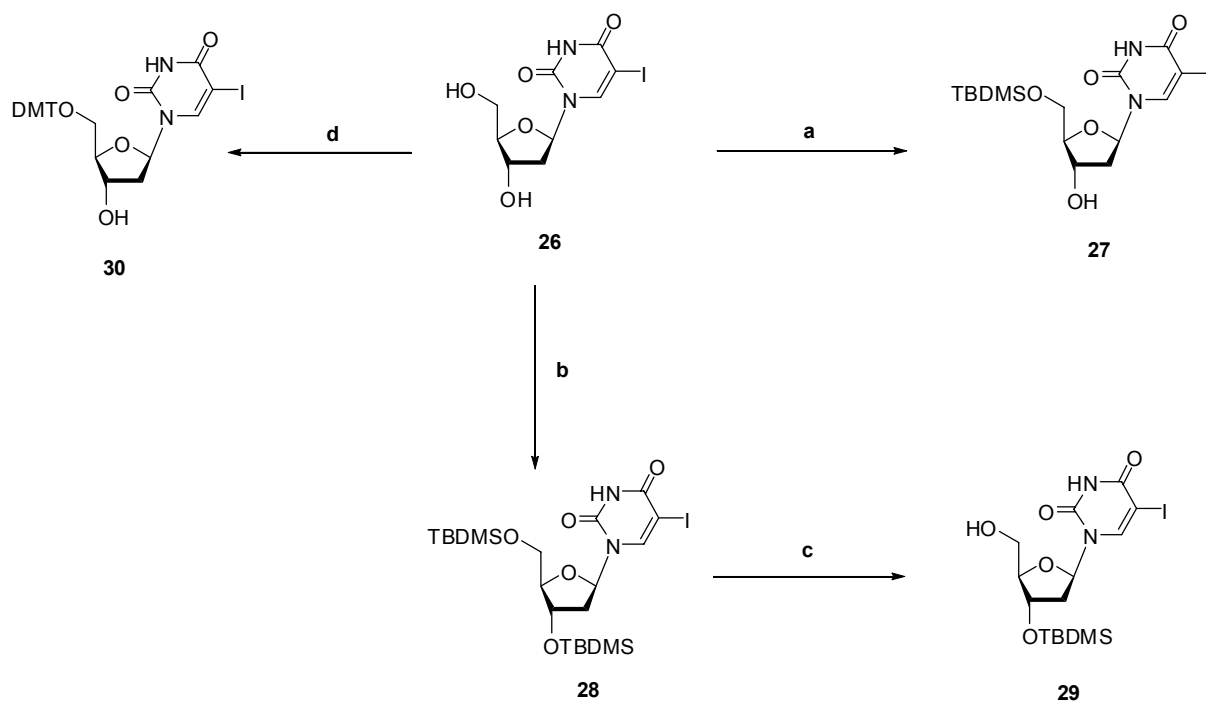
The unsymmetrical porphyrin **22** was one of three possible products and was synthesised *via* a statistical procedure (the other two products being the symmetrical di-phenyl and the symmetrical di-protected ethynyl porphyrins). The reaction sequence began with an acid catalysed condensation of two equivalents of the  $\alpha$ -free dipyrromethane **20**, with one equivalent of the benzaldehyde **26**, and 1.5 equivalent of protected alkynyl benzaldehyde **3**. Subsequent DDQ oxidation of the ensuing porphyrinogen gave a statistical mixture of symmetrical and unsymmetrical porphyrins. In each case, the unsymmetrical porphyrin was one of the three possible products. The desired porphyrin **22** could then be isolated, after several column chromatographies on silica gel. The deprotection of the acetylene group with sodium methoxide, and the final metalation with zinc acetate gave the acetylene Zinc porphyrin complex ZnDPP(AcO)<sub>2</sub>. The DDP **22** was obtained in 4% yield when the ester chain was not hydrolysed by the sodium methoxyde.

According to the same procedure, the DDP **24** was synthesised from 2 equivalents of dipyrromethane **21**, one equivalent of the benzaldehyde **26**, and 1.5 equivalent of protected alkynyl benzaldehyde **3**. We obtained the DDP **24** in low yield 5%, but when we used the *tert*-butylbenzaldehyde **7** instead of the benzaldehyde **26**, we increased the yield of the DDP **25** to 8%.

The DPP **23** was obtained using the same procedure from 2 equivalents of dipyrromethane **21**, one equivalent of the phosphonate benzaldehyde **10**, and 1.5 equivalent of protected alkynyl benzaldehyde **3** in good yield (9%).

## 2.2 Nucleotide Synthesis

Thymidine and its demethylated derivative 2'-deoxy-uracile represent the ideal nucleobase for this study. In contrast to the other bases, it does not require the use of protecting groups. The 5'-Iodo-uracil is commercially available. Selective TBDMS and DMT protections of the deoxyribose for the 5'- or 3'- positions were used for the ribose as shown in scheme 10.<sup>[72-74]</sup> First, we chose the TBDMS protecting group to protect the 5' or 3' position for possible further dimerisation of the porphyrin-nucleoside in solution. The synthesis of 5'-TBDMS-dU **27** was carried out by selective protection of the 5' position. The protection was achieved with 1.5 equivalent of TBDMS-OTf and Imidazole in DMF for 1 hour at 0°C followed by an additional hour at ambient temperature. To obtain the 3'-TBDMS-dU **29**, we protected the 5'- and the 3'- position of the 5-Iodo-Uracil with 2 equivalents of TBDMS-OTf in presence of two equivalents of Imidazole in dry DMF, and doubled reaction time to four hours. In both reactions, the products were obtained in high yields after usual workup and recrystallisation in CHCl<sub>3</sub>-Hexane. The doubly protected 3',5'-di-TBDMS-dU **28** can be deprotected selectively at the 5'- position with acetic acid in H<sub>2</sub>O/THF mixture at 40°C for three days.



(a) 1.5 eq TBDMS-OTf, 1.5 eq Imidazole, DMF, 1h 0°C, 1h rt, 22 %; (b) 2 eq TBDMS-OTf, 2 eq Imidazole, DMF, 2h 0°C, 2h rt, 90 %; (c) AcOH, H<sub>2</sub>O-THF 1:1, 3d at 40°C, 36 %, (d) DMTr-Cl, TEA, 24 h at rt, 63 %.

**Scheme 10:** Selective protection of 5-Iodo-Uracil.

Then, we chose the DMT-protection to be compatible with DNA synthesis. This protecting group reacts selectively with the 5'-OH and is easily removed by acidic treatment. The nucleoside was stirred with 1.3 equivalent of dimethoxytrityl chloride in dry pyridine overnight, followed by a hydrogenocarbonate treatment to avoid a significant amount of detritylation. We obtained the 5'-O-protected Iodo-uracil **30** in good yield.

The same strategy for the protection deprotection can also be applied to the porphyrin-nucleoside but we obtained lower yield. The protection of the nucleobase before the coupling reaction gave higher yields compared to the protection of the porphyrin-nucleoside.

We found that TBDMS or DMT-protection of the hydroxyl groups on the sugar moiety did not affect the efficiency of the coupling, thus we used pre-protected 5-I-dU for the coupling with the alkynyl porphyrin.

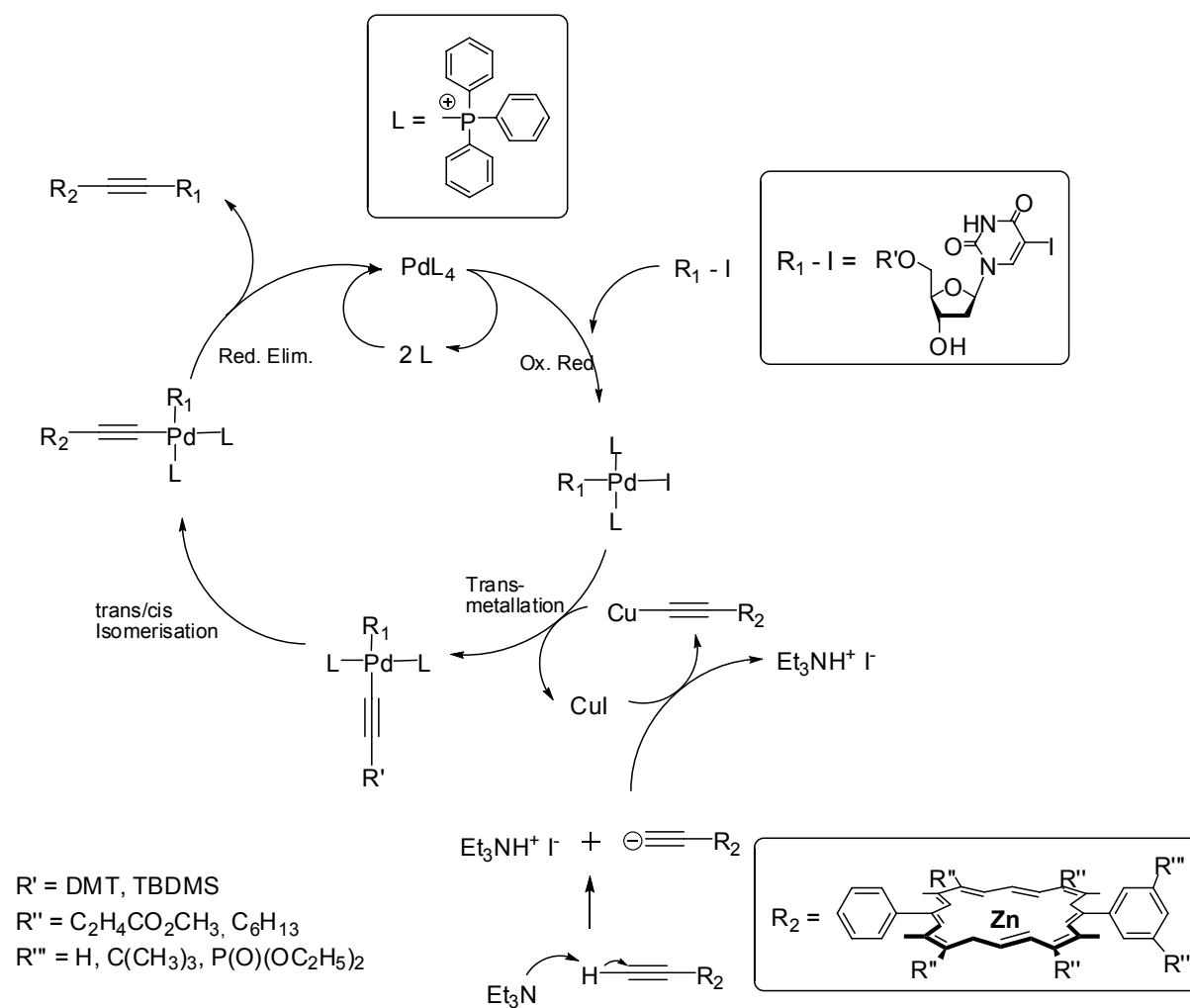
## 2.3 Synthesis of the Porphyrin Building Blocks

### 2.3.1 Methodology

Using a Sonogashira coupling<sup>[51, 55]</sup> with acetylene porphyrins (**22-25**) and 2'-deoxyuridine (**27, 29, 30**) lead to the desired building blocks. To demonstrate the possible diversity, several different structural porphyrins (chapter 2.1.5) can be incorporated into DNA in solution or using solid support by phosphoramidite chemistry.

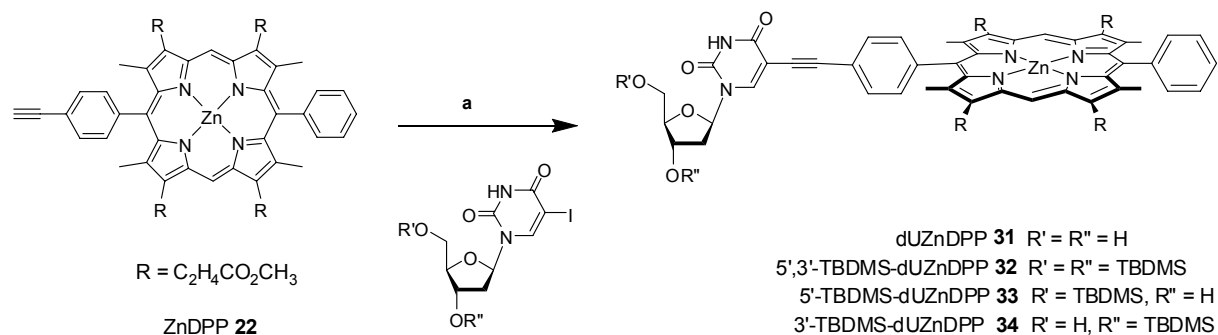
### 2.3.2 Results

The coupling of the porphyrin to the nucleobase to obtain the building blocks **31** to **38** was performed using Sonogashira coupling by adapting a published procedure.



**Scheme 11:** Sonogashira coupling mechanism.

The coupling, between the 5-Iodo-uracile and the porphyrin acetylene groups was achieved using tetrakis(triphenylphosphine)palladium (0) as catalyst and iodide copper (I) as co-catalyst. Triethylamine was used as a base to deprotonate the acetylene group.



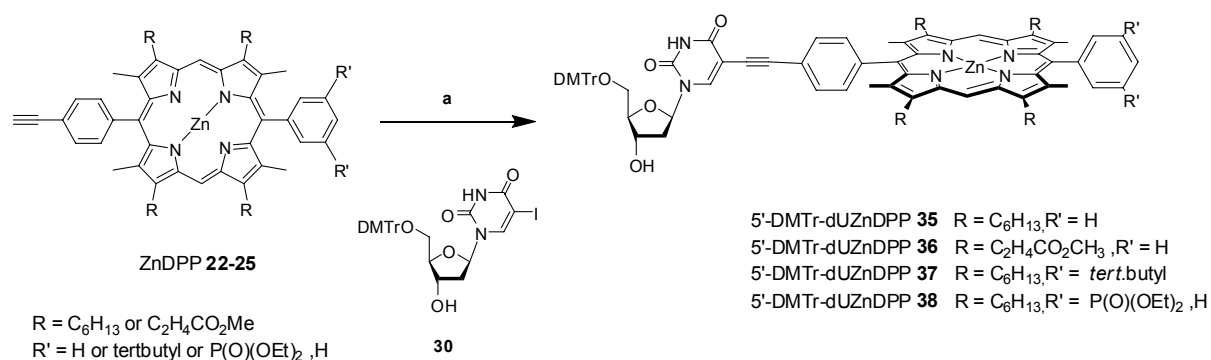
(a)  $Pd(PPh_3)_4, CuI, NEt_3, DMF, rt, 24h.$

**Scheme 12:** Synthesis of the diphenyl porphyrin substituted TBDMS nucleosides.

Using 3 equivalents of the nucleoside, and increasing the quantity of palladium catalyst to 40% with respect to the nucleoside, increased the yield substantially. The coupling reaction was monitored by TLC, and products were identified by MALDI-TOF MS analysis and NMR spectroscopy. The reaction time varied from two to four days, and we obtained the porphyrin-nucleoside (**31-38**) with 30%-98% yield.

With TBDMS protection, the impurities from the residual catalyst were not always removed by purification on silica gel and recrystallisation. For the products **33** and **34**, we needed a final purification on Lipophilic Sephadex LH20 using  $CH_2Cl_2/MeOH$  1:1 as eluent to give pure material, which can be proved by  $^1H$  NMR spectroscopy. The impurities, detected by a multiplet at 7 ppm, disappeared. Then, we could use these building blocks **33** and **34** to synthesise the dimer in solution via phosphoramidite chemistry, as it is shown in scheme **15**.





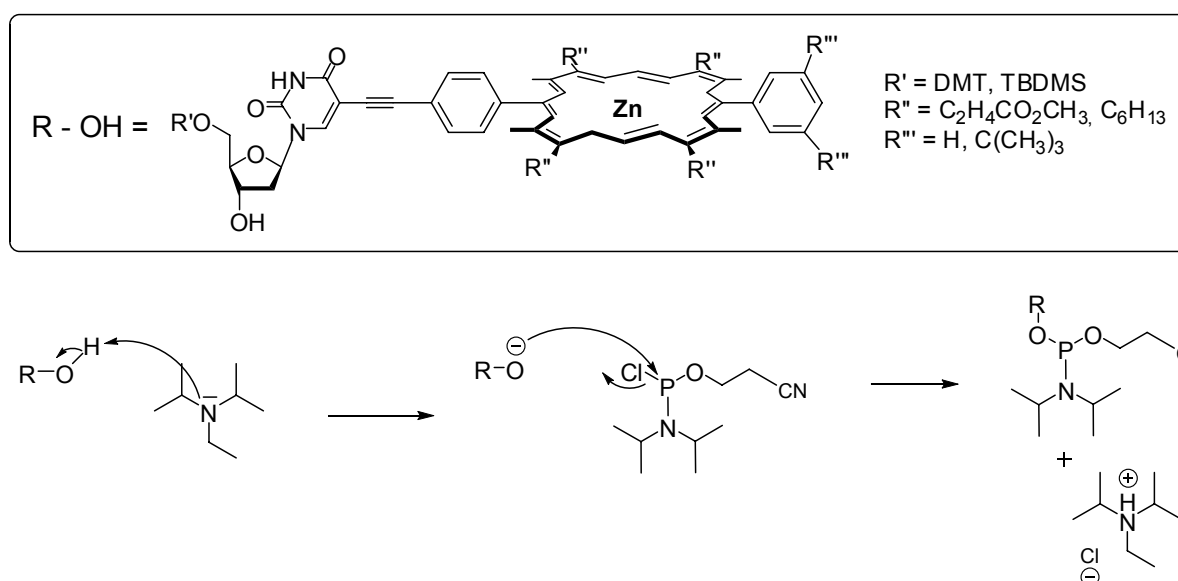
(a) Pd(PPh<sub>3</sub>)<sub>4</sub>, CuI, NEt<sub>3</sub>, DMF, rt, 24h, 43-98%.

### Scheme 13: Synthesis of the diphenyl porphyrin substituted DMT nucleosides.

With the DMT-protection, purification on silica gel and recrystallisation gave the pure product **35-38**, which will further be used to synthesis modified DNA on solid support (chapter 4). We obtained the building block with alkyl chain **35** and **37** in good yield (97-98%) compared to the one with ester chain **36**, where the coupling yield achieved was only 43%.

## 2.4 Synthesis of the Phosphoramidite Building Blocks

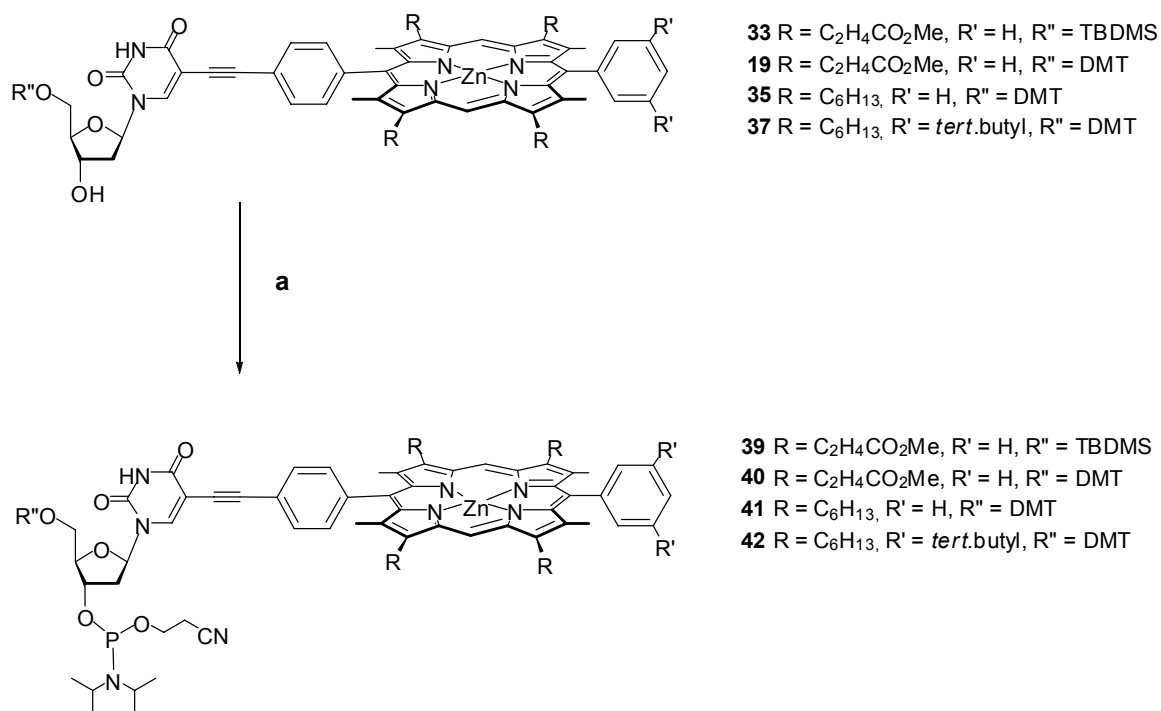
### 2.4.1 Methodology



Scheme 14: Mechanism of the phosphoramidite synthesis.

The alcohol group is activated by the DIEA base; the thus obtained nucleophile attacks the CEP-Cl phosphate followed by chloride elimination and ammonium chloride formation. The phosphoramidite obtained is very sensitive to oxygen; and readily forms the inactive phosphine oxide.

## 2.4.2 Results



(a) N(C<sub>3</sub>H<sub>6</sub>)<sub>3</sub>, CEP-Cl, CH<sub>2</sub>Cl<sub>2</sub>, 2h30, 70-98%.

### Scheme 15: Phosphoramidite synthesis.

Due to the phosphine sensitivity, inert atmosphere techniques were applied during all the phosphoramidite manipulation; i.e. synthesis, purification and utilisation.

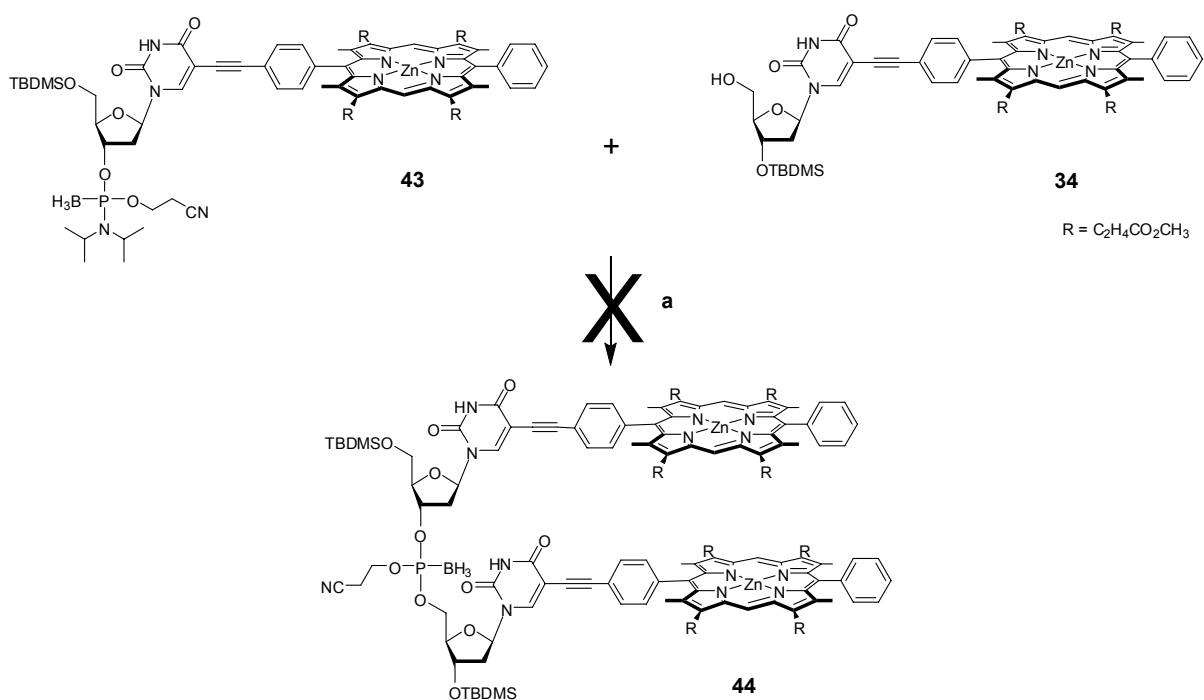
The porphyrin-substituted nucleotides (**19**, **33**, **35**, and **37**) were converted to the phosphoramidite (**39-42**) by treatment with CEP-Chloride and DIEA. The conversion into the phosphoramidite could be achieved up to 98% yield. The phosphoramidite was characterized by NMR (<sup>31</sup>P) which shows a peak at 145.5 ppm.

### 3 Porphyrin-Substituted Dinucleotides

The next step of the project was the dinucleotide synthesis with two porphyrin building blocks. The building blocks were dimerised to the corresponding homo- and hetero-porphyrin dinucleotides. The synthesis was performed in solution and/or on solid phase in order to compare the reactivity of the phosphoramidite building blocks under both conditions. We then studied the formation of duplexes with the complementary diadenosine using spectroscopy methods.

#### 3.1 Modified Dinucleotides Synthesis

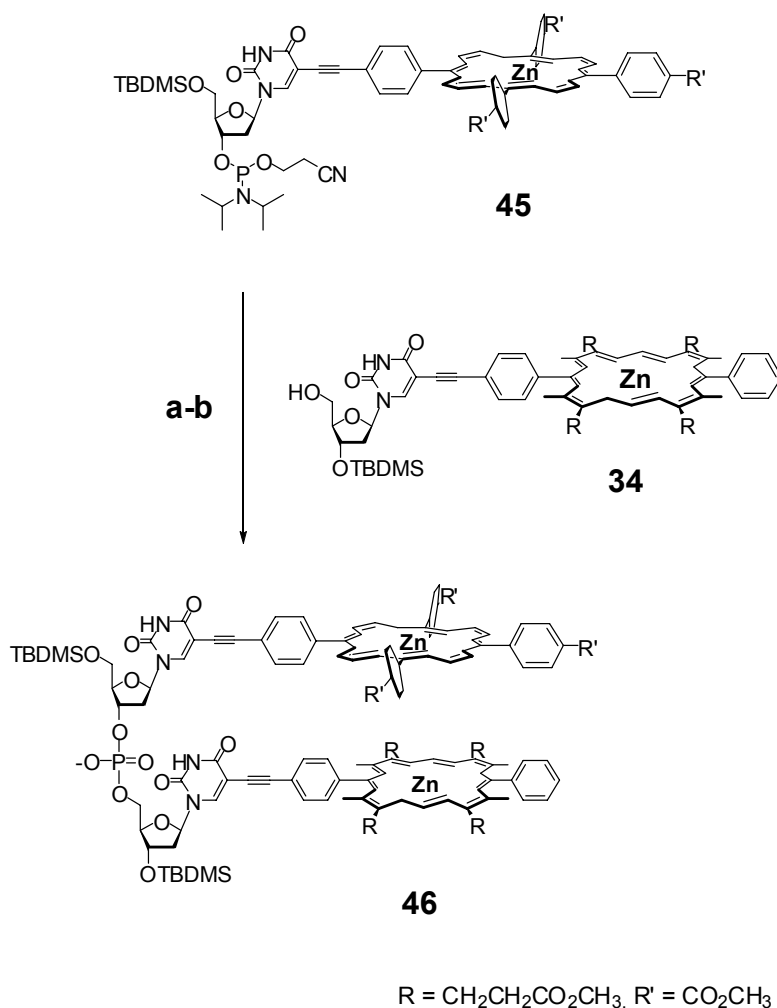
##### 3.1.1 Dimerisation in solution



(a) 1H-tetrazole, DCM, 2h.

**Scheme 16:** Synthesis of the dimer **44** in solution.

The 5'-TBDMS protected phosphoramidite building block was obtained using the standard phosphorylation procedure described in chapter 2.4. We found that our phosphoramidite building block is more sensitive to oxidation, compared to a sole phosphoramidite nucleobase, due to the presence of the porphyrin as a photosensitiser.<sup>[75]</sup> In the presence of both light and oxygen, the phosphoramidite is rapidly converted to the inactive phosphate. We therefore investigated the use of borane as protecting group. After the formation of the phosphoramidite **39**, 3.5 equivalents of borane were added for in-situ protection. The reaction mixture was stirred overnight under inert atmosphere and in the dark. A chromatography column under argon with ethyl acetate gave the desired product **43** in good yield (63%) and was characterised by NMR spectroscopy and Maldi-TOF spectrometry. The borane, acting as a Lewis acid, formed a dative bond with phosphorus to prevent the phosphine oxidation. The building block **43** was dissolved in CH<sub>2</sub>Cl<sub>2</sub> and transferred *via* Teflon canula into a CH<sub>2</sub>Cl<sub>2</sub> solution of the corresponding ZnDPP substituted porphyrinyl deoxyuridine **34**. This solution contained 5 equivalents of 1H-Tetrazole as activating agent for the coupling reaction. The desired dimer **44** was not formed, and we suppose that in this case the dative bond was too strong and was not cleaved during the process, thus preventing activation and coupling to occur. Then, the dimer synthesis was performed using a different activating agent and two different building blocks.



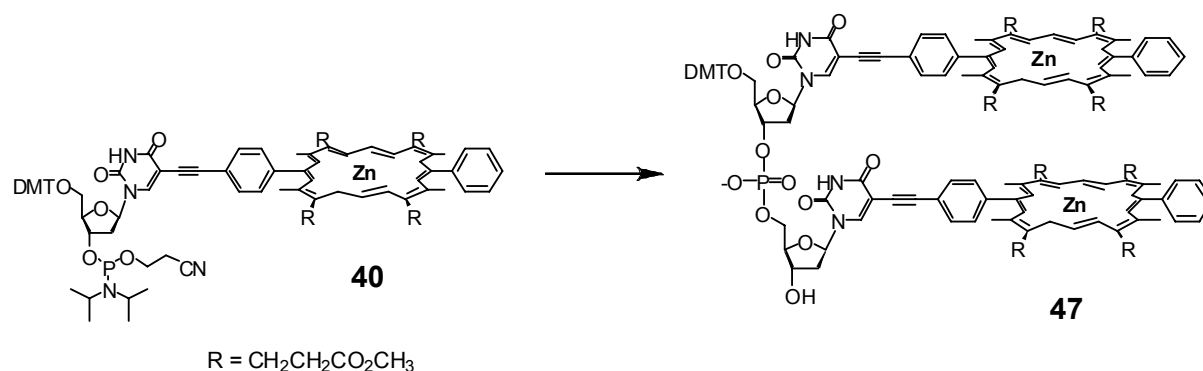
(a) *N*-(phenyl)imidazolium triflate, DCM, 2h; (b) <sup>t</sup>BuOOH, 15 min.

**Scheme 17:** Synthesis of the dimer **46** in solution.

The 5'-TBDMS protected phosphoramidite building block **45** was obtained using the same standard phosphorylation procedure. For the solution-phase synthesis of the heteroporphyrin dimers, the phosphoramidite **45** was used without any further purification, and transferred *via* Teflon canula into a CH<sub>2</sub>Cl<sub>2</sub> solution of the ZnDPP substituted 3'-TBDMS porphyrinyl deoxyuridines. The solution, containing 1.5 equivalents of *N*-(phenyl)-imidazolium triflate as activating agent<sup>[76]</sup> for the coupling reaction, was stirred for two hours. Then, the phosphonate was oxidised by addition of <sup>t</sup>BuOOH and stirring the reaction mixture continued for 15 min. After work up with NaHCO<sub>3</sub>/Na<sub>2</sub>S<sub>2</sub>O<sub>3</sub> (1:1, v/v), the product was isolated by successive chromatography using preparative TLC (CH<sub>2</sub>Cl<sub>2</sub>/MeOH, 10:1) and then by sephadex column LH20 (CH<sub>2</sub>Cl<sub>2</sub>/MeOH, 5:1) to remove side products. The purified

dinucleotide was finally dissolved with ammonium hydroxide (25%) in methanol (1:3, v/v) and stirred overnight to remove the  $\beta$ -cyanoethoxy group. The desired hetero-porphyrin dinucleotide **46** was obtained in 5% yield.

### 3.1.2 Dimerisation on solid phase



**Scheme 18:** Synthesis of the dimer **47** on solid support.

In order to compare the phosphoramidite reactivity, we dimerised the 5'-DMT protected nucleotide **40** under solid phase conditions. The dimer synthesis was achieved on a universal solid support II (15  $\mu\text{mol}$ ) and was performed following a modified standard procedure for deprotection, oxidation, and capping in an automated DNA synthesizer. This procedure is described in chapter 4. The coupling of the building block to the solid support and the formation of the internucleosidic linkage were done manually outside the synthesizer. First, the solid support was washed with the activator solution (1H-Tetrazole in acetonitrile), and then the first building block (15 mM in  $\text{CH}_2\text{Cl}_2$ ) was passed through the column with 1ml activator for 20 min until the synthesis was completed.

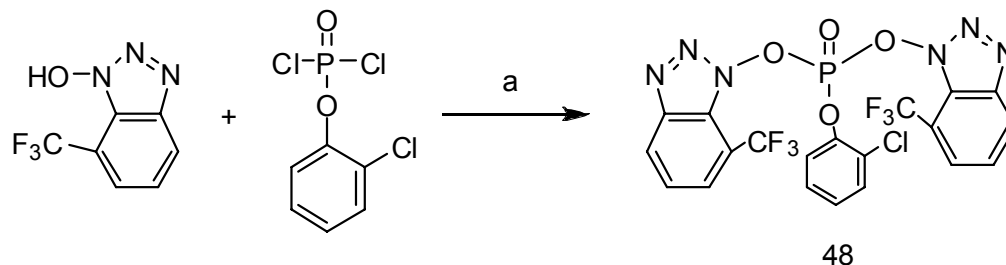
The DMT-protecting group was left on the 5'-position of the second building block for solubility reasons. The dinucleotide was cleaved from the solid support and the phosphate group was deprotected with ammonium hydroxide (25%) in methanol (1:3, v/v) overnight at room temperature.

The homo-porphyrin dinucleotide was purified by LH20 sephadex column ( $\text{CH}_2\text{Cl}_2/\text{MeOH}$ , 1:1) and obtained as a mixed free base and metallated dimer

5'-DMT $dU^{ZnDPP}$  $dU^{DPP}$ , because the first Zn metallated porphyrin was demetallated during the DMT deprotection under acid condition (3% trichloroacetic acid in  $CH_2Cl_2$ ). The dimer **47** was re-metallated with zinc acetate in  $CHCl_3/MeOH$  (1:3, v/v), followed by a final Sephadex column to obtain the pure  $d(U^{ZnDPP})_2$  in less than 1 mg. The low yield cannot be rationalised because the trityl monitoring showed a coupling efficiency of ~90%.

### 3.2 Syntheses of the Adenosine dimer

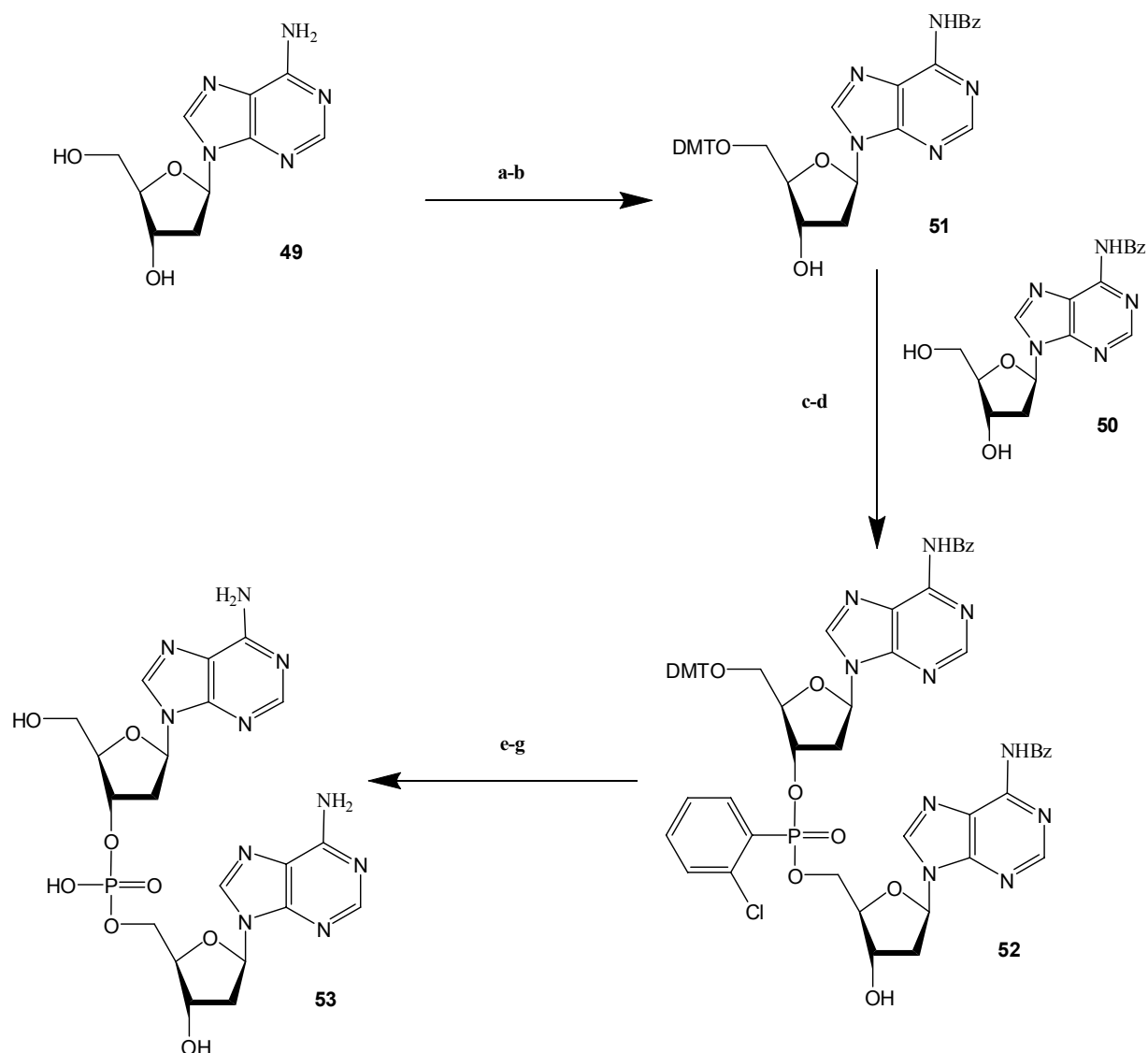
In this project, it is important for the modified oligonucleosides to retain the ability to form duplexes with the complementary natural nucleic acid. To study the interaction between the porphyrin-modified dimer with the complementary base, we synthesised the adenosine dimer. The adenosine dimer was prepared using a standard procedure. The phosphotriester synthesis is shown in the scheme 19.



(a) Dioxane, pyridine, 1h, rt.

**Scheme 19:** Synthesis of the phosphotriester **48**.

A solution of 2-Chlorophenyldichloridate in dioxane was added dropwise to a solution containing 1-hydroxy-6-methyl-benzotriazoles and pyridine in dioxane. The reaction mixture was stirred for 1h and the pyridinium chloride formed was filtered off under argon. A 0.2 M stock solution of phosphorylating agent **48** was obtained by this procedure. The chemical synthesis of nucleosides *via* the phosphotriester **48** implies the preparation of appropriately protected building blocks.



(a) Benzoylchloride,  $(\text{CH}_3)_3\text{SiCl}$ , pyridine, 44 %; (b) DMTrCl, TEA, rt, 24 h, 78 %, (c) Phosphorylating agent, pyridine, 15 min, rt; (d) compound **22**, pyridine, 1h, rt, 87 %; (e)  $1 \text{ CCl}_2\text{C}(\text{O})_2\text{H}$  in DCM, 10 min, 57 %; (f) Syn-2-pyridine-2-calboxaldoxime, Tetramethylguanidine, pyridine, 20h at  $25^\circ\text{C}$ ; (g)  $\text{NH}_3$  32 %, 2h at  $50^\circ\text{C}$ .

**Scheme 20:** Synthesis of the adenosine dimer **53**.

The benzoylation of the amine position of the adenosine with benzoylchloride and trimethylchlorosilane in pyridine gave the  $6'\text{N}$ -benzoyl adenosine **50**. The  $5'$ -OH- position was protected with dimethoxytrityl chloride in pyridine and gave the  $5'$ -DMT- $6'\text{N}$ -benzoyl adenosine **51**. The coupling reaction in dioxane between the protected adenosine **51** and the partly protected nucleoside component **50** was performed using the phosphorylating agent **48**,



which gave the protected dimer **52** in 87% yield. The DMT was cleaved with dichloroacetic acid in DCM, the chlorophenyl group could be cleaved in presence of *syn*-2-pyridine-2-carboxaldoxime and tetramethylguanidine. The adenosine dimer **53** was obtained in 80% yield after a final deprotection of the benzoyl group in presence of ammonia and purification by RP-HPLC.

### 3.3 Duplex Formation (or spectroscopy analysis)

The Uv-vis absorption spectra of the dinucleotides are shown in figure 35 (straight lines), together with the calculated spectra obtained from a superposition of the individual building blocks (dotted lines). The data are compiled in table 1. It should be noted that an accurate measurement of the extinction coefficients of **47** was not possible due to the low amount of material obtained; however, from the absorbance we estimate the solution to be around  $10^{-6}$  M in **47**. A comparison of the calculated and measured spectra reveals that the absorption maxima of the dinucleotides do not exactly match with the calculated spectra, thus electronic interactions between the chromophores occur. The strength of the interaction is highly dependent on the structure of the porphyrins in the dimers. The homo-porphyrin dinucleotide **46a**,<sup>[77]</sup> synthesised in solution, was added to this study. The dimer is substituted by a tetraphenylporphyrin (TPP). Slight blue shifts are observed in the case of **46a** ( $\Delta\lambda \sim 1$  to 2 nm). The steric hindrance due to the *meso*-phenyl groups obviously does not allow the porphyrin cores to approach close enough to induce strong electronic coupling. The mixed dimer **46b** shows a spectrum which differs greatly from the calculated spectrum of  $dU^{ZnTPP}dU^{ZnDPP}$ : the absorbance seems to be dominated by the electronic properties of the TPP part, and small red shifts for the B-band and Q-band absorptions are observed. In the DPP homodinucleotide **47**, the B-band absorption at 419 nm is marginally shifted by about 3 nm to lower energy, but in the Q-band region an additional peak at 629 nm is observed. This additional absorption maximum is not due to incomplete metallation, because in the mixed free base–zinc dinucleotide originally isolated three additional weak maxima at 648, 711 and 740 nm are visible (data not shown), which are absent in **47**. Also, the free base DPP does not exhibit any absorbance in this region.<sup>[78]</sup>

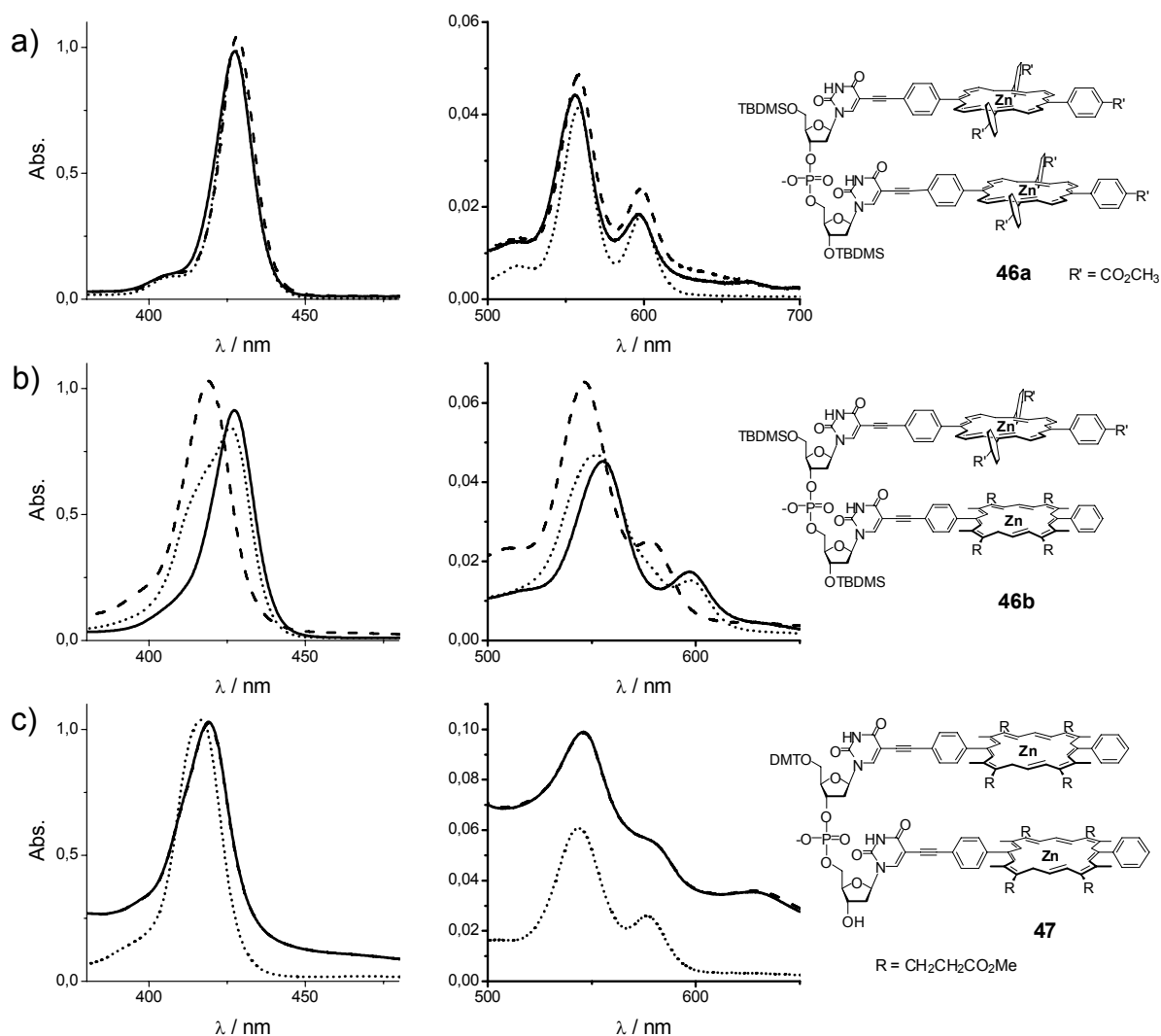


**Figure 35:** Uv-Vis absorption spectra of the dinucleotides **46** and **47** (solid lines), the duplexes with the complementary d(A)<sub>2</sub> (dashed lines), and of the calculated spectra of the dimers (dotted lines). The measurements were performed in CHCl<sub>3</sub> solutions (10<sup>-6</sup> M).

In order to check the interaction with the complementary strand, a saturated methanolic solution of the complementary diadenosine **53** was added to the porphyrin dimer solution (1.5 ml). A titration from 10 μl to 100 μl by ten fractions was done. The absorption changed gradually until 60 μl were added, then the maxima intensity decreased due to the dilution. The spectra of the mixture after addition of 60 μl are represented in figure 35 (dashed line).

In the case of **46a**, the extinction coefficients slightly increased, but again the shifts of the absorption maxima hardly changed. The  $dA_2$ - $dU^{ZnTPP}$  $dU^{ZnDPP}$  duplex show a large shift in the B-band and the Q-band regions and the values for  $\lambda_{max}$  are in-between those of **46b** and **47**. The titration experiment with **47** resulted in no change of the spectrum. Since **47** was not soluble in pure  $CHCl_3$  unlike **46a** and **46b**, a minimum of 10% of methanol was necessary to solubilise **47**. Thus, the duplex formation with  $d(A)_2$  was suppressed due to the high content of the protic solvent which normally destabilises hydrogen bonded systems.

In the dinucleotides, the two chromophores may approach sufficiently close to show electronic interactions, which are stronger in the case of the sterically less hindered DPP derivatives **46b** and **47**. Upon formation of the helical duplex  $d(A)_2$ -**46b**, the porphyrins might be rotated away from each other, and the weaker electronic coupling results in an overall blue shift of the absorbance of the dimer. However, to determine the exact nature of the interactions more spectroscopic investigations will be necessary. In the case of  $d(A)_2$ -**46a**, no significant changes are observed.

	B-band	Q-bands	
<b>46a</b>	427 (5.96)	556 (4.65)	598 (4.24)
$d(A)_2$ - <b>46a</b>	428 (6.01)	558 (4.81)	598 (4.40)
$d(U^{ZnTPP})_2$ calcd.	428 (5.93)	559 (4.67)	598 (4.18)
<b>46b</b>	427 (5.96)	555 (4.65)	598 (4.24)
$d(A)_2$ - <b>46b</b>	418 (6.01)	546 (4.81)	578 (4.40)
$dU^{ZnTPP}$ $dU^{ZnDPP}$ calcd.	426 (5.93)	551 (4.67)	597 (4.18)
<b>47</b>	419	546	577 (sh)      629
$d(U^{ZnDPP})_2$ calcd.	416	543	577

**Table 1:** Absorption maxima  $\lambda_{max}$  ( $\log \epsilon$ ) of the dinucleotides, the duplexes with  $d(A)_2$ , and of the calculated spectra obtained by addition of the building blocks. Measurements were performed in  $CHCl_3$  ( $10^{-6}$  M,  $25^\circ C$ ).

In the MALDI-TOF mass spectrometer, irradiation with the laser induced photolytic fragmentation of the dinucleotides, probably due to radicals generated from the photoexcited state of the porphyrins. We had previously observed cleavage of functional groups and atom

transfer in MALDI-TOF MS.<sup>[79]</sup> Suppression of this fragmentation could be achieved to some extent by varying the matrix use,<sup>[80]</sup> and most useful proved to be a combination of dihydroxy acetophenone together with *p*-nitro aniline. When the dinucleotides are mixed with an excess (50 equivalents) of the complementary d(A)<sub>2</sub>, formation of the duplex is also observed. For **47**, the complexation was much less obvious, and d(A)<sub>2</sub>-**53** displayed *m/z* peaks corresponding to multiple salt adducts.

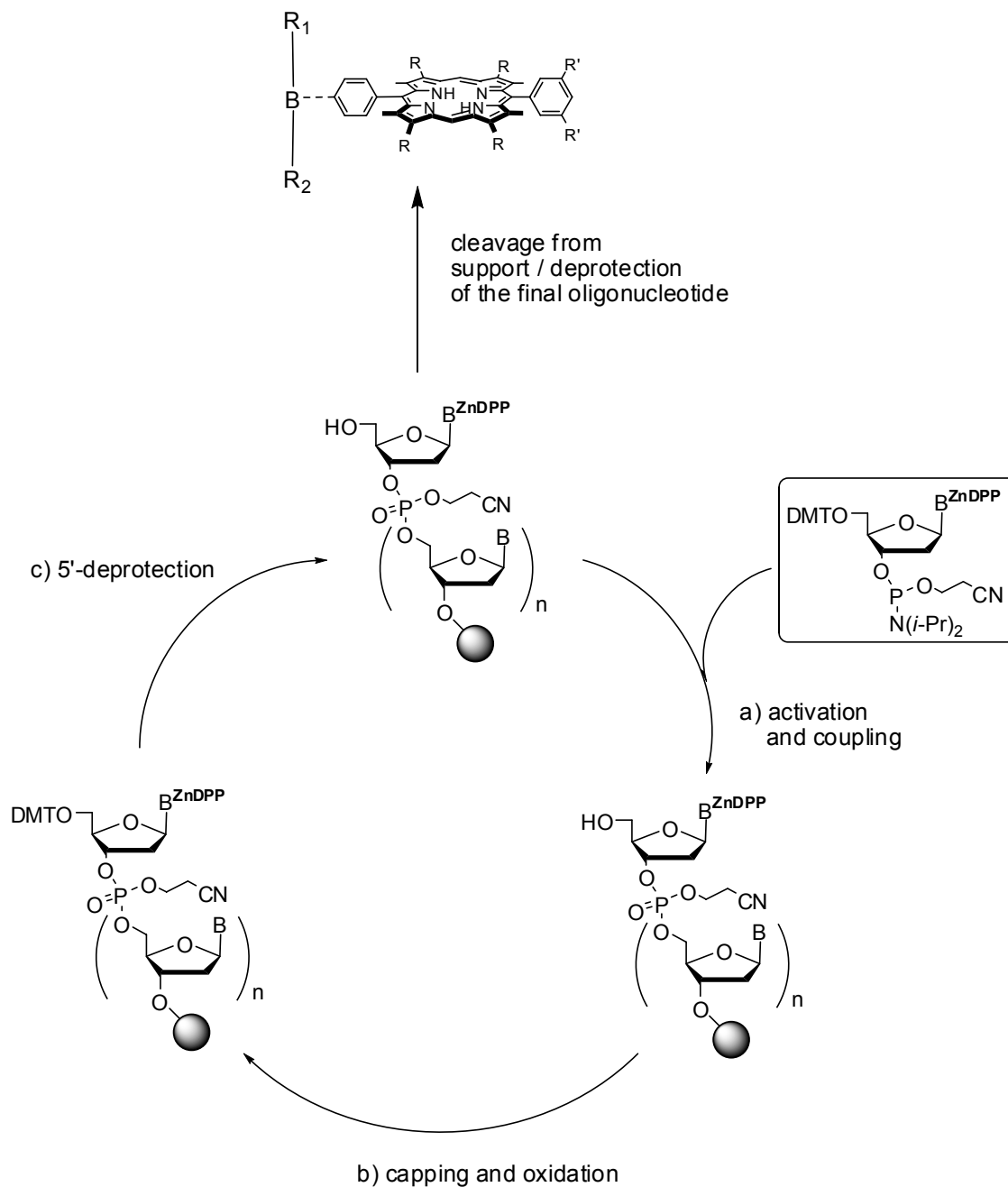
## 4 Tri- and tetranucleotide porphyrin arrays

The next step was the incorporation of porphyrin substituted nucleotides into tetranucleotides using phosphoramidite chemistry on solid support in a DNA synthesiser. Both diphenyl and tetraphenyl porphyrin nucleosides were used as building blocks to introduce chirality into the porphyrinic arrays. We synthesised a trinucleotide in order to compare the reactivity of the diporphyrin arrays with the individual porphyrins. Using spectroscopic methods, we studied the duplex formation with the complementary tetra-adenosine. Because no interaction between the porphyrin arrays and the complementary strands were evident, we used the PNA as neutral complementary strand to obtain more information on possible duplex formation.

### 4.1 Methodology

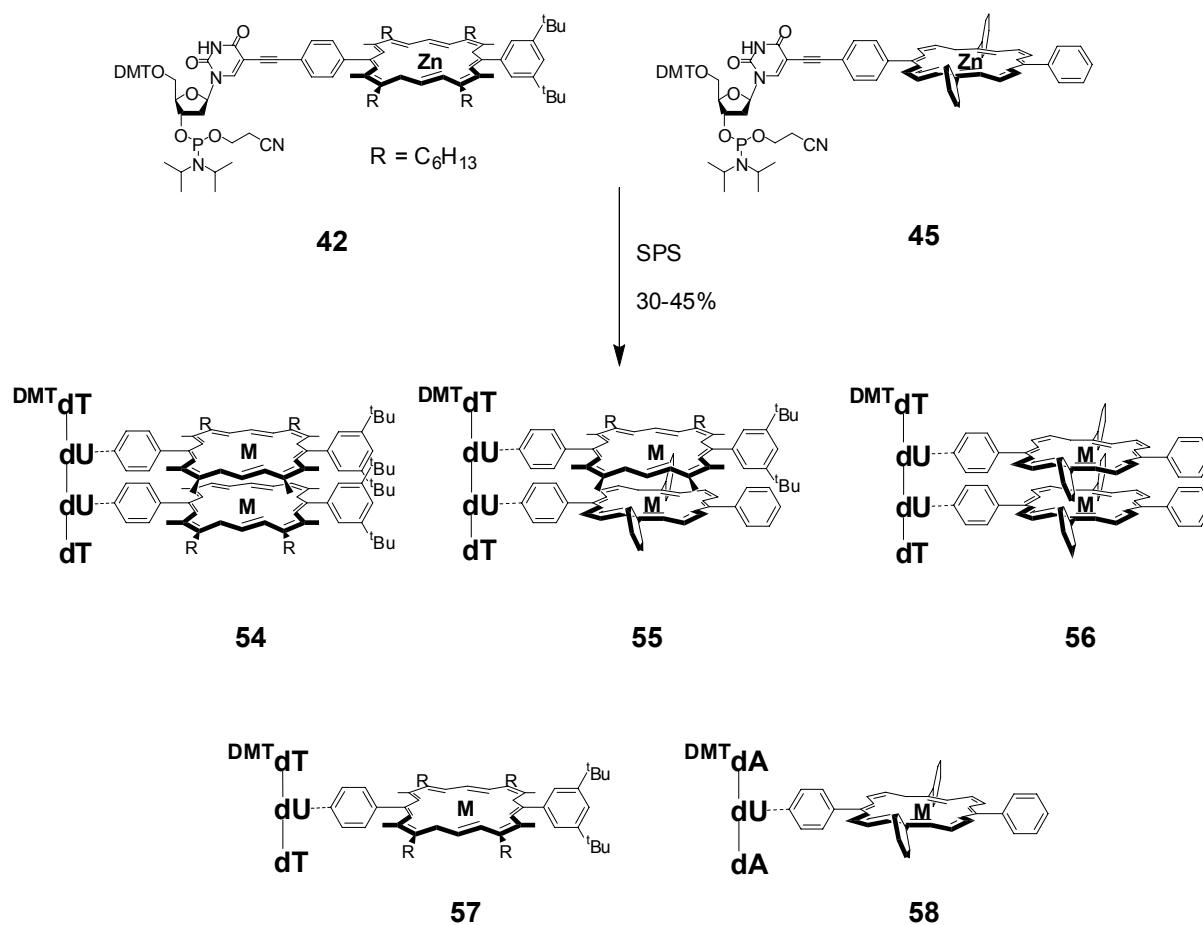
The predominant method for oligonucleotide synthesis nowadays is the phosphoramidite approach introduced by Beaucage and Caruthers.<sup>[81]</sup> The synthesis is performed on a solid phase like glass with controlled pore width (CPG) and starts with the 5'-end deprotection of the CPG-bound nucleoside (scheme 21). The 5'-O-positions of the phosphoramidite building blocks are usually protected by the acid-labile 4,4'-dimethoxytrityl group, which was introduced in 1962 by Khorama and co-workers, and which allows a convenient optical in-line monitoring of the coupling efficiencies. The generated free hydroxyl group reacts with the 3'-phosphoramidite of the following nucleoside which has to be activated with 1*H*-tetrazole for a smooth and fast reaction. Remaining hydroxyl groups are capped to prevent elongation of failure strands. The resulting dinucleoside phosphite is oxidized to the corresponding phosphate with a mixture of iodine in water, and the cycle starts again. During the synthesis, the porphyrin building block is introduced instead of one of the unmodified base with increasing the coupling time to 10 min. At the end of the synthesis, ammonia is used to release the product from the solid support and to deprotect the exocyclic amino groups of the nucleobases. Generally, the nucleophilic NH<sub>2</sub> groups of the adenine, guanine and cytosine nucleosides are masked by acylation. Up to date, optimization of the phosphoramidite approach led to the synthesis of oligonucleotides with coupling times lower than one minute and coupling efficiencies higher than 99% per base for DNA. Regarding the

modular system of this synthetic procedure, the covalent introduction of fluorescent groups at specific positions of any DNA sequence is easily performed.

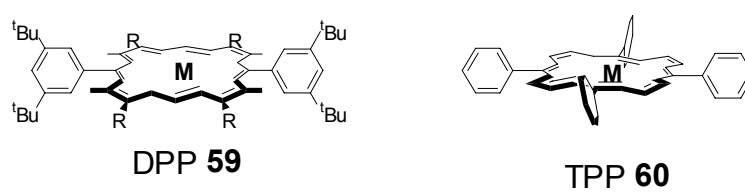


**Scheme 21:** Solid support modified DNA synthesis.<sup>[82]</sup>

## 4.2 Synthesis of the tri- and tetranucleotide



**Scheme 22:** Solid phase synthesis of tri- and tetranucleotide porphyrin arrays with  $M = H, Zn$ .



**Scheme 23:** Reference porphyrins with  $M = H, Zn$ .

The two phosphoramidite building blocks **42** and **45**, obtained from the DMT-protected porphyrin nucleotides,<sup>[77, 78]</sup> were used for both the tri- and tetranucleotide synthesis. DCM solutions (20 mM) of the building blocks were prepared and used for the synthesis of the porphyrin-oligonucleotides **54** to **58** in an automated DNA synthesiser in standard mode (trityl on) on a 15  $\mu$ mol scale; the coupling time for the modified building blocks was increased to 15 minutes. This method allowed the synthesis of chiral homo- and heteroporphyrin tetramers. The incorporation of the two successive porphyrins introduced chirality into the arrays through the DNA's ribose moiety without the need of enantioselective synthesis. Cleavage from the solid support was achieved with a mixture of 25% ammonium hydroxide and methanol at 40°C over night. Due to the low solubility of **54**, **55** and **57** in this solvent mixture, a second treatment of the solid support was necessary using 25% ammonium hydroxide and dioxane 1:1 at 40°C over night. The crude products were purified on lipophilic sephadex (LH 20, DCM-MeOH 1:1). The yields of the final products as free-base porphyrins **H<sub>2</sub>-54** to **H<sub>2</sub>-58** were in the range of 30 to 45%. The products were characterised by MALDI-ToF mass spectrometry (figure 36) which showed the expected  $m/z$  peaks for porphyrin arrays for the diporphyrins **H<sub>2</sub>-54** to **H<sub>2</sub>-56**. The porphyrin arrays are initially isolated in the free base form. Remetallation of the porphyrin arrays to give the zinc derivatives **Zn-54** to **Zn-58** was performed using the standard methods for porphyrin metallation with zinc acetate in DCM-methanol.<sup>[78]</sup> Excess zinc salts were removed on a second lipophilic sephadex column.

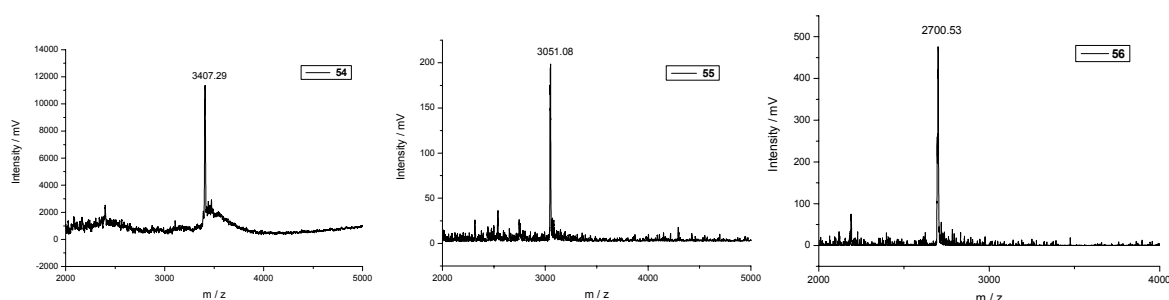


**Figure 36:** Maldi-Tof mass spectra of the free-base tetranucleotides **54-56**.



To gain insight into the influence of the porphyrin substitution on the structure and the stability of the modified DNA, we have performed absorption, emission, and CD spectroscopy. These techniques were also used to determine the duplex formation. The absorbance and emission spectra were determined using chloroform solutions of  $2.5 \times 10^{-6}$  M and  $2.3 \times 10^{-8}$  M concentration, respectively. The concentrations used for the circular dichroism spectroscopy were variable and are indicated in figure 40. The  $^1\text{H}$  NMR spectra were recorded either in  $\text{CDCl}_3$  (0 or 10 mM TBA- $\text{PF}_6$ ) or  $\text{CD}_3\text{CN}$  using a 600 MHz Bruker NMR spectrometer as  $8.4 \times 10^{-4}$  M solutions. All solvents were degassed and filtered through basic alumina prior to preparing the samples. All oligonucleotides were soluble under the conditions indicated, and no aggregation was observed in any experiment

### 4.3 Complementary DNA strand synthesis

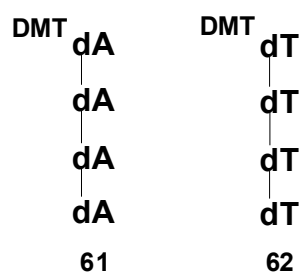


**Figure 37:** Tetra-adenosine **61** and tetra-thymidine **62** synthesis on solid support.

Using the same method as before, the complementary tetra-adenosine **61** and the unmodified tetra-thymidine **62** were synthesised in the DNA synthesiser using the standard mode (trityl on) on a 15  $\mu\text{mol}$  scale (figure 37). For solubility reasons, the DMT group was kept on the non-modified DNA strands. Cleavage from the solid support was achieved with a mixture of 25% ammonium hydroxide and methanol at  $40^\circ\text{C}$  over night. A first purification step on lipophilic sephadex gave no pure material. Then, the crude products were purified by HPLC and were characterised by MALDI-ToF mass spectrometry which showed the expected  $m/z$  peaks for the  $\text{dA}_4$  and  $\text{dT}_4$ . The relative amount were determined by UV-visible spectroscopy using the calculate extinction coefficient ( $\epsilon = 55\,400$  for  $\text{dA}_4$  and  $\epsilon = 33\,000$  for  $\text{dT}_4$ ). The  $^1\text{H}$  NMR spectra were recorded in  $\text{CD}_3\text{CN}$  using a 600 MHz Bruker NMR spectrometer.

## 4.4 UV-Visible Spectroscopy

The spectra of the free base trinucleotides **57** and **58** containing one of the porphyrins are identical to the spectra of either diphenyl porphyrin ( $H_2DPP$  **H<sub>2</sub>-59**) or tetraphenyl porphyrin ( $H_2TPP$  **H<sub>2</sub>-60**). The presence of the DNA backbone therefore does not influence the absorbance of the porphyrins, and no electronic interactions between the chromophores and the nucleobases occur, as was already observed in the porphyrin nucleotide building blocks (chapter 2).

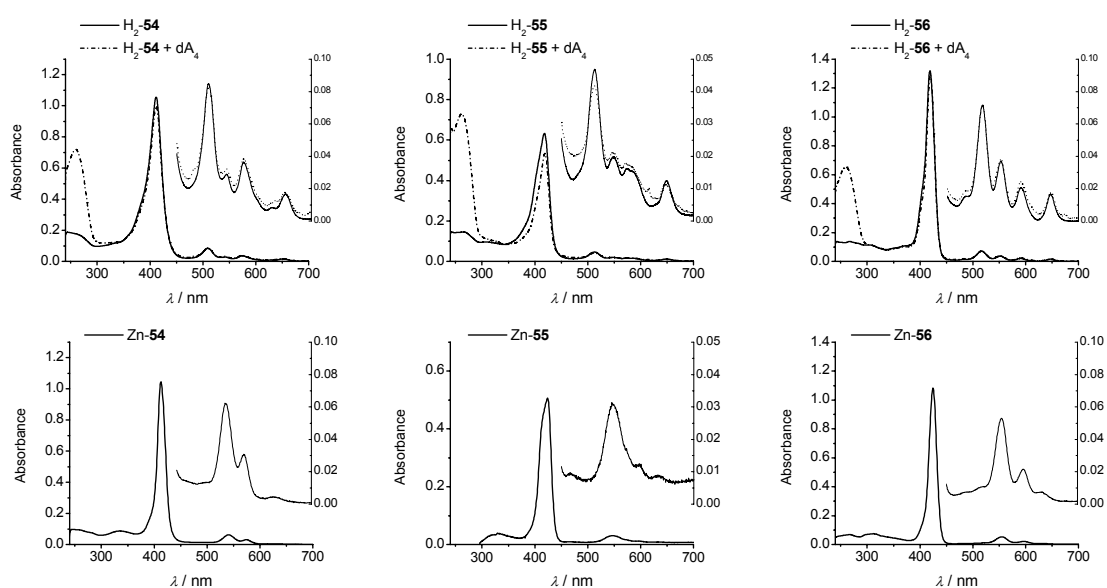


**Figure 38:** Uv-vis spectra of the diporphyrin arrays. The insets show the expanded Q-band region of the porphyrins.

In contrast to the dinucleotide-diporphyrin arrays described in chapter 2, the spectra obtained from the tetranucleotides can be reproduced by a superposition of the spectra of either the individual building blocks or the trinucleotide arrays. The UV-vis absorbance spectra of the diporphyrin arrays **H<sub>2</sub>-54**, **H<sub>2</sub>-55** and **H<sub>2</sub>-56** are shown in figure 38. The absorbance maxima  $\lambda_{\max}$  ( $\log \epsilon$ ) of the porphyrinic absorptions in the arrays are compiled in Table 2. The B-band absorbances are 411 nm (5.62) for **H<sub>2</sub>-54**, 418 nm (5.40) for **H<sub>2</sub>-55**, and 419 nm (5.72) for **H<sub>2</sub>-56**, which are expected values for porphyrins. The four Q-band absorbances can be found in the 450 nm to 700 nm region which is typical for free base

porphyrins. Upon addition of the complementary tetra-adenosine dA<sub>4</sub> the absorbances remain largely unchanged apart from a small hypochromism in the array **H<sub>2</sub>-55** (figure 38). Apparently, no change in the electronic environment is induced by addition of the tetra-adenosine.

The corresponding zinc derivatives **Zn-54**, **Zn-55** and **Zn-56** (table 2) show maxima for the B-band absorbances which are red-shifted only marginally in **3**, and by about 6 nm in **55** and **56** compared to the free base porphyrins (the spectra are displayed in Figure 38 bottom). This shift difference is a common value for zinc metallated porphyrins; the values found are 413 nm ( $\lg\epsilon = 5.32$ ) for **Zn-54**, 424 nm (4.76) for **Zn-55**, and 425 nm (5.48) for **Zn-56**. Again, upon addition of the complementary tetra-adenosine no significant change in the electronic spectra could be observed. The electronic ground state of the porphyrins therefore is not altered when incorporated into the oligonucleotide, nor is it influenced by the absence or presence of the complementary strand. Excitonic coupling does not occur because unhindered rotation around the internucleosidic linkage seems to prevent a close contact.

	B-band absorption		Q-band absorptions		
<b>H<sub>2</sub>-54</b>	412 (5.30)	510 (4.21)	541 (3.81)	576 (3.88)	652 (3.53)
<b>Zn-54</b>	413 (5.32)		540 (4.10)	574 (3.78)	
<b>H<sub>2</sub>-55</b>	418 (4.75)	513 (3.63)	544 (3.49)	575 (3.37)	648 (3.20)
<b>Zn-55</b>	424 (4.76)		545 (3.13)	598 (3.68)	
<b>H<sub>2</sub>-56</b>	419 (5.38)	516 (4.15)	553 (3.96)	592 (3.75)	646 (3.63)
<b>Zn-56</b>	425 (5.48)		555 (4.08)	596 (3.51)	
<b>H<sub>2</sub>-57</b>	417 (4.79)	509 (3.30)	544 (3.43)	575 (3.08)	
<b>H<sub>2</sub>-58</b>	418 (4.86)	515 (3.76)	552 (3.57)	591 (3.39)	645 (3.28)

**Table 2:** Uv-vis absorbance data for the diporphyrin arrays **54** to **58**. Data are recorded in CHCl<sub>3</sub>,  $c = 2.5 \times 10^{-6}$  M, T = 25°C.

## 4.5 Steady state emission spectroscopy

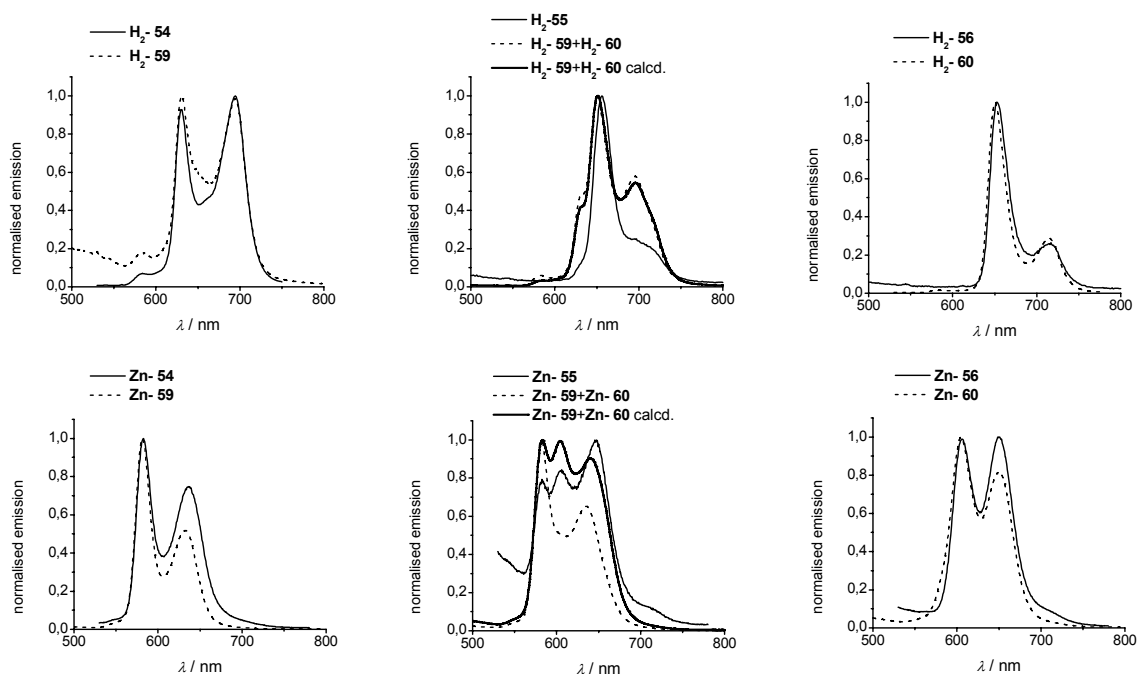


**Figure 39:** Normalised steady state emission spectra of the free-base (top) and zinc metallated (bottom) porphyrin arrays.

The steady state emission spectra of the diporphyrin systems when irradiated at 420 nm show emission maxima between 600 and 750 nm which are characteristic for the fluorescence from the first singlet excited state S1 of porphyrins. In figure 39, the normalised spectra are shown for the diporphyrin arrays as well as for the individual porphyrins. There are no differences in the shape of the spectra of all the homo-porphyrin oligonucleotides when compared to the fluorescence of the model free-base porphyrins diphenyl porphyrin **59** and tetraphenyl porphyrin **60** alone or the combination of **59** and **60**. Comparison with the monoporphyrin trinucleotide shows that the presence of the DNA backbone also has no influence on the excited state behaviour of the porphyrins (data not shown). Some differences in the relative intensities of the emission bands are detectable in the zinc metallated arrays.

The mixed porphyrin arrays **H<sub>2</sub>-55** and **Zn-55**, on the other hand, behave very differently compared to a mixture of the building blocks. Both the shape and the relative

intensities of the normalised spectra do not correspond to a simple superposition of either the porphyrin building blocks or the trinucleotide porphyrin systems.

In an equimolar mixture of the free base porphyrins **H<sub>2</sub>-59** and **H<sub>2</sub>-60**, the spectrum corresponds well to a superposition of the emission spectra of the individual porphyrins (blue lines in Figure 39), whereas in the case of the zinc metallated porphyrins **Zn-59** and **Zn-60**, the spectrum is dominated by the emission of the diphenyl porphyrin **Zn-59**. It should be noted that the relative intensity of the emission of the two porphyrins is almost equal in the free base form, but in the zinc metallated form the tetraphenyl porphyrin has an emission intensity which is about 25 % that of the diphenyl porphyrin.

In **H<sub>2</sub>-55** and **Zn-55**, the contribution of the tetraphenyl porphyrin seems much more enhanced. In **H<sub>2</sub>-55**, the spectrum is very close in shape to the spectrum of H<sub>2</sub>TPP, which indicates that the emission of the DPP part is greatly diminished. Here, also the calculated spectrum which is obtained from the normalized spectra of **H<sub>2</sub>-59** and **H<sub>2</sub>-60** represents the spectrum of the equimolar porphyrin mixture rather than of the diporphyrin array **H<sub>2</sub>-55**. Similarly, for **Zn-55** the emission spectrum is very different from the spectrum of an equimolar mixture of the porphyrins. The emission of the DPP porphyrin does not seem to be completely quenched, but the contribution of the TPP part is significantly enhanced. The spectrum actually is very close to the calculated spectrum obtained from the normalized emission spectra of **Zn-59** and **Zn-60**. It can therefore be assumed that in the arrays an energy transfer from the DPP to the TPP part occurs, which increases the emission of the tetraphenyl porphyrin and quenches the emission of the diphenyl porphyrin. Since this effect is not detected in a mixture of the porphyrins at this low concentration, the enforced close proximity of the two chromophores through the oligonucleotide backbone leads to an intramolecular electronic communication between the porphyrins.

	$\lambda_{\max}$ (rel. Intensity)		
<b>H<sub>2</sub>-54</b>	630 (0.92)	695 (1)	
<b>Zn-54</b>	582 (1)	636 (0.75)	
<b>H<sub>2</sub>-55</b>	655 (1)	704 (sh)	
<b>Zn-55</b>	583 (0.78)	605 (0.84)	646 (1)
<b>H<sub>2</sub>-56</b>	653 (1)	716 (0.24)	
<b>Zn-56</b>	606 (0.99)	650 (1)	
<b>H<sub>2</sub>-57</b>	631 (1)	691 (0.75)	
<b>Zn-57</b>	582 (0.58)	656 (1)	
<b>H<sub>2</sub>-58</b>	651 (1)	715 (0.22)	
<b>Zn-58</b>	602 (1)	648 (0.98)	

**Table 3:** Steady state emission data for the diporphyrin arrays **54** to **58**. Data are recorded in CHCl<sub>3</sub>,  $c = 2.3 \times 10^{-8}$  M,  $T = 25^\circ\text{C}$ .

#### 4.6 Circular dichroism spectroscopy

The arrays were analysed by circular dichroism (CD) spectroscopy in order to determine whether structural changes upon dimerisation with the complementary tetra-adenosine occur. Induced circular dichroism has become a valuable tool to determine changes in the helicity of oligonucleotides, and the porphyrins provide a chromophore allowing to detect subtle changes in the supramolecular chirality.<sup>[11, 83-88]</sup> The CD spectra of the arrays **H<sub>2</sub>-54** to **H<sub>2</sub>-56** are shown in Figure 4. The UV-regions of the CD spectra do not show clear features, thus the spectra do not indicate highly ordered structures with respect to the oligonucleotide backbone.

Regarding the B-band region of the porphyrins, all three complexes show a similar signature in their spectra. The single strand arrays show an induced negative cotton effect at 416, 424 and 420 nm for **H<sub>2</sub>-54**, **H<sub>2</sub>-55** and **H<sub>2</sub>-56**, respectively. The values for  $\lambda_{\max}$  are red-shifted by one to six nm compared to the B-band absorbance of the arrays. A negative cotton effect in DNA-porphyrin complexes is normally observed upon intercalation of cationic porphyrins into G-C rich sequences.<sup>[87, 88]</sup> In the absorbance spectra, neither hypochromism nor a bathochromic shift is observed for any of the arrays as compared to the building blocks, which would be expected if strong  $\pi$ -interactions with the nucleobases upon

intercalation would occur. The negative cotton effect can thus be explained by an induced chirality from the oligonucleotide backbone of the diporphyrin array. Noteworthy, the CD signal is strongest for the array **56**, where a sharp signal was also observed. The signal of **54** is slightly broadened with a decreased intensity compared to **56**. The broadest and also weakest induced signal is observed in the array **55**. Upon addition of the complementary tetra-adenosine, the spectra did not change.

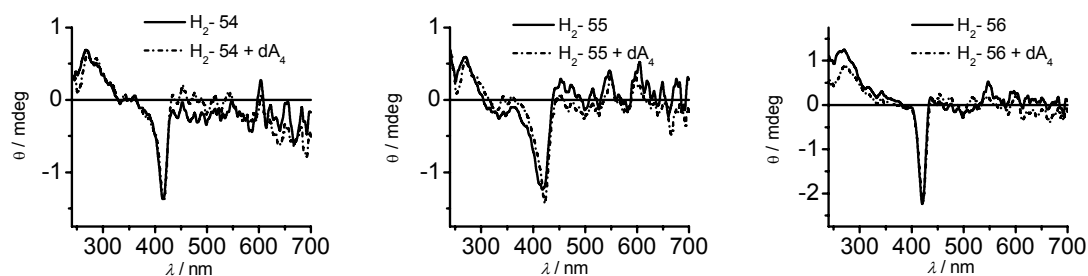


**Figure 40:** CD spectra of the free-base porphyrin arrays. Spectra are recorded in  $\text{CHCl}_3$  ( $T = 25^\circ\text{C}$ ) at  $c = 5 \times 10^{-6}$  M (**H<sub>2</sub>-54**),  $13.4 \times 10^{-6}$  M (**H<sub>2</sub>-55**) and  $3.75 \times 10^{-6}$  M (**H<sub>2</sub>-56**).

## 4.7 $^1\text{H}$ NMR Spectroscopy

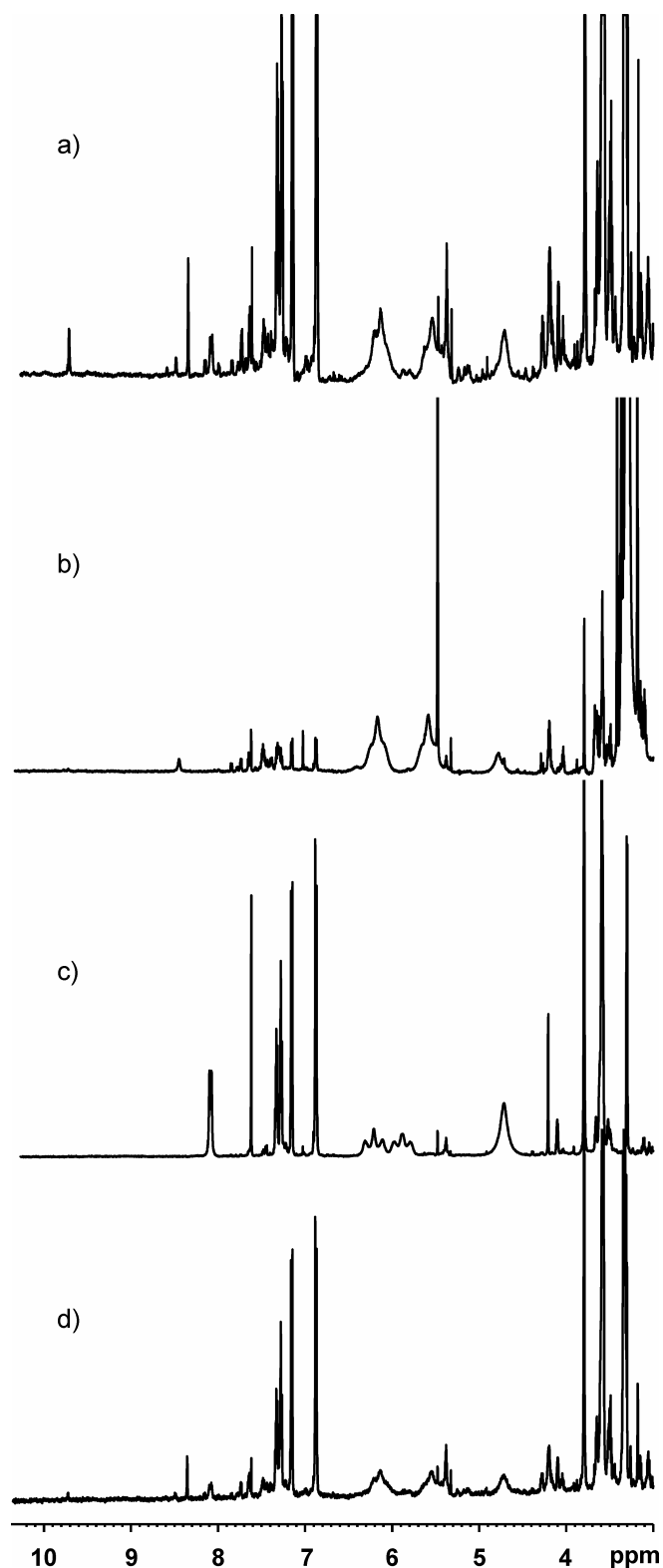


**Figure 41:** Region of the  $^1\text{H}$  NMR spectra of the tetra-nucleotides: a)  $\text{H}_2\text{-54} + \text{dA}_4 \text{61}$ , b)  $\text{dT}_4 \text{62}$ , c)  $\text{dA}_4 \text{61}$ , d)  $\text{dT}_4 \text{62} + \text{dA}_4 \text{61}$ . The spectra shown are recorded in  $\text{CDCl}_3$  (10 mM TBA- $\text{PF}_6$ ) for a) and in  $\text{CD}_3\text{CN}$  for b)-d).  $c = 8.4 \cdot 10^{-4}$  M,  $T = 22^\circ\text{C}$ .



It is expected that in aqueous solution, where the calculated melting point of a tetramer would be below 10 °C, no duplex formation with the complementary strand takes place. This, however, does not necessarily extend to organic solutions. In chloroform, a much stronger interaction between an A-T base pair was reported, and the association constant was determined to be about  $10^2 \text{ M}^{-1}$  [89] which could lead to an association constant of up to  $10^8 \text{ M}^{-1}$  in a tetranucleotide.

In order to verify the presence or absence of any interactions between the arrays and the complementary strand, we studied the tetra-nucleotides by  $^1\text{H}$  NMR spectroscopy. The arrays were dissolved, and the complementary strand was added until equimolar amounts were present. Either neat  $\text{CDCl}_3$  solutions or 10 mM TBA- $\text{PF}_6$  solutions in  $\text{CDCl}_3$  were used. However, no changes in the  $^1\text{H}$  NMR spectra were observed upon addition of the complementary strand, which is shown in figure 41a with the array **H<sub>2</sub>-54** as representative example. Further experiments were performed using both the unmodified tetra-thymidine and tetra-adenosine (figure 41 b-d). The spectrum of the equimolar mixture of  $\text{dT}_4$  and  $\text{dA}_4$  is a superposition of the individual  $^1\text{H}$  NMR spectra. No changes in the resonances assigned to the sugar-phosphate backbone or in the nucleobase region were seen. Also, no low field resonances were detected at ~10-15 ppm which would be expected for the nucleobase protons when they are integrated into an A-T hydrogen bonding system.<sup>[90]</sup> The spectra of the natural oligo-nucleotides were also measured under different conditions, e.g. in both  $\text{CDCl}_3$  and  $\text{CD}_3\text{CN}$  solutions, and in the presence and absence of the non-coordinating buffer TBA- $\text{PF}_6$ , leading to the same results. Also heating to 80 °C for two hours and slow cooling to room temperature to simulate the annealing of natural DNA did not have any influence on the outcome of the spectra. The same applies for recording the spectra at 5 °C. We therefore conclude that the interactions between the two complementary tetra-nucleotides in organic solvents are very weak even in unmodified oligonucleotides where the steric repulsion from the bulky porphyrins is not present.

We decided then to probe the use of PNA as neutral complementary strand to obtain more information on possible duplex formation and to understand the nature of the electronic interactions between the chromophores.

## 4.8 Peptide Nucleic Acid

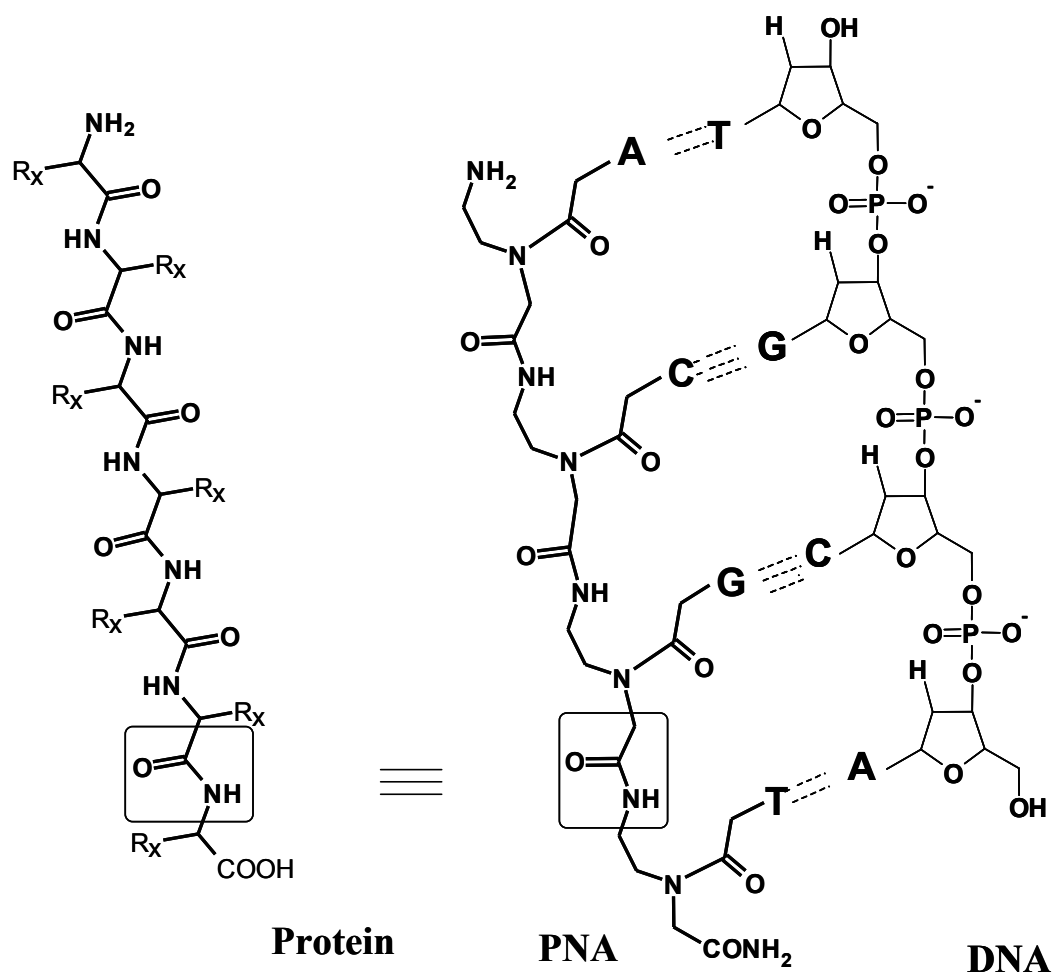


**Figure 42:** PNA, DNA and Protein structures.

Peptide nucleic acids (PNAs) are one of the most interesting of DNA mimics and were first reported in 1991 by Nielsen. Since this time, a vast number of studies have been reported covering their synthesis, properties and applications. In PNAs, the phosphoribose backbone of natural oligonucleotide is made from repeating N-(2-aminoethyl)-glycine units linked by peptide bonds. The different bases (purines and pyrimidines) are linked to the backbone by methylene carbonyl linkages. Their oligomerization is thus carried out using standard peptide chemistry such as Fmoc or Boc chemistry with suitable protecting groups for the purine or pyrimidine heterocycles. One protecting groups for the N terminus and one other for the nucleobase are required. Unlike DNA or other DNA analogs, PNAs do not contain any pentose sugar moieties or phosphate groups. PNAs are depicted like peptides with the N-terminus at the first (left) position and the C-terminus at the right. The PNA backbone is

not charged, this confers to this polymers a much stronger binding to DNA strands as shown in figure 42 This is due to the lack of charge repulsion between PNA and DNA strand. Moreover, PNA is resistant to biological degradation by nucleases or proteases, properties which make PNA an ideal tool in a number of different areas of research such as gene therapy or mRNA profiling.

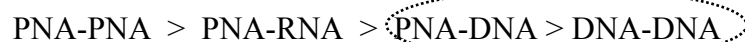
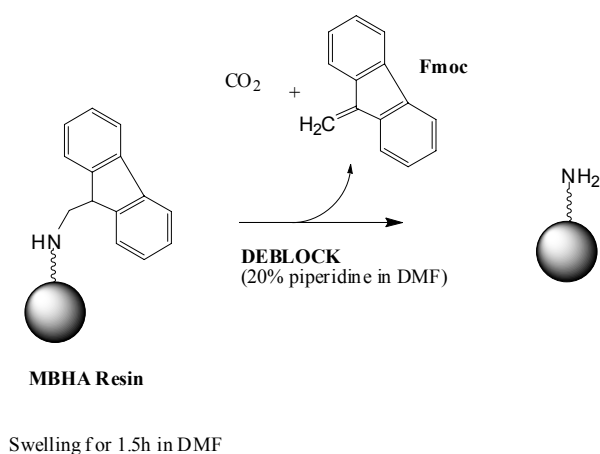


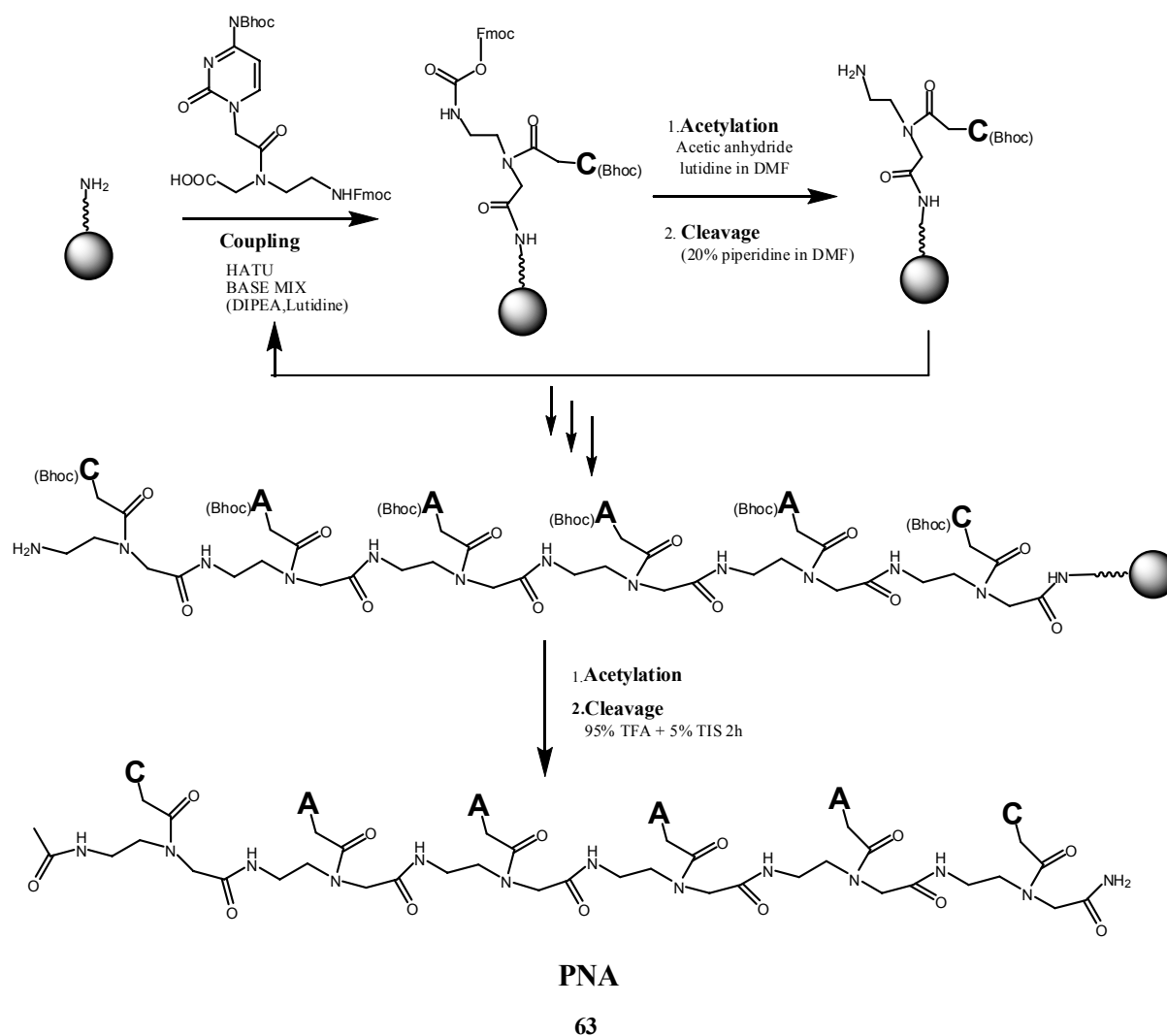
**Figure 42:** Relative thermal stability of the hybrid duplexes and natural DNA.

#### 4.8.1 Solid-Phase PNA Synthesis



**Scheme 24:** Preparation of the resin.

Manual peptide synthesis<sup>[91]</sup> was accomplished in a fritted-filter reaction vessel (Merrifield vessel) with a two-way valve fitted onto a 25 ml side arm vacuum flask by way of a 1-hole stopper. One valve was used to bubble nitrogen through the reaction mixture and the other valve was used to evacuate excess reaction solutions and wash solvent using a vacuum flask. PNAs are synthesised in a similar way common peptide synthesis is performed, whereas the growing chain is elongated by a monomer protected with an N-terminal Fmoc and an additional side-chain protection group. After coupling is completed, the terminal Fmoc-protection group is removed and subsequent cycles are performed until the desired molecule is assembled.



**Scheme 25:** Manual synthesis of the PNA.

The PNA molecules were synthesised on Fmoc-protected Rink resin, the Rink Amide MBHA resin with a substitution of about 0.4-0.8 mmol/g. After swelling the resin for 1 h in N,N'-dimethylformamide (DMF), 50 mg were distributed to each Merrifield vessel. The coupling cycle was started with the cleavage of the Fmoc protection groups. This was done by two successive incubations (1 and 5 min) with 4 ml 20% piperidine in DMF. The Fmoc groups and piperidine were removed and the resin was washed away five times with 6 ml DMF followed by a double coupling (2 x 45 min) of the first monomer (base C). Each of the two coupling solutions consisted of 185  $\mu$ l Fmoc-PNA-monomer (0.3 M in 1-methyl-2-pyrrolidone (NMP), 185  $\mu$ l O-(7-azabenzotriazol-1-yl)-N,N,N',N'-tetramethyluronium hexafluorophosphate (HATU) (0.6 M in DMF) and 185  $\mu$ l base mix (0.6 M diisopropylethylamine (DIPEA) and 0.9 M 2,6-lutidine in DMF). After coupling, the resin

was washed three times with 6 ml DMF. Not elongated sequences were acetylated by incubation in 1.5 ml capping mix (5% acetic anhydride and 6% 2,6-lutidine in DMF) for 5 min. Finally the resin was washed another five times with 6 ml DMF. The cycle was repeated until the synthesis of the desired PNA sequence was completed. The progress of amino acid couplings can be followed using ninhydrin. The ninhydrin solution turned dark blue (positive result) in the presence of a free primary amine but was otherwise colourless (negative result). Finally the terminal Fmoc group was removed and the final free amine was acetylated as described above. The resin was washed another five times with 6 ml DMF and three times with 6 ml 1,2-dichloroethane. After synthesis, the final PNA molecules were cleaved from the dried resin and the Bhoc protecting groups were removed by incubation in 6 ml of 95% trifluoroacetic acid (TFA) and 5% triisopropylsilane (TIS) mixture for 2 h. After elution of the molecules with another 6 ml cleavage mix, precipitation of PNAs was done by adding 30 ml of ice-cold ether. PNAs were washed another four times with ether, and dried. The PNA was first precipitated in acetonitrile and then purified by RP-HPLC. The desired PNA strand CAAAAC **63** was obtained in 37% yield. Quality control of the synthesised PNAs was done by MALDI-TOF mass spectrometry. The absorption spectra measured in water; shows a peak at 259 nm. The PNA extinction coefficient ( $\epsilon=63\ 344$ ), which was calculated using the UV-visible spectroscopy, was determined close to the calculated value of  $\epsilon=66\ 920$  using literature data for the PNA-base (A=13.7, C=6.06, G=11.7, T=8.6, ml/ $\mu$ mol-cm). However, to determine the PNA concentration in solution the measured value for  $\epsilon$  was used.

## 4.8.2 Spectroscopy studies with tetra-nucleotides

### 4.8.2.1 UV-Visible Spectroscopy

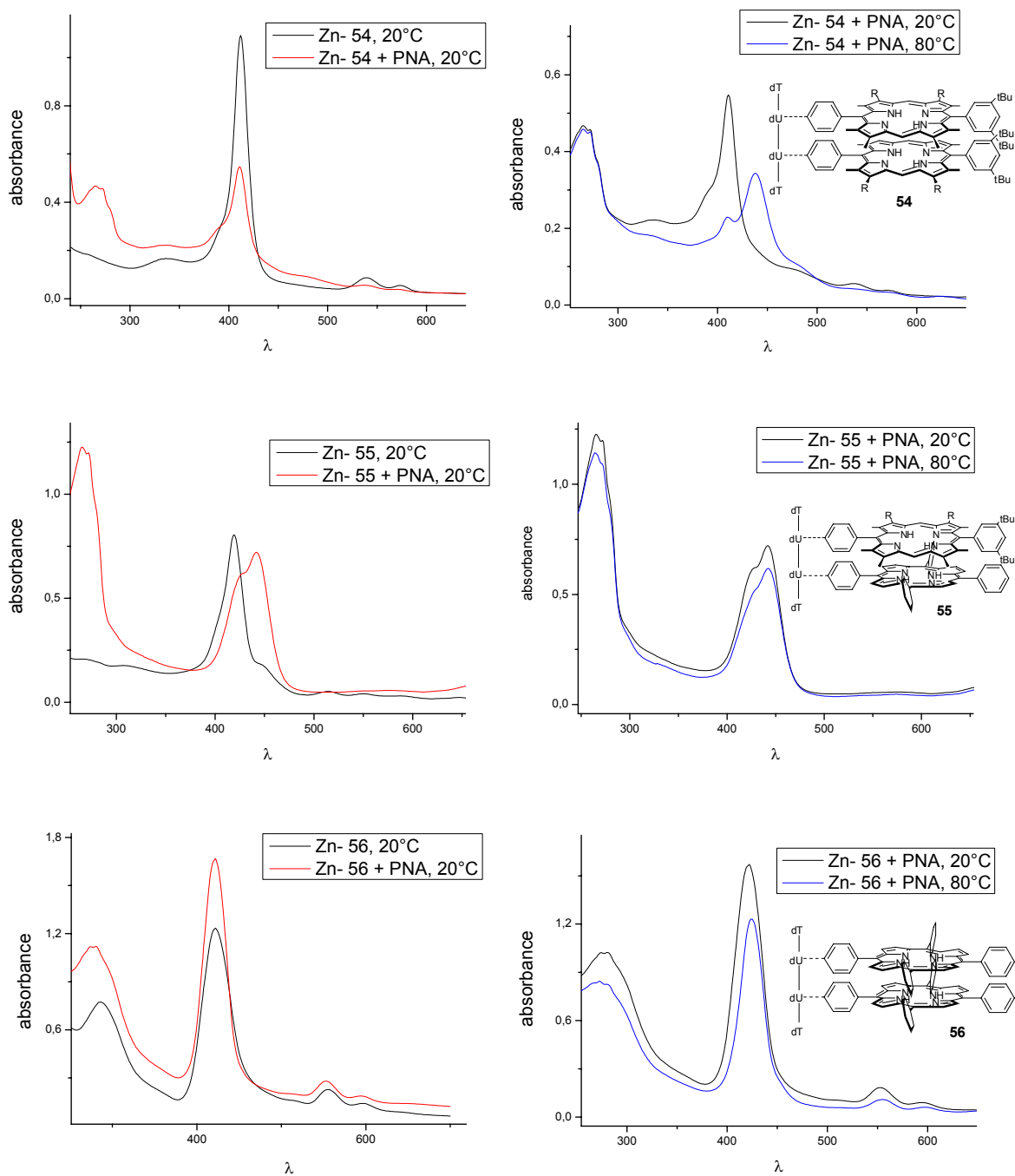


**Figure 43:** Uv-vis spectra of the diporphyrin arrays **54** to **56** with the complementary PNA **63**. Data are recorded in dichloroethane at 20°C and 80°C.

In an equimolar mixture of the diporphyrin arrays with the PNA, the relative intensities for the B-band absorbance changed compared to the single tetramers. The absorbance maximum decreases about 50% for Zn-54., and increases about 25% for Zn-56. In the case of the mixed tetramer, the duplex formation leads to a red-shifted by about 22 nm and the spectrum shows a second B-band absorbance at 426 nm. The data of the porphyrinic absorptions in the arrays are compiled in table 3. In order to study the temperature influence on the possible duplex formation, the solutions were slowly heated up to 80°C and cooled down to 20°C. The relative absorption is quite the same for Zn-55 and Zn-56 with a hypochromicity of 5%. In the case of Zn-54, the spectrum shows a maximum which is red-shifted by about 26 nm. The value found is 436 nm. Upon addition of the complementary PNA 63, significant changes in the electronic spectra could be observed in all cases.

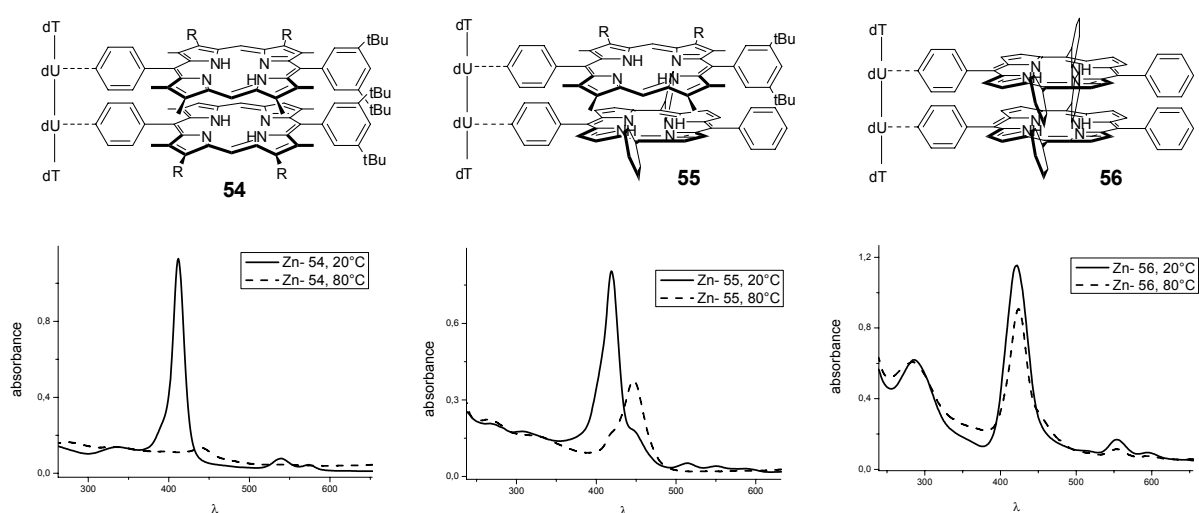


**Figure 44:** UV-vis spectra of the diporphyrin arrays **54-56** at 20°C and 80°C. Data are recorded in dichloroethane.

The UV-vis absorbance spectra of the single strand zinc diporphyrin arrays after heating are shown in figure 44. In order to compare the spectra, the tetramers solutions were heated and cooled down in the same condition as the equimolar mixture with the PNA. The absorbance maxima for Zn-56 decrease about 25%, in contrast to Zn-54 where no more absorbance is observed. We supposed that the compound Zn-54 was decomposed during the heating. This experiment was performed several times with fresh solutions, by changing the concentration and the UV cell length, but the results were the same. The absorbance

maximum for **Zn-55** decreases about 50% and is red-shifted about 28 nm. The value found is 447 nm. The same experiments have been done with the CD spectroscopy as shown in the following section.

The electronic ground state of the porphyrins change in the presence of the complementary PNA, especially for the **Zn-54**. The single strand tetramer **54** which decomposed upon heating, in the presence of the PNA, leads to a spectrum where  $\lambda_{\max}$  is red-shifted. We assumed that the duplex formed a more stable compound when it is heated up. Similarly, for **Zn-56** the duplex formed is more stable than the single strand tetramer with respect to the decomposition.

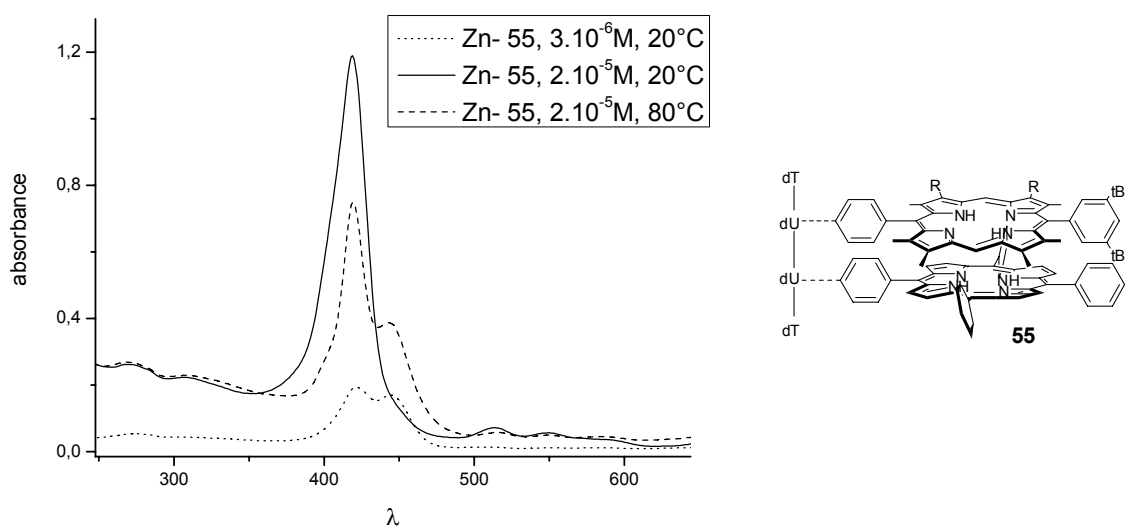


**Figure 45:** UV-vis spectra of the diporphyrin array **55** at 20°C and 80°C for  $c=3.10^{-6}$  M and  $c=2.10^{-5}$  M. Data are recorded in dichloroethane.

The UV-vis absorbance spectrum of the single strand **Zn-55** shows one maxima at 419 nm for a high concentration ( $c=2.10^{-5}$  M) which splits into two peaks at 423 and 445 nm for a lower concentration ( $c=3.10^{-6}$  M). This complex shows a different spectrum when the measurement is performed at higher temperature. For the higher concentration, a hypochromicity of 35% is observed at 80°C and a second smaller peak at 445 nm appears. At this point, there is no clear explanation for this observation.



	Temp.	B-band absorption		Q-band absorptions	
Zn-54	20°C	412 (5.34)		539 (4.24)	573 (4.04)
Zn-54+PNA	20°C	411 (5.04)		536 (4.05)	571 (3.88)
Zn-54+PNA	80°C	438 (4.83)	410(sh)	539 (3.92)	571 (3.83)
Zn-55	20°C	419 (4.70)		514 (3.51)	550 (3.40)
Zn-55+PNA	20°C	442 (4.65)	428(sh)	-	-
Zn-55+PNA	80°C	442 (4.59)		-	-
Zn-56	20°C	422 (5.52)		553 (4.74)	595 (4.57)
Zn-56+PNA	20°C	422 (5.48)		555 (4.65)	597 (4.45)
Zn-56+PNA	80°C	424 (5.39)		555 (4.34)	597 (4.09)

**Table 3:** UV-Vis absorbance data for the diporphyrin arrays **54** to **56**. Data are recorded in dichloroethane,  $c=1.6 \cdot 10^{-5}$  M for Zn-55,  $c=5 \cdot 10^{-6}$  M for Zn-54 and Zn-56,  $T = 20^\circ\text{C}$ .

## 4.8.2.2 Circular Dichroism Spectroscopy

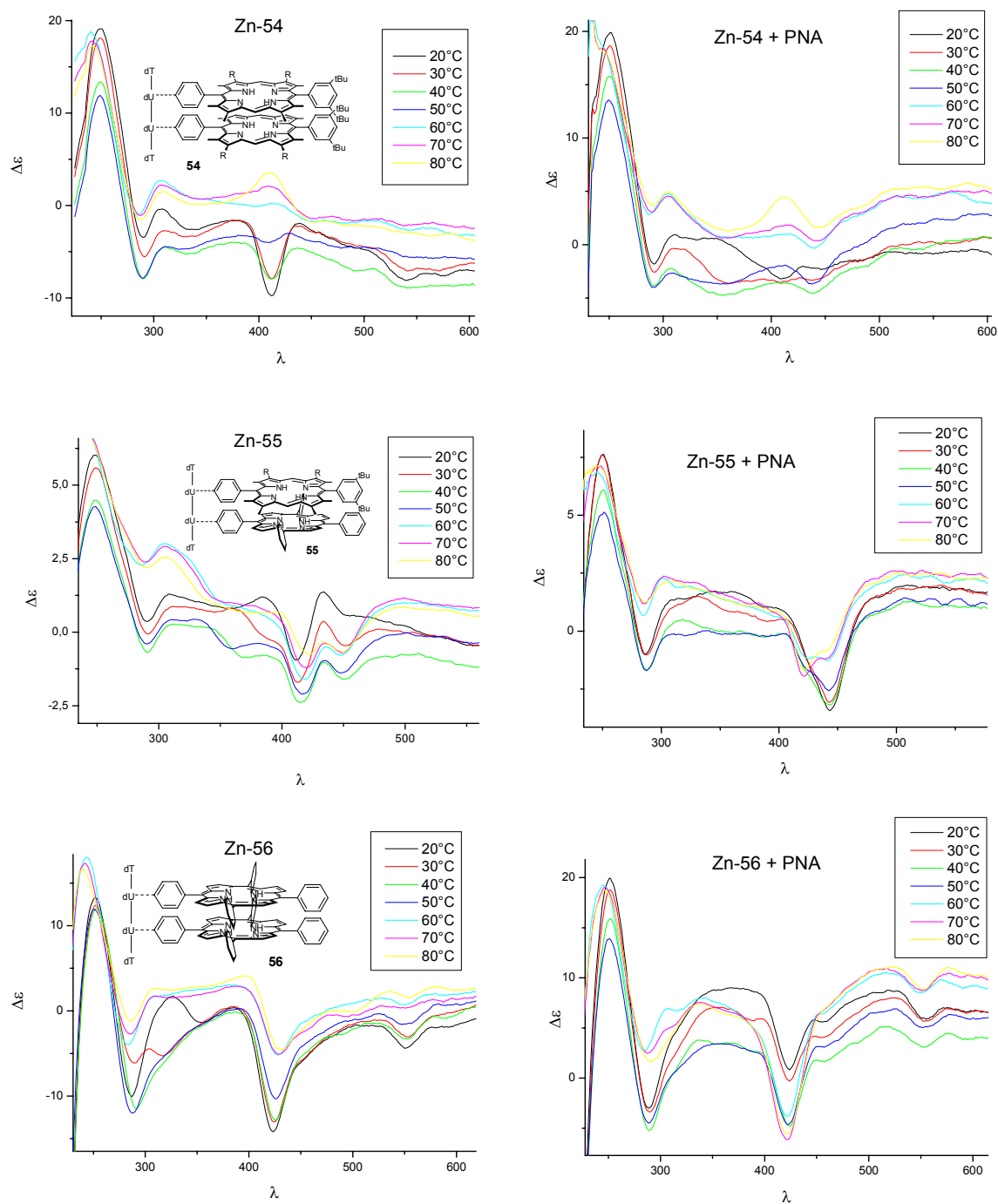


**Figure 46:** CD spectra of modified tetranucleotides **54-56**. Single stands (left) and double strands (right) from 20°C to 80°C.

The arrays were then analysed by CD spectroscopy in order to determine the structural changes upon dimerisation with the complementary PNA. The CD spectra of the arrays Zn-**54** to Zn-**56** are shown in figure 46. For the duplexes, the UV-regions of the CD spectra show the expected signal, the intensity double with the PNA addition. The spectra indicate ordered structures with respect to the oligonucleotide backbone.

Regarding the B-band region of the porphyrins, all three complexes show different spectra when the measurements were performed at higher temperature as shown in figure 46. The induced CD signal for the porphyrin in the B-band regions shows a weak negative peak at 424 nm for Zn-**56**, and at 412 nm for Zn-**54**. In Zn-**55** case, the spectrum indicates a bisignate CD signal with a negative peak at 412 nm and a positive peak at 433 nm. When the measurements were performed at higher temperature, this signal increased for Zn-**55** and decreased for Zn-**56** with a bathochromic shift of 6 nm. The most interesting effect is noticed for Zn-**54**, the negative peak becomes positive.

Upon addition of PNA, the spectra show a hypochromicity of 50% for Zn-**56** and a bathochromic shift of 31 nm for Zn-**55** on going from the single strand to the double strand at 20°C. At higher temperature, this signal increases for Zn-**56**, whereas it decreases for Zn-**55** and the broad negative peak at 443 nm split into two negative peaks at 421 and 439 nm. In Zn-**55** case, an additional bathochromic shift ( $\Delta\lambda=17$  nm) is measured. A hypochromicity (65 %) for Zn-**54** is observed, and the same effect as in the double strand at higher temperature is observed, the negative peak becomes positive.

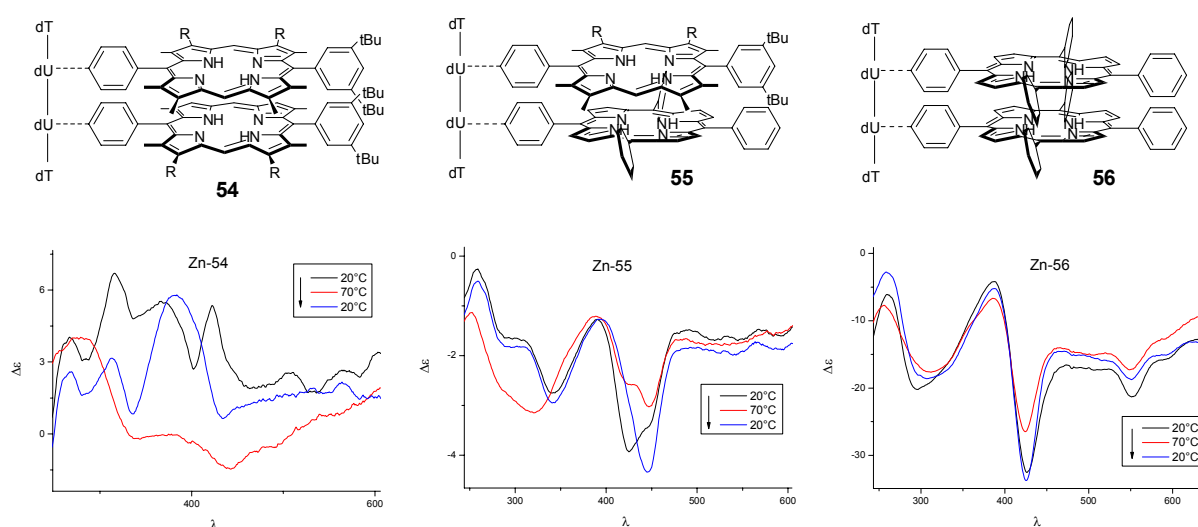


**Figure 47:** CD spectra of modified tetranucleotides **54-56**. Single stands at 20°C, heated at 80°C and cooled down at 20°C.

We are currently performing a detailed study of a diphenyl-tetraphenyl porphyrin hybrid system based on a tetranucleotide scaffold (**54** to **56**) using time- and energy-resolved laser spectroscopy. The tetranucleotide scaffold is used to make diporphyrin arrays of either homo porphyrinic or heteroporphyrinic composition. Preliminary results from laser photolysis show that energy transfer occurs from the diphenyl porphyrin, which acts as a donor, to the tetraphenyl porphyrin, which is the acceptor. No energy transfer is observed simply by mixing the individual porphyrins in solution, thus the DNA scaffold provides the close spatial arrangement necessary to induce the energy transfer. Though the electronic features of the donor and acceptor porphyrin do not differ greatly, the energy transfer is sufficient to proof the concept (manuscript in preparation).

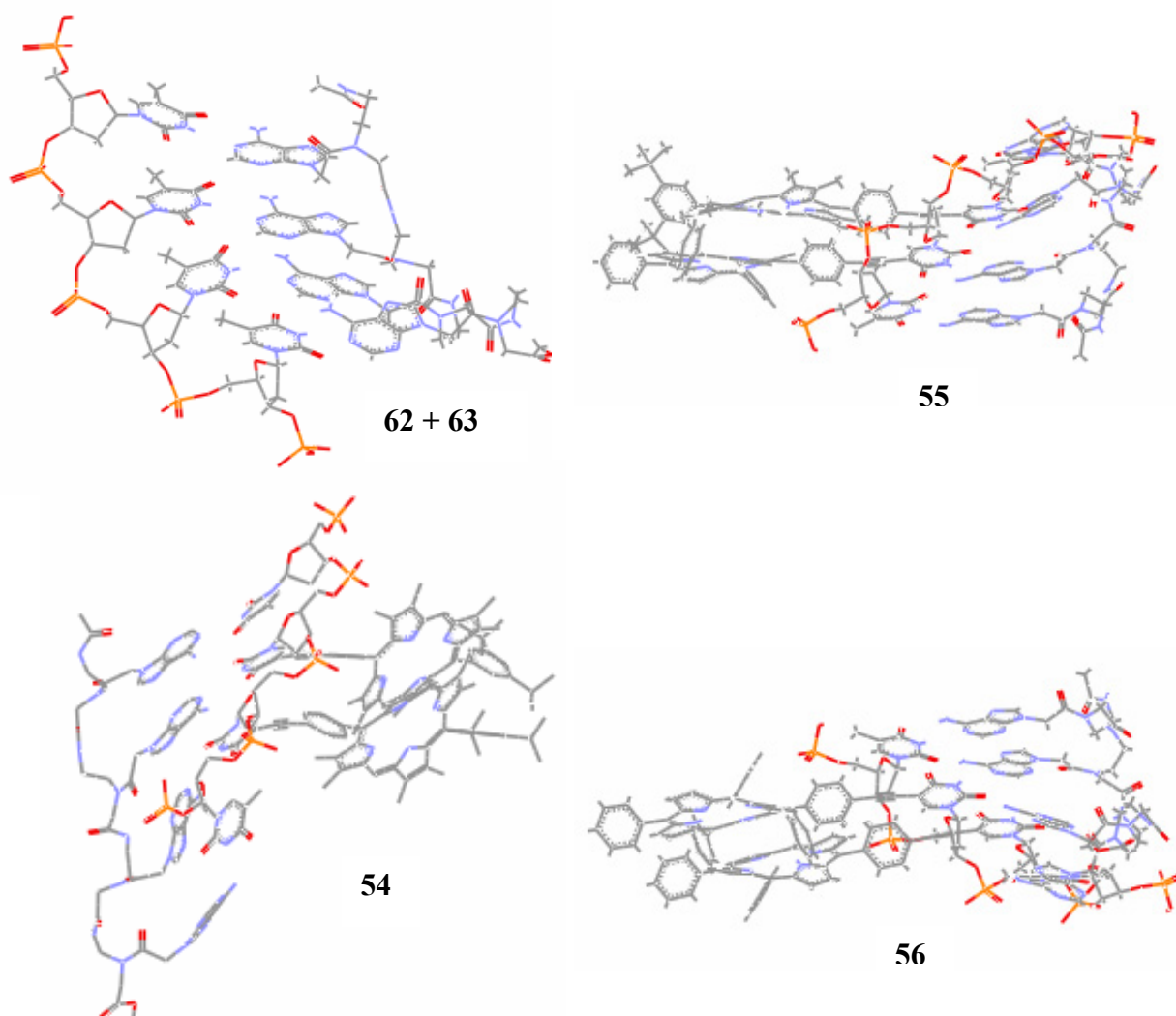


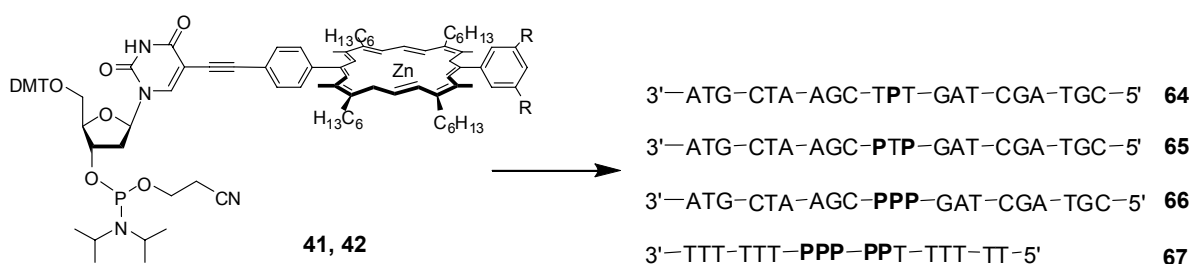
**Figure 48:** Force-field (AMBER\*, MacroModel) minimised structures of the tetramers with the PNA. (The cytosine bases are missing.)

The structure calculations of the modified tetramers **54-56** with PNA and the non-modified tetramers **63-64** were done by Dr Eugen Stulz (figure 48).

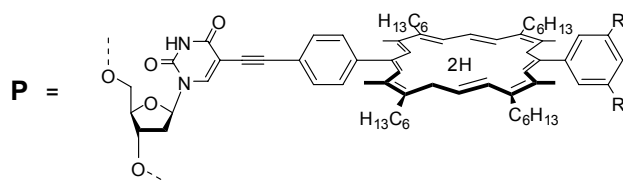
## 5 21-mer Oligonucleotides

We have shown in the previous chapter that the phosphodiester linkage of nucleotides is suitable to connect two different porphyrins which leads to an enhanced electronic interaction between the chromophores.<sup>[77, 92]</sup> The next step of this work is to further explore the use of longer oligonucleotides (ODN's) to create multiporphyrin arrays. We have performed more spectroscopic studies (absorption, emission and CD spectroscopy) to determine the influence of the porphyrin substitution on structure, the thermodynamic stability of the modified DNA, and to see whether the electronic properties of the porphyrins are altered upon placement in the major-groove of the double stranded DNA (dsDNA).

### 5.1 Synthesis

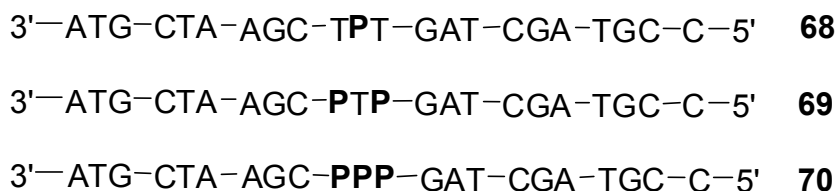


R = H, C(CH<sub>3</sub>)<sub>3</sub>



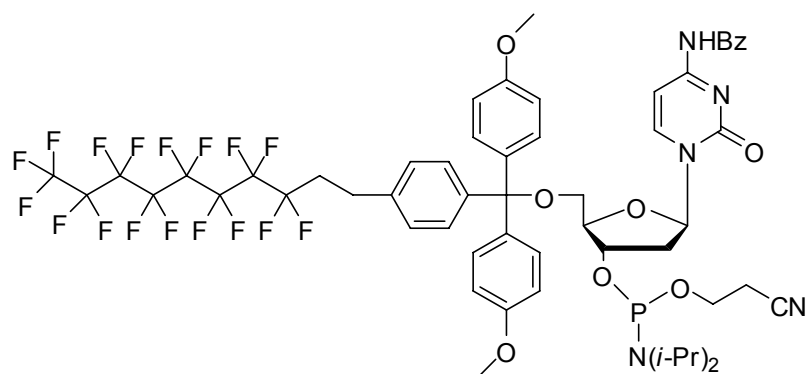
**Scheme 26:** Structure of the phosphoramidite building block and sequences of the DNA strands.

The diphenylporphyrin (DPP) derivatised phosphoramidite building blocks **41**, and **42**<sup>[92]</sup> were incorporated site specifically into longer oligo-deoxynucleotides (ODN's) **64-67** (scheme 26) using the standard solid phase automated DNA synthesis described in previous chapters. The nucleotides were synthesised on a 1.0  $\mu\text{mol}$  scale. The building blocks were incorporated site specifically into a 21-mer. It should be pointed out that either 41 or 42 was used; no mixed porphyrin strands were made. We incorporated first one central porphyrin, then two porphyrins separated by one thymidine, finally three, and five consecutive porphyrins. In a parallel project, using the tetraphenylporphyrin (TPP) derivatised phosphoramidite building block **45**, the same modified DNA strands were synthesised and up to eleven consecutive porphyrins were incorporated. The successful incorporation of different amounts of porphyrins in a row into the sequence shows that there seems to be no synthetic limitation in the amount of modifications per DNA strand. The synthesis was carried out in both trityl-OFF mode and trityl-ON mode. The solid phases were dried under argon and incubated overnight with 1 ml concentrated ammonium hydroxide at 45°C. The porphyrins are obtained in the free-base form and can be re-metallated by standard metallation procedure using  $\text{Zn}(\text{OAc})_2$  in  $\text{H}_2\text{O}$ .



**Scheme 27:** DNA strands sequences with the fluoros tag.

For oligonucleotides **69-70**, we introduced an additional oligonucleotide bearing a fluoros dimethoxytrityl (FDMT) group at the 5'-position ("FDMT-on synthesis") for the last coupling step with increasing the coupling time to 3 min. The 5'-*O*-FDMT-dC-phosphoramidite (scheme 27) was used as 0.1 M solution in acetonitrile for the installation of a single FDMT-on nucleotide (figure 49) at the 5' terminus, which was used for fluoros affinity chromatography purification.

FDMT-N<sup>4</sup>-Bz-dC CEP**Figure 49:** 5'-O-FDMT-dC-phosphoramidite.

## 5.2 DNA Strands Purifications

Different approaches were made to find the appropriate method for a successful purification. Using standard methods like HPLC, column chromatography (silica or sephadex) or gel electrophoresis gave no pure material. Finally, all the strands were purified by recognition of the complementary strand on solid support or by Prof. Bannwarth's method of fluoruous affinity chromatography which lead to a satisfying purification.

### 5.2.1 Purification *via* Solid Support

**65** 3' - ATG - CTA - AGC - **PTP** - GAT - CGA - TGC - 5'

**71** 5' - TAC - GAT - TCG - AAA - CTA - GCT - ACG - TTT - TA ——— 

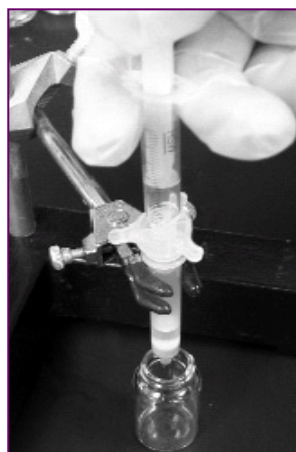
Spaceur

**OAS**

**Figure 50:** Sequence of DNA strand on OAS for DNA purification.

The complementary strand **71** was synthesized on oligo affinity support (OAS) which uses a polystyrene bead. In contrast to CPG (controlled pore glass), the base deprotection was achieved using ammonium hydroxide without cleaving the strand from the resin. The attachment to the support is through the N<sup>6</sup>-position of Adenosine and the oligonucleotide can only be cleaved specifically from the support by periodate oxidation followed by  $\beta$ -elimination to yield the 3'-phosphate. Then, the purification of the modified DNA strand was done by hybridizing with the complementary strand in PTT buffer at 80°C for 10 min, and then slowly cooled down to 4°C. After washing the OAS with water, the desired pure strand was cleaved with methanol.

### 5.2.2 Purification *via* Fluorous Purification System



Using Prof. Bannwarth's method for oligonucleotide purification, the introduced fluororous tag allows the tagged oligonucleotide to be selectively retained on the Fluoro-Pak™ column. The affinity of the fluororous tag on the oligonucleotide for the Fluoro-Pak™ adsorbent is high, much higher than the affinity of a DMT group for an RP adsorbent. The non-fluorous components of the mixture are less well retained than they would be with normal RP adsorbents. Without removing the ammonia used in the deblocking step, the crude deprotected FDMT-on oligonucleotide was passed through the column. The fluororous purification system, in a solid-phase extraction (SPE) mode, promotes complete adsorption of the fluororous-tagged oligonucleotide onto the column, which allows non-fluorous impurities to be washed away. Removal of the fluororous tag with diluted TFA, affords the desired oligonucleotide. To quantify the final oligonucleotide, we determined the optical density at 260 nm.



### 5.3 UV-Visible Spectroscopy

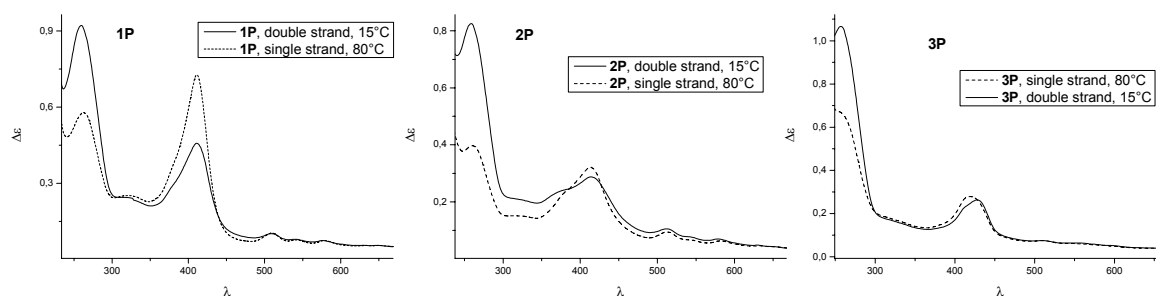


**Figure 51:** UV-vis spectra of X in the dsDNA-form (black) and ssDNA (red); dsDNA at 15°C, ssDNA at 80°C.

The electronic absorption spectra show that the total porphyrin absorbance decreases with increasing the amount of porphyrin modification per DNA strand. The spectra do not change immediately after mixing of the porphyrin-DNA with the complementary strand at ambient temperature, but when the system is heated up to 80°C, and cooled down to 15°C, a substantial increase in absorbance occurs.

In the multi-porphyrin modified strands, a substantial broadening of the porphyrin B-band absorption at ~410 nm indicates electronic interactions between the chromophores. The interactions are present even if the porphyrins are separated by a non-modified nucleotide. The figure 51 shows the single strand ss-**1P**, ss-**2P** and ss-**3P** at 80°C when the bases become unstacked, the wavelength of maxima absorbance does not change but a hyperchromicity of 10% is observed compared to the single strands at 15°C. An additional small bathochromic shift ( $\Delta\lambda = 3$  nm) is measured in ss-**3P** case.

When the UV-vis spectra of the single strand are recorded at 80°C, the spectrum of **3P** shows the same absorption coefficient with a red-shift of 10 nm compared to ds-**3P**. The porphyrin B-band absorption shows a hyperchromicity of 12% and 40% for **2P** and **1P**, respectively. But the largest change occurring in ds-**2P** at 15°C, the absorbance maximum at 414 nm becomes two maxima at 414 and 371 nm. The interactions between the two porphyrins seem to be stronger in the double strand. In the dsDNA at 15°C and in the ssDNA at 80°C, the porphyrin extinction coefficient decreases linearly from **1P** to **3P**.

The structure calculations of the 21-mer oligonucleotides substituted by one, two and three porphyrins (figure 52) were done by Dr Eugen Stulz.

ODN-Strand	Temp.	absorption maxima [nm (lgε)]
ss- <b>1P</b>	80°C	411 (5.21)
ds- <b>1P</b>	20°C	411 (5.41)
ss- <b>2P</b>	80°C	370 (sh), 414 (5.11)
ds- <b>2P</b>	20°C	413 (5.16)
ss- <b>3P</b>	80°C	428 (4.90)
ds- <b>3P</b>	20°C	428 (4.92)

**Table 4:** UV-Vis absorbance data for the modified single strand and double strands. Data are recorded in PTT buffer. For **1P**,  $c = 2.8 \cdot 10^{-6}$  M, for **2P**,  $c = 2.2 \cdot 10^{-6}$  M and for **3P**,  $c = 3.3 \cdot 10^{-6}$  M.

## 5.4 Circular Dichroism Spectroscopy

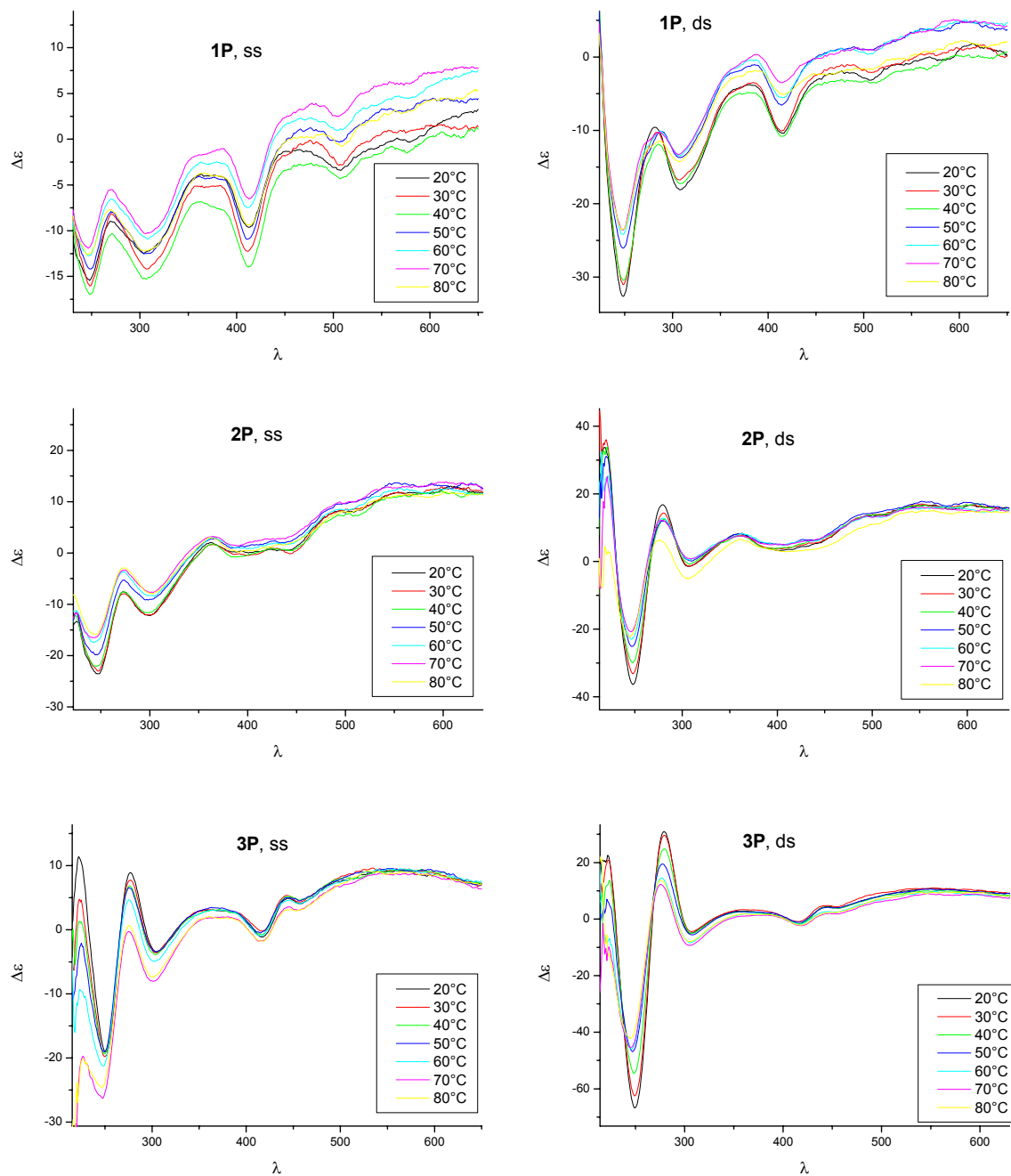


**Figure 53:** CD spectra of modified porphyrin-DNA arrays **1P-3P**. Single strands on the left and double strands on the right.

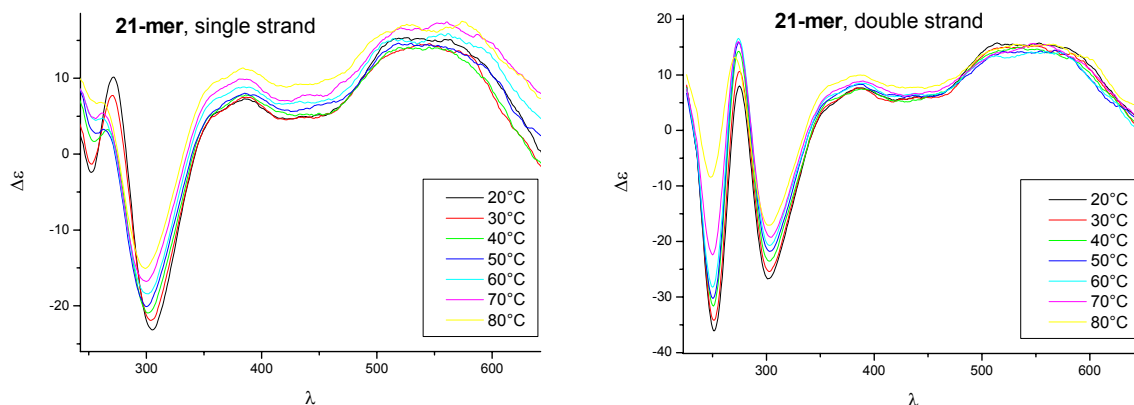


**Figure 54:** CD spectra of unmodified 21-mer.

The CD spectra of strands **1P-3P** shows features of B-type DNA for all strands with a bisignate CD profile (figure 53). Also for the single stranded forms, the base stacking increases substantially compared to the natural DNA (figure 54), even when measured at higher temperatures. The spectra of single strands show an increase in the 250 nm signal with increasing the amount of porphyrin modifications. The induced CD signal for the porphyrin in the B-band region shows a relatively broad signal for **2P** and a negative peak at 416 nm for **1P**. In the case of **3P**, the spectrum indicated a bisignate CD profile which could be interpreted by a major groove stacking of the porphyrins in the double strand.<sup>[93]</sup> This is in contrast to the spectra of **1P** and **2P**. The previously analysed building block **37** gave an induced negative signal as well.

Normally, a negative induced signal indicates intercalation of the porphyrin within the base-stacking of the DNA. This, however, is not a feasible alternative structure. Firstly, the porphyrins are covalently attached to the nucleobase, and intercalation would have to be accompanied by base flipping of the uridine. The porphyrin then cannot be accommodated in the DNA unless the adjacent base is also flipped out. Secondly, the linker would dictate the porphyrin into a position where severe steric clashes with the complementary strand would occur. Thus, a much larger destabilisation of the dsDNA would be expected as is measured. Steric effects also play a crucial role in tetra-aryl porphyrin intercalation and do not favour this structure. In addition, the melting experiments with the mismatched complementary strand support hydrogen bonding in the system. Thus, the negative induced signal can only be explained by the intrinsic properties of the array. It seems that the acetylene linker<sup>[94]</sup> inhibits the chiral perturbation which the DNA should transfer onto the porphyrin B-band. Even

---

though the porphyrins interact with each other electronically (see below), their electronic environment is only locally perturbed by the chiral deoxyribose, leading to a negative Cotton effect within the B-band region, as seen in the CD spectra. The building blocks themselves give rise to a strong negative induced CD signal, and also tetranucleotides with two tetraphenyl porphyrins show the same spectral characteristics. It seems that in our case induced CD spectroscopy is not applicable for structure determination as compared to non-covalent DNA-porphyrin and DNA-drug interactions, or where the chromophore is attached to the DNA via sp<sup>3</sup>-carbon containing linkers.

## 5.5 Melting temperature

Thermal denaturing experiments of the porphyrin-DNA duplexes were measured using CD spectroscopy. The porphyrins incorporated into the DNA strand destabilized the duplex. The ODN with one central porphyrin shows a melting temperature of 42.4 °C compared to the unmodified DNA strand with a higher one (63.5 °C). The ODN, which contains two porphyrins, shows a lower melting temperature of 37.1 °C; here, the destabilisation effect of the duplex increases. But the incorporation of the three consecutive porphyrins increases the melting temperature to 41.6 °C; this system seems to stabilise the porphyrin-DNA duplexes, due to the hydrophobic interactions between the porphyrins. For ODN **3P**, the melting temperature, obtained with CD spectroscopy (41.6 °C) is approximately the same as obtained with the UV-vis peltier machine (42.2 °C). The CD measurements therefore give an accurate  $T_m$  value.

ODN- strand	Conc. (mol/l)	$\epsilon$ (calc.)	$T_m$ [°C] by CD	$T_m$ [°C] by UV
<b>21-mer</b>	$5 \cdot 10^{-6}$ M	207 000	65	63.5
<b>1P</b>	$2.8 \cdot 10^{-6}$ M	198 904	42.4	-
<b>2P</b>	$2.2 \cdot 10^{-6}$ M	195 708	37.1	-
<b>3P</b>	$3.3 \cdot 10^{-6}$ M	193 112	41.6	42.2

**Table 5:** Melting temperatures of ODN's in PTT buffer (500 mM NaCl, 50 mM  $\text{KH}_2\text{PO}_4$ , pH 7.0).  $T_m$ : melting temperature of the duplex with the complementary strand.

## 5.6 On-bead hybridisation

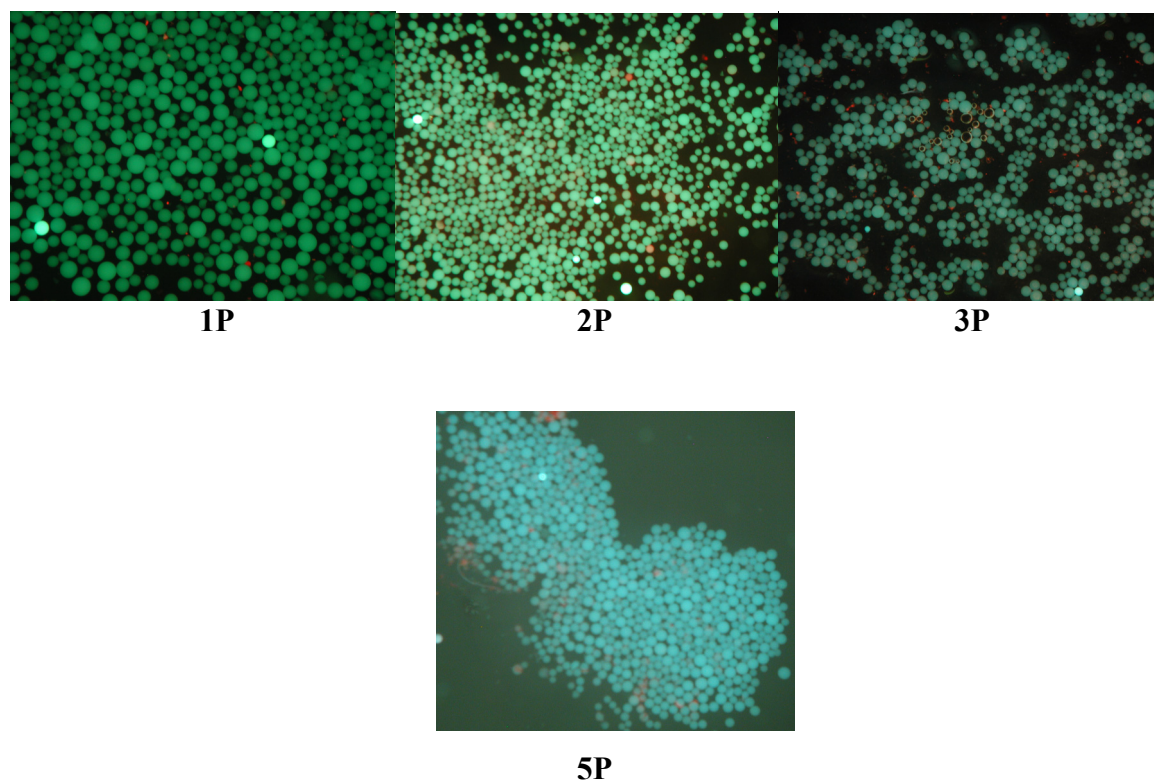


**Figure 55:** Hybridization of OAS with the modified DNA-strand using the BV filter.

After hybridizing with the complementary strand in PTT buffer (chapter 5.2.1), the DNA strands were kept on the oligo affinity support (OAS). The beads were washed with water and suspended in TEAA buffer to be observed under the microscope using the BV filter (excitation at 400-440 nm, emission at 475 nm). In the case of the **1P**, **2P**, **3P**, and **5P**, the beads were found to be fluorescent. These measurements were done a second time in water and gave the same results. This study shows the possibility to attach the porphyrins to beads *via* a non-covalent binding mode.





## 6 Summary and outlook

### 6.1 Summary

In conclusion, we have shown a general route to porphyrin modified uridine and deoxyuridine, where the substitution pattern and the metallation state of the porphyrin are variable without affecting the synthetic route and the solubility can be tuned by varying the substituents on the porphyrins.

Then, we have presented the synthesis of porphyrin dimers based on dinucleotide formation, where the building blocks are connected through a phosphate diester backbone in analogy to the natural DNA structure. The general route to substituted nucleosides *via* Sonogashira coupling allows introduction of a much larger diversity of structurally different porphyrins, and the mode of connection is independent of the substitution pattern of the porphyrin. Both solution and solid phase synthesis can be applied, and by varying the building blocks the composition of the dimer can be chosen. In this case, the solid support synthesis is advantageous due to the much easier purification of the product, even if the yield was low. Both UV-vis spectroscopy and mass spectrometry reveal that the presence of two consecutive porphyrins does not hinder the specific recognition of the complementary nucleobase.

The oligonucleotide backbone was shown to be a suitable template for the synthesis of both homo- and heteroporphyrinic diporphyrin arrays. We have shown that the electronic ground state properties of the porphyrins are largely unaffected upon incorporation into the oligonucleotide when measured in organic solvents. But the excited state is strongly influenced by the presence or absence of a neighbouring porphyrin, and electronic interactions occur depending on the structure of the adjacent porphyrin. The photophysical properties of the diporphyrin array can therefore be tuned simply by reprogramming the sequence of the incorporated building blocks. There was no spectroscopic evidence for the formation of any duplex with the complementary tetra-adenosine; this is also supported by the fact that the  $^1\text{H}$  NMR spectra of the mixtures are represented by a superposition of the individual  $^1\text{H}$  NMR spectra under different conditions. But the use of PNA, as neutral complementary strand, leads to a duplex formation. Both CD and UV-vis spectroscopy indicate an interaction between the two strands which is different with the three tetramers. Especially with the tetramer **54**, no decomposition was observed in presence of PNA when the temperature was increased.

Finally, we have incorporated different amount of porphyrin in a 21-mer DNA strand, which indicate that the backbone of natural DNA can be used to sequence specifically assemble porphyrin, leading to new stacked arrays on the nanometre scale. The synthesis of new strands in combination with other porphyrins and more detailed spectroscopic evaluations are currently under way, i.e. evaluation of energy or electron transport for which this system is a promising candidate. DNA will certainly lead to new functional molecules on the nanometre scale when substituted with a diversity of electronically active molecules such as porphyrins, transition metal complexes or amino acid side-chain derived groups which we anticipate in future.

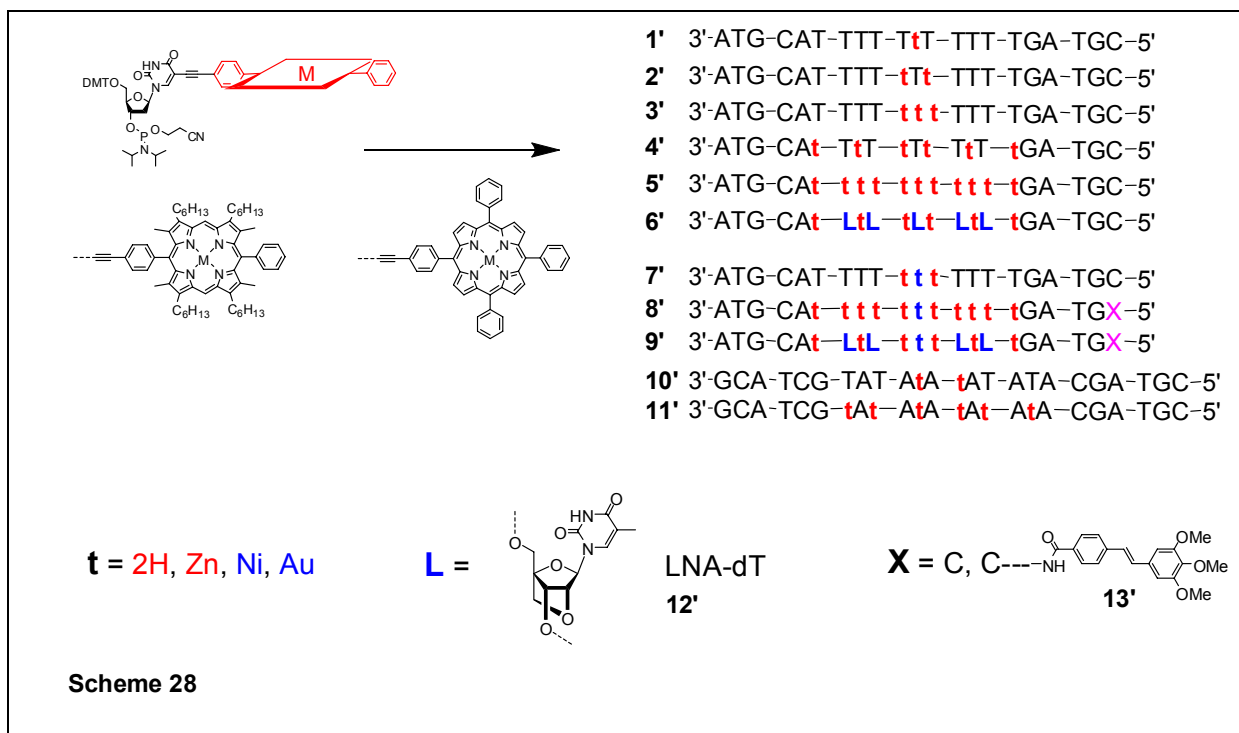
## 6.2 Outlook

The next steps of this project is divided into four stages: i) synthesis of specific DNA porphyrin sequences for structure and physical analysis; ii) evaluation of the constructs for structure and energy and/or electron transfer; iii) study of the arrays towards their ability to function as electronic wires in artificial membranes and between nano-gaps (part iv). The results of the two first parts will be used to design the exact composition of the final porphyrin arrays for the desired purpose. To achieve the goals, the following strategic tasks are planned.

### 6.2.1 Synthesis of DNA porphyrin arrays for structural studies

To obtain a better understanding of the structural aspects of the modified DNA and physical properties of the porphyrin arrays, a set of ODN's (**1'** to **5'**) with various amounts of porphyrins will be synthesised, which is different from our first DNA strands (Scheme 2). This will allow a more precise analysis of the impact of the porphyrin substituents on the stability and structure of the dsDNA. The introduction of mismatches in the complementary strand is necessary to proof the base-pairing ability of the modified nucleotide. In this part, other modifications of the DNA to obtain more stable duplexes will be introduced (ODN's **6'**, **8'** to **9'**). These include the use of LNA-nucleotides (**12'**)<sup>[95-97]</sup> and capping nucleotides such as stilbenes (**25**).<sup>[98, 99]</sup> The use of peptide nucleic acids (PNA) as complementary strand was

shown to greatly stabilise the duplex in DNA-PNA hybrids.<sup>[100, 101]</sup> This will also be applied to our system, and two different approaches are anticipated. A complementary strand comprising of only PNA units will show whether the porphyrin-DNA part can form DNA (porphyrin)-PNA hetero-duplexes of similar thermodynamic stability as natural DNA-PNA hetero-duplexes. The use of a PNA-DNA(porphyrin)-PNA hybrid system will be used to determine whether the stability of the flanking sequences of the porphyrin array alters the overall physical properties of the chromophore system. All the porphyrin arrays described will be thoroughly studied using absorption and emission spectroscopy (steady state and time resolved, in collaboration with Dr Pavlos Lagoudakis, Southampton), and CD spectroscopy. If applicable, the use of NMR spectroscopy and X-ray crystallography is anticipated to determine the structure of the arrays. The arrays will also be adsorbed on surfaces and analysed using AFM and STM techniques (in collaboration with Dr Iris Nandhakumar, School of Chemistry, Southampton). Cyclic voltammetry studies and EHMO calculations can be performed at Southampton and in the laboratories of Dr Fabrizia de Biani (Siena, Italy). A further strategically important system to be studied in this part is a self-complementary strand. Here, in the duplex the alternating porphyrin units will be on adjacent strands (ODN's **10'** and **11'**) so that the same porphyrin array is obtained as with the DNA-DNA(porphyrin) system. This study is necessary to determine whether the substituents can be attached to complementary strands and the functional molecule is obtained by hybridisation (see also part below).



## 6.2.2 Synthesis of Donor-Acceptor systems

Time resolved fluorescence spectroscopy will be performed to study the energy transfer mechanisms and efficiencies between the porphyrin units. The photophysical analysis will be done by Dr Pavlos Lagoudakis who has the required instrumentation to undertake these studies. For this purpose, either Ni(II) or Au(II) porphyrins as central unit will be incorporated into the arrays (Scheme 28). With these systems, either quenching of the fluorescence (nickel) or enhancement of the fluorescence (gold) is expected giving better access to the rates and quantum yields of the energy transfer. Whether or not LNA nucleotides, capping reagents or different counter strands will be used is depending on the outcome of part a). In addition to changing the central metal of the porphyrin, we will also use different porphyrin structures (DPP or TPP) to study the electronic interactions in the arrays. As we have observed with the mixed porphyrin arrays, energy transfer from one porphyrin to another is possible. Since the efficiency of energy transfer between porphyrins of the same metallation state is not very efficient, the combination of porphyrins containing different central metals will be much more informative due to the enhanced quantum yield of the

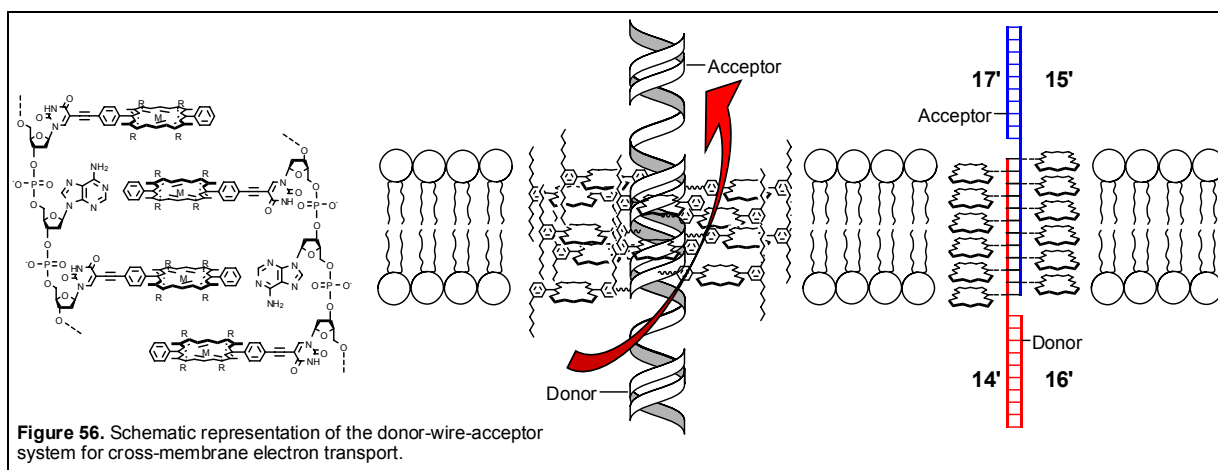
energy transfer. With the results obtained in this part of the project we will be able to design the best system for the applications in energy and electron transfer (see below).

### 6.2.3 Synthesis of electronic wires for charge separation through artificial membranes

The incorporation of up to eleven porphyrins into the DNA strand has already been achieved. Assuming a dsDNA structure which is not too far away from the natural DNA this means that we have a porphyrin array of  $\sim 4$  nm at hand. This length is sufficient to span a lipid bilayer similar in size to a cellular membrane. Aim of this part of the project is to incorporate the conjugates within the membrane of either phospholipid vesicles or within a membrane which separates two compartments in order to obtain functionalized polymolecular assemblies that will allow the transport of electron across the bilayers.<sup>[15, 102, 103]</sup> The conjugates will have at one end an electron acceptor and on the other end an electron donor, as schematically shown in Figure 2. Attachment of alkyl chains to the *meso*-phenyl group of the porphyrin may be necessary to direct the porphyrins into the lipid bilayer and for orienting the units appropriately. The functional membranes, for example based on 1-palmitoyl-2-oleoyl-sn-glycero-3-phosphocholine (POP),<sup>[104]</sup> will be prepared and characterized by dynamic light scattering, electron microscopy, absorption and emission spectroscopy and possibly NMR spectroscopy, in collaboration with Prof. Peter Walde (ETHZ, Switzerland).

The specific composition of the porphyrin array for the cross-membrane electronic molecular wire will strongly depend on the outcome of the studies of parts a) and b). So far, the following design is anticipated: two DNA strands of the sequence  $(dX)_{15}(dU^{\text{Porph}}dA)_6$  (**14** and **15'**) will be synthesised, where the dX-sequence is non-identical in the two strands. The alternating sequences  $(dU^{\text{Porph}}dA)_6$  of the two strands will then be hybridised within the lipid bilayer. If the self-complementarity in the sequences proves problematic, the formation of homo-duplexes may be prevented by extending the  $dU^{\text{Porph}}dA$ -sequence by a few nucleotides with a different sequence in **14'** and **15'**. This approach has advantages over the synthesis of a DNA strand having the full length of the porphyrin array: i) the shorter overall length of the DNA and the smaller amount of porphyrins which are separated by an unmodified nucleotide predicts an increase in the yield of the DNA synthesis and should facilitate the purification of the porphyrin-DNA; ii) the hydrophobic porphyrin modification should be a driving force to

direct this part of the DNA into the lipid bilayer, thus the two strands **14'** and **15'** can be added from the opposite side and hybridise within the bilayer; iii) the remaining unmodified sequences of the DNA will be directed into the aqueous environment and can be used to attach complementary strands which are modified with either electron donor (e.g. boron-dipyrin, ferrocene; strand **16'**) or acceptor (e.g. anthraquinone, pyrromellitimide; strand **17'**) moieties.<sup>[105-107]</sup> The donor and acceptor units can be placed at various distances to the electronic wire. To additionally improve the photoinduced electron transfer, the donor site can contain viologens and the acceptor site NADH or analogues thereof. The project will focus on the use of DPP and TPP, either in the free base or metallated form, to create the wire (the two-strand approach would also allow to have an alternating free base-metallo porphyrin array). The diphenyl porphyrin is expected to have  $\pi$ - $\pi$ -overlap of about 5-10 % between the individual building blocks in the double helix, thus behaving as an extended  $\pi$ -conjugated system along the periphery of the DNA. The tetraphenyl porphyrin, on the other hand, will not do so, which could have a profound impact on the electron transfer capability of the wire. The conjugates will serve as a system to study the electron transfer in multiporphyrin systems in a hydrophobic environment that will help to stabilise the photophysically active units in analogy to the natural antenna complex of the photosynthetic system, and create a system capable of charge separation upon photo-irradiation.









## **Experimental Part**



## 7 General experimental conditions

### 7.1 Reaction instruments and physical data

#### Nucleic acid synthesizer

Device: PerSeptive Biosystems Expedite 8909 nucleic acid synthesis system. The DNA synthesis related chemicals were supplied by Glen Research. For this work, only 500 Å pore CPG columns were used.

#### <sup>1</sup>H NMR spectroscopy

Devices: Varian Gemini VXR400 (400 MHz), Bruker dpx500 (500 MHz). Chemical shifts ( $\delta$ ) are indicated in ppm, relative to SiMe<sub>4</sub> ( $\delta = 0.00$ ) or based on the solvent signals of the partially deuterated nuclei of chloroform-d<sub>1</sub> ( $\delta = 7.26$  ppm), dimethylsulfoxid-d<sub>6</sub> ( $\delta = 2.50$  ppm) or methanol-d<sub>4</sub> ( $\delta = 3.31$  ppm). All spectra are interpreted by first order Fourier transformation and the coupling constants ( $J$ ) were given in Hertz (Hz). The signals were abbreviated as followed: s = singlet, d = doublet, t = triplet, q = quartet, m = multiplet. All solvents were provided by Cambridge Isotope Laboratories, Inc..

#### <sup>13</sup>C NMR spectroscopy

Devices: : Varian Gemini VXR400 (101 MHz), Bruker dpx500 (125 MHz). Chemical shifts ( $\delta$ ) are indicated in ppm and are relative to the following solvent signals: chloroform-d<sub>1</sub> ( $\delta = 77.0$ ). The spectra were broad-band proton decoupled; the classification of the signals was achieved by APT or DEPT.

### **<sup>31</sup>P NMR spectroscopy**

Devices: Bruker dpx400 (162.0 MHz). Chemical shifts ( $\delta$ ) are indicated in ppm and are relative to the spectra reference of an external standard of triphenylphosphate in chloroform ( $\delta = -18$ ). The spectra were broad-band proton decoupled.

### **UV-Vis and fluorescence spectroscopy**

Devices: Perkin-Elmer Bio-Lambda II spectrometer, featuring a PTP-6 Peltier unit and FluoroMax-2. Molar extinction coefficients ( $\epsilon_M$ ) are referred to a cell path of 1 cm at 260 nm for oligonucleotides and at 420 nm for porphyrins. The background was done with appropriate solvent before measurement.

### **Melting points**

Devices: Büchi 530 and Hund Wetzlar V200. The melting points are given in degrees centigrades [ $^{\circ}\text{C}$ ] and are uncorrected.

### **Circular dichroism spectroscopy**

Device: Chirascan Circular Dichroism Spectrometer, 150 W Xe arc, air cooled. The ellipticity is referred to a cell path of 1 cm and the data were collected from 650 nm to 200 nm (1s/nm). The data was given in mdeg and corrected to delta epsilon using the formula:

$$\Delta\epsilon = \theta / (10 \times \text{conc} \times \text{pathlength} \times 3298)$$

Molar ellipticity ( $\theta$ ) = 3298  $\Delta\epsilon$

$\Delta\epsilon = \theta / (10 \times \text{conc} \times \text{pathlength} \times 3298)$

ellipticity ( $\theta$ ) is as measured by the instrument in mdeg

conc is in mol/litre

pathlength is in centimetres.

## Fluorescence microscopy

Devices: Olympus Microscope SZX12, and Olympus Camera Camedia C-3000 Zoom. The Microscope was used with three different filters:

Filter	Excitation	Emission
BU	330-385	420
U	400-440	475
GFPA	460-490	510-550

## MALDI-TOF mass spectroscopy (Matrix-assisted Laser Desorption Ionization Time-of-Flight)

Device: Perseptive Biosystems Voyager-DE PRO. The spectrometer was run in linear mode at 25 KV acceleration voltages for both positive and negative ions. Probes desorption and ionisation was induced by a N2-LASER (337 nm, 3 ns pulses, 0.2 mJ per pulse, and acquisition of 10 to 100 pulses). The signals are referred to the unfragmented, single charged molecule ions  $[M-H]^-$  and  $[M+H]^+$ . The data are given in mass units per charge (m/z).

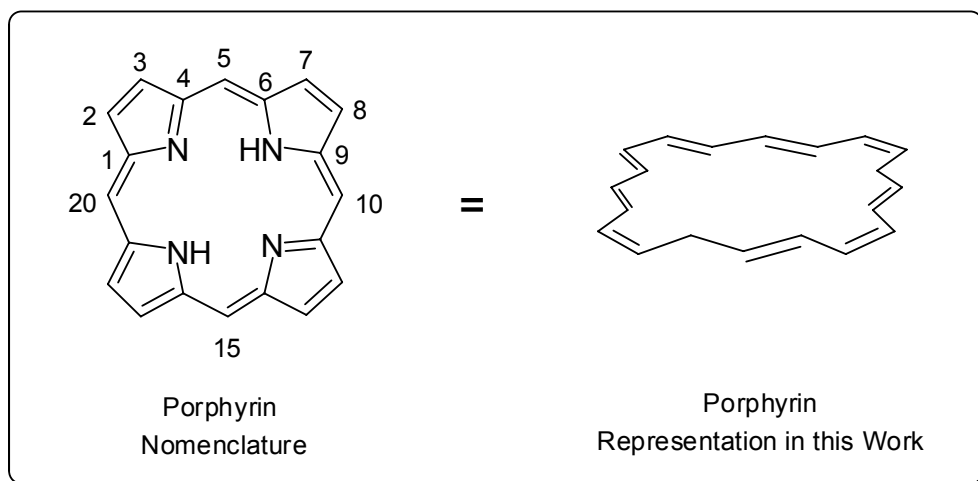
### Matrix preparation for Maldi-Tof

- **Matrix A:** 2-4 mg p-nitroaniline was dissolved in 0.2 ml DCM.
- **Matrix B:** 0.6 ml of solution 1 was mixed with 0.3 ml of solution 2:
  - Solution 1: 2-4 mg 2,6-dihydroxyacetophenone was dissolved in 1 ml MeCN/H<sub>2</sub>O.
  - Solution 2: a 0.5 M solution of ammoniumtartrate (92 mg in 1 ml H<sub>2</sub>O) was prepared.
- **Matrix C:** 2-4 mg sinapinic acid was dissolved in 0.2 ml acetonitrile/water or acetonitrile/0.1% TFA.

- **Matrix D:** a saturated solution of 3-hydroxypicolinic acid (139.1 g/mol) in acetonitrile/water was prepared.

## 7.2 Assignment of protons in the $^1\text{H}$ NMR spectra

### Porphyrin nomenclature

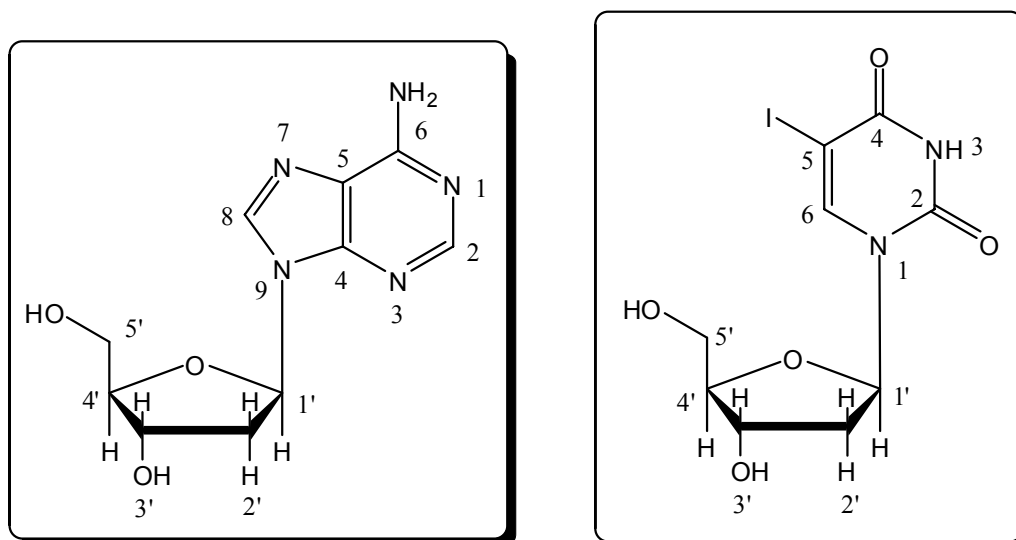


**Scheme 29:** Nomenclature of the porphyrin.

The nomenclature as shown above is normally used in the literature. The positions 5, 10, 15 and 20 are referred as meso-position. In this work, we represented the porphyrin as described in scheme 29. The protons in the  $^1\text{H}$  NMR spectra were numbered in the same way as the related carbon atoms.

### Numbering of the nuclei

The protons in the  $^1\text{H}$  NMR spectra are numbered the same as the related carbon atoms. Atoms within the sugar backbone of the nucleotides are marked by an additional prime. If geminal hydrogen atoms show distinguished signals, the high-field and the low-field shifted nuclei are set apart by an additional “a” or “b”, respectively. Scheme 30 demonstrates the numbering of the atoms in 2'-deoxyadenosine and 5-Iodouracil.



**Scheme 30:** Nomenclature of the 2'-deoxyadenosine and 5-Iodouracil.

### 7.3 Separation and purification methods

#### Thin layer chromatography (TLC)

The reactions were monitored by TLC using Merck silica gel 60 F<sub>254</sub> aluminium sheets (0.2 mm layer). The compounds were detected by two subsequent procedures:

1. fluorescence quenching detection at 254 nm,
2. dipping into a solution consisting of:
  - a) Cerium sulphate, or
  - c) 15% H<sub>2</sub>SO<sub>4</sub> in methanol, or
  - d) Potassium permanganate,

followed by heating.

The compounds containing porphyrins were detected by fluorescence quenching detection at 366 nm.

TLC retention factors ( $R_f$ ) were indicated together with the appropriate solvent mixture.

### **Flash column chromatography (FC)**

Flash column chromatography was performed on silica gel Fluka 60 (40–63  $\mu\text{m}$ ). The solvents used were of technical grade and were re-distilled prior to use. The mixture ratios of solvents were referred to the parts of the volume.

### **High performance liquid chromatography (HPLC)**

Devices: Hewlett-Packard 1050 chromatograph, Kontron Instruments, and Thermo Finnigan Spectra System with UV detection at 260 nm. Columns for reversed-phase HPLC: Merck (VWR) LiChroSpher 100 (RP-18e, 5  $\mu\text{m}$ , 250 x 4 mm, Flow: 1.0  $\text{ml min}^{-1}$ ) and Merck (VWR) LiChroSpher 100 (RP-18e, 10  $\mu\text{m}$ , 250 x 10 mm, Flow: 7.5  $\text{ml min}^{-1}$ ). Solvents used were acetonitrile HPLC grade (Fisher scientific), Methanol HPLC analysed (J.T.Baker), 0.1 M aqueous TEAA (solution purchased as 1.0 M stock solution from Fluka and diluted by 9 parts of nanopure water prior to use), 0.1 M aqueous TEAA with 1% acetonitrile, and 1 mM aqueous TFA (J.T.Baker).

### **Size exclusion chromatography (Gel Permeation) of oligonucleotides and building blocks**

The compounds were purified using the appropriate column's size and sephadex:

- Sephadex (Sigma-Aldrich, dry bead diameter: 40-120  $\mu\text{m}$ ) G10 ( $M_w > 700$ ), G15 ( $M_w > 1500$ ), and G25 ( $1\text{K} < M_w < 5\text{K}$ ) were used with  $\text{H}_2\text{O}/\text{MeOH}$  (1:1) as eluent.
- Lipophilic Sephadex (Sigma-Aldrich) LH 20 (dry bead diameter: 25-100  $\mu\text{m}$ ) was used with  $\text{DCM}/\text{MeOH}$  (1:1) as eluent.



## **7.4 Further Instruments**

### **Centrifuge, thermomixer and vortexer**

Devices: Picofuge and Eppendorf 5415 C centrifuges. Eppendorf 5436 thermomixer. Bender & Hobein AG Vortex Genie 2.

### **Drying of DNA containing probes**

Devices: Eppendorf Concentrator 5301.

### **Syringes and micropipette**

Syringes 5  $\mu$ l, 10  $\mu$ l, 25  $\mu$ l, 50  $\mu$ l, 100  $\mu$ l, 250  $\mu$ l, 500  $\mu$ l (Hamilton) and syringe 2.5 ml (Schmidlin) were used for samples preparations.

Micropipette 1-5  $\mu$ l, 10  $\mu$ l, 100  $\mu$ l (SOCOREX) and 200  $\mu$ l, 1000  $\mu$ l (Gilson Pipetman).

### **Precision cells**

The UV-Vis cells (110 Quartz SUPRASIL, 10 mm) and the Fluo cells (119 Quartz SUPRASIL, 10 mm) were provided from Hellma.

## 7.5 Solvents and chemicals

### Solvents

Technical grade solvents for extraction and flash column chromatography were distilled prior to use. HPLC grade solvents, provided by Fluka, J.T.Baker and Fisher were used for Sephadex column Chromatography. For all other reaction in water-free environment, or for analytic purposes, absolute solvents from Fluka were used without further purification. The THF, DCM and MeOH used for reactions still contained their chemical stabilizers. Nanopure Water for buffer preparation was provided by Barnstead ultrapure water system. Acetone freshly distilled over CaSO<sub>4</sub> semihydrat was used for synthesis (34g of CaSO<sub>4</sub> for 300 ml acetone).

### Chemicals

5-Iodo-2'-deoxyuridine was purchased from BERRY & Associates. Chemicals for DNA synthesis were provided by Glen Research and TEAA (1M) stock solutions were obtained from Fluka. All other chemicals were provided by Fluka, Aldrich, Acros, Merck, Scharlau and Fisher, and were highest grade available.

## 7.6 Buffer and solution

### Preparation of PTT (phosphate buffer saline) 50 mM buffer, pH=7:

0.05 M KH<sub>2</sub>PO<sub>4</sub> (0.68 g, 5 mmol) and 0.5 M NaCl (2.92 g, 50 mmol) were mixed together in 100 ml nanopure water. The pH of the solution was adjusted to 7.0 with 10 N aq. NaOH solution.

**Preparation of 0.1 M TEAA buffer ( $\pm$  1% acetonitrile):**

TEAA (1M, 100 ml) (Fluka) was diluted in 900 ml nanopure water and 10 ml acetonitrile was added if necessary.

**Preparation of 10 mM TRIS buffer, pH=7:**

Tris(hydroxymethyl)aminomethane (0.30 g) and Boric acid (2 g) were mixed together in 250 ml nanopure water. The pH of the solution was adjusted to 7.0 with 10 N aq. NaOH solution.



## 8 General Synthetic Procedure

### 8.1 Syntheses

All reactions were carried out in standard laboratory glassware of appropriate dimensions. Most of the reactions at ambient pressure were performed under argon atmosphere.

### 8.2 Reversed-Phase HPLC

Generally, reversed-phase columns provided by Merk (LiChroSpher 100-5, RP-18e, 250 x 4 mm, Flow: 1.0 ml min<sup>-1</sup> and LiChroSpher 100-10, RP-18e, 250 x 10 mm, Flow: 7.5 ml min<sup>-1</sup>) were used. For separation of oligonucleotides an acetonitrile gradient was applied, whereas detection was achieved by UV absorption at 260 nm. Most of the tritylated oligonucleotides eluted at an acetonitrile fraction range between 25%-30%. For PNA purification, an acidic buffer was used. In order to avoid aggregation effects, the column temperature was always set to 55°C.

	Solvent A	Solvent B
Program 1	0.1 M TEAA	Acetonitrile
Program 2	0.1 M TEAA + 1% acetonitrile	Acetonitrile
Programme 3	0.1 M TEAA	0.1 % TFA

### 8.3 Formation of the double-stranded DNA

Equal amounts of the complementary single strands were dissolved in 1.0 ml of buffer solution (pH = 7.0 with NaOH, 50 mM KHPO<sub>4</sub>, 500 mM NaCl), heated to 75°C for 5 min, and then cooled to RT over 2h to provide a clean annealing.

## 8.4 Quantification of oligonucleotides via UV absorption

Firstly, the micromolar extinction coefficients at 260 nm ( $\epsilon_{\mu\text{m}, 260}$ ) of the oligonucleotides were calculated according to a standard incremental method, which applies the following empirical equation. (Eq. 1)<sup>[109, 110]</sup>:

$$\epsilon_{\mu\text{m}, 260} = [ (8.8 \times \text{nT}) + (7.3 \times \text{nC}) + (11.7 \times \text{nG}) + (15.4 \times \text{nA}) ] \times 0.9 \quad (1)$$

Secondly, the absorption at 260 nm of the corresponding aqueous oligonucleotides solutions was determined using a Quartz UV-transparent cell ( $d = 10 \text{ mm}$ ), and the amount calculated applying the Beer-Lambert Law (Eq. 2):

$$\text{AU} = \epsilon \cdot c \cdot d \quad (2)$$

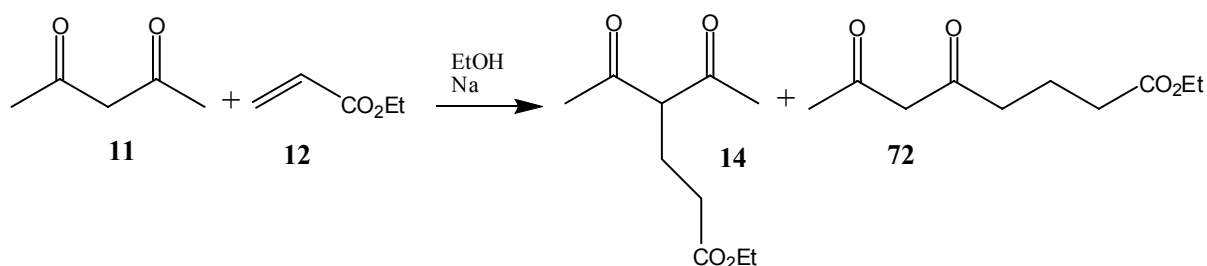
## 8.5 Mass determination

Probes which contained salts were de-salted by Reversed-Phase ZipTip (MILLIPORE) prior to mass determination. A solution of the analyte ( $1 \mu\text{l}$ ) was mixed on the sample plate together with the appropriate matrix solution and crystallized on air. Tetraphenylporphyrin ( $M_w = 614.2$ ) and tetraestertryphenylporphyrin ( $M_w = 846.27$ ) were used for the calibration of the spectrometer device.

## 9 Preparation of components for the porphyrin synthesis

### 9.1 Synthesis of the dipyrromethane with ester chain

#### 3-ester-2, 4-diketone **14**:



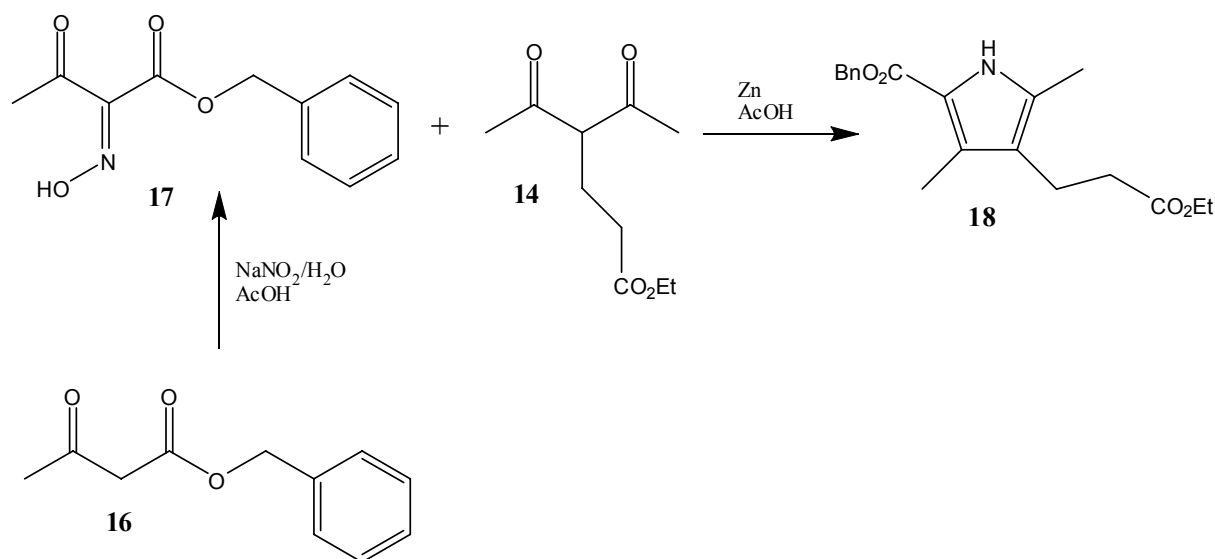
Sodium (0.44 g, 0.02 mol) was dissolved in ethanol (300 ml), then 2,4-pentadione **11** (103 ml, 1 mol, 1 eq) was added after the sodium was dissolved, followed by ethyl acrylate **12** (109 ml, 1 mol, 1.0 eq). The reaction mixture was heated under reflux for 2h, and then kept at RT overnight. Acetic acid (0.66 g, 0.01 mol) was added and the solution stirred for an additional 30 min. After removal of all volatiles under reduced pressure, ethyl 4-acetyl-5-oxohexanoate **14** (110 g, 0.55 mol, 55 %) could be isolated as a yellowish oil after distillation under vacuum.

**C<sub>10</sub>H<sub>16</sub>O<sub>4</sub>**: 200.10 g/mol

**bp**: 110°C at 0.13 mbar

**TLC**: R<sub>f</sub> = 0.32; EA:Hex (1:3)

**<sup>1</sup>H-NMR** (400 MHz, CDCl<sub>3</sub>): δ (ppm) = 4.14 (2H, m, -OCH<sub>2</sub>CH<sub>3</sub>); 3.75 (1H, t, <sup>3</sup>J<sub>HH</sub> = 7.0 Hz, -CHCOCH<sub>3</sub>); 2.3 (2H, m, -CH<sub>2</sub>-CO<sub>2</sub>Et); 2.21 (6H, s, -COCH<sub>3</sub>); 2.16 (2H, dt, <sup>3</sup>J<sub>HH</sub> = 7.2 Hz, <sup>4</sup>J<sub>HH</sub> = 2 Hz, -CH<sub>2</sub>-CH<sub>2</sub>CO<sub>2</sub>Et), 1.26 (3H, t, <sup>3</sup>J<sub>HH</sub> = 7.2 Hz, -CO<sub>2</sub>CH<sub>2</sub>CH<sub>3</sub>).

**Ester derivated pyrrol 18:**

A solution of sodium nitrite (47.7 g, 0.68 mol, 3 eq) in water (100 ml) was added to a well stirred solution of benzoyl acetoacetate **16** (100.3 g, 0.52 mol, 1 eq) in acetic acid (165 ml, 2.6 mol, 5 eq) over an hour at  $10^\circ\text{C}$ . After stirring the cooled solution for 4 further h, it was kept at RT overnight to yield oxime **17**.

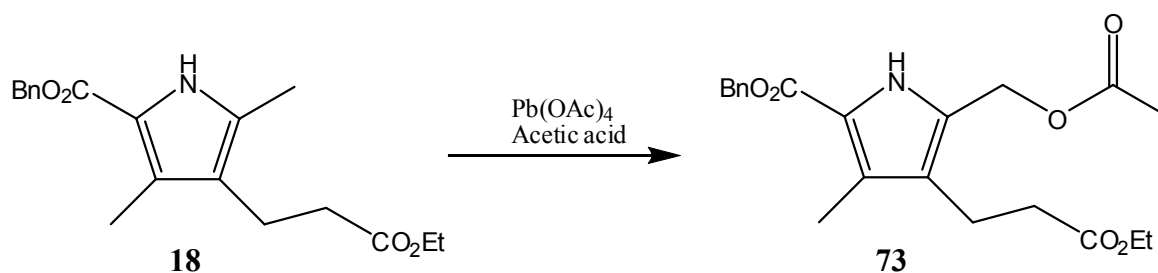
The previous reaction mixture was added to a suspension of 3-hexyl-2,4-diketone **14** (110 g, 0.55 mol, 1 eq) and Zinc dust (68.9 g, 1.04 mol, 2 eq.) in acetic acid (165 ml, 2.7 mol, 5.2 eq) over 1h at  $60^\circ\text{C}$ . The solution was stirred at  $100^\circ\text{C}$  for 45 min then 1h at RT. The reaction mixture was poured into an ice-water bath. The ester was separated by filtration, washed with water, dissolved in DCM and evaporated. Recrystallisation in ethanol at  $-18^\circ\text{C}$  gave the ester derivated pyrrol **18** (142,5 g, 0.43 mol, 83 %).

$\text{C}_{19}\text{H}_{23}\text{NO}_4$ : 329.16 g/mol

**TLC:**  $R_f = 0.28$ , EA:Hex (1:3), turns orange with phosphomolybdic acid solution.

**$^1\text{H-NMR}$**  (400 MHz,  $\text{CDCl}_3$ ):  $\delta$  (ppm) = 8.89 (1H, s,  $-\text{NH}$ ); 7.36 (5H, m,  $-\text{C}_6\text{H}_5$ ); 5.27 (2H, s,  $-\text{OCH}_2-\text{C}_6\text{H}_5$ ); 4.11 (2H, m,  $-\text{CO}_2\text{CH}_2\text{CH}_3$ ); 2.68 (2H, t,  $^3J_{\text{HH}} = 8$  Hz,  $-\text{CH}_2\text{CO}_2\text{Et}$ ); 2.40 (2H, m,  $-\text{CH}_2\text{CH}_2\text{CO}_2\text{Et}$ ); 2.28 (3H, s,  $-\text{CH}_3$  ( $\alpha$ )); 2.19 (3H, s,  $-\text{CH}_3$  ( $\beta$ )); 1.22 (3H, t,  $-\text{CO}_2\text{CH}_2\text{CH}_3$ ).

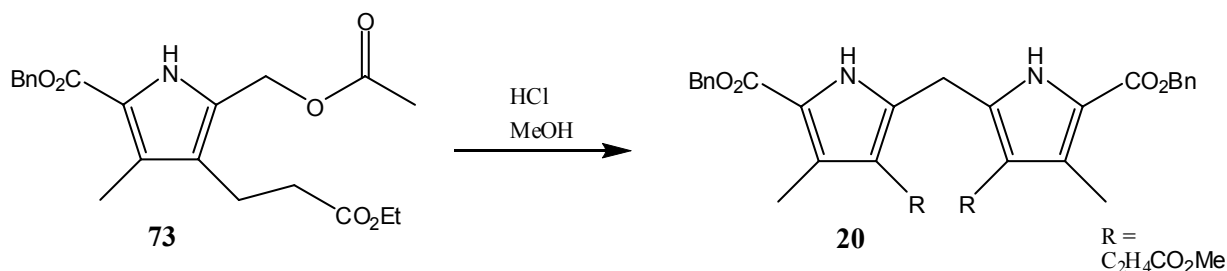


**$\alpha$ -Acetyl ester derived pyrrole 73:**

The  $\alpha$ -acetylation of the ester-derived pyrrole **18** (142.5 g, 0.43 mol, 1 eq) was achieved by treatment with lead acetate (230 g, 0.52 mol, 1.2 eq) in acetic acid (220 ml, 3.5 mol, 8 eq). The reaction mixture was stirred for 3h at RT, then 100ml methanol was added and the mixture was kept in the fridge ( $-18^\circ\text{C}$ ) to obtain a white precipitate **73** (116 g, 0.31 mol, 73 %) which was filtered and kept under inert atmosphere (else it turns pink).

$\text{C}_{21}\text{H}_{25}\text{NO}_6$ : 387.17 g/mol

$^1\text{H-NMR}$  (400 MHz,  $\text{CDCl}_3$ ):  $\delta$  (ppm) = 9.38 (1H, s,  $-\text{NH}$ ); 7.40 (5H, m,  $-\text{C}_6\text{H}_5$ ); 5.27 (2H, s,  $-\text{OCH}_2-\text{C}_6\text{H}_5$ ); 5.02 (2H, s,  $-\text{CH}_2\text{CO}_2\text{CH}_3$ ); 4.09 (2H, m,  $-\text{CO}_2\text{CH}_2\text{CH}_3$ ); 2.73 (4H, m,  $-\text{C}_2\text{H}_4\text{CO}_2\text{Et}$ ); 2.26 (3H, s,  $-\text{CO}_2\text{CH}_3$ ); 2.02 (3H, s,  $-\text{CH}_3$  ( $\beta$ )); 1.21 (3H, t,  $-\text{CO}_2\text{CH}_2\text{CH}_3$ ).

**Dipyrromethane with ester chain 20**

Dimerisation of acetylated pyrrole **73** (116 g, 0.31 mol) was obtained by refluxing compound **73** in hydrochloric acid 37% (155 ml) and methanol (400 ml) for 3h, then the solvent was evaporated. The crude product was dissolved in DCM, washed with a sat. aqueous  $\text{NaHCO}_3$  solution and water. Recrystallisation in MeOH at  $-18^\circ\text{C}$  gave the dipyrromethane **20** (22.9 g, 37 mmol, 12%) as a yellowish powder.

$\text{C}_{35}\text{H}_{38}\text{N}_2\text{O}_8$ : 614.26 g/mol

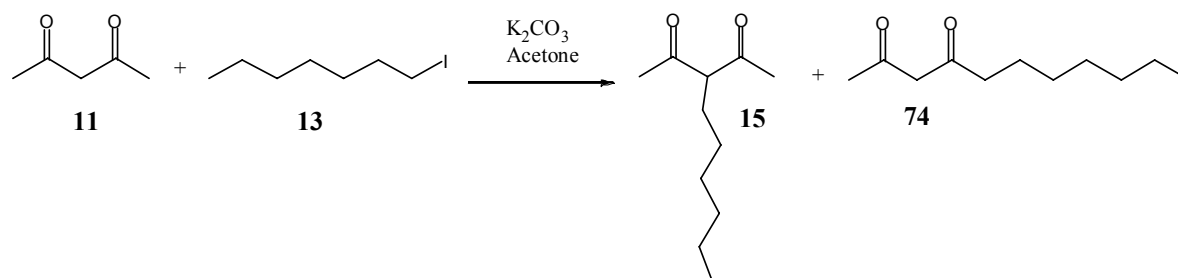
**MALDI-TOF**: m/z: 614.02  $[\text{M}]^+$

**TLC**:  $R_f = 0.1$ ; Hex/EA, (5:1)

$^1\text{H-NMR}$  (400 MHz,  $\text{CDCl}_3$ ):  $\delta$  (ppm) = 9.08 (2H, s,  $-\text{NH}$ ); 7.36-7.39 (10H, m,  $-\text{C}_6\text{H}_5$ ); 5.24 (4H, s,  $-\text{OCH}_2-\text{C}_6\text{H}_5$ ); 3.96 (2H, s,  $-\text{CH}_2-$  meso); 3.56 (6H, s,  $-\text{CH}_3$  ( $\beta$ )); 2.75 (4H, t,  $^3J_{\text{HH}} = 7.0$  Hz,  $-\text{CH}_2\text{CH}_2\text{CO}_2\text{Et}$ ); 2.51 (4H, t,  $^3J_{\text{HH}} = 7.0$  Hz,  $-\text{CH}_2\text{CH}_2\text{CO}_2\text{Et}$ ); 2.28 (6H, s,  $-\text{CO}_2\text{CH}_3$ ).

## 9.2 Synthesis of the dipyrromethane with hexyl chain

### 3-hexyl-2,4-diketone **15**:



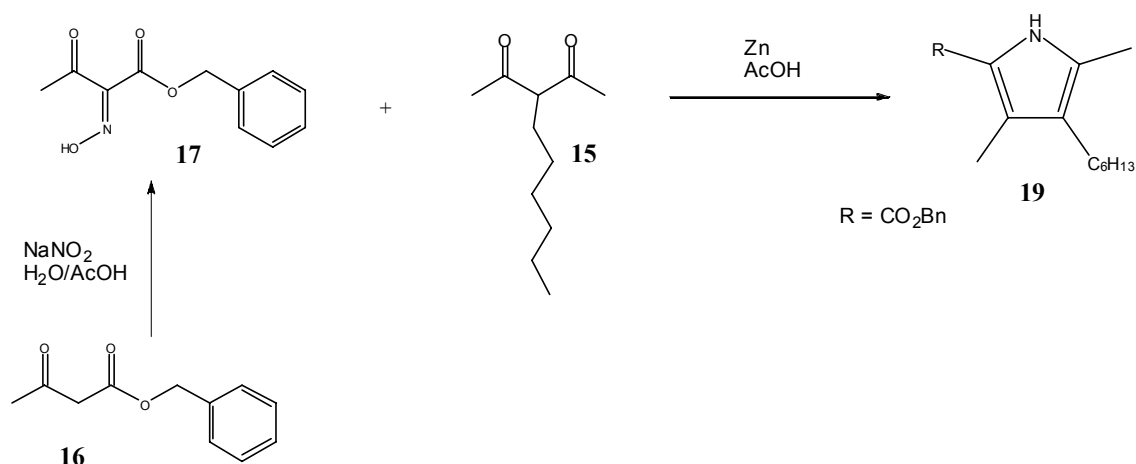
1-Iodoheptane **13** (100 ml, 0.68 mol, 1.07 eq) and 2, 4-pentadione **11** (65.3 ml, 0.64 mol, 1 eq) were treated with potassium carbonate (93.7 g, 0.68 mol, 1.07 eq) in 250 ml acetone for 24 h at 60°C, to give 3-hexyl-2,4-diketone **15** and undecane-2,4-dione **74**. The reaction mixture was filtered and washed with acetone. After removal of all volatiles under reduced pressure, 3-hexyl-2, 4-diketone **15** (73 g, 0.39 mol, 58%) could be isolated as a yellow oil after distillation under vacuum.

$C_{11}H_{20}O_2$ : 184.15 g/mol

**bp**: 68°C with 0.06 mbar (Lit.:<sup>[111]</sup> 123-124°C with 21.3 mbar).

**TLC**:  $R_f = 0.56$ , PE:EA (1:1)

**$^1H$ -NMR** (400 MHz,  $CDCl_3$ ):  $\delta$  (ppm) = 3.62 (1H, t,  $^3J_{HH} = 7.0$  Hz,  $-CH_{\text{meso}}$ ); 2.18 (6H, s,  $-CH_3$ ); 1.84 (2H, dt,  $^3J_{HH} = 7.3$  Hz,  $^3J_{HH} = 7.0$  Hz,  $-CH_2-C_5H_{11}$ ); 1.31 (8H, m,  $-CH_2-C_4H_8-CH_3$ ); 0.88 (3H, t,  $^3J_{HH} = 6.7$  Hz,  $-C_5H_{10}-CH_3$ ).

**hexyl derivated pyrrol 19:**

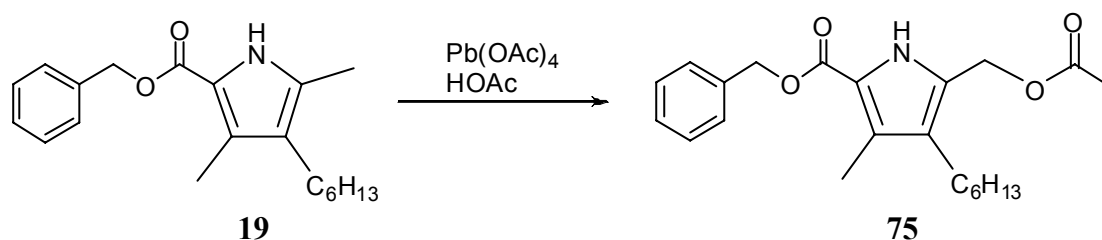
Sodium nitrite (12.0 g, 0.17 mol, 1.0 eq) in water (27 ml) was added to benzoyl acetoacetate **16** (30 ml, 0.17 mol, 1.0 eq) in acetic acid (33.8 ml, 0.59 mol, 3.4 eq) over one hour at 10°C. Then, the mixture was stirred at 10°C for 4h, and at RT overnight, to yield oxime **17**.

The previous reaction mixture was added to a suspension of 3-hexyl-2,4-diketone **15** (32 g, 0.17mol) and Zinc dust (33.7 g, 0.52 mol, 3.0 eq.) in acetic acid (46 ml) over 1h at 60°C. The solution was stirred at 100°C for 45 min and 1h at RT. The reaction mixture was poured into an ice-water bath. The ester was separated by filtration, washed with water, dissolved in DCM and evaporated. Recrystallisation in ethanol at -18°C gave the hexyl derivated pyrrol **19** (9 g, 28 mmol, 17%).

$\text{C}_{20}\text{H}_{27}\text{NO}_2$ : 313.20 g/mol

TLC:  $R_f = 0.69$ ; PE:EA (2:1)

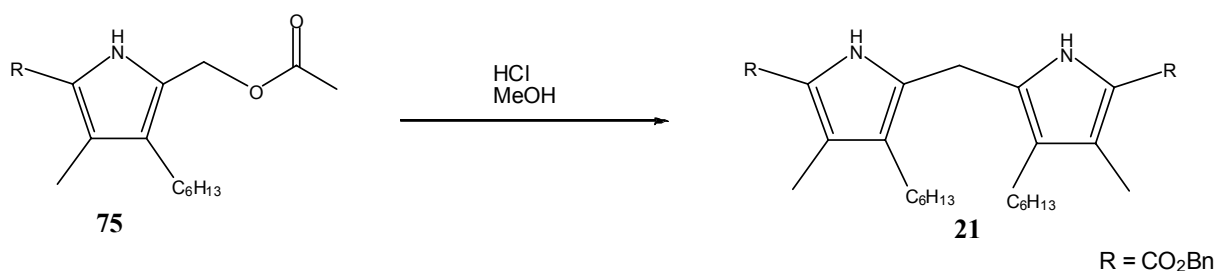
$^1\text{H-NMR}$  (400 MHz,  $\text{CDCl}_3$ ):  $\delta$  (ppm) = 8.73 (1H, t, s,  $-\text{NH}$ ); 7.36-7.33 (5H, m,  $-\text{C}_6\text{H}_5$ ); 5.29 (2H, s,  $-\text{OCH}_2-\text{C}_6\text{H}_5$ ); 2.33 (2H, t,  $^3J_{\text{HH}} = 7.6$  Hz,  $-\text{CH}_2-\text{C}_5\text{H}_{11}$ ); 2.28 (3H, s,  $-\text{CH}_3$ ), 2.17 (3H, s,  $-\text{CH}_3$ ); 1.40 (2H, m,  $-\text{CH}_2-\text{CH}_2-\text{C}_4\text{H}_9$ ); 1.28 (6H, m,  $-\text{C}_2\text{H}_4-\text{C}_3\text{H}_6-\text{CH}_3$ ); 0.88 (3H, t,  $^3J_{\text{HH}} = 7.0$  Hz,  $-\text{C}_5\text{H}_{10}-\text{CH}_3$ ).

**$\alpha$ -Acetyl hexyl derived pyrrole 75:**

The  $\alpha$ -acetylation of hexyl-derived pyrrole **19** (9 g, 28.9 mmol, 1 eq) was achieved by treatment with lead acetate (12.3 g, 28.7 mmol, 1 eq) in acetic acid (45 ml). The mixture was stirred for 30 min at 120°C and 1h at RT. The reaction mixture was evaporated to a volume of 20 ml, and 50 ml of methanol were added to crystallise the product. A white precipitate **75** (2.45 g, 6.6 mmol, 23%) which was filtered and kept under inert atmosphere (else it turns to pink).

$C_{22}H_{29}NO_4$ : 371.21 g/mol

$^1H$ -NMR (400 MHz,  $CDCl_3$ ):  $\delta$  (ppm) = 9.12 (1H, s, -NH); 7.37-7.34 (5H, m, -C<sub>6</sub>H<sub>5</sub>); 5.00 (2H, s, -CH<sub>2</sub>-CO<sub>2</sub>CH<sub>3</sub>); 2.42 (2H, t,  $^3J_{HH} = 7.6$  Hz, -CH<sub>2</sub>-C<sub>5</sub>H<sub>11</sub>); 2.28 (3H, s, -CH<sub>3</sub>), 2.06 (3H, s, -CO<sub>2</sub>CH<sub>3</sub>); 1.31-1.29 (8H, m, -CH<sub>2</sub>-C<sub>4</sub>H<sub>8</sub>-CH<sub>3</sub>); 0.88 (3H, t,  $^3J_{HH} = 6.7$  Hz, -C<sub>5</sub>H<sub>10</sub>-CH<sub>3</sub>).

**Dipyrromethane with hexyl chain 21:**

Dimerisation of acetylated pyrrole **75** (2.45 g, 6.85 mmol) was obtained by refluxing in hydrochloric acid 37% (1.3 ml) and methanol (40 ml). The mixture was refluxed for 3h, and the solvent was evaporated. The crude product was dissolved in DCM, washed with a solution of NaHCO<sub>3</sub> sat. and water. Recrystallisation in MeOH (-18°C) overnight gave the dipyrromethane **21** (1.45 g, 2.38 mmol, 35%) as a brown precipitate.

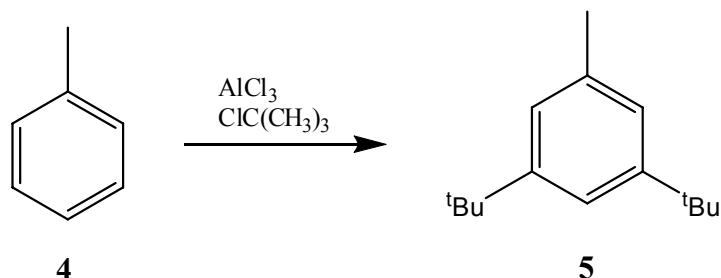
**C<sub>39</sub>H<sub>50</sub>N<sub>2</sub>O<sub>4</sub>**: 610.38

**TLC**: R<sub>f</sub> = 0.1; Hex/EA, (5:1)

**<sup>1</sup>H-NMR** (400 MHz, CDCl<sub>3</sub>): δ (ppm) = 9.12 (2H, s, -NH); 7.35-7.32 (10H, m, -C<sub>6</sub>H<sub>5</sub>); 5.27 (4H, s, -CH<sub>2</sub>-CO<sub>2</sub>CH<sub>3</sub>); 3.82 (2H, s, -CH<sub>2</sub>-meso); 2.34 (4H, t, <sup>3</sup>J<sub>HH</sub> = 7.6 Hz, -CH<sub>2</sub>-C<sub>5</sub>H<sub>11</sub>); 2.28 (6H, s, -CH<sub>3</sub>); 1.25-1.22 (8H, m, -CH<sub>2</sub>-C<sub>4</sub>H<sub>8</sub>-CH<sub>3</sub>); 0.86 (6H, t, <sup>3</sup>J<sub>HH</sub> = 6.8Hz, -C<sub>5</sub>H<sub>10</sub>-CH<sub>3</sub>).

### 9.3 Synthesis of the derivate benzaldehyde

#### 3, 5-Di-*tert*-butyltoluene 5:

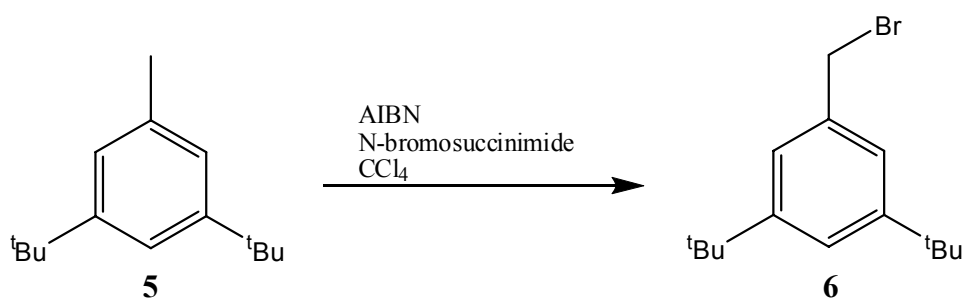


Aluminium trichloride (3.96 g, 0.03 mol) was added in 8 portions, over 8h, to a rapidly stirred solution of 2-chloromethylpropane (166 ml, 1.53 mol, 2 eq) in toluene **4** (81.6 ml, 0.77 mol, 1 eq) in a 500 ml round bottomed flask fitted with a silicon oil bubbler. After 12h, water was added and the product was extracted with  $\text{Et}_2\text{O}$ . The solvent was removed under reduced pressure and the residue purified by vigreux distillation. The crude crystalline product **5** (81.1 g, 0.39 mol, 52 %) was used without further purification.

$\text{C}_{15}\text{H}_{24}$ : 204.35 g/mol

$^1\text{H-NMR}$  (400 MHz,  $\text{CDCl}_3$ ):  $\delta$  (ppm) = 7.25-7.49 (m, 2H,  $\text{H}_{\text{aro}}$ ); 7.05-7.02 (m, 1H,  $\text{H}_{\text{aro}}$ ); 2.36 (s, 3H,  $-\text{CH}_3$ ); 1.33 (18H, s,  $-\text{C}(\text{CH}_3)_3$ ).

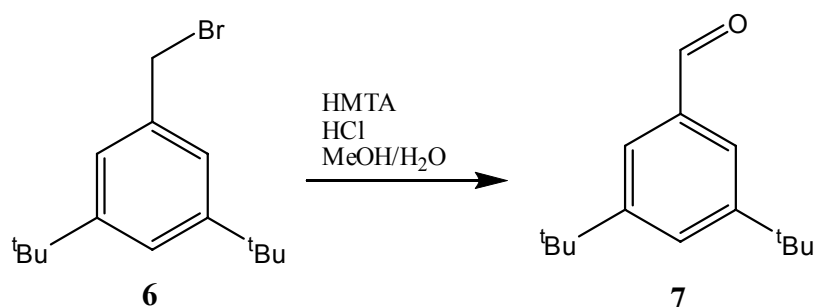
#### 3,5-Di-*tert*-butyl-bromomethylbenzene 6:



A mixture of 3,5-Di-*tert*-butyltoluene **5** (35.95 g, 0.176 mol), N-Bromosuccinimide (47.3 g, 0.23 mol, 1.3eq), and AIBN (azo-bis-isobutyronitrile) (157.6 mg, 0.88 mmol) in tetrachloromethane (130 ml) was refluxed for 3h. The solution was cooled and the solvent was removed by distillation. The residue was dissolved in dichloromethane, the precipitated filtered and the product concentrated by distillation. The crude product **6** (22g, 78 mmol, 44%) was used without further purification in the next step.

$C_{15}H_{23}Br$ : 282.10 g/mol

### 3,5-Di-*tert*-butylbenzaldehyde **7**:

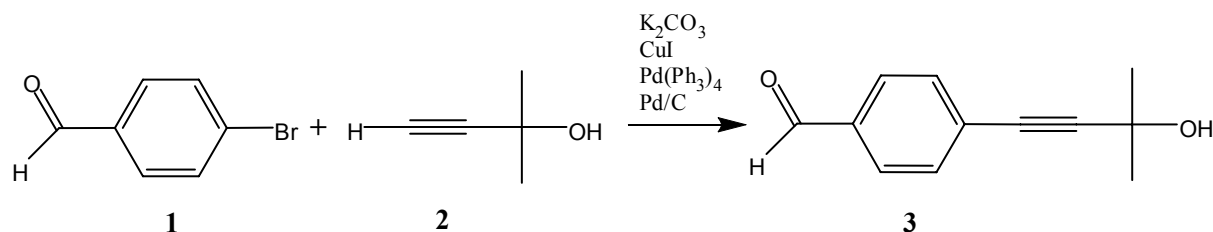


A mixture of 3,5-Di-*tert*-butyl-bromomethylbenzene **6** (22g, 78 mmol) and HMTA (hexamethylenetetramine) (102.4 g, 0.73 mol) in methanol/water (200 ml, 1:1) was refluxed for 4h. Concentrated aqueous HCl (60 ml) was added dropwise and the mixture refluxed for 0.5h. The solution was cooled and extracted into dichloromethane (3x150 ml), the solvent removed under reduced pressure and the residue recrystallised from ethanol/water to give the compound **7** (12 g, 55 mmol, 70%) as a white crystalline solid.

$C_{15}H_{22}O$ : 218.17 g/mol

$^1H$ -NMR (400 MHz, CDCl<sub>3</sub>):  $\delta$  (ppm) = 10.00 (1H, s,  $\underline{C}HO$ ); 7.71 (m, 3H, H<sub>aro</sub>); 1.33 (18H, s, -C( $\underline{C}H_3$ )<sub>3</sub>).

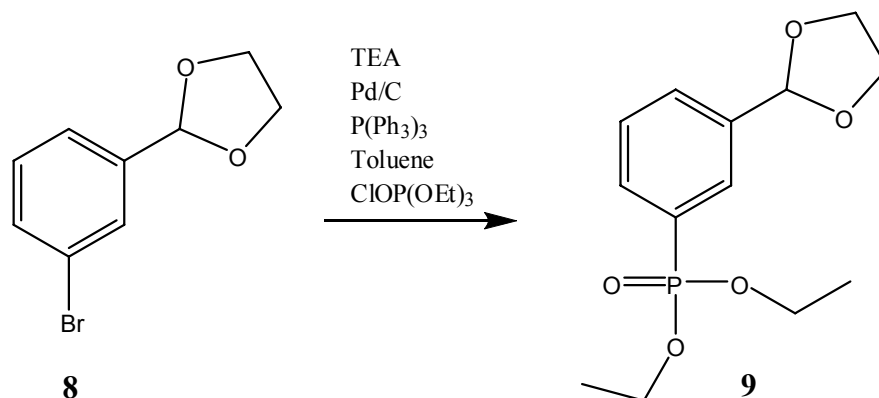


**4-(3-hydroxy-3-methylbut-1-ynyl)benzaldehyde 3:**

A suspension of 4-bromobenzaldehyde **1** (10 g, 50 mmol),  $K_2CO_3$  (34.3 g, 250 mmol, 5 eq),  $CuI$  (0.77 g, 4 mmol, 0.08 eq), triphenylphosphine (2.1 g, 8 mmol, 0.16 eq), palladium on activated charcoal (2.1 g, 2 mmol, 0.08 eq) in dimethoxyethane/water (60 ml/60ml) was degassed with argon and stirred at RT for 30 min. Then, 2-methylbut-3-yn-2-ol **2** (24.5 ml, 250 mmol, 5 eq) was added dropwise via syringe, and the mixture heated at  $80^\circ C$  for 16h. The suspension was filtered over celite, extracted with 35 ml acetic acid. The organic phase was washed with water (2x20 ml), dried over  $MgSO_4$  and evaporated. The residue was purified by flash chromatography (ethyl acetate/hexane, gradient from 1:4 to 1:3) to obtain the pure product **3** (8.8 g, 47 mmol, 87 %) as yellow oil.

$C_{12}H_{12}O_2$ : 188.08 g/mol

$^1H$ -NMR (400 MHz,  $CDCl_3$ ):  $\delta$  (ppm) = 9.93 (1H, s,  $-CHO$ ), 7.75 (2H, d,  $J = 8.29$ ,  $-C_6H_5$ ), 7.49 (2H, d,  $J = 8.29$ ,  $-C_6H_5$ ), 1.89 (1H, s,  $-OH$ ), 1.57 (6H, s,  $-CH_3$ ).

**Diethyl 3-(dioxolan-2'-yl)phenylphosphonate 9:**

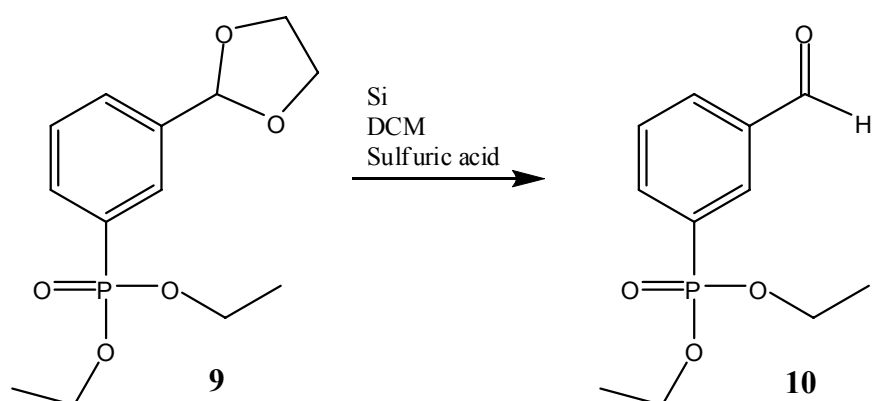
Diethyl phosphonate (3.3 ml, 21.8 mmol, 1.1 eq) and triethylamine (3.4 ml, 24 mmol, 1.1 eq) were added *via* syringe to 2-(3-bromophenyl)-1,3-dioxolane **8** (3.32 ml, 24 mmol, 1 eq) in toluene (5 ml) under argon. Palladium on activated Charcoal (1.6 g, 1.22 mmol, 0.05 eq.) and triphenylphosphine (1.6 g, 4.88 mmol, 0.22 eq) were added, and the reaction was heated to 95°C for 36 h. The crude product was filtered through Celite, washed with ether-hexane (50:50 as eluent) and all volatiles were evaporated to yield the crude product as a deep yellow oil, purified by flash column chromatography (EE/Hex, 4:1) to give diethyl-3-(dioxolan-2'-yl)phenylphosphonate (550 mg, 1.9 mmol, 10 %) as a yellow oil.

**C<sub>13</sub>H<sub>19</sub>O<sub>5</sub>P**: 286.10 g/mol

**TLC**: R<sub>f</sub> = 0.20, EA, turned yellow with KMNO<sub>4</sub>

**<sup>1</sup>H-NMR** (400 MHz, CDCl<sub>3</sub>): δ (ppm) = 7.40–7.90 (4 H, m, -C<sub>6</sub>H<sub>4</sub>); 5.78 (1 H, s, -CH(OR)); 4.10-3.98 (8H, m, -CH<sub>2</sub>CH<sub>3</sub>, -OCH<sub>2</sub>CH<sub>2</sub>O-); 1.29 (6 H, t, *J* = 6.2, -CH<sub>2</sub>CH<sub>3</sub>).

**<sup>31</sup>P-NMR** (167 MHz, CDCl<sub>3</sub>): δ (ppm) = 13.3 (s)

**1-diethyl (3-carbonylphenyl)phosphonate 10:**

Aqueous 15% sulfuric acid (0.6 ml) was adsorbed onto silicagel (5 g) suspended in DCM (14 ml). Diethyl 3-(dioxolan-2-yl)-phenylphosphonate **9** (0.55 g, 1.9 mmol) was then added in DCM (14 ml) and the reaction stirred for 24 h at RT. The mixture was filtered, washed with DCM (150 ml), and solvent removed *in vacuo*. The crude product was purified by flash column chromatography to afford diethyl (3-carbonylphenyl)phosphonate **10** (0.25 g, 1 mmol, 54 %) as a yellow oil.

**C<sub>11</sub>H<sub>15</sub>O<sub>4</sub>P**: 242.07 g/mol

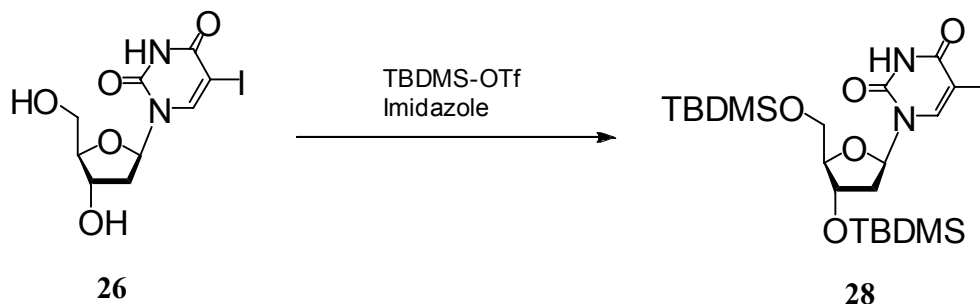
**TLC**: R<sub>f</sub> = 0.28, EA/PE, (70:30)

**<sup>1</sup>H-NMR** (400 MHz, CDCl<sub>3</sub>): δ (ppm) = 10.0 (1H, s, -CHO), 8.31 (1H, ddt, <sup>4</sup>J<sub>HH</sub> = 0.6 Hz, <sup>3</sup>J<sub>HH</sub> = 1.5 Hz, <sup>3</sup>J<sub>HP</sub> = 12.8 Hz, -CH<sub>(o)</sub>), 8.05-8.09 (2H, m, -CH<sub>(o)</sub> and -CH<sub>(p)</sub>), 7.45-7.66 (1H, m, -CH<sub>(m)</sub>), 4.10-4.20 (4H, m, -CH<sub>2</sub>CH<sub>3</sub>), 1.36 (6H, t, J = 6.7, -CH<sub>2</sub>CH<sub>3</sub>),

**<sup>31</sup>P-NMR** (167 MHz, CDCl<sub>3</sub>): δ (ppm) = 13.5 (s)

## 9.4 Synthesis of the protected oligonucleotides

### 3',5'-Bis-O-tert.-butyldiphenylsilyl-5'-iodo-uracil **28**:



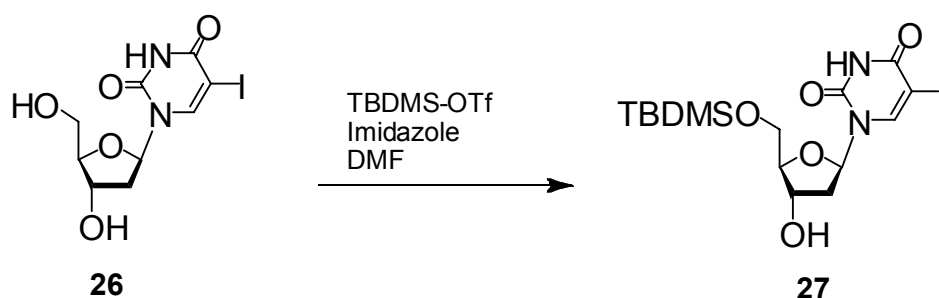
1 g (2.82 mmol, 1 eq.) of 5-iododeoxyuridine **26** was dried three times by co-evaporation with pyridine (3×2 ml), and suspended in DMF (10 ml). 0.81 g (11.8 mmol, 4.2 eq.) of imidazole was added, followed by a slow addition of tert.-butyldimethylsilylchloride (1.3 ml, 5.7 mmol, 2 eq.) *via* syringe in a ice bath. The reaction mixture was stirred for 2h at 0°C and then 2h at RT. The solution was poured into 10 ml of 10 % aqueous tartaric acid, and the mixture was extracted 3 times with AcOEt. The organic phase was washed with H<sub>2</sub>O (25 ml), NaCl sat. and dried over Na<sub>2</sub>SO<sub>4</sub>. After removal of all the solvent under reduced pressure, the residue was kept in the Kugelrohr at 40°C for 3h. A flash chromatography on silica gel (CH<sub>2</sub>Cl<sub>2</sub>/MeOH 50:1) gave the protected iodouracil **28** (1.46 g, 2.51 mmol, 90 %) as a white foam.

**C<sub>21</sub>H<sub>39</sub>I<sub>N</sub><sub>2</sub>O<sub>5</sub>Si<sub>2</sub>**: 582.14 g/mol

**Maldi-TOF**: m/z: 582.73 [M]<sup>+</sup>

**TLC**: R<sub>f</sub>: 0.58, DCM/MeOH (10:1)

**<sup>1</sup>H-NMR** (400 MHz, CDCl<sub>3</sub>): δ (ppm) = 8.16 (s, 1H, -NH), 8.09 (s, 1H, H-(6)), 6.28-6.25 (m, 1H, H-1'), 4.40-4.38 (m, 1H, H-3'), 3.99-3.98 (m, 1H, H-4'), 3.90-3.86 (m, 1H, H-5'), 3.77-3.74 (m, 1H, H-5'), 2.28 (m, 1H, H-2'), 2.01-1.98 (m, 1H, H-2'), 0.94 (s, 9H, -SiC<sub>5</sub>(CH<sub>3</sub>)<sub>3</sub>), 0.89 (s, 9H, -SiC<sub>3</sub>(CH<sub>3</sub>)<sub>3</sub>), 0.14 (d, *J* = 4.28 Hz, 6H, -Si(CH<sub>3</sub>)<sub>2</sub>), 0.07 (d, *J* = 3.28 Hz, 6H, -Si(CH<sub>3</sub>)<sub>2</sub>).

**5'-O-tert.-butyldimethylsilyl-5'-iodo-uracil 28:**

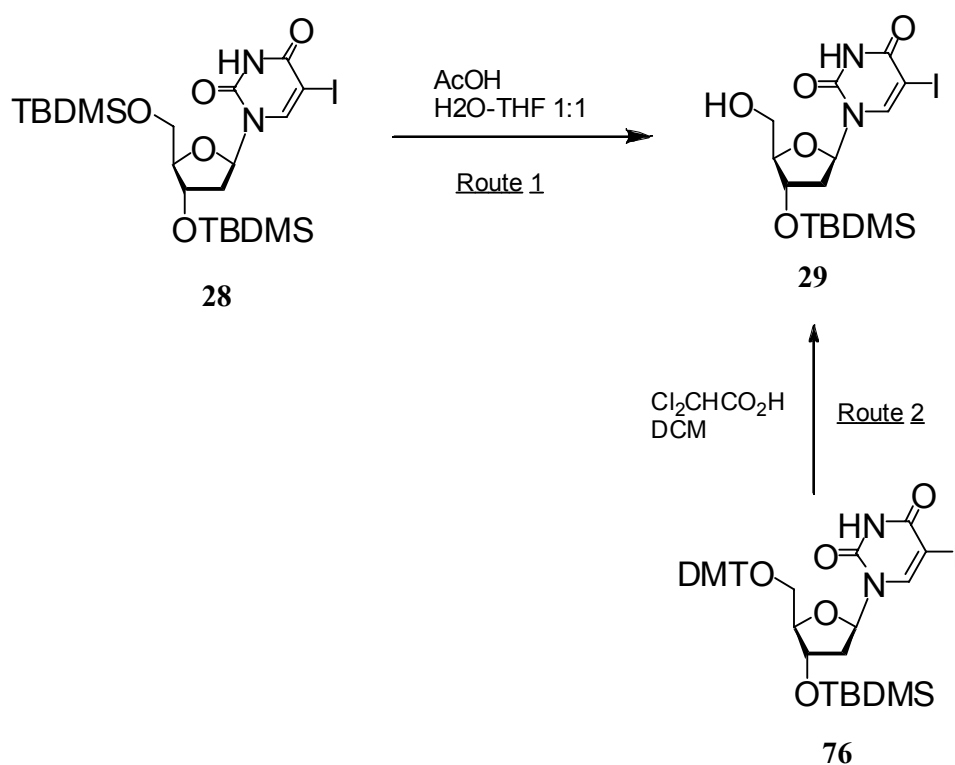
The 5'-O-tert.-butyldiphenylsilyl-5'-iodo-uracil **27** was prepared according to the general procedure described for derivative **28**. The reaction time was reduced to the half. The residue was diluted in warm CH<sub>2</sub>Cl<sub>2</sub> (4 ml) and precipitated with hexane (15 ml). The precipitate was filtrated and washed with hexane. The compound **27** was obtained as white foam (362 mg, 0.62 mmol, 22 %).

**C<sub>15</sub>H<sub>25</sub>IN<sub>2</sub>O<sub>5</sub>Si**: 468.06 g/mol

**TLC**: R<sub>f</sub>: 0.72, CH<sub>2</sub>Cl<sub>2</sub>/MeOH (3:2)

**Maldi-TOF**: m/z: 468.37 [M]<sup>+</sup>

**<sup>1</sup>H-NMR** (400 MHz, CDCl<sub>3</sub>): δ (ppm) = 8.52 (s, 1H, -NH), 8.10 (s, 1H, H-(6)), 6.31-6.28 (m, 1H, H-1'), 4.48-4.47 (m, 1H, H-3'), 4.09-4.08 (m, 1H, H-4'), 3.90-3.89 (dd, 1H, H-5'), 3.85-3.84 (dd, 1H, H-5'), 2.44-2.39 (m, 2H, H-2'), 2.08 (m, 1H, 3'-OH), 0.93 (s, 9H, -SiC<sub>5</sub>(CH<sub>3</sub>)<sub>3</sub>), 0.14 (s, 6H, -Si(CH<sub>3</sub>)<sub>2</sub>).

**3'-O-tert-butyldimethylsilyl-5-iodo-uracil 29:**Synthetic route 1:

400 mg (0.69 mmol, 1eq) of 3',5'-bis(tert-butyldimethylsilyl)5-iodo-uracil **28** were dissolved in THF (4 ml) followed by addition of a mixture of acetic acid (3.3 ml) and H<sub>2</sub>O (1 ml). The reaction mixture was stirred at 35°C for 4 days under argon, and diluted with CH<sub>2</sub>Cl<sub>2</sub> (7 ml). The organic layer was washed with NaHCO<sub>3</sub> (3 × 12 ml), H<sub>2</sub>O (2 × 8 ml), NaCl (1 × 12 ml), and dried over Na<sub>2</sub>SO<sub>4</sub>. Filtration and evaporation of the solvent under reduced pressure yielded the crude product which was purified by a flash chromatography on silica gel (CH<sub>2</sub>Cl<sub>2</sub>/MeOH 100:0.5) to yield 117 mg (0.25 mmol, 36 %) of 3'-O-tert-butyldimethylsilyl-5-iodo-uracil **29** as a white foam.

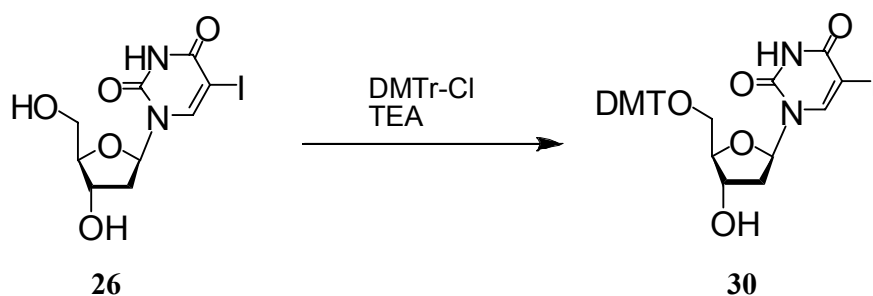
Synthetic route 2:

300 mg (0.369 mmol, 1eq) of 3'-(tert-butyldimethylsilyl)-5'-O-DMT-iodo-uracil **76** were dissolved in DCM (10 ml), and 0.3 ml of dichloroacetic acid were added. The reaction mixture was stirred at RT for 30 min. The organic layer was washed with NaHCO<sub>3</sub> and dried over Na<sub>2</sub>SO<sub>4</sub>. Filtration and evaporation of the solvent under reduced pressure yielded the crude product which was purified by a flash chromatography on silica gel (CH<sub>2</sub>Cl<sub>2</sub>/MeOH) from 0.5 % to 10 % to yield 135 mg (0.29 mmol, 75 %) of 3'-O-tert-butyldimethylsilyl-5'-iodo-uracil **29** as a white foam.

**C<sub>15</sub>H<sub>25</sub>IN<sub>2</sub>O<sub>5</sub>Si**: 468.06 g/mol

**TLC**: R<sub>f</sub>: 0.52, CH<sub>2</sub>Cl<sub>2</sub>/MeOH (10:1)

**<sup>1</sup>H-NMR** (400 MHz, CDCl<sub>3</sub>): δ (ppm) = 8.22 (s, 1H, -NH), 8.03 (s, 1H, H-(6)), 6.14-6.15 (m, 1H, H-1'), 4.49-4.48 (m, 1H, H-3'), 3.98-3.97 (m, 2H, H-5'), 3.81-3.78 (m, 1H, H-4'), 2.28-2.27 (m, 2H, H-2'), 2.00 (m, 1H, 5'-OH), 0.89 (s, 9H, -SiC<sub>3</sub>(CH<sub>3</sub>)<sub>3</sub>), 0.08 (s, 6H, -Si(CH<sub>3</sub>)<sub>2</sub>).

**5'-O-DMT-iodo-uracile 30:**

5'-iodo-uracil **26** (2 g, 5.65 mmol, 1 eq) was co-evaporated with 3×2 ml pyridine and dissolved in 15 ml of pyridine with molecular sieves (4 Å) under argon. After one and a half hours, TEA (1.6 ml, 11.29 mmol, 2 eq) was added followed by the addition of dimethoxytrityl chloride (2.49 g, 7.34 mmol, 1.3 eq). The reaction mixture was stirred overnight at RT, and diluted with AcOEt (100 ml). The solution was washed with NaHCO<sub>3</sub> (2 × 100 ml) and H<sub>2</sub>O (75 ml). The aqueous layer was extracted again with AcOEt and the combined organic layers were dried over NaSO<sub>4</sub>. After removal of all volatiles under reduced pressure, flash chromatography (CH<sub>2</sub>Cl<sub>2</sub>/MeOH 20:1 + 1 % TEA) afforded 2.32 g (3.54 mmol, 63 %) of 5'-O-DMT-5'-iodo-uracile **30** as white foam.

**C<sub>30</sub>H<sub>29</sub>I<sub>N<sub>2</sub>O<sub>7</sub></sub>**: 656.10 g/mol

**Maldi-TOF**: m/z: 656.47 [M]<sup>+</sup>

**TLC**: R<sub>f</sub>: 0.7, CH<sub>2</sub>Cl<sub>2</sub>/MeOH (20:1) +1% TEA

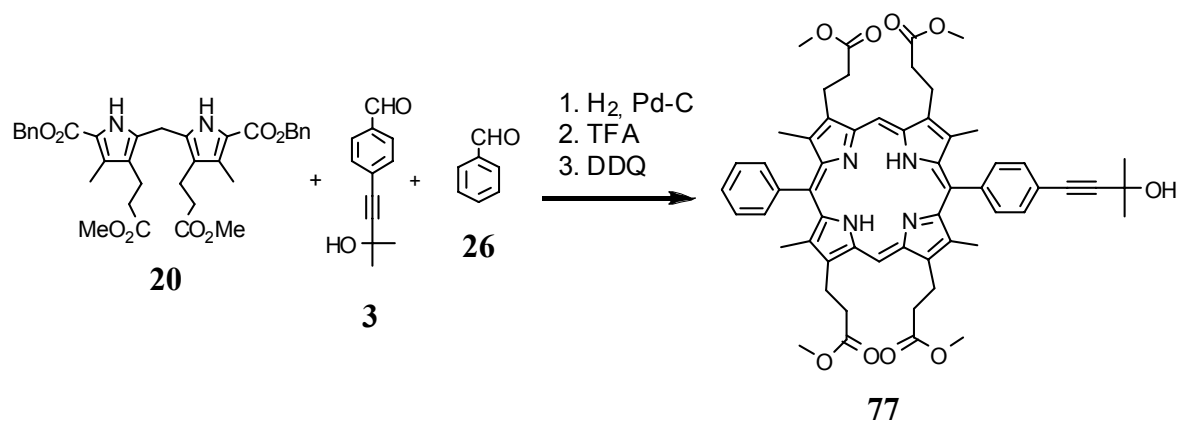
**<sup>1</sup>H-NMR** (400 MHz, CDCl<sub>3</sub>): δ (ppm) = 8.13 (s, 1H, -NH), 7.41 (d, *J* = 7.2 Hz, 2H, H<sub>aro</sub>), 7.33-7.24 (m, 6H, H<sub>aro</sub>), 7.22 (s, 1H, H-(6)), 6.85 (d, *J* = 9.2 Hz, 4H, H<sub>aro</sub>), 6.33-6.28 (m, 1H, H-1'), 4.55-4.54 (m, 1H, H-3'), 4.09-4.08 (m, 1H, H-4'), 3.80 (s, 6H, -O-CH<sub>3</sub>) 3.40-3.37 (m, 2H, H-5'), 2.50-2.45 (m, 2H, H-2'), 2.30 (m, 1H, 3'-OH).



## 10 Porphyrin Synthesis

### 10.1 Zn Diphenylporphyrin with ester chain

#### Protected acetylene porphyrin **77**



To a solution of dipyrromethane **20** (4 g, 6.8 mmol, 2 eq) in THF (50 ml), MeOH (6 ml), TEA (2 ml), and finally 320 mg of Pd/C (10%) were added. The reaction mixture was degassed with H<sub>2</sub> for 30 min, and kept under H<sub>2</sub> for 2h at rt. After filtration of the reaction mixture *via* canula under Ar, the residue was washed twice with a 10:1 degassed mixture of THF and MeOH. After removal of the solvent under reduced pressure, the oily residue was dried at the vacuum line for several hours to give a white foam (rf = 0, Hex/EE, 5:1). The resulting deprotected dipyrromethane was dissolved in degassed TFA (35 ml) at 0°C under Ar. The reaction mixture was stirred in the dark at 0°C for 10 min, and then at RT for 1.5 h until everything was dissolved. 0.34 ml (3.4 mmol, 1 eq.) of benzaldehyde and 0.96 g (10.2 mmol, 1.5 eq.) of the alkyne-aldhyde were dissolved in 70 ml of MeOH, the solution was degassed with Ar, and added to the reaction mixture over a period of 30 min at -10°C *via* canula. The mixture was allowed to stir at RT for 2h, and DDQ (2.32 g, 10.2 mmol) was added. The dark green solution was stirred for 1.5 h (in the light), diluted with CH<sub>2</sub>Cl<sub>2</sub> (50 ml) and neutralised with TEA (36 ml) in an ice bath. The organic layer was washed 3 times with water and NaCl sat., dried over Na<sub>2</sub>SO<sub>4</sub>, and filtered. After removal of all volatiles under reduced pressure, flash chromatography (CH<sub>2</sub>Cl<sub>2</sub>/AcOEt 10:1) followed by a crystallisation (CHCl<sub>3</sub>/MeOH) afforded 552 mg (574 μmol, 8.5%) of the protected diphenylporphyrin as a purple solid.

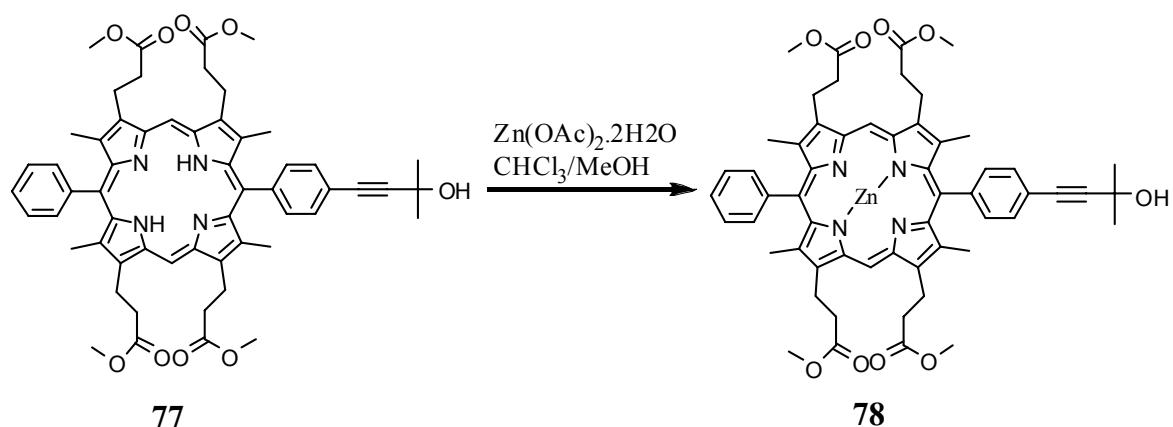
$C_{57}H_{60}N_4O_9$ : 944.4 g/mol

**Maldi-TOF:**  $m/z$ : 946.11  $[M]^+$

**TLC:**  $R_f$  = 0.33,  $CH_2Cl_2/AcOEt$  (10:1)

**$^1H$ -NMR** (400 MHz,  $CDCl_3$ ):  $\delta$  (ppm) = 10.26 (s, 2H, H-meso), 8.04-8.01 (m, 4H, H-aro), 7.99-7.74 (m, 5H, H-aro), 4.35 (m, 8H,  $-CH_2-CH_2-CO_2Me$ ), 3.66 (s, 12H,  $-OCH_3$ ), 3.15 (m, 8H,  $-CH_2-CH_2-CO_2Me$ ), 2.50 (d,  $J$  = 12.4 Hz, 12H,  $-CH_3$ ), 1.79 (s, 6H,  $-C(CH_3)_2OH$ ), 2.43 (s, 2H,  $-NH$ ).

### Zinc protected acetylene diphenylporphyrin **78**:



To a solution of protected diphenylporphyrin **77** (150 mg, 156  $\mu$ mol, 1eq) in a 1:5 mixture of MeOH and  $CHCl_3$  (6ml), 1.71 g (7.8 mol, 50 eq.) of zinc acetate were added. The mixture was refluxed for 5 min. After removal of the solvent under reduced pressure, the residue was dissolved in  $CH_2Cl_2$ ; the white solid was filtered off and washed with  $CH_2Cl_2$ . The solvent was removed under reduced pressure, and the zinc protected diphenylporphyrin **78** (160 mg, 156  $\mu$ mol, 100%) were isolated as a red solid.

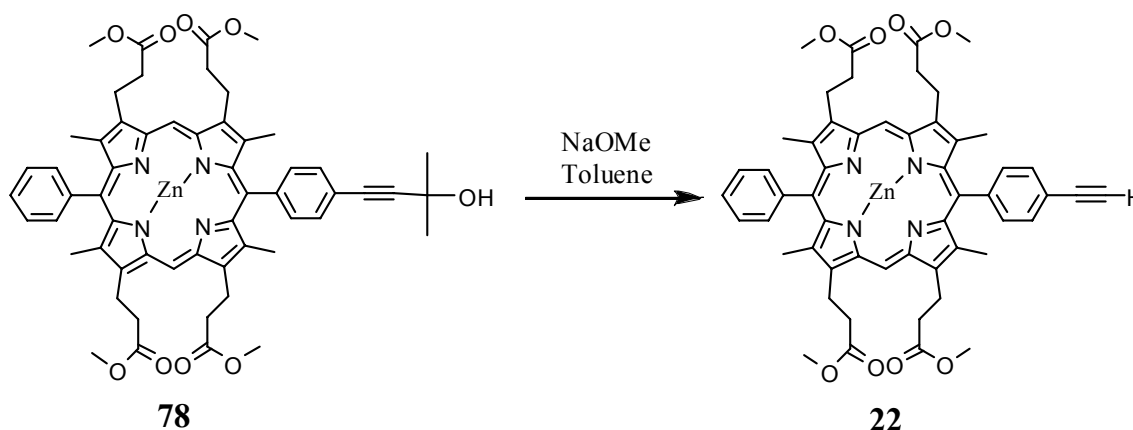
$C_{57}H_{58}N_4O_9Zn$ : 1006.35 g/mol

**Maldi-TOF:** m/z: 1009.3  $[M]^+$

**TLC:**  $R_f = 0.35$ ,  $CH_2Cl_2/AcOEt$  (10:1)

**$^1H$ -NMR** (400 MHz,  $CDCl_3$ ):  $\delta$  (ppm) = 10.20 (s, 2H, H-meso), 8.04-8.01 (m, 4H, H-aro), 7.99-7.74 (m, 5H, H-aro), 4.34-4.30 (m, 8H,  $-CH_2-CH_2-CO_2Me$ ), 3.68 (s, 12H,  $-O-CH_3$ ), 3.15 (m, 8H,  $-CH_2-CH_2-CO_2Me$ ), 2.46 (d,  $J = 12.4$  Hz, 12H,  $-CH_3$ ), 1.79 (s, 6H,  $-C(CH_3)_2OH$ ).

### Zinc acetylene diphenylporphyrin **22**:



Zinc protected diphenylporphyrin **78** (160 mg, 159  $\mu$ mol, 1 eq.) was dissolved in anhydrous toluene (25 ml), and sodium methoxide (260 mg, 4.68 mmol, 30 eq.) was added. The reaction mixture was refluxed under Ar for 4h. The solution was diluted with toluene (20 ml), and the organic layer was washed with 2M HCl ( $2 \times 10$  ml), brine ( $2 \times 10$  ml), and dried over  $NaSO_4$ . After removal of all volatiles at reduced pressure, recrystallisation from  $CHCl_3/MeOH$  gave the diphenylporphyrin **22** (110 mg, 114  $\mu$ mol, 73%) as a red solid.

$C_{54}H_{52}N_4O_8Zn$ : 948.31 g/mol

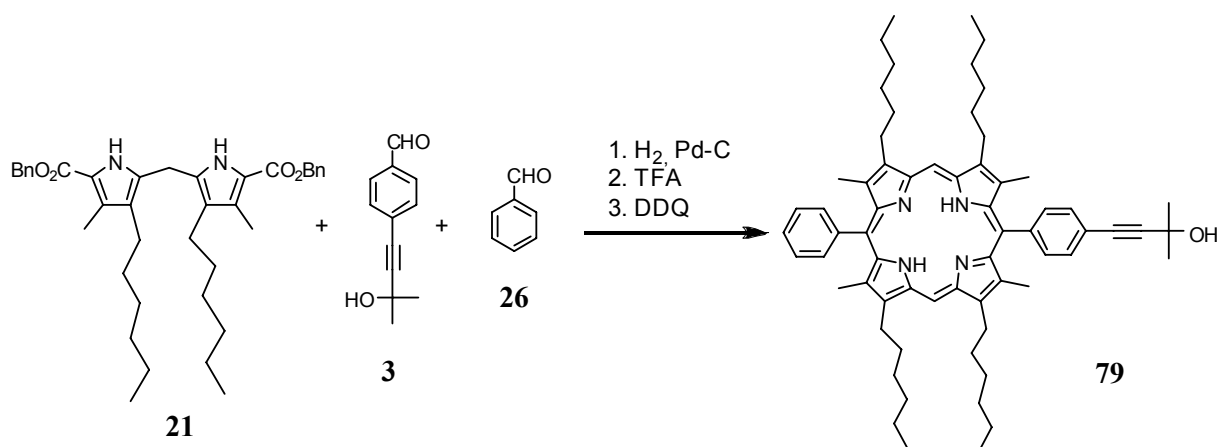
**Maldi-TOF:** m/z: 949.6  $[M]^+$

**TLC:**  $R_f = 0.85$ ,  $\text{CH}_2\text{Cl}_2/\text{AcOEt}$  (10:1)

**$^1\text{H-NMR}$**  (400 MHz,  $\text{CDCl}_3$ ):  $\delta$  (ppm) = 10.21 (s, 2H, H-meso), 8.05-8.03 (m, 4H, H-aro), 7.90-7.70 (m, 5H, H-aro), 4.32-4.30 (m, 8H,  $-\text{CH}_2-\text{CH}_2-\text{CO}_2\text{Me}$ ), 3.66 (s, 12H,  $-\text{OCH}_3$ ), 3.34 (s, 1H,  $-\text{CH}$ ), 3.14 (m, 8H,  $-\text{CH}_2-\text{CH}_2-\text{C O}_2\text{Me}$ ), 2.50 (d, , 12H,  $J = 12.4$  Hz,  $-\text{CH}_3$ ).

## 10.2 Zinc diphenylporphyrin with hexyl chain

### Protected acetylene diphenylporphyrin **79**:



To a solution of dipyrromethane **21** (4 g, 6.8 mmol, 2 eq.) in THF (50 ml), MeOH (6 ml) and TEA (2 ml), Pd/C (320 mg, 10%) were added. The reaction mixture was degassed by bubbling  $\text{H}_2$  for 30 min, and kept under  $\text{H}_2$  for 2h at RT. After filtration of the reaction mixture *via* canula under Ar pressure, the residue was washed twice with a 10:1 degassed mixture of THF and MeOH. After removal of the solvent under reduced pressure, the oil residue was dried at the vacuum line for several hours to give white foam. The resulting deprotected dipyrromethane was dissolved in degassed TFA (35 ml) at  $0^\circ\text{C}$  under Ar. The reaction mixture was stirred in dark at  $0^\circ\text{C}$  for 10 min, and then at RT for 0.5 h until everything was dissolved. Benzaldehyde (0.34 ml, 3.4 mmol, 1 eq) and the alkynylbenzaldehyde (0.96 g, 10.2 mmol, 1.5 eq) were dissolved in MeOH (65 ml); the solution was

degassed with Ar, and added to the reaction mixture over 30 min at  $-10^{\circ}\text{C}$  *via* canula. The mixture was allowed to stir at RT for 2h, and DDQ (2.32 g, 10.2 mmol) was added. The dark green solution was stirred overnight (in the light), diluted in  $\text{CH}_2\text{Cl}_2$  (50 ml) and neutralised with TEA (36 ml) in an ice bath. The organic layer was washed 3 times with water and NaCl sat., dried over  $\text{Na}_2\text{SO}_4$ , and filtered. After removal of all volatiles at reduced pressure, flash chromatography ( $\text{CH}_2\text{Cl}_2/\text{MeOH}$ , 50:1) afforded (253 mg, 270  $\mu\text{mol}$ , 4.2%) of the protected diphenylporphyrin **79** as a purple solid.

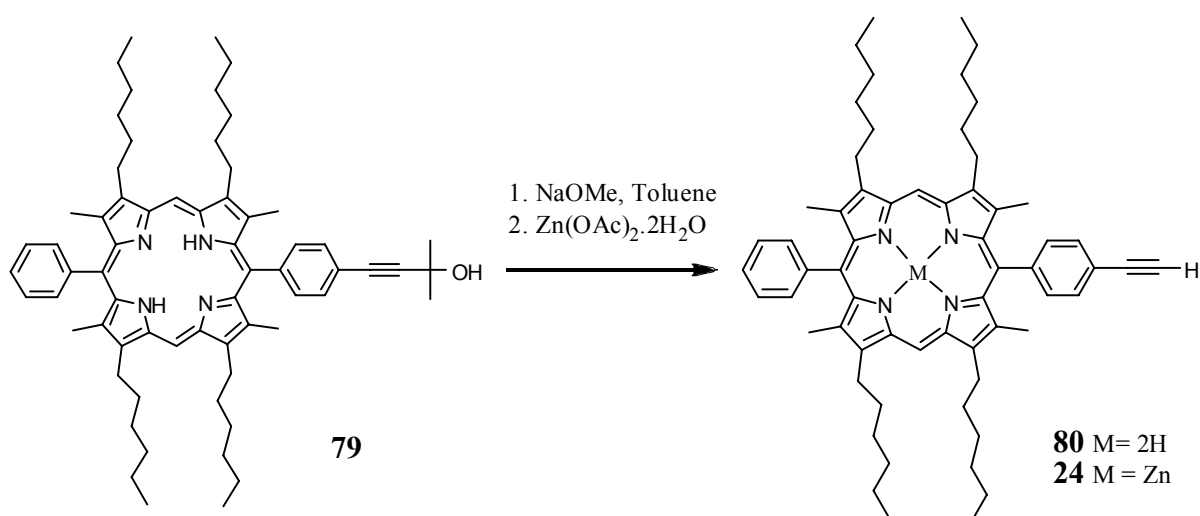
$\text{C}_{65}\text{H}_{84}\text{N}_4\text{O}$ : 936.66 g/mol

**Maldi-TOF**:  $m/z$ : 936.05  $[\text{M}]^+$

**TLC**:  $R_f = 0.45$ , DCM/EA (95:5)

**$^1\text{H-NMR}$**  (400 MHz,  $\text{CDCl}_3$ ):  $\delta$  (ppm) = 10.17 (s, 2H, H-meso), 8.08-8.05 (m, 4H, H-aro), 7.89-7.73 (m, 5H, H-aro), 3.95 (m, 8H,  $-\text{CH}_2-\text{C}_5\text{H}_{11}$ ), 2.48 (d,  $J = 10$  Hz, 12H,  $-\text{CH}_3$ ), 2.16 (m, 8H,  $-\text{CH}_2-\text{CH}_2-\text{C}_4\text{H}_9$ ), 1.83 (s, 6H,  $-\text{C}(\text{CH}_3)_2\text{OH}$ ), 1.71 (m, 8H,  $-\text{C}_2\text{H}_4-\text{CH}_2-\text{C}_3\text{H}_7$ ), 1.50-1.25 (m, 16H,  $-\text{C}_3\text{H}_6-\text{C}_2\text{H}_4-\text{CH}_3$ ), 0.89-0.91 (m, 12H,  $-\text{C}_5\text{H}_{10}-\text{CH}_3$ ), -2.45 (s, 2H,  $-\text{NH}$ ).

### Zinc acetylene diphenylporphyrin **24**:



Protected diphenylporphyrin **79** (250 mg, 0.27 mmol, 1 eq.) was dissolved in anhydrous toluene (50 ml), and sodium methoxide (406 mg, 7.52 mmol, 30 eq) was added. The reaction mixture was stirred at reflux under Ar for 3h. The solution was diluted with toluene (40 ml), and the organic layer was washed with 2M HCl (2×20 ml), brine (2×20 ml), and dried over NaSO<sub>4</sub>. Filtration and removal of all volatiles under reduced pressure gave the deprotected diphenylporphyrin **80** (150 mg, 150 μmol, 56%) as a purple solid.

The deprotected diphenylporphyrin **80** (150 mg, 150 μmol, 1eq) was in a 1:5 mixture of MeOH and CHCl<sub>3</sub> (6ml), and zinc acetate (1.65 g, 7.5 mmol, 50 eq) was added. The mixture was refluxed for 5 min. After removal of the solvent at reduced pressure, the residue was dissolved in CH<sub>2</sub>Cl<sub>2</sub> and the white solid was filtered off and then washed with CH<sub>2</sub>Cl<sub>2</sub>. The solvent was removed at reduced pressure, and flash chromatography (CH<sub>2</sub>Cl<sub>2</sub>/AcOEt, 50:1) afforded 141 mg (150 μmol, 100%) of the diphenylporphyrin **24** as a red solid.

**C<sub>62</sub>H<sub>76</sub>N<sub>4</sub>Zn**: 940.66 g/mol

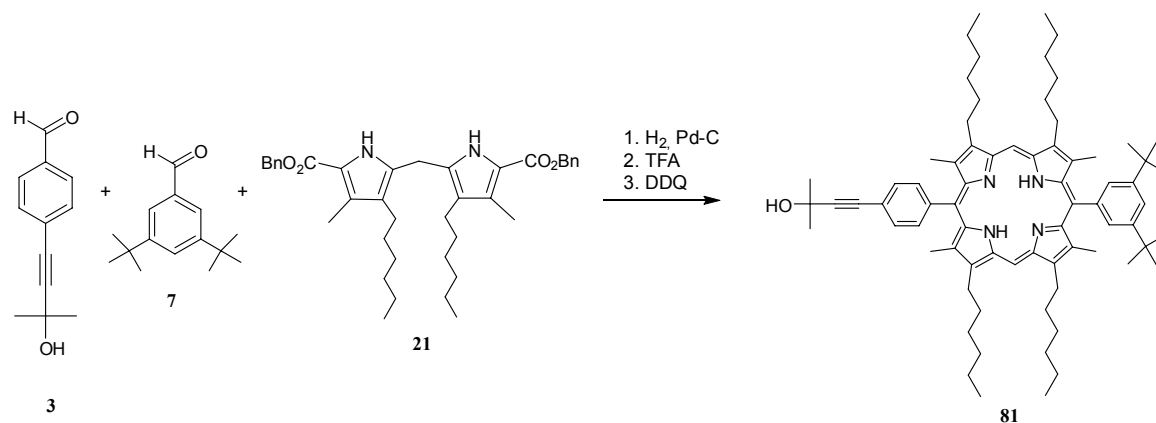
**Maldi-TOF**: m/z: 940.54 [M]<sup>+</sup>

**TLC**: R<sub>f</sub> = 0.90, DCM/EA (95:5)

**<sup>1</sup>H-NMR** (400 MHz, CDCl<sub>3</sub>): δ (ppm) = 10.17 (s, 2H, H-meso), 8.08-8.05 (m, 4H, H-aro), 7.89-7.73 (m, 5H, H-aro), 3.95 (m, 8H, -CH<sub>2</sub>-C<sub>5</sub>H<sub>11</sub>), 3.33 (s, 1H, -CH), 2.48 (d, *J* = 10 Hz, 12H, -CH<sub>3</sub>), 2.16 (m, 8H, -CH<sub>2</sub>-CH<sub>2</sub>-C<sub>4</sub>H<sub>9</sub>), 1.71 (m, 8H, -C<sub>2</sub>H<sub>4</sub>-CH<sub>2</sub>-C<sub>3</sub>H<sub>7</sub>), 1.50-1.25 (m, 16H, -C<sub>3</sub>H<sub>6</sub>-C<sub>2</sub>H<sub>4</sub>-CH<sub>3</sub>), 0.89-0.91 (m, 12H, -C<sub>10</sub>H<sub>5</sub>-CH<sub>3</sub>).

### 10.3 Zinc diphenylporphyrin bearing hexyl chain and di-tertbutylbenzaldehyde

#### Protected acetylene diphenylporphyrin **81**:



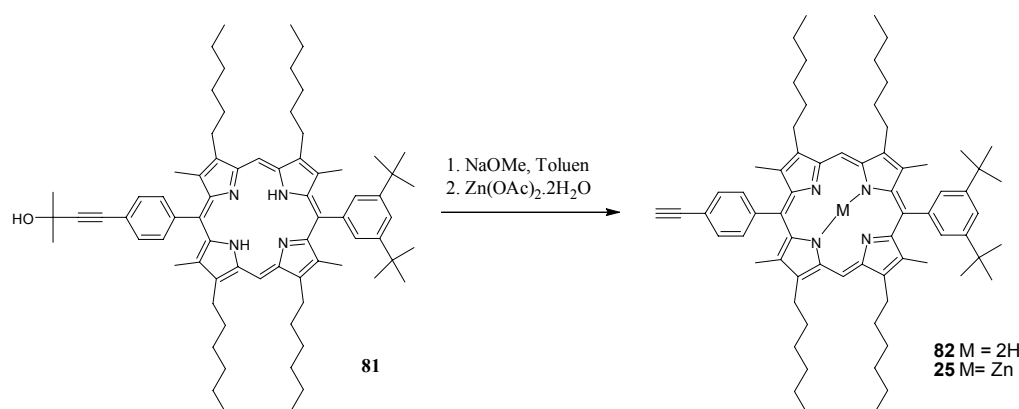
To a solution of dipyrromethane **21** (4 g, 6.8 mmol, 2 eq.) in THF (50 ml), MeOH (6 ml), TEA (2 ml), and finally Pd/C (320 mg, 10%) was added. The reaction mixture was degassed with H<sub>2</sub> for 30 min, and kept under H<sub>2</sub> for 2h at RT. After filtration of the reaction mixture *via* canula under Ar pressure, the residue was washed twice with a 10:1 degassed mixture of THF and MeOH. After removal of the solvent under reduced pressure, the oil residue was dried at the vacuum line for several hours to give white foam. The resulting deprotected dipyrromethane was dissolved in degassed TFA (35 ml) at 0°C under Ar. The reaction mixture was stirred in dark at 0°C for 10 min, and then at RT for half an hour until everything was dissolved. 0.72 g (3.4 mmol, 1 eq) of di-tertbutylbenzaldehyde **7** and 0.96 g (5.25 mmol, 1.5 eq) of the alkyne-benzaldehyde **3** were dissolved in MeOH (65 ml); the solution was degassed with Ar, and added to the reaction mixture in 30 min at -10°C *via* canula. The mixture was allowed to stir at RT for 2h, and DDQ (2.32 g, 10.2 mmol) was added. The dark green solution was stirred overnight (in the light), diluted in CH<sub>2</sub>Cl<sub>2</sub> (50 ml) and neutralised with TEA (36 ml) in an ice bath. The organic layer was washed 3 times with water and NaCl sat., dried over Na<sub>2</sub>SO<sub>4</sub>, filtered and evaporated under reduced pressure. First flash chromatography on basic alox (DCM) removed the first porphyrin (symetric di-tertbutylporphyrin), a second flash chromatography on silica gel (CH<sub>2</sub>Cl<sub>2</sub>/MeOH, 50:1)

gave the desired porphyrin. A final recrystallisation ( $\text{CHCl}_3/\text{MeOH}$ ) afforded 356 mg (0.34 mmol, 10%) of the protected diphenylporphyrin **81** as a purple solid.

$\text{C}_{73}\text{H}_{100}\text{N}_4\text{O}$ : 1048.79 g/mol

**Maldi-TOF**: m/z: 1048.6  $[\text{M}]^+$

### Zinc acetylene diphenylporphyrin **25**:



The protected diphenylporphyrin **81** (356 mg, 0.34 mmol, 1 eq) was dissolved in anhydrous toluene (60 ml), and 850 mg (0.15 mol, 45 eq) of sodium methoxide was added. The reaction mixture was stirred at reflux under Ar for 4h. The solution was diluted with toluene (60 ml), and the organic layer was washed with 2M HCl ( $2 \times 30$  ml), brine ( $2 \times 30$  ml), dried over  $\text{NaSO}_4$  and evaporated at reduced pressure. We obtained the deprotected diphenylporphyrin (247 mg, 0.25 mmol, 73%) **82** as a red solid.

To a solution of deprotected diphenylporphyrin **82** (247 mg, 0.25 mmol) in a 1:5 mixture of MeOH and  $\text{CHCl}_3$  (25ml), 2.7 g (12.5 mmol, 50 eq) of zinc acetate was added. The mixture was refluxed for 5 min. After removal of the solvent under reduced pressure, the residue was dissolved in  $\text{CH}_2\text{Cl}_2$  and the white solid was filtered off and then washed with  $\text{CH}_2\text{Cl}_2$ . The



solvent was removed under reduced pressure, and a flash chromatography ( $\text{CH}_2\text{Cl}_2$ ) gave the desired diphenylporphyrin **25** (256 mg, 0.25 mmol, 74%) as a red solid.

$\text{C}_{70}\text{H}_{92}\text{N}_4\text{Zn}$ : 1052.66 g/mol

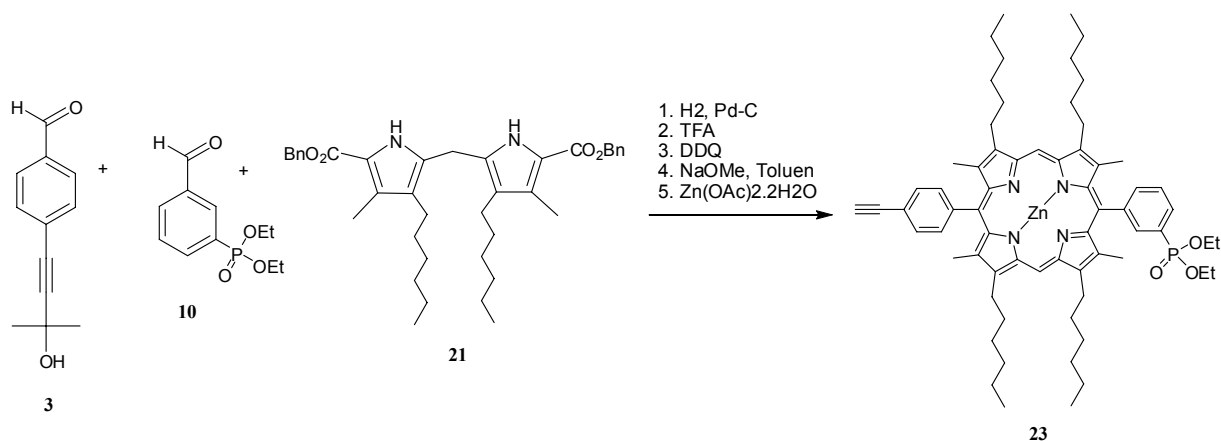
**Maldi-TOF**:  $m/z$ : 1052.5  $[\text{M}]^+$

**TLC**:  $R_f = 0.95$ , ( $\text{CH}_2\text{Cl}_2$ )

**$^1\text{H-NMR}$**  (400 MHz,  $\text{CDCl}_3$ ):  $\delta$  (ppm) = 10.19 (s, 2H, H-meso), 8.06 (m, 2H,  $\text{H}_{(\text{m})}\text{-C}_6\text{H}_4$ ), 7.92 (m, 2H,  $\text{H}_{(\text{o})}\text{-C}_6\text{H}_3$ ), 7.87 (m, 2H,  $\text{H}_{(\text{o})}\text{-C}_6\text{H}_4$ ), 7.80 (m, 1H,  $\text{H}_{(\text{p})}\text{-C}_6\text{H}_3$ ), 3.96 (m, 8H,  $\text{-CH}_2\text{-C}_5\text{H}_{11}$ ), 3.33 (s, 1H,  $\text{HC}\equiv\text{C-}$ ), 2.45 (d, 12H,  $J = 10$  Hz, 4x  $\text{-CH}_3$ ), 2.17 (m, 8H,  $\text{-CH}_2\text{-CH}_2\text{-C}_4\text{H}_9$ ), 1.73 (m, 8H,  $\text{-C}_2\text{H}_4\text{-CH}_2\text{-C}_3\text{H}_7$ ), 1.53-1.48 (m, 26H,  $\text{-C}_3\text{H}_6\text{-CH}_2\text{-C}_2\text{H}_5$  +  $\text{-C}(\text{CH}_3)_3$ ), 1.38 (m, 8H,  $\text{-C}_4\text{H}_8\text{-CH}_2\text{-CH}_3$ ), 0.90 (m, 12H,  $\text{-C}_{10}\text{H}_5\text{-CH}_3$ ).

## 10.4 Zinc diphenylporphyrin bearing hexyl chain and phosphonate group

### Synthesis of the acetylene phosphonate diphenylporphyrin **23**:



To a solution of dipyrromethane **21** (0.82 g, 1.34 mmol, 2 eq.) in THF (12 ml), MeOH (1.5 ml) and TEA (0.3 ml), Pd/C (70 mg, 10%) was added. The reaction mixture was degassed with H<sub>2</sub> for 30 min, and kept under H<sub>2</sub> for 2h at RT. After filtration of the reaction mixture *via* canula under Ar, the residue was washed twice with a 10:1 degassed mixture of THF and MeOH. After removal of the solvent under reduced pressure, the oil residue was dried at the vacuum line for several hours to give white foam. The resulting deprotected dipyrromethane was dissolved in degassed TFA (8 ml) at 0°C under Ar. The reaction mixture was stirred in dark at 0°C for 10 min, and then at RT for half an hour until everything was dissolved. Diethyl 3-formylphenylphosphonate (250 mg, 1 mmol, 0.75 eq) and 0.96 g (253 mg, 1.34 mmol, 1 eq) of the alkynyl-benzaldehyde were dissolved in MeOH (13 ml) and DCM (2 ml) (diethyl 3-formylphenylphosphonate was not soluble in MeOH). The solution was degassed with Ar, and added to the reaction mixture in 30 min at -10°C *via* canula. The mixture was allowed to stir at RT for two and half hours, and DDQ (0.47 g, 2 mmol) was added. The dark green solution was stirred overnight (in the light), diluted in CH<sub>2</sub>Cl<sub>2</sub> (15 ml) and neutralised with TEA (10 ml) in an ice bath. The organic layer was washed 3 times with water and NaCl sat., dried over Na<sub>2</sub>SO<sub>4</sub>, and filtered. After removal of all volatiles at reduced pressure, a flash chromatography (CH<sub>2</sub>Cl<sub>2</sub>/MeOH, 50:1 to 25:1), then a recrystallisation in

CHCl<sub>3</sub>/MeOH gave the protected diphenylporphyrin (94 mg, 87 μmol, 6.5%) as a purple solid.

**TLC:** R<sub>f</sub> = 0.48, CH<sub>2</sub>Cl<sub>2</sub>/MeOH (25:1)

To a solution of protected diphenylporphyrin (94 mg, 87 μmol) in a 1:5 mixture of MeOH and CHCl<sub>3</sub> (3ml), 0.94 g (4.4 mmol, 50 eq) of zinc acetate were added. The mixture was refluxed for 5 min. After removal of the solvent under reduced pressure, the residue was dissolved in CH<sub>2</sub>Cl<sub>2</sub> and the white solid was filtered off and then washed with CH<sub>2</sub>Cl<sub>2</sub>. The solvent was removed at reduced pressure, and we obtained the protected Zn diphenylporphyrin (100 mg, 88 μmol, 99 %) as a red solid.

**TLC:** R<sub>f</sub> = 0.24, CH<sub>2</sub>Cl<sub>2</sub>/MeOH (50:1)

The protected Zn diphenylporphyrin (100 mg, 88 μmol, 1 eq) was dissolved in anhydrous toluene (17 ml), and 250 mg (4.63 mmol, 30 eq) of sodium methoxide were added. The reaction mixture was stirred at reflux under Ar for 4h. The solution was diluted with toluene (20 ml), and the organic layer was washed with 2M HCl (2×10 ml), brine (2×10 ml), and dried over NaSO<sub>4</sub>. After filtration and removal of all volatiles at reduced pressure, a flash chromatography column (CH<sub>2</sub>Cl<sub>2</sub>/MeOH, 50:1) afforded the diphenylporphyrin **23** (60 mg, 55.6 μmol, 63%) as a red solid.

**C<sub>66</sub>H<sub>85</sub>N<sub>4</sub>O<sub>3</sub>PZn:** 1076.57 g/mol

**Maldi-TOF:** m/z: 1076.08 [M]<sup>+</sup>

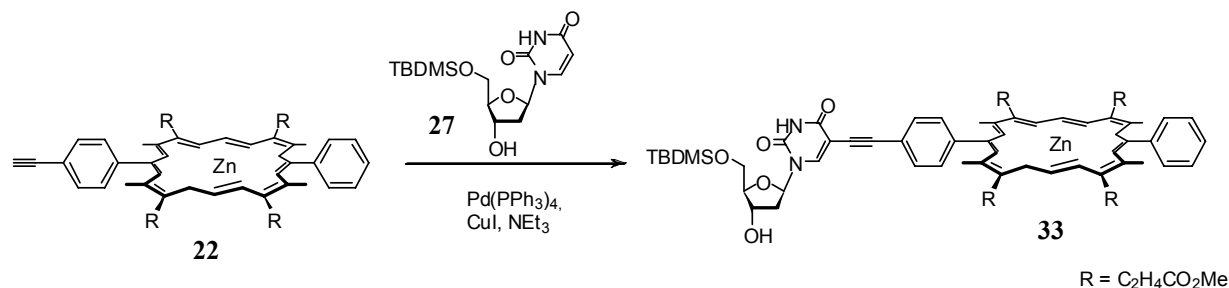
**TLC:** R<sub>f</sub> = 0.33, CH<sub>2</sub>Cl<sub>2</sub>/MeOH (50:1)

**<sup>1</sup>H-NMR** (400 MHz, CDCl<sub>3</sub>): δ (ppm) = 10.19 (s, 2H, H-meso), 8.56 (m, 8H, H<sub>(aro)</sub>), 4.24 (m, 4H, -CH<sub>2</sub>CH<sub>3</sub>), 3.95 (m, 8H, -CH<sub>2</sub>-C<sub>5</sub>H<sub>11</sub>), 3.33 (s, 1H, HC≡C-), 2.43 (d, 12H, J = 16 Hz, -CH<sub>3</sub>), 2.16 (m, 8H, -CH<sub>2</sub>-CH<sub>2</sub>-C<sub>4</sub>H<sub>9</sub>), 1.73 (m, 8H, -C<sub>2</sub>H<sub>4</sub>-CH<sub>2</sub>-C<sub>3</sub>H<sub>7</sub>), 1.48 (m, 8H, -C<sub>3</sub>H<sub>6</sub>-CH<sub>2</sub>-C<sub>2</sub>H<sub>5</sub>), 1.37 (m, 14H, -C<sub>4</sub>H<sub>8</sub>-CH<sub>2</sub>-CH<sub>3</sub> + -CH<sub>2</sub>CH<sub>3</sub>), 0.90 (m, 12H, -C<sub>5</sub>H<sub>10</sub>-CH<sub>3</sub>).



## 11 Synthesis of the building blocks

### 11.1 5'-O-TBDMS-dU<sup>ZnDPP</sup> **33**



To a solution of 5'-TBDMSO-iodouracile **27** (76 mg, 0.13 mmol, 1.5 eq.) in DMF (2 ml), CuI (6.3 mg, 0.033 mmol, 40 %) was added in the dark under Argon. TEA (46  $\mu$ l, 0.33 mmol, 4 eq.) was added when all the CuI was dissolved. The porphyrin **22** (80 mg, 83  $\mu$ mol) was dissolved in 2ml of DMF and added to the mixture. Finally, 19 mg (0.017, 20%) of Pd(PPh<sub>3</sub>)<sub>4</sub> was added, the reaction mixture was stirred under an inert atmosphere for 4 days. The solution was diluted with 80 ml of AcOEt, washed with a solution of H<sub>2</sub>O/NaCl (1:1, 6 $\times$ 25 ml) and dried over Na<sub>2</sub>SO<sub>4</sub>. Evaporation of the solvent at reduced pressure yielded the crude product which was purified by column chromatography on silica gel (gradient of CH<sub>2</sub>Cl<sub>2</sub>/MeOH from 100:0.5 to 50:1). This afforded the 5'-O-TBDMS-dU<sup>ZnDPP</sup> **33** (124 mg, 0.09 mmol, 95%) as a red solid.

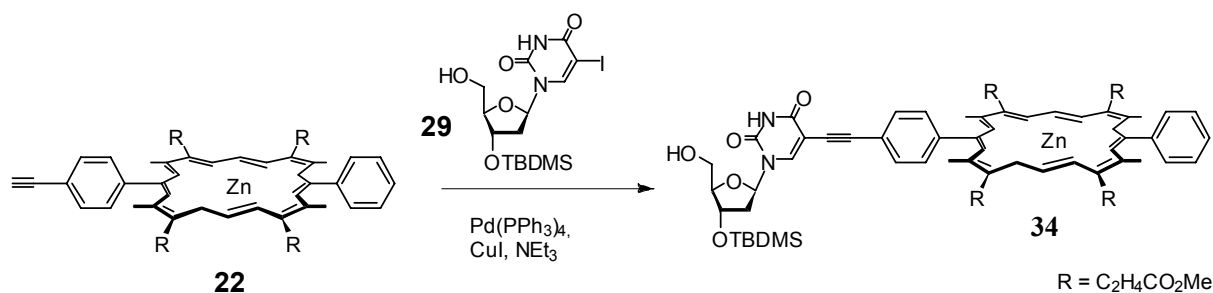
**C<sub>69</sub>H<sub>76</sub>N<sub>6</sub>O<sub>13</sub>SiZn**: 1288.45 g/mol

**Maldi-TOF**: m/z: 1291.6 [M]<sup>+</sup>

**TLC**: R<sub>f</sub> = 0.63, DCM/MeOH (10:1)

**<sup>1</sup>H-NMR** (400 MHz, CDCl<sub>3</sub>):  $\delta$  (ppm) = 10.09 (2H, s, H-meso), 8.05 (s, 1H, -NH), 8.05-7.98 (m, 5H, H-aro), 7.85-7.77 (m, 6H, H-aro), 6.22-6.20 (m, 1H, H-1'), 5.36-5.35 (m, 1H, H-3'), 4.22-4.21 (m, 8H, -CH<sub>2</sub>-CH<sub>2</sub>-CO<sub>2</sub>Me), 3.95-3.92 (m, 2H, H-5'), 3.83-3.81 (m, 1H, H-4'), 3.54 (s, 12H, -O-CH<sub>3</sub>), 3.12-3.08 (m, 8H, -CH<sub>2</sub>-CH<sub>2</sub>-CO<sub>2</sub>Me), 2.47 (d,  $J$  = 10, 12H, -CH<sub>3</sub>), 2.21-2.19 (m, 2H, H-2'), 0.99 (s, 9H, -SiC<sub>5</sub>(CH<sub>3</sub>)<sub>3</sub>), 0.21 (d,  $J$  = 6 Hz, 6H, -Si(CH<sub>3</sub>)<sub>2</sub>).

## 11.2 3'-O-TBDMS-dU<sup>ZnDPP</sup> **34**



To a solution of 3'-TBDMSO-iodouracil **29** (76 mg, 0.13 mmol, 1.5 eq.) in DMF (2 ml), CuI (6.3 mg, 0.033 mmol, 40 %) was added in dark under Argon. TEA (46  $\mu\text{l}$ , 0.33 mmol, 4 eq.) was added when all the CuI was dissolved. The porphyrin **22** (80 mg, 83  $\mu\text{mol}$ ) was dissolved in DMF (2ml) and added to the mixture. Finally, Pd(PPh<sub>3</sub>)<sub>4</sub> (19 mg, 0.0166, 20%) was added, the reaction mixture was stirred under an inert atmosphere for 4 days. The solution was diluted with 80 ml of AcOEt, washed with a solution of H<sub>2</sub>O/NaCl (1:1, 6  $\times$  25 ml) and dried over Na<sub>2</sub>SO<sub>4</sub>. Evaporation of the solvent at reduced pressure yielded the crude product which was purified first by column chromatography on silica gel (gradient of CH<sub>2</sub>Cl<sub>2</sub>/MeOH from 100:0.5 to 100:1.2), then by column chromatography on sephadex G15 (CH<sub>2</sub>Cl<sub>2</sub>/MeOH 1:1) afforded the 3'-O-TBDMS-dU<sup>ZnDPP</sup> **34** (98 mg, 0.07 mmol, 82%) as a red solid.

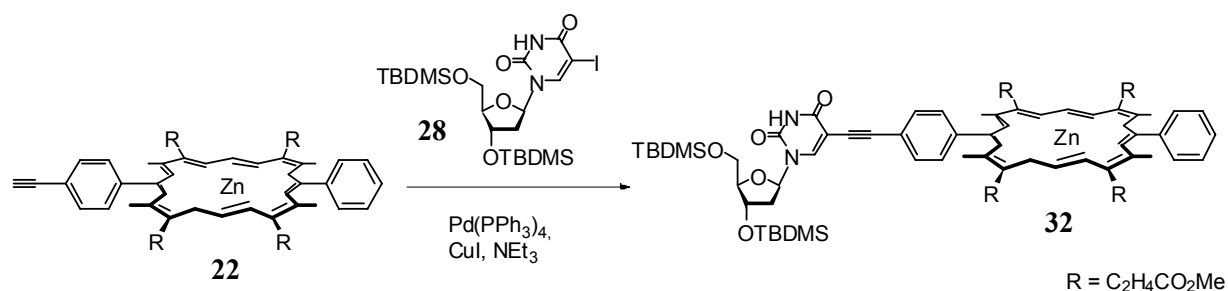
**C<sub>69</sub>H<sub>76</sub>N<sub>6</sub>O<sub>13</sub>SiZn**: 1288.45 g/mol

**Maldi-TOF**: m/z: 1291.6 [M]<sup>+</sup>

**TLC**: R<sub>f</sub> = 0.52, DCM/MeOH (20:1)

**<sup>1</sup>H-NMR** (400 MHz, CDCl<sub>3</sub>):  $\delta$  (ppm) = 10.09 (2H, s, H-meso), 8.03 (s, 1H, -NH), 8.05-8.03 (m, 5H, H-aro, H-(6)), 7.91-7.74 (m, 5H, H-aro), 6.17 (m, 1H, H-1'), 4.99 (m, 1H, H-3'), 4.32-4.30 (m, 8H, -CH<sub>2</sub>-CH<sub>2</sub>-CO<sub>2</sub>Me), 4.10-4.08 (m, 2H, H-5'), 3.69 (m, 1H, H-4'), 3.68 (d,  $J = 8.08$  Hz, 12H, -O-CH<sub>3</sub>), 3.15-3.13 (m, 8H, -CH<sub>2</sub>-CH<sub>2</sub>-CO<sub>2</sub>Me), 2.31-2.30 (m, 2H, H-2'), 2.46 (d,  $J = 6.32$  Hz, 12H, -CH<sub>3</sub>), 0.83 (s, 9H, -SiC<sub>5</sub>(CH<sub>3</sub>)<sub>3</sub>), 0.05 (d,  $J = 10.4$  Hz, 6H, -Si(CH<sub>3</sub>)<sub>2</sub>).

### 11.3 3',5'-Bis-O-TBDMS-dU<sup>ZnDPP</sup> **32**



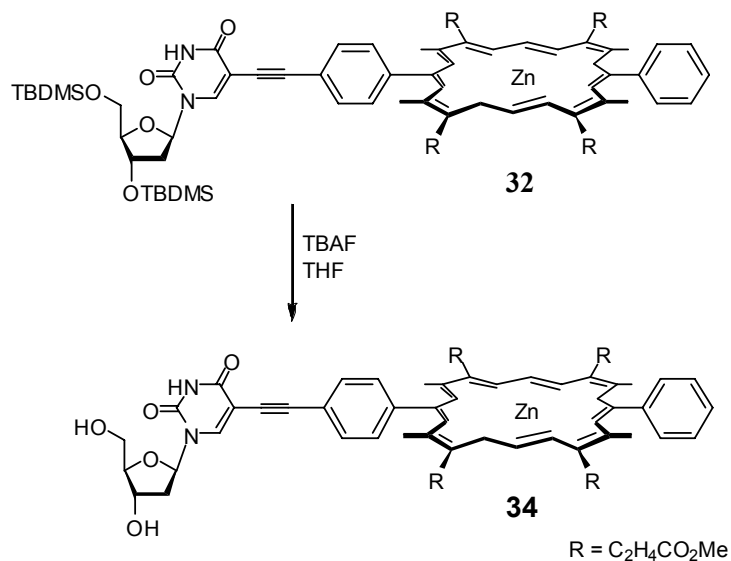
To a solution of 3',5'-Bis-O-TBDMS-iodouracil **28** (60.3 mg, 0.10 mmol, 1 eq) in DMF (4 ml), CuI (7.9 mg, 41.6  $\mu$ mol, 40 %) was added in dark under Argon. TEA (31  $\mu$ l, 416  $\mu$ mol, 4 eq.) was added when all the CuI was dissolved. The porphyrin **22** (100 mg, 104  $\mu$ mol, 1 eq) was dissolved in DMF (2ml) and added to the mixture. Finally, the Pd(PPh<sub>3</sub>)<sub>4</sub> (24 mg, 20.8  $\mu$ mol, 20%) was added, the reaction mixture was stirred under an inert atmosphere for 2 days. The solution was diluted with 60 ml of AcOEt, washed with a solution of H<sub>2</sub>O/NaCl (1:1, 6  $\times$  20 ml) and dried over Na<sub>2</sub>SO<sub>4</sub>. Evaporation of the solvent at reduced pressure yielded the crude product which was purified first by column chromatography on silica gel (gradient of CH<sub>2</sub>Cl<sub>2</sub>/AcOEt 10:1), then by crystallisation (CHCl<sub>3</sub>/Hexane). This afforded the 3',5'-Bis-O-TBDMS-dU<sup>ZnDPP</sup> **32** (45 mg, 31  $\mu$ mol, 30%) as a purple solid.

**C<sub>75</sub>H<sub>90</sub>N<sub>6</sub>O<sub>13</sub>Si<sub>2</sub>Zn**: 1402.54 g/mol

**Maldi-TOF**: m/z: 1404.78 [M]<sup>+</sup>

**TLC**: R<sub>f</sub> = 0.8, CH<sub>2</sub>Cl<sub>2</sub>/EA (10:1)

**<sup>1</sup>H-NMR** (400 MHz, CDCl<sub>3</sub>):  $\delta$  (ppm) = 10.19 (2H, s, H-meso), 8.16 (s, 1H, -NH), 8.06-7.98 (m, 5H, H-aro, H-(6)), 7.85-7.74 (m, 5H, H-aro), 6.19 (m, 1H, H-1'), 5.16-5.15 (m, 1H, H-3'), 4.36-4.32 (m, 8H, -CH<sub>2</sub>-CH<sub>2</sub>-CO<sub>2</sub>Me), 4.03-4.02 (m, 2H, H-5'), 3.30-3.29 (m, 1H, H-4'), 3.70 (d,  $J$  = 3.5 Hz, 12H, -O-CH<sub>3</sub>), 3.16-3.15 (m, 8H, -CH<sub>2</sub>-CH<sub>2</sub>-CO<sub>2</sub>Me), 1.97-1.95 (m, 2H, H-2'), 2.48 (d,  $J$  = 15, 12H, -CH<sub>3</sub>), 0.90 (s, 9H, -SiC<sub>5</sub>-(CH<sub>3</sub>)<sub>3</sub>), 0.88 (s, 9H, -SiC<sub>3</sub>-(CH<sub>3</sub>)<sub>3</sub>), 0.14 (s, 6H, -Si(CH<sub>3</sub>)<sub>2</sub>), 0.07 (s, 6H, -Si(CH<sub>3</sub>)<sub>2</sub>).

**dUZnDPP 34**

To a solution 10 mg (6.96  $\mu\text{mol}$ , 1 eq) of 3',5'-Bis-O-TBDMS-dU<sup>ZnDPP</sup> **32** in THF (3 ml), 8  $\mu\text{l}$  (2.87  $\mu\text{mol}$ , 4 eq) tetrabutylammoniumfluorid (TBAF) was added. The reaction mixture was stirred in an ice bath for 24h under argon. An additional quantity of TBAF (4  $\mu\text{l}$ , 1.43  $\mu\text{mol}$ , 2 eq) was added and the mixture was stirred for an additional 24 h. The solution was diluted in CH<sub>2</sub>Cl<sub>2</sub>, and a small quantity of CaCl<sub>2</sub> was added, and the organic layer was washed with H<sub>2</sub>O (3 $\times$ 5 ml). Drying over Na<sub>2</sub>SO<sub>4</sub> and evaporation of all the solvent at reduced pressure gave dU<sup>ZnDPP</sup> **34** (7.5 mg, 6.74  $\mu\text{mol}$ , 97%) as a purple solid.

**C<sub>63</sub>H<sub>64</sub>N<sub>6</sub>O<sub>13</sub>**: 1112.45 g/mol

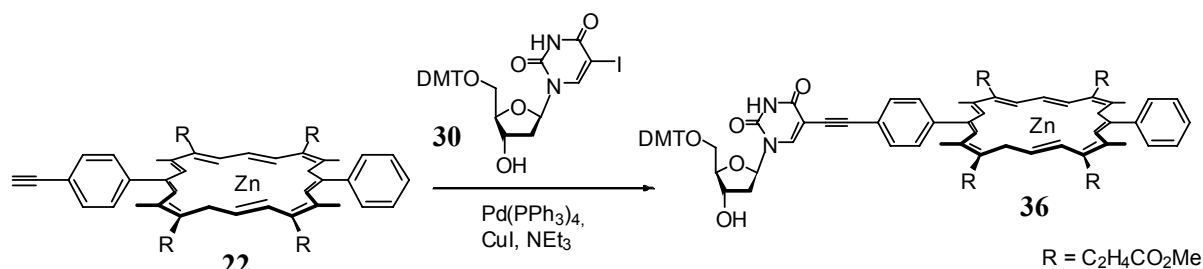
**Maldi-TOF**: m/z: 1111.03 [M]<sup>+</sup>

**TLC**: R<sub>f</sub> = 0.43, CH<sub>2</sub>Cl<sub>2</sub>/MeOH (10:1)

**<sup>1</sup>H-NMR** (400 MHz, CDCl<sub>3</sub>):  $\delta$  (ppm) = 10.09 (2H, s, H-meso), 8.55 (s, 1H, -NH), 8.30 (s, 1H, H-(6)), 8.04-7.98 (m, 4H, H-aro), 7.89-7.76 (m, 5H, H-aro), 6.20 (m, 1H, H-1'), 5.27-5.26 (m, 1H, H-3'), 4.23-4.22 (m, 8H, -CH<sub>2</sub>-CH<sub>2</sub>-CO<sub>2</sub>Me), 3.90-3.89 (m, 1H, H-4'), 3.78-3.63 (m, 2H, H-5'), 3.55 (d,  $J = 2$  Hz, 12H, -O-CH<sub>3</sub>), 3.11-3.10 (m, 8H, -CH<sub>2</sub>-CH<sub>2</sub>-CO<sub>2</sub>Me), 2.27-2.20 (m, 2H, H-2'), 2.37 (d,  $J = 25$ , 12H, -CH<sub>3</sub>).



### 11.4 5'-O-DMT-dU<sup>ZnDPP</sup> **36**



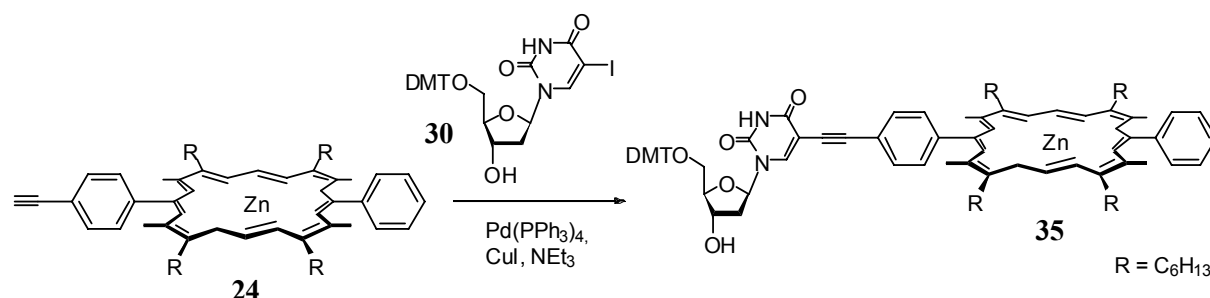
To a solution of 5'-O-DMT-iodouracil **30** (150 mg, 0.23 mmol, 3 eq) in DMF (2 ml), CuI (5.7 mg, 30.2  $\mu$ mol, 40 %) was added in dark under Argon. TEA (25  $\mu$ l, 0.3 mmol, 4 eq.) was added when all the CuI was dissolved. The porphyrin **22** (73 mg, 75.6  $\mu$ mol) was dissolved in DMF (2 ml) and added to the mixture. Finally, the Pd(PPh<sub>3</sub>)<sub>4</sub> (17 mg, 15.1  $\mu$ mol) was added, the reaction mixture was stirred under an inert atmosphere for 3 days. The solution was diluted with 100 ml of AcOEt, washed with a solution of H<sub>2</sub>O/NaCl (1:1, 6 $\times$ 30 ml) and dried over Na<sub>2</sub>SO<sub>4</sub>. Evaporation of the solvent at reduced pressure yielded the crude product which was purified by column chromatography on silica gel (gradient of CH<sub>2</sub>Cl<sub>2</sub>/MeOH from 100:0.5 to 100:1), afforded the 5'-O-DMT-dU<sup>ZnDPP</sup> **19** (48 mg, 32.5  $\mu$ mol, 43%) as a purple solid.

**C<sub>84</sub>H<sub>80</sub>N<sub>6</sub>O<sub>15</sub>Zn**: 1476.50 g/mol

**Maldi-TOF**: m/z: 1477.6 [M]<sup>+</sup>

**<sup>1</sup>H-NMR** (400 MHz, CDCl<sub>3</sub>):  $\delta$  (ppm) = 10.18 (s, 2H, H-meso), 7.84 (s, 1H, -NH), 7.34-7.20 (m, 19H, H<sub>aro</sub>, H-(6)), 6.83-6.80 (m, 4H, H<sub>aro</sub>), 5.86-5.85 (m, 1H, H-1'), 4.62 (m, 2H, H-3' + H-4'), 4.17 (m, 1H, -OH(3')), 3.66 (m, 2H, H-5'), 2.58 (m, 2H, H-2'), 4.36-4.35 (m, 8H, -CH<sub>2</sub>-CH<sub>2</sub>-CO<sub>2</sub>Me), 3.78 (s, 12H, -OCH<sub>3</sub>), 3.65-3.62 (m, 8H, -CH<sub>2</sub>-CH<sub>2</sub>-CO<sub>2</sub>Me), 3.18-3.11 (m, 12H, -CH<sub>3</sub>).

## 11.5 5'-O-DMT-dU<sup>ZnDPP</sup> **35**



To a solution of 5'-O-DMT-iodouracile **30** (96.3 mg, 146.8  $\mu\text{mol}$ , 3 eq) in DMF (1 ml) with molecular sieves (4 Å), CuI (7.4 mg, 39  $\mu\text{mol}$ , 80 %) was added in dark under Argon. TEA (40  $\mu\text{l}$ , 0.48 mmol, 4 eq.) was added when all the CuI was dissolved. The porphyrin **24** (46 mg, 48.9  $\mu\text{mol}$ , 1eq) was dissolved in 2 ml of DMF and added to the mixture. Finally, the Pd(PPh<sub>3</sub>)<sub>4</sub> (22.1 mg, 19  $\mu\text{mol}$ , 40%) was added, the reaction mixture was stirred at inert atmosphere for 24 h. The solution was diluted with AcOEt (80 ml), washed with a solution of H<sub>2</sub>O/NaCl (1:1, 6 $\times$ 25 ml) and dried over Na<sub>2</sub>SO<sub>4</sub>. Evaporation of the solvent at reduced pressure yielded the crude product which was purified by column chromatography on silica gel (gradient of CH<sub>2</sub>Cl<sub>2</sub>/MeOH from 100:0.5 to 100:1), afforded the 5'-O-DMT-dU<sup>ZnDPP</sup> **35** (70 mg, 47.7  $\mu\text{mol}$ , 97%) as a purple solid.

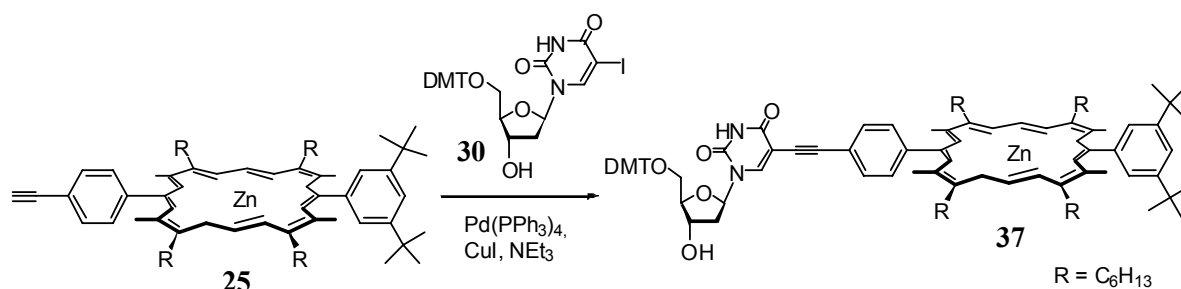
**C<sub>92</sub>H<sub>104</sub>N<sub>6</sub>O<sub>7</sub>Zn**: 1468.73 g/mol

**Maldi-TOF**: m/z: 1468.5 [M]<sup>+</sup>

**TLC**: R<sub>f</sub> = 0.37, DCM/EA (1:1)

**<sup>1</sup>H-NMR** (400 MHz, CDCl<sub>3</sub>):  $\delta$  (ppm) = 10.13 (2H, s, H-meso), 8.16 (s, 1H, -NH), 8.05-7.85 (m, 4H, H-aro), 7.75-7.72 (m, 3H, H-aro), 7.49-7.48 (m, 2H, H-aro), 7.41-7.33 (m, 9H, H-aro), 6.88-6.86 (m, 4H, H-aro), 6.44 (m, 1H, H-1'), 4.66 (m, 2H, H-3' + H-4'), 4.09 (m, 1H, -OH(3')), 3.97-3.95 (m, 8H, -CH<sub>2</sub>-C<sub>5</sub>H<sub>11</sub>), 3.65 (m, 2H, H-5'), 2.55 (m, 2H, H-2'), 2.41 (d,  $J$  = 15 Hz, 12H, -CH<sub>3</sub>), 2.17-2.15 (m, 8H, -CH<sub>2</sub>-CH<sub>2</sub>-C<sub>4</sub>H<sub>9</sub>), 1.76-1.75 (m, 8H, -C<sub>2</sub>H<sub>4</sub>-CH<sub>2</sub>-C<sub>3</sub>H<sub>7</sub>), 1.51-1.48 (m, 8H, -C<sub>3</sub>H<sub>6</sub>-CH<sub>2</sub>-C<sub>2</sub>H<sub>5</sub>), 1.40-1.39 (m, 8H, -C<sub>4</sub>H<sub>8</sub>-CH<sub>2</sub>-CH<sub>3</sub>), 0.89-0.91 (m, 12H, -C<sub>10</sub>H<sub>5</sub>-CH<sub>3</sub>).

## 11.6 5'-O-DMT-dUZnDPP 37



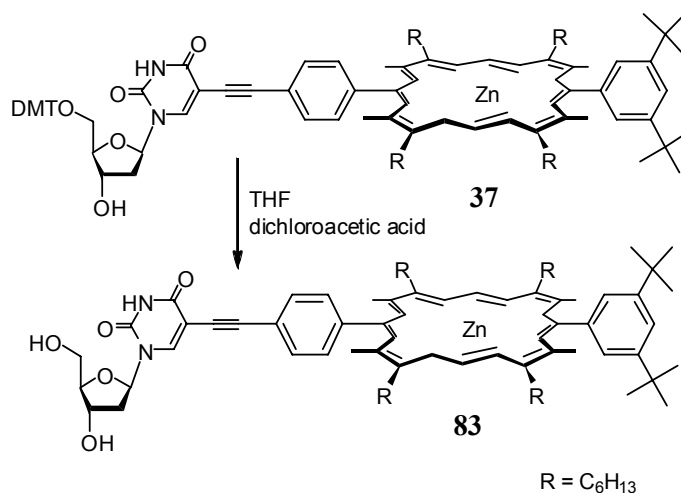
To a solution of 5'-O-DMT-iodouracile (374 mg, 0.57 mmol, 3 eq) in DMF (4 ml) with molecular sieves (4 Å), CuI (29.2 mg, 0.45 mmol, 80 %) was added in the dark under Argon. TEA (0.16 ml, 0.76 mmol, 4 eq.) was added when all the CuI was dissolved. The porphyrin (200 mg, 0.19 mmol, 1eq) was dissolved in DMF (4 ml) and added to the mixture. Finally, 88.5 mg (0.23 mmol, 40%) of the Pd(PPh<sub>3</sub>)<sub>4</sub> was added, the reaction mixture was stirred under argon for 48 h. The solution was diluted with AcOEt (80 ml), washed with a solution of H<sub>2</sub>O/NaCl (1:1, 6×35 ml) and dried over Na<sub>2</sub>SO<sub>4</sub>. Evaporation of the solvent at reduced pressure, followed by a chromatography column on silica gel (gradient of CH<sub>2</sub>Cl<sub>2</sub>/MeOH from 100:0.5 to 100:1) afforded the 5'-O-DMT-dU<sup>ZnDPP</sup> **18** (294 mg, 0.18 mmol, 98%) as a purple solid.

**C<sub>100</sub>H<sub>120</sub>N<sub>6</sub>O<sub>7</sub>Zn**: 1580.85 g/mol

**Maldi-TOF**: m/z: 1581.4 [M]<sup>+</sup>

**TLC**: R<sub>f</sub> = 0.44, DCM/MeOH (100:3).

**<sup>1</sup>H-NMR** (400 MHz, CDCl<sub>3</sub>): δ (ppm) = 10.11 (s, 2H, H-meso), 8.16 (s, 1H, -NH), 7.94 (m, 2H, H-aro), 7.85 (m, 3H, H-aro), 7.77 (m, 4H, H-aro), 7.59 (m, 2H, H-aro), 7.49 (m, 4H, H-aro), 7.40 (m, 3H, H-aro), 6.92 (m, 4H, m-Bz<sub>(m)</sub>), 6.39 (m, 1H, H-1'), 4.59 (m, 2H, H-3' + H-4'), 4.15 (m, 1H, -OH(3')), 3.97 (m, 8H, -CH<sub>2</sub>-C<sub>5</sub>H<sub>11</sub>), 3.62 (m, 2H, H-5'), 2.58 (m, 2H, H-2'), 2.45 (d, 12H, J = 8 Hz, -CH<sub>3</sub>), 2.19 (m, 8H, -CH<sub>2</sub>-CH<sub>2</sub>-C<sub>4</sub>H<sub>9</sub>), 1.77 (m, 8H, -C<sub>2</sub>H<sub>4</sub>-CH<sub>2</sub>-C<sub>3</sub>H<sub>7</sub>), 1.52 (m, 26H, -C<sub>3</sub>H<sub>6</sub>-CH<sub>2</sub>-C<sub>2</sub>H<sub>5</sub> + -C(CH<sub>3</sub>)<sub>3</sub>), 1.40 (m, 8H, -C<sub>4</sub>H<sub>8</sub>-CH<sub>2</sub>-CH<sub>3</sub>), 0.92 (m, 12H, -C<sub>10</sub>H<sub>5</sub>-CH<sub>3</sub>).

11.7 dU<sup>ZnDPP</sup> **83**

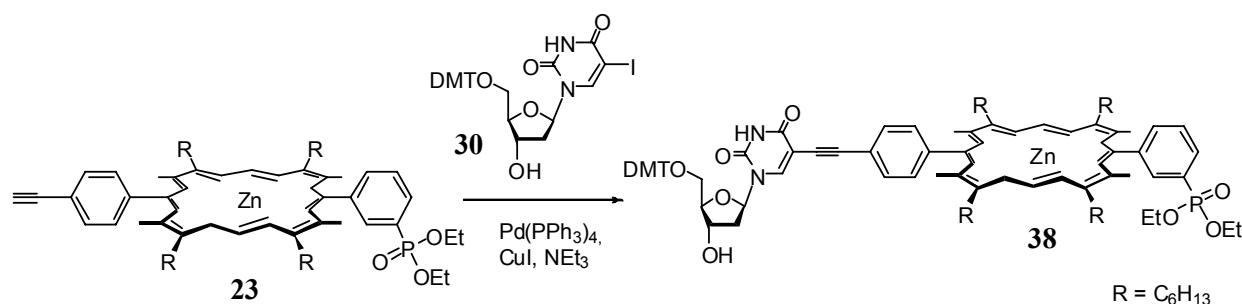
5'-DMT-dU<sup>ZnDPP</sup> **37** (88 mg, 55.5 μmol, 1 eq) was dissolved in dry DCM (5 ml), and 0.25 ml of dichloroacetic acid was added. The reaction mixture was stirred at RT for 30 min. The organic layer was washed with NaHCO<sub>3</sub> and dried over Na<sub>2</sub>SO<sub>4</sub>. Filtration and evaporation of the solvent at reduced pressure yielded the crude product which was purified by a flash chromatography on silica gel (CH<sub>2</sub>Cl<sub>2</sub>/MeOH, 20:1) to yield 20 mg (16 μmol, 28%) of dU<sup>ZnDPP</sup> **83** as purple solid.

**C<sub>79</sub>H<sub>104</sub>N<sub>6</sub>O<sub>5</sub>**: 1216.81 g/mol

**Maldi-TOF**: m/z: 1217.31 [M]<sup>+</sup>

**TLC**: R<sub>f</sub> = 0.17, CH<sub>2</sub>Cl<sub>2</sub>/MeOH (20:1)

**<sup>1</sup>H-NMR** (400 MHz, CDCl<sub>3</sub>): δ (ppm) = 10.19 (s, 2H, H-meso), 8.18 (s, 1H, -NH), 8.06 (m, 2H, H<sub>(m)</sub>-C<sub>6</sub>H<sub>4</sub>), 7.92 (m, 2H, H<sub>(o)</sub>-C<sub>6</sub>H<sub>3</sub>), 7.87 (m, 2H, H<sub>(o)</sub>-C<sub>6</sub>H<sub>4</sub>), 7.80 (m, 1H, H<sub>(p)</sub>-C<sub>6</sub>H<sub>3</sub>), 6.39 (m, 1H, H-1'), 4.59 (m, 2H, H-3' + H-4'), 4.07 (m, 1H, -OH(5')), 4.15 (m, 1H, -OH(3')), 3.96 (m, 8H, -CH<sub>2</sub>-C<sub>5</sub>H<sub>11</sub>), 3.33 (s, 1H, HC≡C-), 3.62 (m, 2H, H-5'), 2.58 (m, 2H, H-2'), 2.45 (d, 12H, J = 10 Hz, 4x -CH<sub>3</sub>), 2.17 (m, 8H, -CH<sub>2</sub>-CH<sub>2</sub>-C<sub>4</sub>H<sub>9</sub>), 1.73 (m, 8H, -C<sub>2</sub>H<sub>4</sub>-CH<sub>2</sub>-C<sub>3</sub>H<sub>7</sub>), 1.53-1.48 (m, 26H, -C<sub>3</sub>H<sub>6</sub>-CH<sub>2</sub>-C<sub>2</sub>H<sub>5</sub> + -C(CH<sub>3</sub>)<sub>3</sub>), 1.38 (m, 8H, -C<sub>4</sub>H<sub>8</sub>-CH<sub>2</sub>-CH<sub>3</sub>), 0.90 (m, 12H, -C<sub>10</sub>H<sub>5</sub>-CH<sub>3</sub>).

**5'-O-DMT-dUZnDPP 38**

To a solution of 5'-O-DMT-iodouracile **30** (109.5 mg, 167  $\mu\text{mol}$ , 3 eq) in DMF (2 ml) with molecular sieves (4  $\text{\AA}$ ), CuI (8.4 mg, 44.4  $\mu\text{mol}$ , 80 %) was added in dark under Argon. TEA (50  $\mu\text{l}$ , 222.4  $\mu\text{mol}$ , 4 eq.) was added when all the CuI was dissolved. The porphyrin **23** (60 mg, 55.6  $\mu\text{mol}$ , 1eq) was dissolved in DMF (2 ml) and added to the mixture. Finally, the Pd(PPh<sub>3</sub>)<sub>4</sub> (25.6 mg, 22.2  $\mu\text{mol}$ , 40%) was added, the reaction mixture was stirred under for 48 h. The solution was diluted with AcOEt (80 ml), washed with a solution of H<sub>2</sub>O/NaCl (1:1, 6 $\times$ 35 ml) and dried over Na<sub>2</sub>SO<sub>4</sub>. Evaporation of the solvent under reduced pressure, followed by a chromatography column on silica gel (CH<sub>2</sub>Cl<sub>2</sub>/MeOH, 50:1) afforded the 5'-O-DMT-dU<sup>ZnDPP</sup> **38** (53 mg, 33  $\mu\text{mol}$ , 60%) as a purple solid.

**C<sub>96</sub>H<sub>113</sub>N<sub>6</sub>O<sub>10</sub>PZn**: 1604.75 g/mol

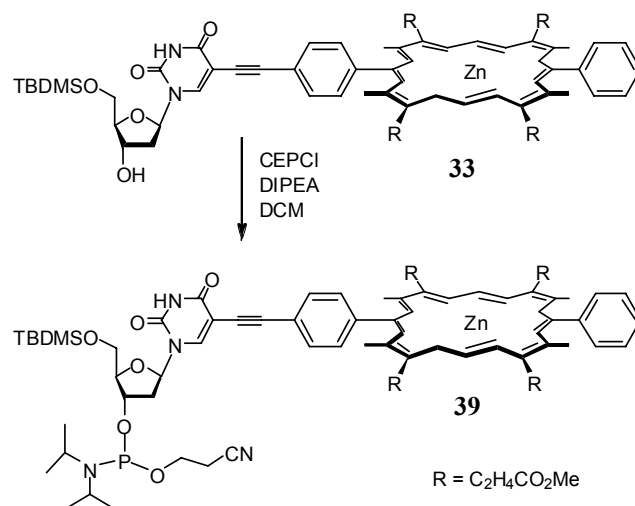
**Maldi-TOF**: m/z: 1605.04 [M]<sup>+</sup>

**TLC**: R<sub>f</sub> = 0.48, DCM/MeOH (50:1).



## 12 Synthesis of the phosphoramidite building block

### 12.1 5'-O-TBDMS-dU<sup>ZnDPP</sup> phosphoramidite **39**



The protected 5'-O-TBDMS-dU<sup>ZnDPP</sup> **33** (20 mg, 15.1 μmol) was co-evaporated three times with dry pyridine, and dried on the vacuum line overnight. The product was dissolved in dry DCM (2 ml) with molecular sieves (powder) and stirred for an hour. Then, diisopropylethylamine (15.4 μl, 90 μmol, 6 eq) and finally the 2-cyanoethyldiisopropylchlorophosphoramidite (13.3 μl, 53 μmol, 3.5 eq) was added and the reaction mixture was stirred for 4h under argon and in dark. The mixture was evaporated and put directly on a chromatography column (EA pure) under argon. We obtained the 5'-O-TBDMS-dU<sup>ZnDPP</sup> phosphoramidite **39** (14.5 mg, 9.7 μmol, 64%) as a purple solid which was kept under argon and in the dark overnight for the next step. (Otherwise, we observed an oxidation of the phosphoramidite.)

**C<sub>78</sub>H<sub>93</sub>N<sub>8</sub>O<sub>14</sub>PSiZn**: 1488.56 g/mol

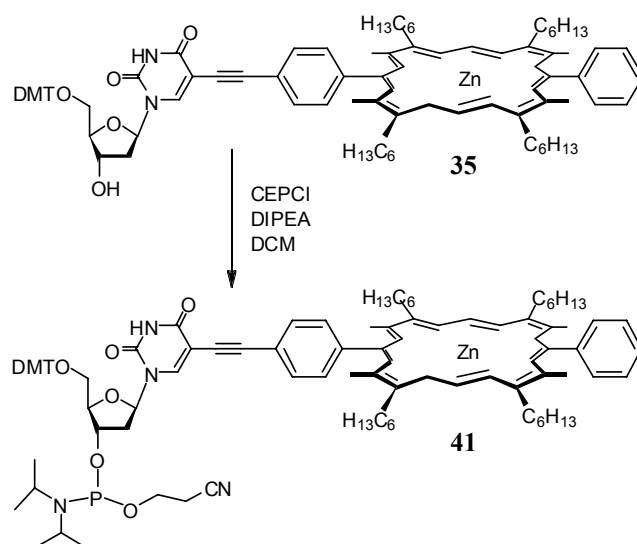
**Maldi-TOF**: m/z: 1488.89 [M]<sup>+</sup>

**TLC**: R<sub>f</sub> = 0.72, EA pure

**<sup>1</sup>H-NMR** (400 MHz, CDCl<sub>3</sub>): δ (ppm) = 10.09 (2H, s, H-meso), 8.05 (s, 1H, -NH), 8.05-7.98 (m, 5H, H-aro), 7.85-7.77 (m, 6H, H-aro), 6.22-6.20 (m, 1H, H-1'), 4.22-4.21 (m, 8H, -CH<sub>2</sub>-CH<sub>2</sub>-C O<sub>2</sub>Me), 3.95-3.92 (m, 2H, H-5'), 3.90-3.93 (2H, m, -CH<sub>2</sub>CH<sub>2</sub>CN); 3.83-3.81 (m, 1H, H-4'), 3.54 (s, 12H, -O-CH<sub>3</sub>), 3.12-3.08 (m, 8H, -CH<sub>2</sub>-CH<sub>2</sub>-CO<sub>2</sub>Me), 2.97-2.92 (2H, m, NCH(CH<sub>3</sub>)<sub>2</sub>); 2.60-2.63 (2H, m, -CH<sub>2</sub>CN); 2.47 (d, *J* = 10, 12H, -CH<sub>3</sub>), 2.21-2.19 (m, 2H, H-2'), 1.07 (12H, s, NCH(CH<sub>3</sub>)<sub>2</sub>); 0.99 (s, 9H, -SiC<sub>5</sub>(CH<sub>3</sub>)<sub>3</sub>), 0.21 (d, *J* = 6 Hz, 6H, -Si(CH<sub>3</sub>)<sub>2</sub>).



## 12.2 5'-O-DMT-dU<sup>ZnDPP</sup> phosphoramidite



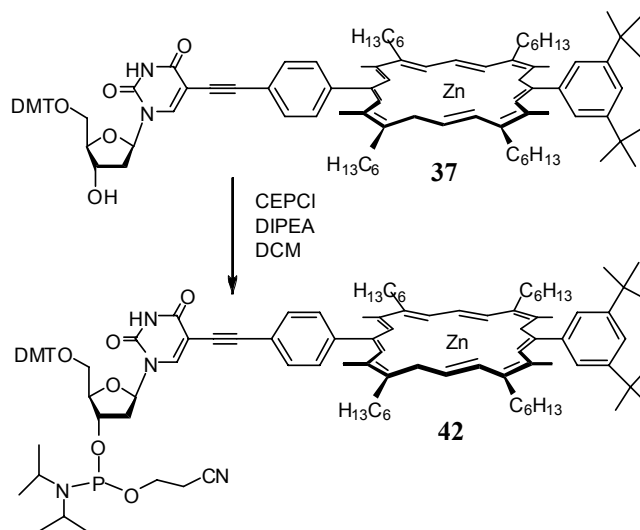
The protected 5'-O-DMT-dU<sup>ZnDPP</sup> **35** (70 mg, 47.7  $\mu\text{mol}$ , 1 eq) was co-evaporated three times with dry pyridine, and dried on the vacuum line overnight. The product was dissolved in dry DCM (1.5 ml) with molecular sieves (powder) and stirred for an hour. Then, diisopropylethylamine (42  $\mu\text{l}$ , 191  $\mu\text{mol}$ , 4 eq) and finally the 2-cyanoethyl diisopropylchlorophosphoramidite (35  $\mu\text{l}$ , 143  $\mu\text{mol}$ , 3 eq) was added and the reaction mixture was stirred for 5h under argon and in the dark. The mixture was evaporated and put directly on a chromatography column (DCM/EA, 1:1) under argon. Prior to use triphenylphosphine on the column, left for 2h and washed with eluent. We obtained the 5'-O-DMT-dU<sup>ZnDPP</sup> phosphoramidite **41** (55.1 mg, 33  $\mu\text{mol}$ , 70%) as a purple solid which was kept under argon and in the dark overnight for the next step. (Otherwise, we observed an oxidation of the phosphoramidite.)

**C<sub>101</sub>H<sub>121</sub>N<sub>8</sub>O<sub>2</sub>PZn**: 1668.83 g/mol

**Maldi-TOF**: m/z: 1668.18 [M]<sup>+</sup>

**TLC**: R<sub>f</sub> = 0.27, Hex/EA, (5:1)

### 12.3 5'-O-DMT-dU<sup>ZnDPP</sup> phosphoramidite **42**



The protected 5'-O-DMT-dU<sup>ZnDPP</sup> **37** (146 mg, 92  $\mu\text{mol}$ , 1 eq) was co-evaporated three times with dry pyridine, and dried on the vacuum line overnight. The product was dissolved in dry DCM (2 ml) with molecular sieves (powder) and stirred for an hour in dark. Then, diisopropylethylamine (70  $\mu\text{l}$ , 368  $\mu\text{mol}$ , 4 eq) and finally the 2-cyanoethyldiisopropylchlorophosphoramidite (62  $\mu\text{l}$ , 276  $\mu\text{mol}$ , 3 eq) was added and the reaction mixture was stirred for two and a half hours under argon and in dark. The mixture was evaporated and put directly on a chromatography column (DCM/EA, 1:1) under argon. Prior to use triphenylphosphine on the column, left for 2h and washed with eluent. We obtained the 5'-O-DMT-dU<sup>ZnDPP</sup> phosphoramidite **42** (131 mg, 73  $\mu\text{mol}$ , 80%) as a purple solid which was kept under argon and in the dark overnight for the next step. (Otherwise, we observed an oxidation of the phosphoramidite.)

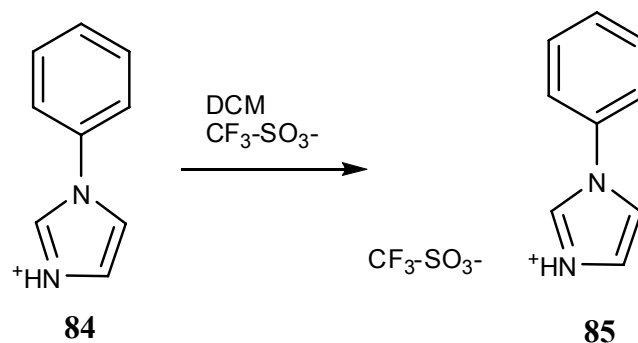
**C<sub>109</sub>H<sub>137</sub>N<sub>8</sub>O<sub>8</sub>PZn**: 1780.96 g/mol

**Maldi-TOF**: m/z: 1781.2 [M]<sup>+</sup>

**TLC**: R<sub>f</sub> = 0.85, DCM/AcOEt (1:1)

## 12.4 Synthesis of the homo- and heterophorphyrinic dimers in solution

### 12.4.1 Synthesis of the 1-phenyl-1H-imidazol-3-ium salt

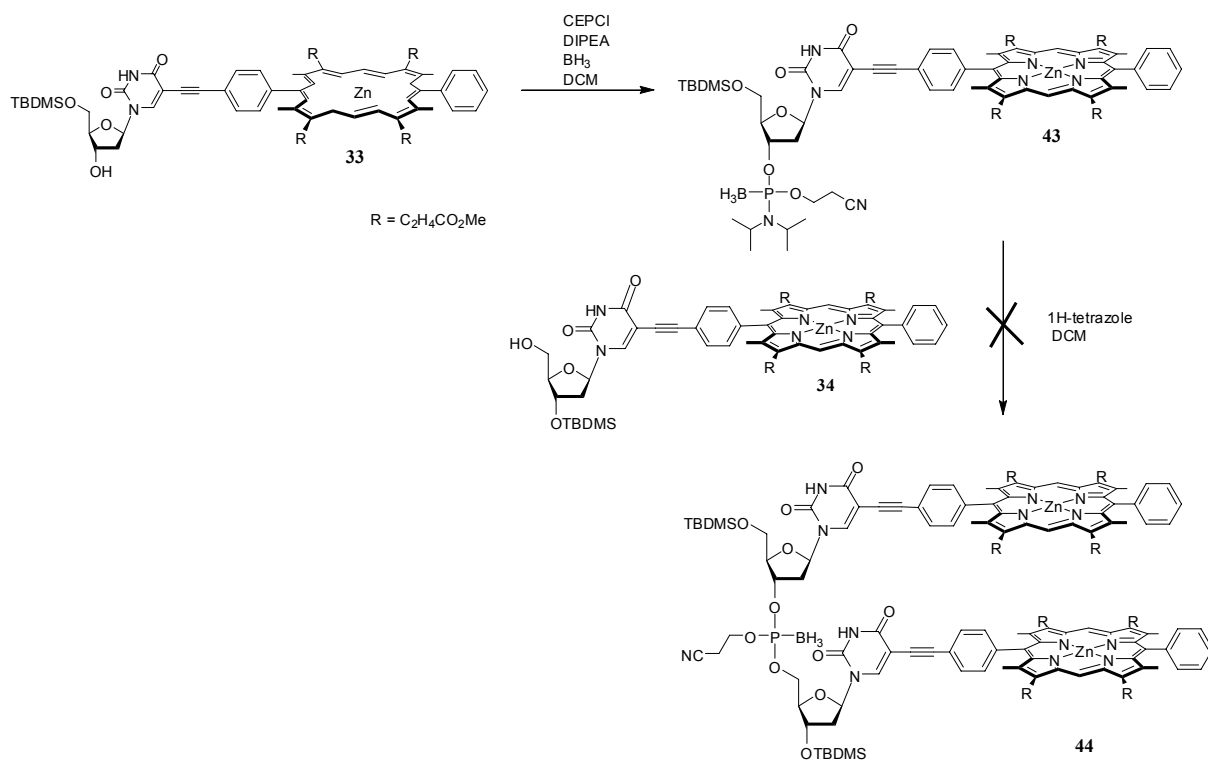


Trifluoromethanesulfonic acid (0.62 ml, 6.95 mmol) was added over 2 min to a solution of 1-phenylimidazole **84** (1g, 6.95 mmol) in DCM (5 ml), and the reaction mixture was stirred for 1h under argon. The reaction mixture was diluted with diethyl ether (5ml). The resultant precipitate was collected by filtration, washed with diethyl ether and dried on the vacuum line overnight. The 1-phenyl-1H-imidazol-3-ium (NPhImT) **85** (1.97 g, 6.68 mmol, 96%) was obtained as a white powder.

$\text{C}_{10}\text{H}_9\text{F}_3\text{N}_2\text{O}_3\text{S}$ : 294.03 g/mol

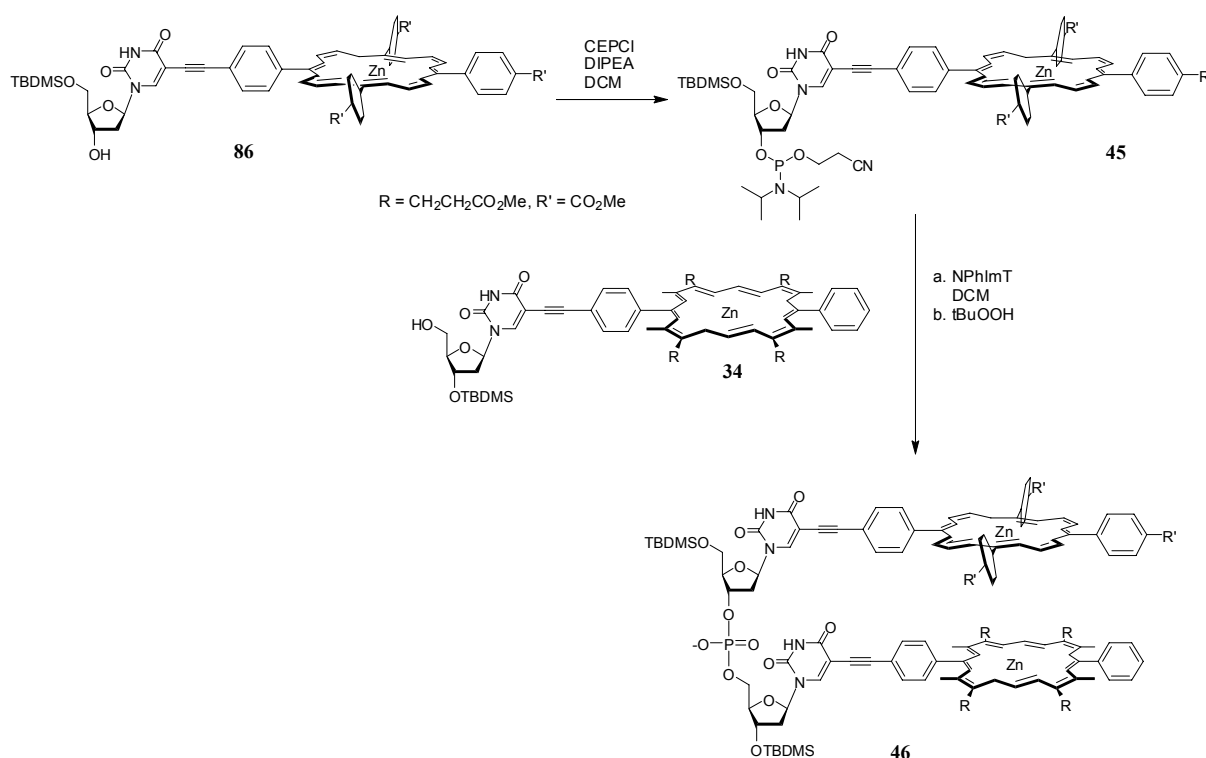
$^1\text{H-NMR}$  (400 MHz,  $\text{CDCl}_3$ ):  $\delta$  (ppm) = 9.46 (s, 1H, H-aro), 8.07 (s, 1H, H-aro), 7.77-7.64 (m, 6H, H-aro).

### 12.4.2 Synthesis of the (dU<sup>ZnDPP</sup>)<sub>2</sub> dimer **44**



The DPP building block **33** (20 mg, 15.1  $\mu\text{mol}$ ) was dissolved in dry DCM (2 ml). Then, CEP-Cl (13.3  $\mu\text{l}$ , 53  $\mu\text{mol}$ , 3.5 eq) and DIEA (14.4  $\mu\text{l}$ , 90  $\mu\text{mol}$ , 6 eq) were added. The reaction mixture was stirred in dark under argon. After four hours, borane was added and the reaction was stirred overnight. The mixture was evaporated and put directly on a chromatography column (EA) under argon. The 5'-O-TBDMS-dU<sup>ZnDPP</sup> phosphoramidite **43** (14.5 mg, 9.5  $\mu\text{mol}$ , 63 %) was obtained as a purple solid which was dissolved in dry DCM (2 ml) with molecular sieves (powder). Then, 1H-tetrazole (5 mg, 71  $\mu\text{mol}$ , 5 eq) and the porphyrin substituted nucleotide **34** (12.5 mg, 9.5  $\mu\text{mol}$ , 1 eq) were added. The reaction mixture was stirred for 2h without formation of the dimer **44**.

### 12.4.3 Synthesis of the (dU<sup>ZnDPP</sup>-dU<sup>ZnTPP</sup>) dimer



The porphyrin substituted nucleotide **86** (22 mg, 19  $\mu$ mol, 1.2 eq) was dissolved in dry DCM (1 ml). Then, CEP-Cl (7.3 mg, 31  $\mu$ mol, 6.9  $\mu$ l, 2 eq) and DIEA (8 mg, 62  $\mu$ mol, 10.5  $\mu$ l, 4 eq) were added. The reaction mixture was stirred for 2h under argon. Finally, the DPP building block **86** (20 mg, 15.5  $\mu$ mol) and NPhImT (17 mg, 58  $\mu$ mol, 3.7 eq) were added. The reaction mixture was stirred overnight. The crude product was purified by silica column chromatography (DCM/EA, from 10:1 to 1:1) and the dimer was obtained as a purple solid (11 mg, 4.2  $\mu$ mol, 27%).

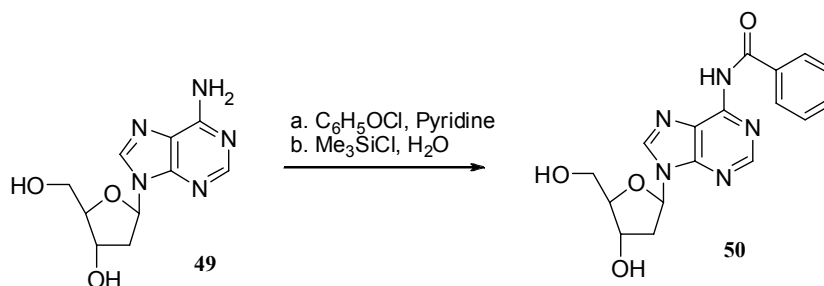
**C<sub>134</sub>H<sub>133</sub>N<sub>12</sub>O<sub>26</sub>PSi<sub>2</sub>Zn**: 2384.9 g/mol

**Maldi-TOF**: m/z: 2384.6 [M]<sup>+</sup>



## 13 Synthesis of diadenosine dimer

### 13.1 6-N-Benzoyl-2'-deoxyadenosine **50**



2'-deoxyadenosine **49** (1 g, 3.7 mmol) was dried by co-evaporation three times with dry pyridine, and resuspended in pyridine (20 ml). Trimethylchlorosilane (2.5 ml, 20 mmol) was added and the reaction mixture was stirred for 15 min. Then, benzoylchloride (2.3 ml, 20 mmol) was added and the reaction was kept at room temperature for 2h. The mixture was then cooled in an ice bath, and 5 ml of H<sub>2</sub>O was added. After 5 min, 5 ml of 32% aqueous ammonia was added, and the mixture was stirred at RT for 1h. The reaction was then evaporated to near dryness and the residue was dissolved in water (100 ml). The solution was washed once with AcOEt portion (25 ml). Crystallisation began immediately after separation of the layers and addition of AcOEt portion (25 ml) to the aqueous phase. After the solution was cooled for one night, the filtration gave the 6-N-benzoyl-2'-deoxyadenosine **50** (0.57 g, 1.6 mmol, 44%) as a white powder.

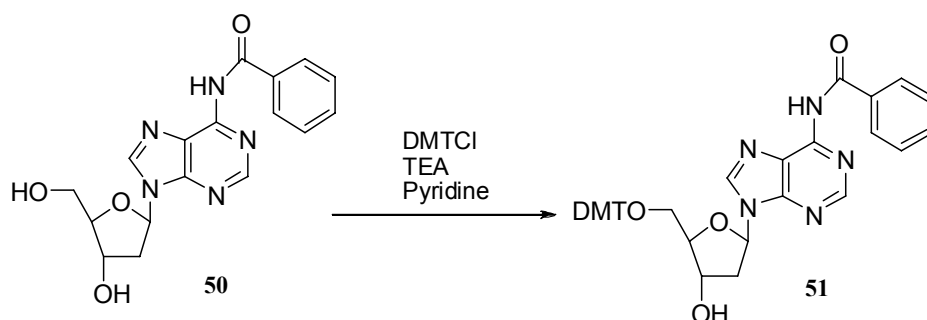
**C<sub>17</sub>H<sub>17</sub>N<sub>5</sub>O<sub>4</sub>**: 355.13 g/mol

**Maldi-TOF**: m/z: 356.38 [M]<sup>+</sup>

**TLC**: R<sub>f</sub> = 0.46, DCM/MeOH (10:1), turned to yellow when revealed with H<sub>2</sub>SO<sub>4</sub> in MeOH

**<sup>1</sup>H-NMR** (400 MHz, CDCl<sub>3</sub>): δ (ppm) = 11.1 (-NH, s, 1H), 8.72 (1H, s, H-8); 8.66 (1H, s, H-2); 8.01 (2H, m, -CH<sub>(o)</sub>); 7.6-7.55 (1H, m, -CH<sub>(p)</sub>); 7.53-7.46 (2H, m, -CH<sub>(m)</sub>); 6.46 (1H, m, H-1'); 5.35 (1H, m, OH-3'); 5.0 (1H, m, OH-5'); 4.43 (1H, m, H-3'); 3.88 (1H, m, H-4'); 3.62-3.5 (2H, m, H-2'), 2.80-2.76 (1H, m, H-5'); 2.36-2.30 (1H, m, H-5').

### 13.2 5'-O-DMT-6-N-Benzoyl-2'-deoxyadenosine **51**



The 6-N-Benzoyl-2'-deoxyadenosine **50** (100 mg, 0.28 mmol, 1 eq.) was dried by co-evaporation with dry pyridine (3×1 ml) and kept overnight on the vacuum line, and redissolved in pyridine (1 ml) and molecular sieves (4 Å). The solution was stirred for one hour, TEA (78  $\mu$ l, 0.56 mmol, 2 eq.) and dimethoxytrityl chloride (105 mg, 0.31 mmol, 1.1 eq.) were added. The reaction mixture was stirred at RT under Ar overnight, pyridine was evaporated, residue freed from pyridine by evaporation of toluene. A column chromatography of the remaining oil (CH<sub>2</sub>Cl<sub>2</sub>/MeOH from 100:1 to 10:1) gave the 5'-O-DMT-6-N-Benzoyl-2'-deoxyadenosine **51** (147 mg, 0.22 mmol, 78%) as a yellow foam.

**C<sub>38</sub>H<sub>35</sub>N<sub>5</sub>O<sub>6</sub>**: 657.26 g/mol

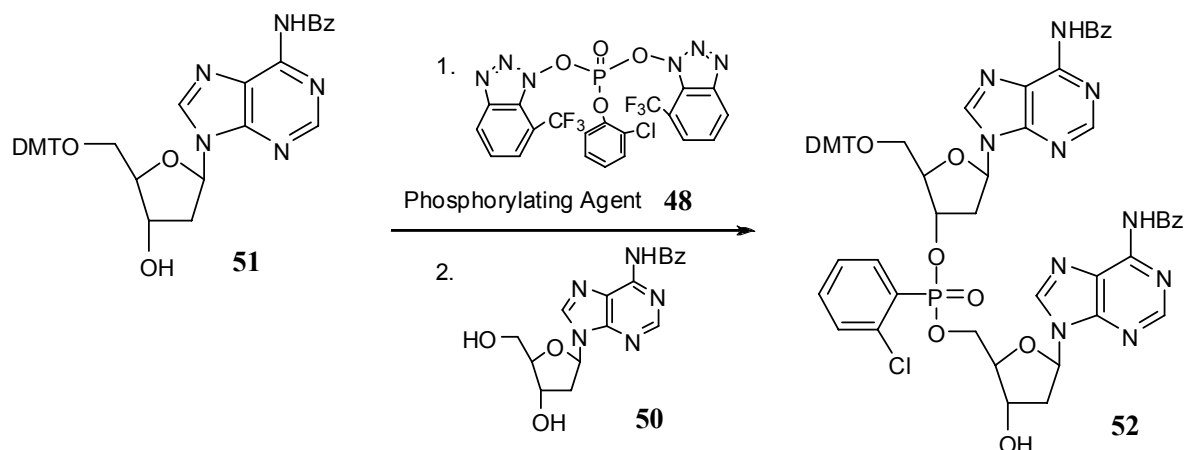
**Maldi-TOF**: m/z: 659.07 [M]<sup>+</sup>

**TLC**: R<sub>f</sub> = 0.35, DCM/MeOH (10:1), turn black with H<sub>2</sub>SO<sub>4</sub> in MeOH

**<sup>1</sup>H-NMR** (400 MHz, CDCl<sub>3</sub>):  $\delta$  (ppm) = 11.17 (-NH, s, 1H), 8.94 (1H, s, H-8); 8.73 (1H, s, H-2); 8.15 (1H, m, Bz-H<sub>(p)</sub>); 8.02 (2H, m, Bz-H<sub>(o)</sub>); 7.63-7.59 (2H, m, Bz-H<sub>(m)</sub>); 7.54-7.39 ((5H, m, Bz-H<sub>(DMT)</sub>); 7.25-7.20 (4H, m, m-Bz-H<sub>(p)</sub>); 6.79 (4H, m, m-Bz-H<sub>(o)</sub>); 6.49 (1H, m, H-1'); 4.73 (1H, m, OH-3'); 4.16 (1H, m, H-3'); 3.75 (1H, m, H-4'); 3.42 (2H, m, H-2'), 2.92-2.88 (1H, m, H-5'); 2.62-2.55 (1H, m, H-5'); 1.40-1.36 (6H, m, -OCH<sub>3</sub>).



### 13.3 5'-O-DMT-6-N-Benzoyl-2'-deoxyadenosine dimer **52**



5'-O-DMT-6-N-Benzoyl-2'-deoxyadenosine **51** (385 mg, 0.57 mmol) was dried by co-evaporated with pyridine (3 × 2 ml) and kept overnight on the vacuum line, redissolved in dioxane (1 ml) with molecular sieves and the phosphorylating agent **48** (3.18ml, 1.1 eq.) was added. After 15 min, TLC indicated the end of the reaction ( $R_f = 0$ ).

6-N-Benzoyl-2'-deoxyadenosine **50** (305 mg, 0.86 mmol, 1.5 eq) was dried by evaporation of pyridine (3×2 ml) and kept overnight on the vacuum line, redissolved in dioxane (1.5 ml) with molecular sieves. The reaction mixture was stirred for 1h at RT under Argon and filtered over celite. The organic phase was washed with triethylammonium Buffer (first 1M , then 0.1M), dried over  $\text{Na}_2\text{SO}_4$  and evaporated. A column chromatography ( $\text{CH}_2\text{Cl}_2/\text{MeOH}$ , from 1 % to 7 %) gave the 5'-O-DMT-6-N-Benzoyl-2'-deoxyadenosine dimer **52** (585 mg, 0.49 mmol, 87 %) as yellow oil.

$\text{C}_{61}\text{H}_{54}\text{ClN}_{10}\text{O}_{11}\text{P}$ : 1168.34 g/mol

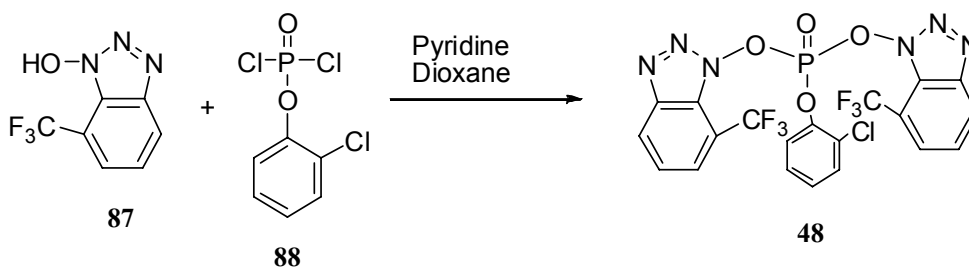
**Maldi-TOF**:  $m/z$ : 1169.3  $[\text{M}]^+$

**TLC**:  $R_f = 0.35$ ,  $\text{DCM}/\text{MeOH}$ , (10:1)

**<sup>1</sup>H-NMR** (400 MHz, CDCl<sub>3</sub>): δ (ppm) = 11.1 (2H, s, -NH), 8.69-8.57 (2H, m, H-8); 8.31-8.24 (2H, m, H-2); 7.95-7.91 (6H, m, Bz-H<sub>(p+o)</sub>); 7.55-7.04 (17H, m, Bz-H<sub>(m)</sub> + m-Bz-H<sub>(o)</sub> + Bz-H<sub>(DMT)</sub> + Cl-C<sub>6</sub>H<sub>4</sub>); 7.85-7.71 (4H, m, m-Bz-H<sub>(m)</sub>); 6.45-6.41 (2H, m, H-1'); 4.50-4.42 (2H, m, H-3'); 4.32-4.25 (2H, m, H-4'); 3.76-3.60 (6H, m, -OCH<sub>3</sub>); 3.38-3.29 (4H, m, H-2'), 2.90-2.75 (2H, m, H-5'); 2.57-2.53 (2H, m, H-5').

**<sup>31</sup>P-NMR** (Hz, CDCl<sub>3</sub>, ppm): -10.9 (s).

### Preparation of stocks of phosphorylation reagent **48** solution 0.2 M:

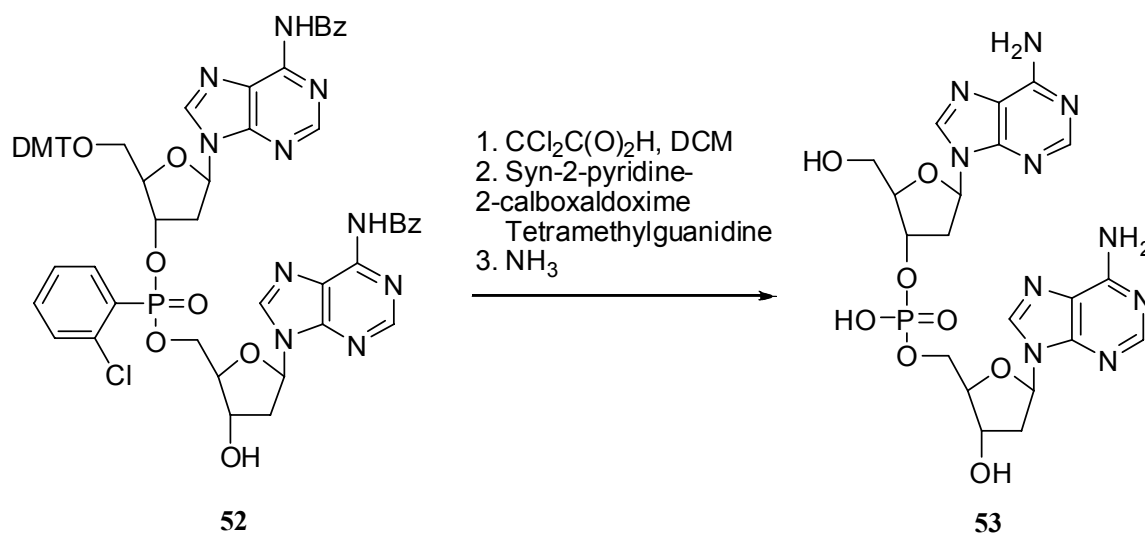


2-chlorophenylphosphorodichloridate **88** (3.1 mmol, 1 eq., 0.5 ml) in 3 ml dioxane was added dropwise to a solution of 1-hydroxy-6-trifluoromethyl-benzotriazoles **87** (2.03 eq., 1.27 g) in dioxane (12.5 ml) and pyridine (0.5 ml, 1.02 eq.). The reaction mixture was then stirred for 1h, and filtered via canula under inert atmosphere. The yellow solution of phosphorylation reagent **48** was stored in the fridge under Argon.

**C<sub>20</sub>H<sub>10</sub>ClF<sub>6</sub>N<sub>6</sub>O<sub>4</sub>P**: 578.01 g/mol

**Maldi-TOF**: m/z: 578.75 [M]<sup>+</sup>

### 13.4 2'-deoxyadenosine dimer 53



To a solution of 5'-O-DMT-6-N-Benzoyl-2'-deoxyadenosine dimer **52** (585 mg, 0.49 mmol, 1 eq) in  $\text{CH}_2\text{Cl}_2$  (5ml), 0.5 ml of dichloroacetic acid were added and the mixture was stirred in an ice bath for 10 min. The solution was washed with  $\text{NaHCO}_3$  and dried over  $\text{Na}_2\text{SO}_4$ . After removal of all volatiles under reduced pressure, flash chromatography ( $\text{CH}_2\text{Cl}_2/\text{MeOH}$  from 100:1 to 10:1) gave the 6-N-Benzoyl-2'-deoxyadenosine dimer (248 mg, 0.28 mmol, 57 %) as yellow oil.

To cleave the chlorophenyl, the product (238 mg, 0.27mmol) was dissolved in pyridine (10 ml). Then syn-2-pyridine-2-calboxaldoxime (1.32 mg, 10.8 mmol) and tetramethylguanidine (1.22 ml, 9.64 mmol) were added. The reaction mixture was stirred for 20h at 25°C.

To deprotect the dimer from the benzoyl group, a solution of ammoniac 32% (20 ml) was added to the mixture and stirred for 2h at 50°C. The reaction mixture was concentrated to about 10 ml under reduced pressure, washed with  $\text{Et}_2\text{O}$ , and evaporated. The yellow oil was kept at the vacuum line for one day. After purification by HPLC, we obtained the 2'-deoxyadenosine dimer **53** (220 mg, 0.39 mmol, 80%) as white oil.

$\text{C}_{20}\text{H}_{25}\text{N}_{10}\text{O}_8\text{P}$ : 564.16 g/mol

**Maldi-TOF**: m/z: 566.50  $[\text{M}]^+$



## 14 Manual PNA Fmoc-synthesis

### 14.1 Solutions for PNA synthesis:

These solutions were prepared in small glass vials.

#### Monomer Solutions.

Monomers were dissolved in NMP at a concentration of 0.3M. This solution provided the base that was necessary for activation on the PNA monomer with HATU prior to coupling.

➤ A (725 g/mol)

➤ C (701 g/mol)

\_ 321 mg (0.9 mmol, 3 eq) Base A was dissolved in 3 ml NMP. (V=0.370 ml for each couplage)

\_ 315 mg (0.45 mmol, 3 eq) Base C was dissolved in 1.5 ml NMP. (V=0.185 ml for each couplage)

**DIPEA solution (1.5 ml DMF):** (V=0.185 ml for each couplage)

\_ 0.6 M DIEA in DMF: 154  $\mu$ l DIEA was mixed in 1.5 ml

\_ 0.9 M 2,6-lutidine in DMF: 156  $\mu$ l 2,6-lutidine mixed in 1.5 ml

**Capping Mix (10 ml DMF):** (V=0.185 ml for each couplage)

\_ 5% acetic anhydride: 500  $\mu$ l in 10 ml

\_ 6% 2,6-lutidine: 600  $\mu$ l in 10 ml

**20 % piperidine in DMF.**

2 ml piperidine was mixed with 8 ml of DMF (dimethylformamide) and stored in an amber bottle in the hood.

### **0.6M HATU in DMF.**

0.844 g (3 eq) HATU (Applied Biosystem) was dissolved in DMF to give a total volume of 3ml. This solution was stored in a glass vial wrapped in aluminium foil in the hood. This reagent crystallised overnight, thus fresh solution was prepared everyday.  $V=0.185$  ml for each couplage

## **14.2 Manual synthesis**

The PNA molecules were synthesized on Rink Amide MBHA resin under argon.

### **14.2.1 Swelling the resin**

50 mg (37  $\mu$ mol, 1 eq) MBHA resin was placed in a small Merrifield vessel and washed three times with DMF for 1 min. The resin was then suspended in a small amount of DMF (4 ml) and was shaken for 1h. The solvent was then drained and the resin was washed twice with DMF. Finally, a few resin beads were sampled to a small glass tube for the Kaiser test. (Qualitative test for the absence or presence of free amino groups)

### **14.2.2 Fmoc-deprotection**

The coupling cycle was started with the cleavage of the Fmoc protecting group. The deprotection was achieved by two successive incubation in piperidine. The resin was shaken with a mixture of 20% piperidine in DMF (4 ml) for 1 min and then 4 min. The solvent was drained and the Fmoc groups and piperidine were washed away five times with DMF during 1 min. At the end of this step, a Kaiser test was performed to check the successful Fmoc deprotection. If the Kaiser test was positive (blue colour), the Fmoc protecting groups were removed and the next amino acid was coupled. And if the Kaiser test was negative (white colour), the coupling was repeated until the entire amino group was deprotected.

### 14.2.3 Coupling reaction

The deprotection step was followed by a double coupling of the monomer (base A or C). 0.185 ml of the first monomer C, 0.185 ml of HATU solution and 0.185 ml of base Mix DIPEA were added, and the mixture was shaken twice for 45 min. The resin was washed thrice with DMF after the second coupling step.

### 14.2.4 Free amine acetylation

After the coupling reaction, we need to capping all the unreacted amino groups as acetamides by adding 1.5 ml of capping Mix. The mixture was shaken for 5 min, and the resin was washed three times with DMF. Then, a Kaiser test was performed to check the successful protection of the free position. The white colour confirmed the completion of the reaction.

Finally, the cycle was repeated from **2.2** to **2.4** until the synthesis of the desired PNA **63** was completed. During the night, the Merrifield vessel with the resin was stored in the fridge under Ar.

The terminal Fmoc was removed as described above (II) and the free NH<sub>2</sub> was acetylated (IV). The resin was washed another 5 times with DMF and 2 times with DCM.

After Synthesis, the final PNA molecule was cleaved from the dried resin.

### 14.2.5 Cleavage of the side chain protecting groups and from MBHA Resin

6 ml of a solution TFA/TIS (95:5) was added, and the mixture was shaken two times for 2h to cleave the resin and the Boc protecting group from the side chain. The solution was drained in a conical glass centrifuge tube, and added 5-fold excess of cold dry ether. The solution was mixed, placed in an ice bath for 10 min, and centrifuged in good for 5 min. The supernatant was poured off carefully, and this step was repeated four times with the following dry ice incubation: 5 min, 2min, 0 min, 0 min. Finally, the supernatants were mixed together and evaporated to dryness. The PNA was stored under Ar at -4°C before purification.

## 14.2.6 Purification and characterisation of PNA

### 14.2.6.1 Purification

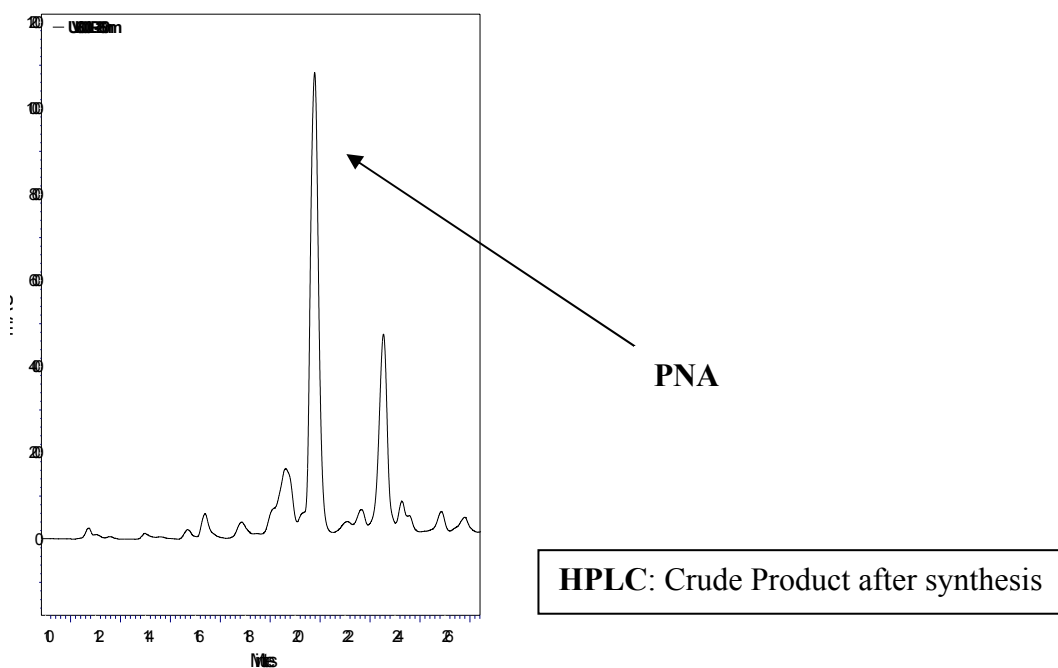
The PNA was precipitated in acetonitrile and the first purification of the PNA strand was done on sephadex LH 20 column (DCM/MeOH, 1:1), but gave no pure material. A second purification on semi-prep HPLC gave pure material (22.6 mg, 13.6  $\mu\text{mol}$ , 37%).

HPLC: from 2% to 11% in 35 min

Temperature: 55°C

$\lambda = 260 \text{ nm}$

Column semi-preparative: RP-18e HPLC LiChrospher





### 14.2.6.2 Characterisation

Quality Control of synthesised PNA was done by MALDI-TOF mass spectrometry.

**C<sub>66</sub>H<sub>83</sub>N<sub>39</sub>O<sub>15</sub>**: 1661.69

**MALDI-TOF**: m/z: 1661.1 [M]<sup>+</sup>

The UV-visible spectra showed an absorption maximum at 260 nm in water. Using different concentration from a 0.33 mM solution and the Beer-Lambert equation, we calculated the extinction coefficient of the PNA strand. The measurements were performed in water at 80°C. We obtained:  $\epsilon_{260} = 63\,344$ , compared to normal DNA strand  $\epsilon_{\text{calcd.}} = 66\,920$ .

**Kaiser Test.**

The “Kaiser Test” is a colorimetric test for the presence of amino groups; we use it to make sure that each coupling step in PNA synthesis goes to completion. It is based on the reaction of ninhydrin with amino groups to form a blue adduct. Therefore, an incomplete coupling cycle will lead to a positive Kaiser test, demonstrated by the development of a blue colour, while coupling to completion will yield a negative (yellow) test.

The following solutions were prepared:

A. Dissolved 8 g phenol in 2 ml absolute ethanol. The solution was warmed to completely dissolve the phenol.

B. Dissolved 13 mg KCN in 20 ml water. Transferred the KCN into a tarred vial in the hood, then it was carried to the balance with the cap on.

C. Diluted 20  $\mu$ l of aqueous KCN solution with 980  $\mu$ l pyridine then added to 100  $\mu$ l of the phenol/ethanol solution. This was the Kaiser (A) solution.

D. Dissolved 1.0 g ninhydrin in 20 ml absolute ethanol. This was the Kaiser (B) solution

E. Stored Kaiser (A) and (B) solutions in amber dropper bottles.

Once the solutions were prepared, the following procedure was performed:

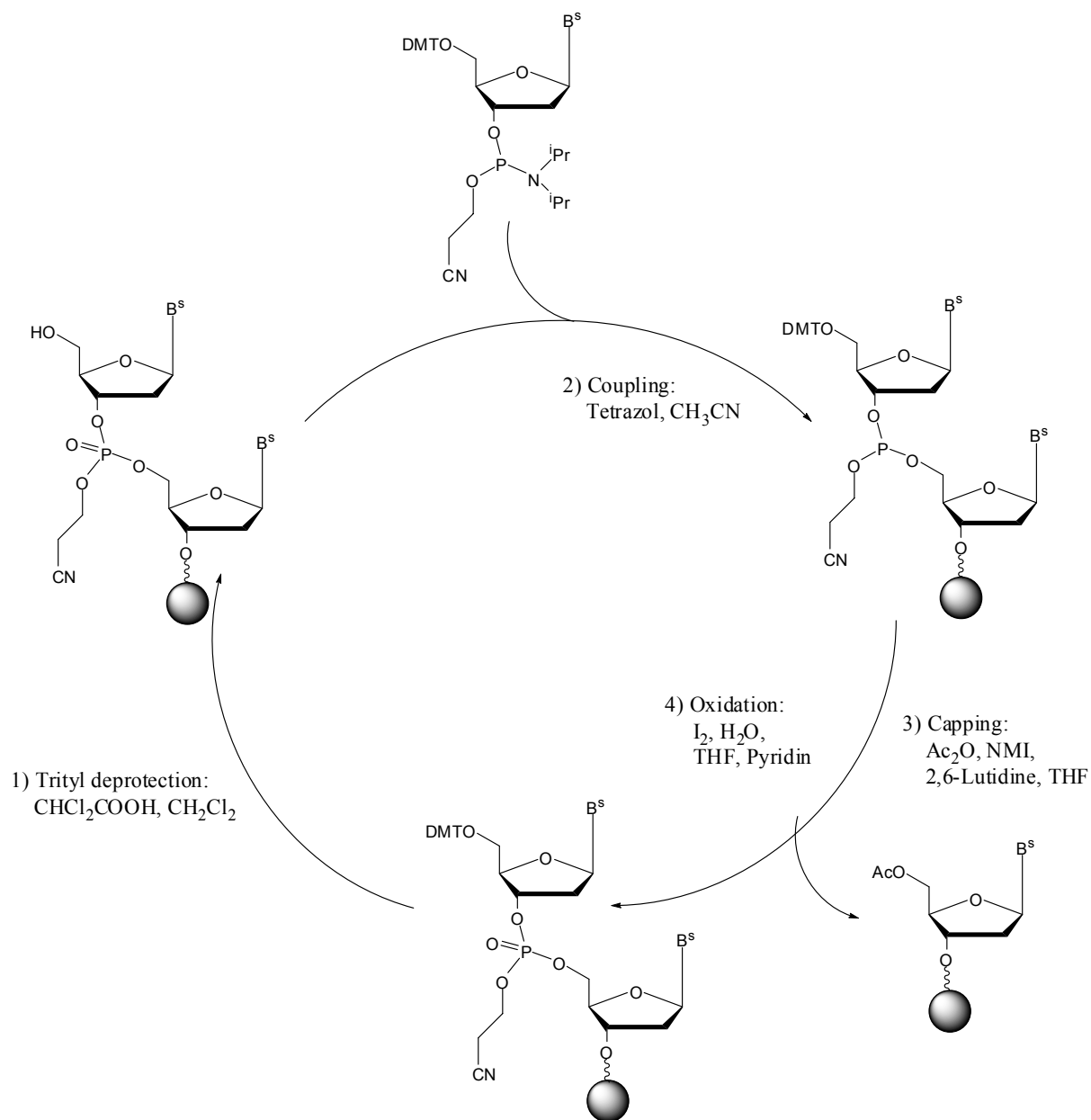
Set a heating block to 100 °C and removed a small amount of resin from the reactor and placed it in a microcentrifuge tube. Then, added two drops each of Kaiser (A) and (B) solutions; placed the tube in the heat block for two minutes. Finally, removed and observed the color: Blue = positive (i.e. amino groups present); Yellow = negative (i.e. no amino groups present).

## 15 Synthesis of oligonucleotides

### 15.1 Principle of the Automated DNA Solid-Phase Synthesis

Synthetic oligonucleotides were usually built up in 3' to 5' direction and the first building block was covalently bound to the solid phase *via* a base-labile succinyl linker. The connection to the solid phase was via an amide bond and the 5' hydroxyl group was protected by acid-labile DMT ether. For this work, only 1  $\mu\text{mol}$  and 15  $\mu\text{mol}$  synthesis scale were used. The monomeric nucleotide building blocks carry a temporary protecting group (DMT), which get cleaved before each coupling step. They also contain permanent protecting groups for the amino functions of A, C and G, as well as for the phosphate function, which are only cleaved after completion of the oligonucleotide synthesis. The DMT group was used for the protection of all 5' hydroxyl groups. The amino groups of A, C, and G were protected as amides or amidines, and the phosphates are protected by the 2-cyanoethyl group.

The first step of oligonucleotide synthesis was the deprotection of the terminal DMT group by 2% trichloroacetic acid. The following, tetrazole activated nucleotide then couples with this free hydroxyl group. In the next step, unreacted 5' hydroxyl groups were capped in a fast and quantitative reaction as acetate, in order to terminate any further synthesis of fault sequences. The subsequent oxidation of the labile P(III) compound to the phosphate was achieved by reaction with iodine/water/pyridine mixture. With the cleavage of the DMT group the next synthesis cycle starts. Upon completion of the synthesis, the oligonucleotide was manually cleaved off the solid phase by treatment with 25 % aqueous ammonia solution at 55°C overnight. All permanent protection groups are also cleaved in this step with exception of the terminal DMT group (scheme 31).



**Scheme 31:** the synthesis cycle of the Phosphoramidite method.

## 15.2 Incorporation of the Building Block

Freshly-prepared the  $^{DMT}dU^{ZnDPP}$  phosphoramidite was dried under high vacuum overnight and was dissolved in anhydrous DCM under argon to give a 17 mM solution. The sequence was synthesised on the 1  $\mu$ mol or 15  $\mu$ mol scales using Trityl-on or Trityl-off procedure. Solution of DMT-CE phosphoramidite bases (0.1 M) in acetonitrile was then prepared and used in the DNA synthesizer. The program was started under standard mode until the desired column length was completed. For the ODN 5-7, the last base added was the F-DMT-dC-CE nucleotide. A 0.1 M solution of F-DMT-CE phosphoramidite in acetonitrile was then prepared and used in the DNA synthesizer. Upon completion of the syntheses, the columns were dried in an argon flow and were incubated by 25% ammonium hydroxide and methanol (or dioxane) (1:1) at 55°C overnight to release the DNA strand. The solution was centrifuged and the supernatant was separated from the solid support. The resin was washed twice with DCM/MeOH (or dioxane) (1:1) and the obtained solution were centrifuged. The supernatants were collected, combined and the thus obtained solution was lyophilized. (In presence of dioxane, the residue was re dissolved in ethanol and lyophilized again)

The purification was dependant of the oligonucleotide length and the amount of porphyrins.

## 15.3 DNA Melting Temperatures

Prior to the DNA melting temperature ( $T_m$ ) measurements, the desired two complementary strands were dissolved in 1.0 ml buffer solution (pH 7.0, 50 mM  $KHPO_4$ , 500 mM NaCl) and annealed according the procedure described in chapter 5.

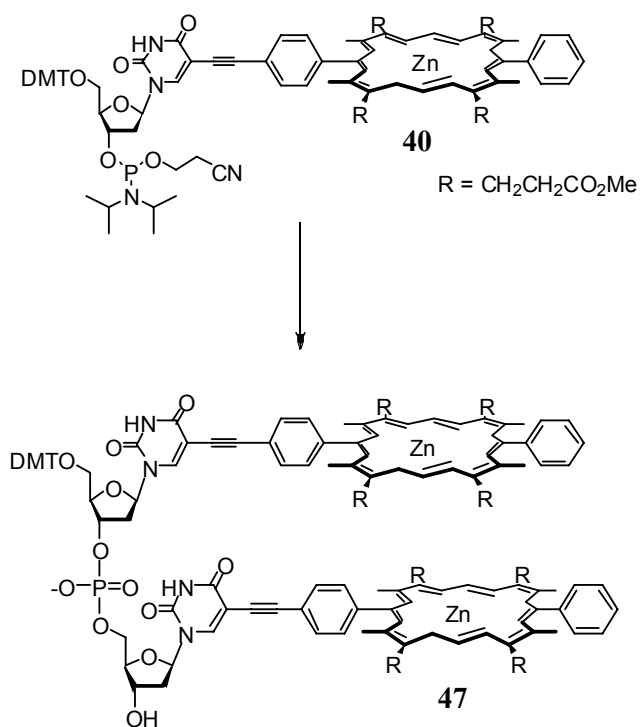
$T_m$  measurements were carried out at 260 nm, 280 nm, 410 nm, and at temperature gradient of 1°C  $min^{-1}$ . The measurements were performed two times and the values given were the mean of the heating and cooling cycles.

## 15.4 Data for the synthesized Oligonucleotides

The identity of all oligonucleotides was verified by MALDI-TOF MS using the appropriate Matrix.

## 15.5 Synthesis

### 15.5.1 Dimer 47

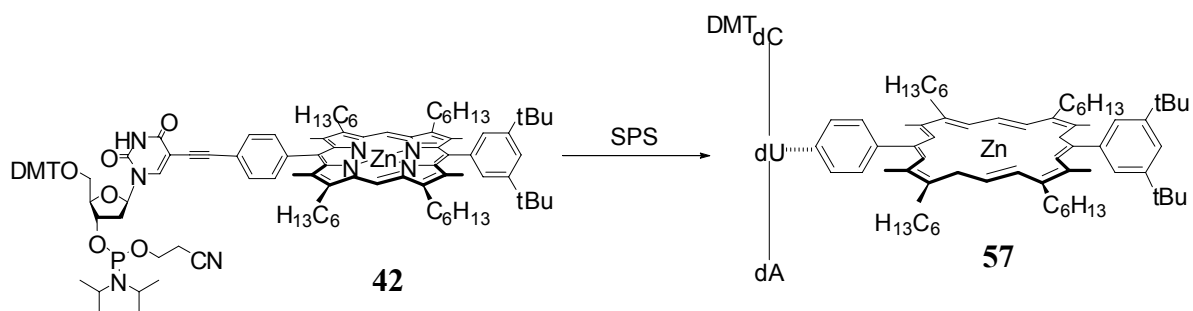


The standard procedure was used to synthesise a dimer **47** starting from the building block **40**. The purification was achieved by preparative TLC using DCM/MeOH (10:1) as eluent to obtain the pure material with 5 % yield.

**C<sub>147</sub>H<sub>142</sub>N<sub>12</sub>O<sub>30</sub>PZn**: 2649.9 g/mol

**MALDI-TOF**: m/z: 2648. 6 [M]<sup>+</sup>

### 15.5.2 Trimer 57

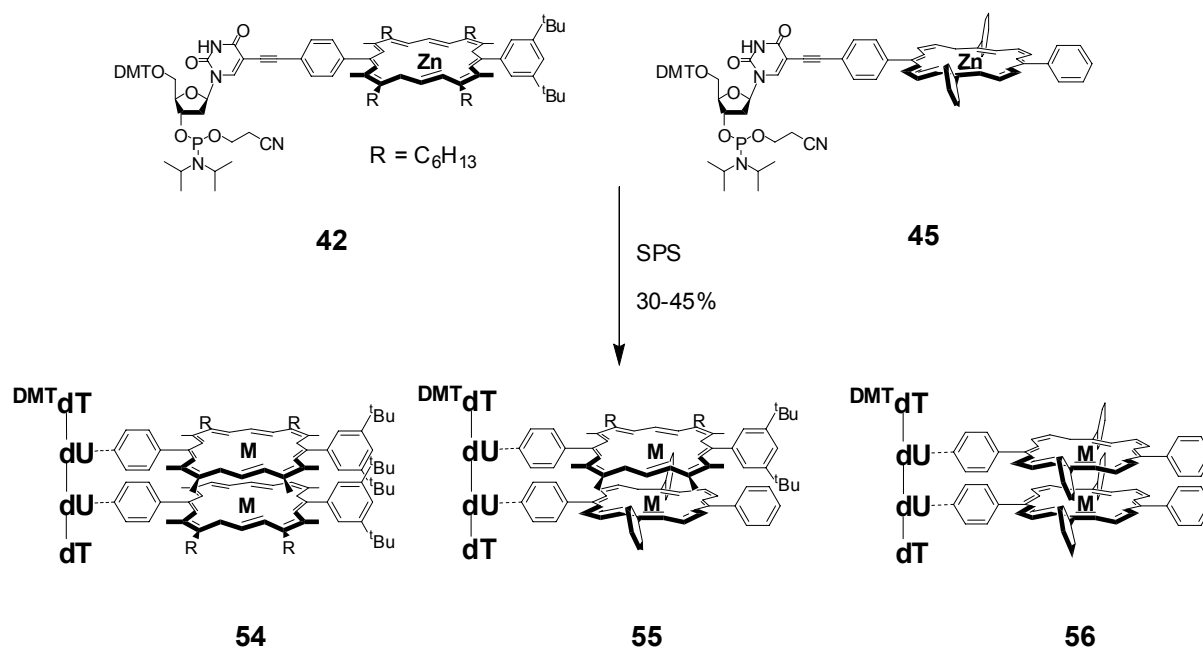


The standard procedure was used to synthesise a trimer with one central modification. This trimer **57** was purified on a sephadex LH20 column ( $l = 2.5$  m,  $\varnothing = 3.5$  cm) and the product was eluted with DCM/MeOH (1:1) as eluent (1 second per drop).

$C_{119}H_{141}N_{14}O_{21}P_3Zn_4$ : 2258,89 g/mol

**MALDI-TOF**: m/z: 2259. 2  $[M]^+$

## 15.5.3 Tetramers



Using the same standard procedure, two homo-porphyrin **54** and **56** were synthesized using the building blocks **42** and **45** respectively. Then the hetero-porphyrin **55** was synthesised. For solubility reason, the DMT group was left on the last position. These tetramers were purified on a sephadex LH20 column ( $l=2.5\text{m}$ ,  $\varnothing=3.5\text{ cm}$ ) and the products were eluted with DCM/MeOH (1:1) as eluent. (1 seconds per drop)

$\text{C}_{199}\text{H}_{250}\text{N}_{16}\text{O}_{28}\text{P}_3^-$  (**54**): 3407.1 g/mol

MALDI-TOF (**54**):  $m/z$ : 3407.2  $[\text{M}]^+$

$\text{C}_{175}\text{H}_{186}\text{N}_{16}\text{O}_{28}\text{P}_3^-$  (**55**): 3052.2 g/mol

MALDI-TOF(**55**):  $m/z$ : 3051.0  $[\text{M}]^+$

$\text{C}_{151}\text{H}_{122}\text{N}_{16}\text{O}_{28}\text{P}_3^-$  (**56**): 2699.7 g/mol

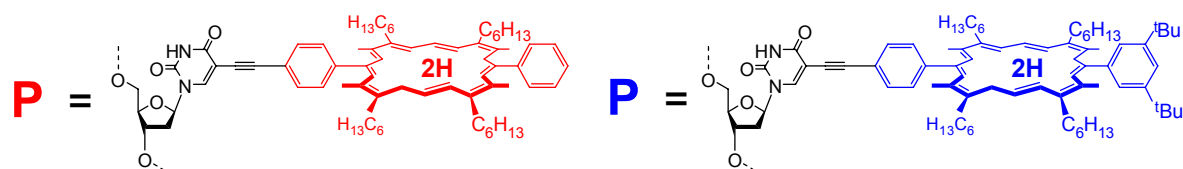
MALDI-TOF(**56**):  $m/z$ : 2700.5  $[\text{M}]^+$

	$\epsilon_{410} / [\text{M}^{-1} \text{cm}^{-1}]$
54	-
Zn-54	208 916
55	56 704
Zn-55	58 392
56	244 152
Zn-56	300 664



## 15.5.4 21mer oligonucleotides

### 15.5.4.1 Modified oligonucleotides (ODN)



The same procedure was used to synthesis longer modified oligonucleotides with different amounts of porphyrins as shown in the table infra. The building blocks **41** or **42** were used. The extinction coefficient was determined in PTT buffer.

Name	Sequence 5' → 3'	DMT	$\epsilon_{260} / [M^{-1} cm^{-1}]$
1 ODN <b>64</b>	ATG CTA AGC <b>PT</b> GAT CGA TGC	ON	198 904
2 ODN <b>65</b>	ATG CTA AGC <b>PTP</b> GAT CGA TGC	ON	195 708
3 ODN <b>66</b>	ATG CTA AGC <b>PPP</b> GAT CGA TGC	ON	193 112
4 ODN <b>67</b>	TTT TTT <b>PPP PPT</b> TTT TT	ON	122 320
5 ODN <b>68</b>	ATG CTA AGC <b>PT</b> GAT CGA TGCC	OFF	204 404
6 ODN <b>69</b>	ATG CTA AGC <b>PTP</b> GAT CGA TGCC	OFF	201 208
7 ODN <b>70</b>	ATG CTA AGC <b>PPP</b> GAT CGA TGCC	OFF	198 612

Name	MW <sub>calcd.</sub>	MW <sub>found.</sub>
ODN <b>64</b>	7755.59	7855.0
ODN <b>65</b>	8731.22	8789.0
ODN <b>66</b>	9706.0	9786
ODN <b>67</b>	10 043.25	10 075
ODN <b>68</b>	8 110.2	
ODN <b>69</b>	9141.24	
ODN <b>70</b>	10 177.9	

### 15.5.4.2 Oligonucleotide synthesis (ON)

Using the same standard procedure on CPG support, we synthesised different non modified oligonucleotides as shown infra.

	Name	Sequence	DMT	$\epsilon_{260} / [M^{-1} cm^{-1}]$
1	ON <b>61</b>	AAA A	ON	55 400 (MeOH)
2	ON <b>62</b>	TTT T	ON	33 000 (MeOH)

### 15.5.4.3 Purification

The purification of these DNA strands was done with two different methods:

➤ **Method A:** Affinity Chromatography

We synthesized the complementary strand of ODN on PS solid support, and then we purified these strands by affinity recognition.

#### Duplex formation:

200  $\mu$ l of PTT buffer was added to the DNA strand, and heated at 50°C overnight in the thermomixer. The solution was filtered, added to the appropriated solid support and heated at 60°C in the thermomixer for 10 min. Then, the suspension was cooled down slowly to 25°C and left in the fridge for one and half hours. The solid support was filtered, suspended in 0.1 M TEAA Buffer (100  $\mu$ l), and left again in the fridge for 1h30. The buffer containing the failure sequences was filtered off.

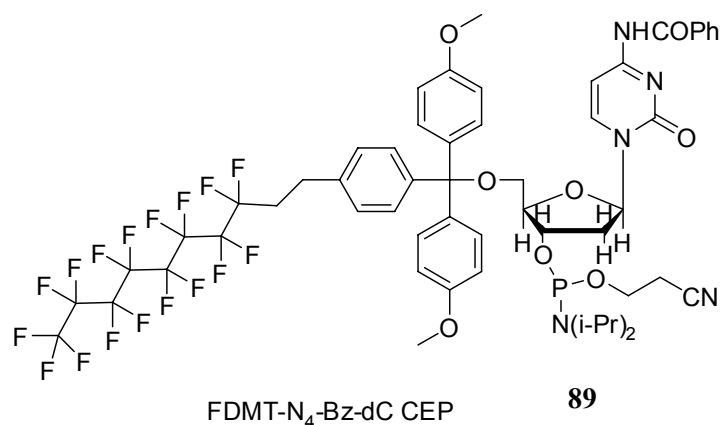
**Cleavage:**

The solid support was suspended in 200  $\mu$ l of MeOH/H<sub>2</sub>O (9:1), heated at 60°C for 5 min filtered and the liquid was collected in an eppendorf (1.5 ml). This last step was repeated twice, and then the solutions were collected, and combined. Water (500  $\mu$ l) was added and the obtained solution was lyophilized up to a 250  $\mu$ l volume reduction. The liquid was co-evaporated thrice with water to obtain the pure ODN. The solid support was washed several times with water and used again for other purifications.

	Name	Sequence 5' $\rightarrow$ 3'	DMT
4	ON 4	TAC GAT TCG AAA CTA GCT AGC TTT TA	OFF
5	ON 5	TGG TTA AAA AAA AAA AAA AAA TTG A	OFF

➤ **Method B: fluorous affinity purification:**

The last step of the fully automated synthesis was the addition of the F-DMT-dC-CE nucleotide **89**. This fluorous tag will be selectively retained on the Fluoro-Pak<sup>TM</sup> column. We applied this method for the ODN 5-7.



### **Sample preparation**

Without removing the ammonia and dioxane used in the deblocking step, the solid was filtered support over filter and the crude was diluted with an equal volume of lading buffer. The final sample volume was 4 ml.

### **Conditioning the column**

In order to prepare the Fluoro-Pak™ column, MeCN (2 ml), 0.1 M aqueous TEAA (2 ml) and loading buffer (2 ml) were passed, at a flow rate of 2 seconds per drop. The first 2-3 drops of MeCN was discoloured.

### **Loading the FDMT-on oligonucleotide**

The sample prepared in 4.2 above was passed through the pre-conditioned column at a flow rate of 5 seconds per drop, these conditions that allow one-pass loading. The loading buffer was used and a slow loading rate was employed.

### **Eluting remaining failure sequences**

Then, 10% MeCN (2 ml) in 0.1 M aqueous TEAA and water (2 ml) were passed at a flow rate of 2 seconds per drop. The acetonitrile/TEAA solution selectively washed the remaining non-fluorous compounds (failure sequences) from the resin, and left the FDMT-on oligonucleotide bound and the water washed the buffer out of the resin prior to the acid-catalyzed detritylation in the next step.

### **On-column detritylation**

3% aqueous TFA (3 ml), 0.1 M aqueous TEAA (1 ml) and water (1 ml) were passed at a flow rate of 2 seconds per drop. The TFA cleaved the FDMT group from the full-length oligonucleotide. A faint yellow colour was appeared on the column due to the trityl cation. The TEAA wash neutralized the residual TFA and ensured that the detritylated oligonucleotide had lipophilic triethylammonium counterions and was thus, retained on the support during the subsequent water wash, which removed excess TEAA buffer.

### Elution of the final detritylated oligonucleotide

Finally, 20% acetonitrile (1 ml) in water was passed at 2 seconds per drop and collected the eluate in an appropriate sample tube. A further 1 ml 20% acetonitrile was collected at higher concentration of acetonitrile (e.g. 50-100 %).

*Fluoro-Pak™ II Columns*: Each column contains 150 mg of adsorbent, and are designed for 1 micromole purifications.

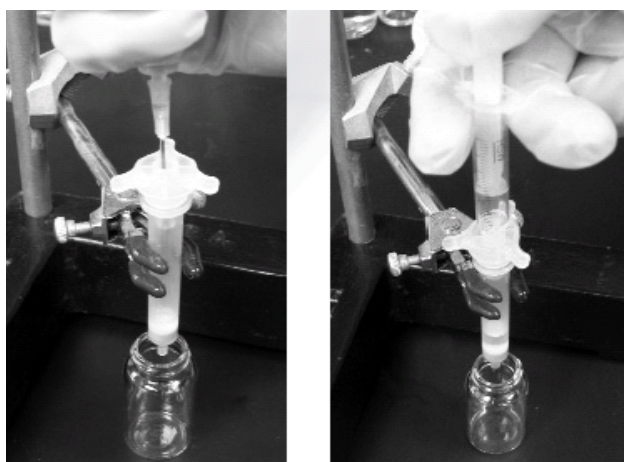


*Figure 1*: Introducing a solution to the column. Use a Syringe with needle to pass the solution through the hole in the luer adaptor.

*Figure 2*: With the desired solution already present in the column, use a syringe to pressurize the column with air, thereby eluting the solution.

Remarks: use here one column for 2\* 1  $\mu$ mol (reactions yield was low)



## Notes and References

- [1] N. Robertson, C. A. McGowan, *Chem. Soc. Rev.* **2003**, 32, 96.
- [2] M. K. C. ski, T. M. Krygowski, M. Wisiorowski, N. J. R. v. E. Hommes, P. v. R. Schleyer, *Angew. Chem.* **1998**, 110, Nr. 1/2.
- [3] M. L. Merla, M. d. Pilar, S. T. Nguyen, J. T. Hupp, *Angew. Chem., Int. Ed.* **2001**, 40.
- [4] A. W. Kleij, M. Kuil, D. M. Tooke, A. L. Spek, J. N. H. Reek, *Inorg. Chem.* **2005**, 44, 7696.
- [5] A. Ambroise, R. W. Wagner, P. D. Rao, J. A. Riggs, P. Hascoat, J. R. Diers, J. Seth, R. K. Lammi, D. F. Bocian, D. Holten, J. S. Lindsey, *Chem. Mater.* **2001**, 13, 1023.
- [6] D. Furutsu, A. Satake, Y. Kobuke, *Inorg. Chem.* **2005**, 44, 4460.
- [7] J. E. Redman, N. Feeder, S. J. Teat, J. K. M. Sanders, *Inorg. Chem.* **2001**, 40, 2486.
- [8] H. Imahori, J. C. Liu, H. Hotta, A. Kira, T. Umeyama, Y. Matano, L. GF, S. Ye, M. Isosomppi, N. Tkachenko, H. Lemmetyinen, *J. Phys. Chem. B* **2005**, 109, 18435.
- [9] J. R. Dunetz, C. Sandstrom, E. R. Young, P. Baker, S. A. Van Name, T. Cathopolous, R. Fairman, J. C. de Paula, K. S. Akerfeldt, *Org. Lett.* **2005**, 7, 2559.
- [10] F. G. Gulino, R. Lauceri, L. Frish, T. Evan-Salem, Y. Cohen, R. D. Zorzi, S. Geremia, L. D. Costanzo, L. Randaccio, D. Sciotto, R. Purrello, *Chem.-Eur. J.* **2006**, 12, 2722.
- [11] M. Balaz, M. De Napoli, A. E. Holmes, A. Mammana, K. Nakanishi, N. Berova, R. Purrello, *Angew. Chem. Int. Ed.* **2005**, 44, 4006.
- [12] A. Mammana, M. De Napoli, R. Lauceri, R. Purrello, *Bioorg. Med. Chem.* **2005**, 13, 5159.
- [13] D. Pomeranc, V. Heitz, J. C. Chambron, J. P. Sauvage, *J. Am. Chem. Soc.* **2001**, 123, 12215.
- [14] Y. H. Kim, D. H. Jeong, D. Kim, S. C. Jeoung, H. S. Cho, S. K. Kim, N. Aratani, A. Osuka, *J. Am. Chem. Soc.* **2001**, 123, 76.
- [15] C. M. Drain, *Proc. Natl. Acad. Sci. U. S. A.* **2002**, 99, 5178.
- [16] K. M. Kadish, K. M. Smith, R. Guilard, *Academic Press: San Diego, CA*, **2003**, 18, 63.
- [17] S. Prathapan, T. E. Johnson, J. S. Lindsey, *J. Am. Chem. Soc.* **1993**, 115, 7519.
- [18] A. J. Amoroso, B. F. G. Johnson, J. Lewis, A. D. Massey, P. R. Raithby, W. T. Wong, *J. Organomet. Chem.* **1992**, 440, 219.
- [19] A. Ambroise, J. Li, L. Yu, J. S. Lindsey, *Org. Lett.* **2000**, 2, 2563.
- [20] R. Takahashi, Y. Kobuke, *J. Am. Chem. Soc.* **2003**, 125, 2372.
- [21] Y. Kuramochi, A. Satake, Y. Kobuke, *J. Am. Chem. Soc.* **2004**, 126, 8668.
- [22] M. S. Choi, T. Aida, T. Yamazaki, I. Yamazaki, *Angew. Chem. Int. Ed.* **2001**, 40, 3194.
- [23] N. Maruo, M. Uchiyama, T. Kato, T. Arai, H. Akisada, N. Nishino, *Chem. Commun.* **1999**, 2057.
- [24] E. K. L. Yeow, K. P. Ghiggino, J. N. H. Reek, M. J. Crossley, A. W. Bosman, A. P. H. J. Schenning, E. W. Meijer, *J. Phys. Chem. B* **2000**, 104, 2596.
- [25] N. Aratani, O. A. Suka, Y. H. Kim, J. D. H. Eong, D. Kim, *Angew. Chem., Int. Ed.* **2000**, 39, 1458.
- [26] K. Ogawa, Y. Kobuke, *Angew. Chem., Int. Ed.* **2000**, 39, 4070.
- [27] D. M. Guldi, *Pure Appl. Chem.* **2003**, 75, 1069.
- [28] C. Luo, D. M. Guldi, M. Maggini, E. Menna, S. Mondini, N. A. Koto, M. Prato, *Angew. Chem., Int. Ed.* **2000**, 39, 3905.

- [29] D. M. Guldi, C. Luo, D. Koktysh, N. A. Kotov, T. D. Ros, S. Bosi, M. Prato, *Nano. Lett.* **2002**, *2*, 775.
- [30] D. M. Guldi, F. Pellarini, M. Prato, C. Granito, L. Troisi, *Nano. Lett.* **2002**, *2*, 965.
- [31] T. Hasobe, S. Hattori, P. V. Kamat, Y. Urano, N. Umezawa, T. Nagano, S. Fukuzumi, *Chemical Physics* **2005**, *319*, 243.
- [32] H. Yan, S. H. Park, G. Finkelstein, J. H. Reif, T. H. LaBean, *Science* **2003**, *301*, 1882.
- [33] J. Wengel, *Org. Biomol. Chem.* **2004**, *2*, 277.
- [34] T. Carell, C. Behrens, J. Gierlich, *Org. Biomol. Chem.* **2003**, *1*, 2221.
- [35] L. H. Eckardt, K. Naumann, W. Matthias Pankau, M. Rein, M. Schweitzer, N. Windhab, G. von Kiedrowski, *Nature* **2002**, *420*, 286.
- [36] M. Li, S. Mann, *J. Mater. Chem.* **2004**, *14*, 2260.
- [37] Z. Li, R. C. Jin, C. A. Mirkin, R. L. Letsinger, *Nucleic Acids Res.* **2002**, *30*, 1558.
- [38] N. C. Seeman, *Chem. Biol.* **2003**, *10*, 1151.
- [39] N. C. Seeman, *Nature* **2003**, *421*, 427.
- [40] S. A. Bejune, A. H. Shelton, D. R. McMillin, *Inorganic Chemistry* **2003**, *42*, 8465.
- [41] D. R. McMillin, A. H. Shelton, S. A. Bejune, P. E. Fanwick, R. K. Wall, *Coord. Chem. Rev.* **2005**, *249*, 1451.
- [42] M. Balaz, B. C. Li, S. Jockusch, G. A. Ellestad, N. Berova, *Angew. Chem. Int. Ed.* **2006**, *45*, 3530.
- [43] M. Balaz, J. D. Steinkruger, G. A. Ellestad, N. Berova, *Org. Lett.* **2005**, *7*, 5613.
- [44] M. Balaz, B. C. Li, S. Jockusch, G. A. Ellestad, N. Berova, *Angew. Chem. Int. Ed.* **2006**, *45*, 3530.
- [45] M. Balaz, B. C. Li, J. D. Steinkruger, G. A. Ellestad, K. Nakanishi, N. Berova, *Org. Biomol. Chem.* **2006**, *4*, 1865.
- [46] M. Endo, T. Shiroyama, M. Fujitsuka, T. Majima, *J. Org. Chem.* **2005**, *70*, 7468.
- [47] M. Endo, N. C. Seeman, T. Majima, *Angew. Chem.-Int. Ed.* **2005**, *44*, 6074.
- [48] R. Rigler, F. Seela, *J. Biotechnol.* **2001**, *86*, 161.
- [49] F. Seela, E. Feiling, J. Gross, F. Hillenkamp, N. Ramzaeva, H. Rosemeyer, M. Zulauf, *J. Biotechnol.* **2001**, *86*, 269.
- [50] D. M. Perrin, T. Garestier, C. Helene, *J. Am. Chem. Soc.* **2001**, *123*, 1556.
- [51] T. Goullain, A. Sidorov, N. Mignet, S. J. Thorpe, S. E. Lee, J. A. Grasby, D. M. Williams, *Nucleic Acids Res.* **2001**, *29*, 1898.
- [52] U. Diederichsen, C. M. Biro, *Bioorg. Med. Chem. Lett.* **2000**, *10*, 1417.
- [53] K. Sakthivel, C. F. Barbas, *Angew. Chem. Int. Ed.* **1998**, *37*, 2872.
- [54] D. J. Hurley, Y. Tor, *J. Am. Chem. Soc.* **2002**, *124*, 3749.
- [55] S. I. Khan, A. E. Beilstein, G. D. Smith, M. Sykora, M. W. Grinstaff, *Inorg. Chem.* **1999**, *38*, 2411.
- [56] S. I. Khan, A. E. Beilstein, M. W. Grinstaff, *Inorg. Chem.* **1999**, *38*, 418.
- [57] O. Thum, S. Jager, M. Famulok, *Angew. Chem.-Int. Edit.* **2001**, *40*, 3990.
- [58] M. A. Augustin, W. Ankenbauer, B. Angerer, *J. Biotechnol.* **2001**, *86*, 289.
- [59] N. Solladie, M. Gross, *Tetrahedron Lett.* **1999**, *40*, 3359.
- [60] N. Solladie, N. Aubert, J.-P. Gisselbrecht, M. Gross, C. Sooambar, V. Troiani, *Chirality* **2003**, *15*, S50.
- [61] M. Morisue, N. Haruta, D. Kalita, Y. Kobuke, *Chem. Eur. J.* **2006**, *12*, 8123
- [62] L. S. Bleicher, N. D. P. Cosford, A. Herbaut, J. S. McCallum, I. A. McDonald, *J. Org. Chem.* **1998**, *63*, 1109.
- [63] M. J. Plater, S. Aiken, G. Bourhill, *Tetrahedron* **2002**, *58*, 2405.
- [64] E. Rose, B. Andrioletti, R. P. Pandian, *J. Porphyrins and Phtalocyanines* **2002**, *6*, 602.
- [65] K. Ishimark, K. Monda, Y. Yamamoto, K.-Y. Akiba, *Synth. com.* **2000**, *30*, 575.



- [66] N. A. Caplan, C. I. Pogson, D. J. Hayes, G. M. Blackburna, *J. Chem. Soc., Perkin Trans. 1* **2000**, 421.
- [67] L. J. Twyman, J. K. M. Sanders, *Tetrahedron Lett.* **1999**, 40, 6681.
- [68] A. Vidal-Ferran, N. Bampos, J. K. M. Sanders, *Inorg. Chem.* **1997**, 36, 6117.
- [69] E. Bullock, A. W. Johnson, E. Markham, K. B. Shaw, *J. Chem. Soc.* **1985**, 287, 1437.
- [70] P. Dolphin, *J. Org. Chem.* **1985**, 50, 5598.
- [71] E. Stulz, S. M. Scott, A. D. Bond, S. Otto, J. K. M. Sanders, *Inorg. Chem.* **2003**, 42, 3086.
- [72] A. M. Sorensen, P. Nielsen, *Org. Lett.* **2000**, 2, 4217.
- [73] G. Wang, P. Middleton, *Nucleosides Nucleotides* **1998**, 17, 1033.
- [74] I. Charles, L. Xue, D. Arya, *Bioorg. Med. Chem. Lett.* **2002**, 12, 1259.
- [75] S. L. Darling, E. Stulz, N. Feeder, N. Bampos, J. K. M. Sanders, *New J. Chem.* **2000**, 24, 261.
- [76] Y. Hayakawa, R. Kawai, A. Hirata, J. Sugimoto, M. Kataoka, A. Sakakura, M. Hirose, R. Noyori, *J. Am. Chem. Soc.* **2001**, 123, 8165.
- [77] I. Bouamaied, E. Stulz, *Chimia* **2005**, 59, 101.
- [78] I. Bouamaied, E. Stulz, *SYNLETT* **2004**, 1579.
- [79] E. Stulz, C. C. Mak, J. K. M. Sanders, *J. Chem. Soc.-Dalton Trans.* **2001**, 604.
- [80] S. Carda-Broch, A. Berthod, D. W. Armstrong, *Rapid Commun. Mass Spectrom.* **2003**, 17, 553.
- [81] Beaucage, Caruthers, *Tetrahedron Lett.* **1981**, 22, 1859.
- [82] C. Wojczewski, K. Stolze, J. W. Engels, *Synlett* **1999**, 10, 1667.
- [83] X. Huang, K. Nakanishi, N. Berova, *Chirality* **2000**, 12, 237.
- [84] T. Kurtan, N. Nesnas, F. E. Koehn, Y. Q. Li, K. Nakanishi, N. Berova, *J. Am. Chem. Soc.* **2001**, 123, 5974.
- [85] T. Kurtan, N. Nesnas, Y. Q. Li, X. F. Huang, K. Nakanishi, N. Berova, *J. Am. Chem. Soc.* **2001**, 123, 5962.
- [86] S. Matile, N. Berova, K. Nakanishi, J. Fleischhauer, R. W. Woody, *J. Am. Chem. Soc.* **1996**, 118, 5198.
- [87] S. Lee, Y. A. Lee, H. M. Lee, J. Y. Lee, D. H. Kim, S. K. Kim, *Biophys. J.* **2002**, 83, 371.
- [88] S. Lee, S. H. Jeon, B. J. Kim, S. W. Han, H. G. Jang, S. K. Kim, *Biophys. Chem.* **2001**, 92, 35.
- [89] Y. Kyogoku, R. C. Lord, A. Rich, *Proc. Natl. Acad. Sci. U. S. A.* **1967**, 57, 250.
- [90] K. Wüthrich, *NMR of proteins and nucleic acids*, John Wiley & Sons, Ltd., New York, **1986**.
- [91] O. Brandt, J. Feldner, S. Hellweg, M. Schröder, A. Stephan, H. F. Arlinghaus, J. D. Hoheisel, A. Jacob, *Appl. Surface Sci.* **2006**, 256, 6935.
- [92] I. Bouamaied, L.-A. Fendt, M. Wiesner, D. Häussinger, N. Amiot, S. Thöni, E. Stulz, *Pure Appl. Chem.* **2006**, 78, 2003.
- [93] X. L. Guo, W. T. An, S. M. Shuang, F. Q. Cheng, C. Dong, *J. Photochem. Photobiol. A-Chem.* **2005**, 173, 258.
- [94] B. M. Znosko, T. W. Barnes, T. R. Krugh, D. H. Turner, *J. Am. Chem. Soc.* **2003**, 125, 6090.
- [95] M. D. Sorensen, M. Petersen, J. Wengel, *Chem. Commun.* **2003**, 2130.
- [96] A. Lauritsen, J. Wengel, *Chem. Commun.* **2002**, 530.
- [97] A. A. Koshkin, S. K. Singh, P. Nielsen, V. K. Rajwanshi, R. Kumar, M. Meldgaard, C. E. Olsen, J. Wengel, *Tetrahedron* **1998**, 54, 3607.
- [98] A. A. Mokhir, C. N. Tetzlaff, S. Herzberger, A. Mosbacher, C. Richert, *J. Comb. Chem.* **2001**, 3, 374.

- [99] Z. Dogan, R. Paulini, J. A. R. Stutz, S. Narayanan, C. Richert, *J. Am. Chem. Soc.* **2004**, *126*, 4762.
- [100] M. Eriksson, P. E. Nielsen, *Nat. Struct. Biol.* **1996**, *3*, 410.
- [101] S. Shakeel, S. Karim, A. Ali, *J. Chem. Technol. Biotechnol.* **2006**, *81*, 892.
- [102] T. van der Boom, R. T. Hayes, Y. Y. Zhao, P. J. Bushard, E. A. Weiss, M. R. Wasielewski, *J. Am. Chem. Soc.* **2002**, *124*, 9582.
- [103] A. S. Lukas, P. J. Bushard, M. R. Wasielewski, *J. Phys. Chem. A* **2002**, *106*, 2074.
- [104] P. Walde, in *Encyclopedia of Nanoscience and Nanotechnology*, Vol. 9 (Ed.: H. S. Nalwa), **2004**.
- [105] D. Holten, D. F. Bocian, J. S. Lindsey, *Accounts Chem. Res.* **2002**, *35*, 57.
- [106] C. S. Rajesh, G. J. Capitosti, S. J. Cramer, D. A. Modarelli, *J. Phys. Chem. B* **2001**, *105*, 10175.
- [107] U. Heinen, T. Berthold, G. Kothe, E. Stavitski, T. Galili, H. Levanon, G. Wiederrecht, M. R. Wasielewski, *J. Phys. Chem. A* **2002**, *106*, 1933.
- [108] H. B. Yin, T. Brown, J. S. Wilkinson, R. W. Eason, T. Melvin, *Nucl. Acids Res.* **2004**, *32*, e118.
- [109] N. D. Sinha, J. Biern, J. McManus, H. Köster, *Nucl. Acids Res.* **1984**, *12*, 4539.
- [110] C. R. Cantor, M. M. Warshaw, H. Shiparo, *Biopolymers* **1970**, *9*, 1059.
- [111] M. Budessinsky, *Collect. Czech. Chem. Comm.* **1959**, *24*, 4022.

Dipl. Chem. Imenne Bouamaied

### **Eidesstattliche Erklärung**

Ich erkläre, dass die Dissertation mit dem Titel:  
**„DNA as Supramolecular Scaffold for Porphyrin Arrays“**  
nur mit der darin angegebenen Hilfe verfasst  
und bei keiner anderen Fakultät eingereicht wurde.

Basel, den 19. juni 2007

Imenne Bouamaied

**The following lectures contributed to my education:**

**University of Basel (CH):** Dr. E. Stulz, Prof. Dr. B. Giese.

**University of Strasbourg (FR):** Prof. Dr. M. Pfeiffer, Prof. Dr. J. J. Bourguignon, Prof. Dr. W. Hosseini, Prof. Dr. G. Solladié, Prof. Dr. J.F. Nicoud, Prof. Dr. D. Uguen, Prof. Dr. L. Gade, Prof. Dr. M. Henry, Prof. Dr. C. Mioskowsky, Prof. Dr.P. Pale, Prof. Dr. J. P. Lepoitevin, Prof. Dr. H. Wipff.

**University of Reading (UK):** Prof. Dr. L. Harwood

**University of College London (UK):** Prof. Dr. K. Hale

## Curriculum Vitae

Imenne Bouamaied

**Date of birth:** March. 12, 1979

**Nationality:** French

## EDUCATION

---

- 2003-2007**            **Ph.D. Student in Organic Chemistry**, University of Basel, Switzerland.
- 2003**                **DEA (M.Sc.) in Organic Chemistry**, University of Strasbourg, France.
- 2002**                **Master in Chemistry**, University of Strasbourg, France.
- 2001**                **Licence in Chemistry**, University of Strasbourg, France.
- 2000**                **DEUG in Science**, University of Strasbourg, France.
- 1997**                **Baccalauréat**, Mulhouse, France.

## PROFESSIONAL EXPERIENCE

---

- 2003-2007**            **Ph. D studies**, Department of Organic Chemistry at the University of Basel, in the group of Prof. Bernd Giese under the supervision of Dr. Eugen Stulz.
- “Porphyrin substituted oligonucleotides synthesis and characterization”*
- 2003**                **DEA (M. Sc.)**, Department of Organic and Inorganic Chemistry, University of Strasbourg, in the group of Prof. Michel Pfeffer.
- “Molecular Recognition of anions by Cobalto Receptors”*
- 2002**                **Master**, Department of Pharmacochemistry, University of Strasbourg, in the group of Prof. Jean-Jacques Bourguignon.
- “Synthesis of functionalized imidazolones”*